WHY DOES MY JOINT HURT: UNDERSTANDING DISEASE PHENOTYPE AND PAIN RELATIONSHIPS USING MOUSE MODELS OF ARTHRITIS

Sanaa Zaki

A thesis submitted in fulfilment of requirements for the degree of Doctor of Philosophy

Faculty of Medicine (Sydney Medical School)

The University of Sydney

November 2016

PREFACE

The research embodied in this thesis was conducted at the Raymond Purves Laboratories of Bone and Joint Research, Kolling Institute of Medical Research, University of Sydney at the Royal North Shore Hospital, St Leonards, Australia. Institutional ethics committee approval was sought and obtained prior to the commencement of all animal experiments. The research was partly funded by Arthritis Australia.

I certify that the intellectual content of this thesis is the product of my own work, including the design, conduct and analysis of experiments presented in this thesis. Contributions of other researchers and all the assistance received in preparing this thesis and relevant sources have been acknowledged. This thesis has not been submitted for any degree or other purpose.

Sanaa Zaki

ACKNOWLEDGEMENTS

My PhD candidature has been a very long journey and I have many colleagues, friends and family that I need to acknowledge for their contribution.

Firstly, I am forever indebted to the support and mentorship of my two supervisors, Mark Connor and Chris Little. They graciously bestowed me with the freedom to pave my own path of scientific discovery, while always being there to guide and redirect me when I needed it the most. I am truly indebted to their academic brilliance, scientific rigor and boundless patience. They are truly inspirational researchers that I can only hope to, one day, emulate.

Secondly, I would like to thank and acknowledge the many contributions of the Raymond Purves Laboratories team. Thank you Cindy Shu for helping me to settle in and always offering assistance when I had a technical problem in the lab. Your endless supply of delicious treats, gorgeous smile and friendship kept me going. Thank you Sue Smith for all your hard work in slide preparation and the perseverance you displayed when I was all but ready to give up after so many failed attempts at IHC. You are definitely the histology guru! Thank you Margaret Smith for showing me how to do RNA extraction and PCR when I first arrived in the lab, and for your help with the tricky statistical analysis; I wouldn't have known where to start otherwise. Thank you Miriam Jackson for letting me borrow/steal your bench equipment and never complaining. Thank you Varshini Ravi for helping me set up my tissue culture protocol and showing me how to do a BCA assay. I really enjoyed sharing a bench with you and the many interesting conversations we had while pipetting. Thank you Kelly McKelvey for been so giving of your time and helping me with formatting my thesis. You are an excellent researcher and a kind and generous human being.

I would also like to acknowledge the support and encouragement I received from colleagues and friends in the Veterinary Faculty, especially Merran Govendir, my special friend that I love and admire so much, and who was always willing to listen to my rants and keep me on track. “Work out what’s really important in your life and focus on that” are definitely words to live by.

Finally, I’ve left the most important people to acknowledge until the end: my family, without whom I could never have gotten through this journey. Thank you to my amazing mum for her endless love and encouragement, and for always being proud of me even during my failures. Thank you to my gorgeous sister Ouafaa who was always there for me and who taught me to allow myself to enjoy the little pleasures life has to offer without feeling guilty. Thank you also for your willingness to proof read chapter after chapter without ever complaining. Thank you to my brother Jassen and my other ‘sister’ Fatima. Without you I don’t know if Aden would have survived this PhD. Thank you to my beautiful boys Ossama, Younis and Aden. The three of you are my inspiration - You are my world. Thank you for always challenging the way I view the world. Thank you for giving me space when I needed it. Thank you for putting a smile on my face after a really tough day. Thank you for making me feel like I’m amazing, even though in my world I’m pretty ordinary. Thank you for your beautiful smiles, amazing hugs and unconditional love.

The last person I would like to acknowledge is my husband. Thank you Mohamed for helping me realise my dream. Thank you for your patience and support even when I wasn’t a very nice person to be around. Thank you for letting me do things my way when I needed to. Thank you for sharing the load to make my life easier. Thank you for allowing me to be more than a mother and a wife. Thank you for putting up with all the late nights and early starts. Thank you for being the amazing, kind and caring

person that you are. Without you to share in my struggles, this achievement would mean nothing.

I would like to dedicate this Thesis, and all the hard work that went into it, to the beautiful men in my life, Mohamed, Ossama, Younis and Aden.

PUBLICATIONS AND PRESENTATIONS

Publications arising from this thesis

1. Kung, L. H., Zaki, S., Ravi, V., Rowley, L., Smith, M.M., Bell, K.M., . . . Little, C. B. (2016). Utility of circulating serum miRNAs as biomarkers of early cartilage degeneration in animal models of post-traumatic osteoarthritis and inflammatory arthritis. *Osteoarthritis Cartilage*. doi:10.1016/j.joca.2016.09.002

Publications related to this thesis

1. Little, C.B., & Zaki, S. (2012). What constitutes an "animal model of osteoarthritis"-the need for consensus? *Osteoarthritis and cartilage / OARS, Osteoarthritis Research Society, 20*(4), 261-267
2. Jackson, M.T., Moradi, B., Zaki, S., Smith, M.M., McCracken, S., Smith, S.M., Jackson, C.J. & Little, C.B. (2014). Depletion of protease-activated receptor 2 but not protease-activated receptor 1 may confer protection against osteoarthritis in mice through extracartilaginous mechanisms. Arthritis & Rheumatology 66(12): 3337-3348.

Conference Abstracts

1. Zaki, S., Smith, M.M., Smith, S.M., Connor, M., & Little, C.B. (2012). Distinct Pain Mechanisms in Two different Models of Arthritis. *Osteoarthritis and Cartilage, 20*, S252-S253.
2. Zaki, S., Smith, M.M., Smith, S., Connor, M., & Little, C.B. (2013). Contrasting Pathophysiology and Behavioural Responses Associated With Osteoarthritis and An Inflammatory Arthropathy. *Arthritis and rheumatism, 65*, S527-S528.
3. Zaki, S., Miller, R. E., Malfait, A. M., Smith, S., Tran, P. B., Ishihara, S., & Little, C. (2014). Characterisation of Pain-Related Behaviours In Association with Joint

Pathology in an 8-Week Antigen-Induced Arthritis Model. *Osteoarthritis and Cartilage, 22*, S36-S37.

4. Miller, R. E., Zaki, S., Ishihara, S., Tran, P. B., Little, C. B., & Malfait, A. M. (2014). Establishing a Method for Measuring Primary Knee Hyperalgesia in the Murine DMM Model of Osteoarthritis. *Osteoarthritis and Cartilage, 22*, S419-S419.
5. Jackson, M. T., Zaki, S., Ravi, V., Moradi, B., Smith, S., Fosang, A., & Little, C. (2016). Defining the Relationship between Joint Pathology and Pain in Osteoarthritis using Genetically Modified Mice. *Osteoarthritis and Cartilage, 24*, S9-S10.
6. Shu, C. C., Ravi, V., Zaki, S., Smith, S. M., Schiavinato, A., Smith, M. M., & Little, C. B. (2016). The Effects of Intra-articular Injection of Mesnchymal Stem Cells versus Hyaluronan Hexadecylamide-Derivative on Post-Traumatic OA: The Relationship Between Synovial Inflammation, Structural Pathology and Pain Sensitisation *Osteoarthritis and Cartilage, 24*, S324-S325.

ABSTRACT

Osteoarthritis (OA), characterised by progressive joint-wide pathology, is a major health problem accounting for 48% of people living with chronic pain. There are no treatments to slow OA progression and symptom managing therapies are at best moderately effective. This failure results from a poor understanding of the mechanisms that drive OA pain. Animal models are widely used to study OA pain molecular pathways, but pre-clinical findings fail to translate into effective therapeutics for patients. In part this may be because animal models have poorly defined phenotypes not mapped to specific sub-types of human OA.

This research aimed to define the relationship between joint tissue pathology, pain behaviour and gene expression in the dorsal root ganglia (DRG), over time comparing models of post-traumatic OA (DMM) and inflammatory arthritis (AIA), and identify differences in what drives pain.

DMM and AIA ultimately displayed similar hallmark histopathology of OA in late stage disease. However, each model had distinct temporal patterns of pathology; associations between articular cartilage, synovium and bone pathology; and risk factors for progression. Both models displayed sensitisation (tactile allodynia, mechanical and thermal hyperalgesia) and altered gait (reduced hindlimb weight bearing, changes in stride length). However, the severity and temporal pattern of occurrence were model-specific. At each phase of OA development, DRG gene expression changes were also model-specific. It was predominantly synovium and bone pathology that were significantly associated with altered DRG gene expression and pain behavior, but differentially in the two models. The DRG expression changes associated with altered pain behaviours were also model specific.

Combined these findings demonstrate that DMM and AIA are phenotypically unique models of OA, defined not only by initiating cause, but temporal pattern and inter-dependence of joint pathology, pain characteristics, and molecular drivers. The results suggest that the mechanisms regulating joint pain are specific to the disease pathophysiology, and confirm the importance of mapping pre-clinical findings to specific human disease phenotypes. This challenges the current way animal models are used to investigate OA pain mechanisms and test therapeutics.

TABLE OF CONTENTS

PREFACE II

ACKNOWLEDGEMENTS III

PUBLICATIONS AND PRESENTATIONS VI

ABSTRACT VIII

TABLE OF CONTENTS X

LIST OF FIGURES XVII

LIST OF TABLES XX

LIST OF ABBREVIATIONS XXII

CHAPTER 1: INTRODUCTION AND LITERATURE REVIEW 1

1.1 OSTEOARTHRITIS 1

1.1.1 Prevalence and disease burden 1

1.1.2 The pathophysiology of OA 2

1.1.3 Articular Cartilage 4

1.1.3.1 Aggrecan 5

1.1.3.2 Collagen 7

1.1.3.3 Tissue inhibitors of metalloproteinase 9

1.1.4 Subchondral bone 9

1.1.5 Inflammation and the immune system 11

1.1.6 OA phenotypes 13

1.1.7 OA therapeutic targets 14

1.2 SENSORY INNERVATION OF THE KNEE JOINT 18

1.2.1 Knee joint afferents 18

1.2.2 Nociceptors 19

1.2.3 Vanilloid 1 receptor 20

1.2.4 Transient Receptor Potential Ankyrin-1 (TRPA1) 22

1.2.5 Transient Receptor Potential Vanilloid-2 (TRPV2) 23

1.2.6 Transient Receptor Potential Vanilloid-4 (TRPV4) *24*

1.2.7 The dorsal root ganglia *25*

1.3 CHRONIC PAIN 26

1.3.1 Sensitisation *26*

1.3.2 OA pain in humans *29*

1.3.3 Mechanisms of OA pain *30*

1.3.3.1 Inflammation 32

1.3.3.2 Neuropathic mechanisms 33

1.3.4 Future therapies for OA pain *38*

1.4 ANIMAL MODELS OF OA 42

1.4.1 Mono-iodoacetate (MIA) induced arthritis *45*

1.4.2 Surgical destabilisation of the medial meniscus (DMM) *47*

1.4.3 Antigen-induced Arthritis (AIA) Model *50*

1.5 LITERATURE REVIEW SUMMARY AND RESEARCH AIMS 51

CHAPTER 2: METHODS 54

2.1 MURINE MODELS OF ARTHRITIS: DESTABILISATION OF THE MEDIAL MENISCUS (DMM) AND ANTIGEN-INDUCED ARTHRITIS (AIA) 54

2.1.1 Randomisation and blinding *55*

2.1.2 Anaesthesia *57*

2.1.3 The DMM model *58*

2.1.3.1 Sham operated mice 62

2.1.3.2 Control mice 62

2.1.4 Antigen induced arthritis model *62*

2.1.4.1 Immunisation: 62

2.1.4.2 Intra articular injection: 63

2.1.4.3 Control mice: 64

2.1.5 Euthanasia *66*

2.2 HISTOLOGY 66

2.2.1 Knee joint processing *66*

2.2.2 Histochemical Staining *68*

2.2.3 Histological Scoring system *68*

2.3 PAIN BEHAVIOUR TESTING 69

2.3.1 Von Frey filament testing *70*

2.3.2 Hotplate test *72*

2.3.3 Pressure Application Measurement *74*

2.3.4 Forceplate *76*

2.3.5 Stride length *78*

2.4 DRG GENE EXPRESSION USING REAL TIME REVERSE TRANSCRIPTION-POLYMERASE CHAIN REACTION (RT-PCR) 80

2.4.1 DRG harvesting *83*

2.4.2 RNA extraction *85*

2.4.3 RNA quantification *86*

2.4.4 Reverse Transcription *86*

2.4.5 Primer design *87*

2.4.6 Quantitative real-time RT-PCR *87*

2.5 IMMUNOHISTOCHEMISTRY 89

2.5.1 Perfusion of mice with paraformaldehyde *89*

2.5.2 DRG Processing *90*

2.5.3 Antibody staining *92*

2.5.3.1 Deparaffinisation 92

2.5.3.2 Primary antibody incubation 92

2.5.3.3 Detection 92

2.5.3.4 Counterstain 93

2.5.3.5 Mounting 93

CHAPTER 3: DEVELOPMENT AND VALIDATION OF METHODS 94

3.1 PAIN ASSESSMENT 94

3.1.1 Mechanical allodynia *101*

3.1.2 Thermal hyperalgesia *108*

3.1.3 Mechanical hyperalgesia *115*

3.1.4 Weight distribution *121*

3.1.5 Stride length *126*

3.1.6 Rotarod *129*

3.1.7 Pain testing Conclusions *132*

3.2 HISTOLOGY SCORING 133

CHAPTER 4: KNEE JOINT HISTOPATHOLOGY FOLLOWING DESTABILIZATION OF THE MEDIAL MENISCUS (DMM) AND ANTIGEN-INDUCED ARTHRITIS (AIA) IN MICE 140

4.1 INTRODUCTION AND AIMS 140

4.2 METHODS, STATISTICAL ANALYSIS AND DATA PRESENTATION 141

4.3 RESULTS 143

4.3.1 Effect of AIA and DMM on inflammation following induction of arthritis *143*

4.3.1.1 Panus 151

4.3.1.2 Bone erosion 151

4.3.1.3 Synovial hyperplasia 151

4.3.1.4 Sub-synovial inflammation 152

4.3.1.5 Synovial exudate 152

4.3.2 Effect of AIA and DMM on articular cartilage degradation following induction of arthritis *154*

4.3.2.1 Proteogylcan loss 154

4.3.2.2 AC structural damage 154

4.3.2.3 Chondrocyte hypertrophy 155

4.3.3 Effect of AIA and DMM on bone following induction of arthritis *159*

4.3.3.1 Osteophytes 159

4.3.3.2 Subchondral bone 160

4.3.4 Time and Treatment effect on joint pathology *165*

4.3.5 Correlation between pathological change in different joint tissues in AIA and DMM when corrected for time *168*

4.3.5.1 Articular cartilage histopathology partial correlations 168

4.3.5.2 Joint inflammation partial correlations 169

4.3.5.3 Bone histopathology partial correlations 169

4.3.6 Comparison of joint tissue pathology relationships in AIA versus DMM *175*

4.4 DISCUSSION 177

CHAPTER 5: PAIN BEHAVIOUR OUTCOMES FOLLOWING DESTABILIZATION OF THE MEDIAL MENISCUS (DMM) AND ANTIGEN-INDUCED ARTHRITIS (AIA) IN MICE 187

5.1 INTRODUCTION AND AIMS 187

5.2 METHODS, STATISTICAL ANALYSIS AND DATA PRESENTATION 189

5.3 RESULTS 190

5.3.1 Effect of AIA and DMM on tactile allodynia following induction of arthritis *190*

5.3.2 Effect of AIA and DMM on thermal hyperalgesia following induction of arthritis *197*

5.3.3 Effect of AIA and DMM on mechanical hyperalgesia following induction of arthritis *201*

5.3.4 Effect of AIA and DMM on hind limb weight distribution following induction of arthritis *208*

5.3.5 Effect of AIA and DMM on stride length following induction of arthritis *212*

5.3.6 Time and treatment effect on pain-related behaviours *224*

5.3.7 Correlation between different pain-related behaviours in AIA and DMM when corrected for time *226*

5.4 DISCUSSION 228

5.4.1 Tactile allodynia *229*

5.4.2 Mechanical hyperalgesia *230*

5.4.3 Hind Limb Weight distribution *231*

5.4.4 Stride length *233*

5.4.5 Thermal hyperalgesia *235*

5.4.6 Summary *237*

CHAPTER 6: GENE EXPRESSION PROFILE OF INFLAMMATORY MEDIATORS AND NEUROTRANSMITTERS IN THE DRG FOLLOWING DESTABILIZATION OF THE MEDIAL MENISCUS (DMM) AND ANTIGEN-INDUCED ARTHRITIS (AIA) IN MICE 241

6.1 INTRODUCTION AND AIMS 241

6.2 METHODS, STATISTICAL ANALYSIS AND DATA PRESENTATION 245

6.3 RESULTS 247

6.3.1 DRG gene expression (real time RT-PCR) *247*

6.3.2 Time and treatment effect on DRG gene expression (real time RT-PCR) *261*

6.3.3 Correlation between different genes in AIA and DMM when corrected for time *263*

6.3.4 DRG protein expression (immunohistochemistry) *269*

6.4 DISCUSSION 279

6.4.1 Summary *289*

CHAPTER 7: ASSOCIATIONS BETWEEN KNEE JOINT HISTOPATHOLOGY, PAIN BEHAVIOR AND PERIPHERAL SENSORY INNERVATION FOLLOWING DESTABILIZATION OF THE MEDIAL MENISCUS (DMM) AND ANTIGEN-INDUCED ARTHRITIS (AIA) IN MICE 291

7.1 INTRODUCTION AND AIMS 291

7.2 METHODS, STATISTICAL ANALYSIS AND DATA PRESENTATION 294

7.3 RESULTS 296

7.3.1 Correlation between joint tissues histopathology and gene expression in right L3/L4 DRG in DMM and AIA when corrected for time 296

7.3.2 Correlation between pain behaviour and gene expression in right L3/L4 DRG in DMM and AIA when corrected for time 299

7.3.3 Correlation between joint tissue histopathology and pain behaviour in DMM and AIA when corrected for time 301

7.4 DISCUSSION 303

7.4.1 Summary 311

CHAPTER 8: CONCLUSIONS AND FUTURE DIRECTIONS 312

8.1 SUMMARY 312

8.2 STUDY LIMITATIONS 319

8.3 QUESTIONS ARISING 321

8.4 FUTURE DIRECTIONS 322

APPENDIX A: REAGENTS AND EQUIPMENT 325

APPENDIX B: REAGENT PREPARATION 329

APPENDIX C: HISTOLOGY SCORING 334

APPENDIX D: MELT CURVES FOR REAL TIME RT-PCR 342

APPENDIX E: THE ROLE OF MACROPHAGE INFILTRATION AND CHEMOKINE PRODUCTION BY SENSORY NEURONES IN DEVELOPMENT OF OA PAIN - PRELIMINARY FINDINGS USING IHC AND DRG TISSUE CULTURE METHODS. 349

REFERENCES: 359

LIST OF FIGURES

Figure 1.1. Schematic diagram of the knee joint 3

Figure 1.2. Schematic diagram of the Pain Pathway 28

Figure 2.1. Destabilisation of the medial meniscus 61

Figure 2.2. Antigen induced arthritis: 65

Figure 2.3a: Von Frey testing chambers and application of filament. 71

Figure2.3b. Hotplate device.....73

Figure 2.3c. Pressure Application Measurement device.....75

Figure 2.3d. Forceplate device.....77

Figure 2.3e. Stride length measurement.....79

Figure 2.4. DRG harvesting 84

Figure 3.1a. Baseline 50% paw withdrawal threshold (PWT) 103

Figure 3.1b. Baseline 50% PWT using von Frey filaments.....103

Figure 3.1c. Development of von Frey test protocol 107

Figure 3.2a. Baseline paw withdrawal latency (PWL) 111

Figure 3.2b. Development of Hotplate test protocol 111

Figure 3.2c. Development of Hotplate test protocol.....114

Figure 3.2d. Development of Hotplate test protocol 114

Figure 3.3a. Pressure Application Measurement (PAM) device 116

Figure 3.3b. PAM protocol restraint method.....116

Figure 3.3c. Development of PAM device protocol 117

Figure 3.3d. Development of PAM device protocol.....120

Figure 3.3e. Development of PAM device protocol 120

Figure 3.4a. Incapacitance device used to measure hind limb weight distribution. .122

Figure 3.4b. Hind limb weight distribution 122

Figure 3.4c. Development of hind limb weight distribution test protocol.....124

Figure 3.4d. Development of hind limb weight distribution test protocol 125

Figure 3.5a. Hind limb paw print trace for stride length measurement.....127

Figure 3.5b. Development of stride length measurement protocol.....127

Figure 3.5c. Development of stride length measurement protocol.....128

Figure 3.6a. Development of rotarod test protocol.....131

Figure 3.6b. Development of rotarod test protocol.....131

Figure 3.7a. Synovial inflammation 135

Figure 3.7b. Inter-observer variability.....136

Figure 3.7c. Serial sagittal section scores 136

Figure 3.7d. Maximum score vs. central weight bearing section 138

Figure 3.7e. Synovial inflammation comparative scores.....138

Figure 4.1a. OA knee joint histopathology – Acute inflammatory phase 146

Figure 4.1b. OA knee joint histopathology – Early progressive OA 148

Figure 4.1c. OA knee joint histopathology – Late chronic OA.....149

Figure 4.2. Knee joint inflammation histopathology I.....150

Figure 4.3. Knee joint inflammation histopathology II 153

Figure 4.4. Knee joint articular cartilage histopathology I 156

Figure 4.5. Knee joint articular cartilage histopathology II.....157

Figure 4.6. Knee joint articular cartilage histopathology III.....158

Figure 4.7. Knee joint osteophyte histopathology I.....161

Figure 4.8. Knee joint osteophyte histopathology II.....162

Figure 4.9. Knee joint subchondral bone histopathology I.....163

Figure 4.10. Knee joint subchondral bone histopathology II.....164

Figure 4.11. Knee joint histopathology associations 173

Figure 5.1a-c. Ipsilateral 50% Paw Withdrawal Threshold (PWT).....194

Figure 5.1d-f. Contralateral 50% Paw Withdrawal Threshold (PWT).....195

Figure 5.1g-h. 50% PWT in immunised only mice.....196

Figure 5.2a. Hotplate paw withdrawal latency (PWL) baseline.....198

Figure 5.2b-e. Hotplate PWL.....200

Figure 5.3a-c. Ipsilateral paw withdrawal threshold (PWT).....205

Figure 5.3d-f. Contralateral paw withdrawal threshold (PWT).....206

Figure 5.3g-h. PWT in immunised only mice.....207

Figure 5.4a-d. Hind limb (HL) weight distribution.....211

Figure 5.5a-c. Stride length I.....218

Figure 5.5d-f. Stride length II.....219

Figure 5.5g-i. Stride length III.....220

Figure 5.5j-l. Stride length IV.....221

Figure 5.5m-n. Stride length V.....222

Figure 6.1a-g. Gene expression for R vs. L L3/L4 DRG.....249

Figure 6.2a-l. Gene expression for R L3/L4 DRG.....252

Figure 6.3a-l. Right to left gene expression ratio for L3/L4 DRG.....256

Figure 6.4a-d. CGRP immunoreactivity (IR).....270

Figure 6.4e-h. Opmr1 immunoreactivity (IR).....275

LIST OF TABLES

Table 1.1. Clinical DMOAD trials in knee osteoarthritis* 16

Table 2.1. Genes selected for RT-PCR analysis and evidence for role in chronic pain states including OA pain 82

Table 3.1. Testing schedule for optimisation of pain behaviour assays 99

Table 3.2: Hotplate Test 113

Table 4.1a Joint histopathology scores in AIA and DMM 144

Table 4.1b Synovitis histolopathology scores in DMM and AIA 145

Table 4.2. Joint histopathology logistic regression analysis 166

Table 4.3. Cartilage pathology, bone pathology and joint inflammation partial correlations in AIA and DMM 170

Table 4.4. Risk factors for OA (cartilage damage) 176

Table 4.5. Risk factors for OA (joint inflammation) 176

Table 5.1. Von Frey (ipsilateral 50% PWT) 192

Table 5.2. Hotplate (52^0C PWL) 199

Table 5.3. PAM device (right knee PWT) 202

Table 5.4. Forceplate (hindlimb weight distribution) 209

Table 5.5a. Stride length (right to left stride - RLS) 213

Table 5.5b. Stride length (left to right stride - LRS) 214

Table 5.5c. Stride length (full stride length right - FSLR) 215

Table 5.5d. Stride length (full stride length left - FSLL) 216

Table 5.6. Time and treatment effect on pain behaviour 225

Table 5.7. Pain related behaviour partial ranked correlations in AIA and DMM when corrected for time. 227

Table 5.8. Summary of pain phenotype for AIA and DMM at different phases of OA 238

Table 6.1. Gene expression of the right vs. left L3/L4 DRG 248

Table 6.2. Gene expression of the right L3/L4 DRG 251

Table 6.3. Right to left DRG (L3 and L4) gene expression ratio 255

Table 6.4. A summary of changes in gene expression profile in the ipsilateral L3/L4 DRG of DMM and AIA mice. 260

Table 6.5. Time and treatment effect on DRG gene expression 262

Table 6.6. Gene expression correlations 264

Table 7.1. Histopathology and gene expression correlations 298

Table 7.2. Pain behavior and gene expression correlations 300

Table 7.3. Histopathology and pain behaviour correlations 302

LIST OF ABBREVIATIONS

AC	articular cartilage
ACLT	Anterior cruciate ligament transection
ADAMTS	a disintegrin and metalloproteinase with thrombospondin
AIA	antigen induced arthritis
ATF3	activated transcription factor-3
BML	bone marrow lesions
BMP	bone morphogenetic protein
CCL	C-C motif chemokine ligand
CCR	C-C motif chemokine ligand receptor
cDNA	complimentary deoxyribonucleic acid
CGRP	calcitonin gene related peptide
ciOA	collagen induced osteoarthritis
DMM	destabilisation of the medial meniscus
DMOAD	disease modifying osteoarthritis drug
DRG	dorsal root ganglia
DXA	dual-energy x-ray absorptiometry
EDTA	ethylenediaminetetraacetic acid
ERK	extracellular-regulated kinase
FBS	fetal bovine serum
FDA	food and drug administration
GAPDH	Glyceraldehyde 3-phosphate dehydrogenase
H&E	haematoxylin and eosin
IHC	immunohistochemistry
IL-1b	interleukin-1b
kDa	kiloDaltons
KO	knock-out
MB	molecular biology grade
mBSA	methylated-Bovine Serum Albumin
MCP	monocyte chemotactic protein
MIA	monoiodoacetate
MML	medial mensical ligament
MMP	matrix metalloproteinase
MRI	magnetic resonance imaging
MSC	mesenchymal stem cell
NBF	neutral buffered formalin
NGF	nerve growth factor
OA	osteoarthritis
OR	ordinal regression
PAR	protein activated receptor
PCR	polymerase chain reaction

PFA	paraformaldehyde
PG	proteoglycan
pH	potential of hydrogen
pi-OA	post inflammatory osteoarthritis
pt-OA	post traumatic osteoarthritis
PWL	paw withdrawal latency
PWT	paw withdrawal threshold
qRT-PCR	quantitative RT-PCR
RNA	ribonucleic acid
RT-PCR	Reverse Transcription- Polymerase Chain Reaction
SCB	subchondral bone
SNL	spinal nerve ligation
TBST	tris-buffered saline and Tween 20
TGF	transforming growth factor
TIMP	tissue inhibitor of metalloproteinase
TJR	total joint replacement
TNF	tumour necrosis factor
TLR	toll-like receptor
TrkA	tropomyosin-related kinase A
TRPA	transient receptor potential ankyrin
TRPV	transient receptor potential vanilloid
VIP	vasoactive intestinal peptide
v/v	volume to volume ratio
w/v	weight to volume ratio

CHAPTER 1: Introduction and literature review

1.1 Osteoarthritis

1.1.1 Prevalence and disease burden

Arthritis is a general term used to describe a range of musculoskeletal conditions characterised by inflammation and/or damage of the joints. The most prevalent form of arthritis is osteoarthritis. Osteoarthritis (OA) is a complex progressive disease of joints that results in pain and reduced mobility. It is a major health problem world-wide, with hip and knee OA ranked the 11th highest contributor to global disability (1). The global prevalence of radiographically confirmed knee OA is 3.8% (2). In the USA, 33.6% of adults aged 65 and older suffer from OA (3). In Australia, 15.3% of the population is affected by arthritis, and 58.9% of those affected have OA (4) . OA is not just a disease of the aged; approximately 64% of OA sufferers are in the working age population (15-64 years) (5). In a recent survey 68% of arthritis sufferers reported that their arthritis is badly managed, translating to persistent pain, disability, impact on work, family and finances (6). The persistent nature of OA means that sufferers live with the disease for a significant portion of their lives and typically develop a chronic pain state. In fact, OA is the major reported cause of chronic pain, accounting for 48% of those living with chronic pain (7). Chronic OA pain negatively impacts both physical and emotional function, leading to depression and reduced social participation (8). All of this results in a huge social and economic disease burden.

The health system expenditure associated with arthritis exceeds expenditure on heart disease, depression, diabetes and asthma. In Australia it was estimated to be $4.2

billion in 2007, with OA accounting for over $1.9 billion (5); in the UK the disease burden cost was estimated at £3.2 billion in 2002 (9); and in the USA the total health expenditure attributable to joint replacements alone was estimated at US$42 billion in 2009 (10).

Despite the huge public health impact of this disease, there are still no effective therapies for treating or preventing OA. Based on the most recent systematic reviews of all randomised clinical trials, current therapy options for the management of hip and knee OA are at best mild to moderately effective and offer only short-term relief of symptoms (11). The exception to this is total joint replacement (TJR) surgery, which accounts in part for the huge financial burden of this disease. However, TJR is not an option when small joints are affected, and a significant proportion of patients that undergo TJR, especially of the knee joint, still report persistent pain (12). Yet, excluding TJR, no advances have been made in how we treat the pain of OA since the introduction of non-steroidal anti-inflammatory drugs (NSAID) at the turn of the last century. Current recommendations for non-surgical management of knee OA include biomechanical interventions, intra-articular corticosteroids, exercise, weight management, strength training and oral and topical NSAID (13).

1.1.2 The pathophysiology of OA

Joints are organs with a biomechanical function that comprise cartilage, subchondral bone, synovium, capsule, ligaments, tendons and muscles (figure 1.1). Each of these tissues is in part made up of extracellular matrices that determine their individual structure and biomechanical function. For example, the physical properties of articular cartilage are imparted by its extracellular matrix (ECM), which comprises a collagen fibre network that enmeshes large hydrophilic proteoglycans, the major one being

aggrecan, that provide resistance to mechanical compression and contribute to the low surface friction necessary for normal joint function (14).

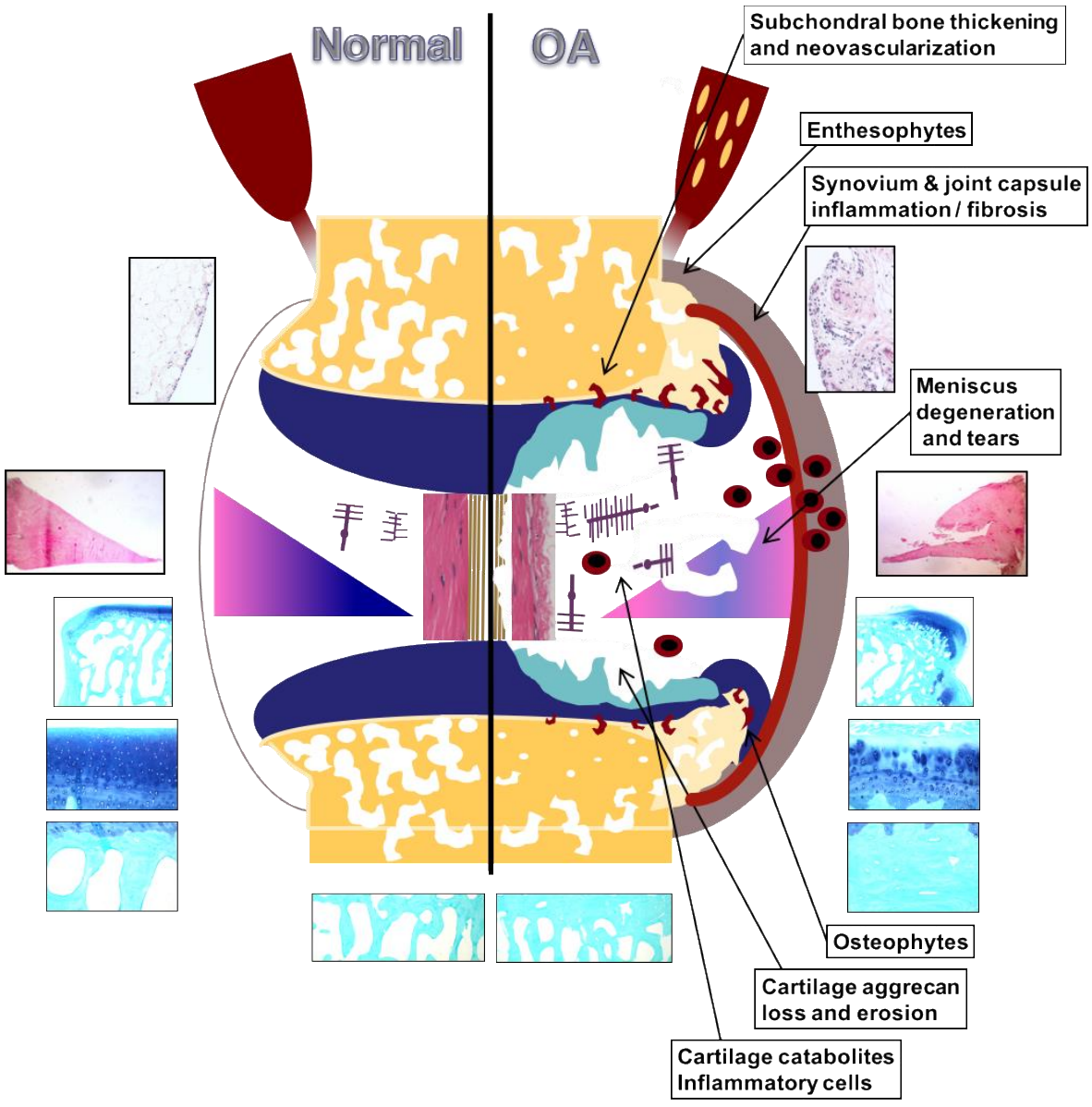

Figure 1.1. Schematic diagram of the knee joint

Diagram depicts normal joint tissue components (left) compared to osteoarthritis (OA) joint tissue pathology (right).

All joint tissues are affected to a greater or lesser extent during the onset and progression of OA. In some tissues such as the articular cartilage the predominant change is progressive degradation and loss while in others like bone there is net tissue formation with resultant subchondral thickening and marginal osteophyte formation. OA is no longer thought of as a disease of individual joint tissues, the new paradigm is to consider that it is a failure of the "joint organ" (figure 1.1). Understanding what drives the pathology in different components of the joint, and how these interact and change with time and/or disease stage is critical to developing new approaches to manage, treat and ultimately cure OA. A great deal has been learned in the last decade, in large part through the development and study of genetically modified mice, about the molecular mechanisms underlying the pathological change. In the following sections I will summarise some of the key mechanisms that contribute to OA pathology in various joint tissues.

1.1.3 Articular Cartilage

Articular cartilage (AC) is comprised of chondrocytes enmeshed in a collagen rich extracellular matrix (ECM) bed. It is a complex tissue with unique properties that present numerous challenges in the face of damage and the need for repair, with little capacity for self-regeneration. AC is hypocellular, with chondrocytes making up only 5 – 10% of the wet tissue weight (15). Chondrocytes are cytoplasmically isolated and rely on paracrine and autocrine communication (16). Yet chondrocytes are responsible for the production and maintenance of the ECM. AC is both aneural and avascular, relying on diffusion for metabolite and nutrient exchange (16).

Cartilage ECM is made up primarily of collagen and proteoglycans, the most abundant by mass being aggrecan (15). Collagen is a major component of many

tissues including AC, bone, tendons, ligaments and muscle, but the specific subtypes and their fibrillar arrangement varies. Collagen is the most predominate protein in AC making up 30-40% of the tissue wet weight, the composite type II/IX/XI fibrils forming an oriented meshwork in the ECM, giving AC its tensile strength (17).

Normal ECM in all tissues undergoes continuous remodelling. Matrix metalloproteinases (MMPs) are a family of more than 25 enzymes involved in normal tissue remodeling as well as many inflammatory and other pathological processes, associated with degeneration. These proteinases cleave ECM proteins and soluble messenger molecules such as cytokines and chemokines. The MMPs involved in articular cartilage degradation are the collagenases (MMP-1, MMP-8, MMP-13), gelatinases (MMP-2, MMP-9) and a distinct group of metalloproteinases belonging to the ADAMTS (a disintegrin and metalloproteinase with thrombospondin motif) family – aggrecanase 1 and 2 (ADAMTS-4 and ADAMTS-5, respectively) (18). Understanding the role of MMP's and ADAMTS in joint disease development has been a major focus of OA research.

1.1.3.1 Aggrecan

Aggrecan is a primary component of articular cartilage ECM. It is a large proteoglycan that consists of a protein core backbone substituted with many sulfated glycosaminoglycans. This imparts a high negative charge density that attracts water and when entrapped in the collagen network provides cartilage with the ability to resist compressive forces. The ADAMTS proteins are a family of zinc-dependent matrix metalloproteinase enzymes several of which cleave the aggrecan core protein with high efficiency at specific sites, in particular the interglobular domain whereby the entire glycosaminoglycan bearing region and load-bearing capacity is lost (19, 20). It is evident in cartilage from all species including humans, that it is cleavage at

the ADAMTS-susceptible sites that is responsible for the majority of pathological aggrecan loss both *in vitro* and *in vivo* (20).

The ADAMTS proteins are made up of an N-terminal pro-domain, a catalytic domain, a disintegrin domain, one or more thrombospondin (TS) motifs, a cysteine-rich domain and a spacer domain of variable length. The two principal aggrecanases, ADAMTS-4 (aggrecanase 1) and ADAMTS-5 (aggrecanase 2) have been cloned and characterised (21, 22). ADAMTS-4 is the shortest member of the family with only one TS motif, while ADAMTS-5 has two. Interest was initially focussed on ADAMTS-4 after researchers demonstrated its regulation by inflammatory cytokines in joint tissue (23, 24). However it has since been shown that ADAMTS-4 knockout (KO) mice demonstrate similar susceptibility to cartilage degradation in OA as wild type (WT) mice (25). In contrast, deletion or inactivation of ADAMTS-5 significantly reduces stimulated cartilage aggrecan loss *in vitro* and in inflammatory and OA models *in vivo*, indicating it is the principle aggrecanase in mouse cartilage (26, 27). Mice deficient in both ADAMTS-4 and ADAMTS-5 do not show any developmental abnormalities, and have similar cartilage protection as ADAMTS-5 KO mice in surgically induced OA (28). Exactly which of these two ADAMTS proteins is the major aggrecanase in human cartilage is still under investigation (29). Furthermore, studies in mice deficient in both ADAMTS-4 and ADAMTS-5 have demonstrated that other aggrecanases may also play a role under specific conditions (30).

Interestingly, ADAMTS-4 and 5 differ with respect to gene regulation. ADAMTS-5 is expressed in human chondrocytes and synovial fibroblasts and is not reliant on induction, whereas ADAMTS-4 expression requires induction by pro-inflammatory cytokines (31). Differential regulation has similarly been seen in MMPs, where

induced transcription occurs for all but MMP-2 and 11, which are constitutively expressed (32, 33).

In addition to its role in cartilage degradation through cleavage of aggrecan, ADAMTS-5 may serve other physiological functions even though some studies would suggest that ADAMTS-5 KO's do not differ phenotypically from WT's (28). More recently investigators have looked at the expression profile of ADAMTS-5 during embryogenesis and in adult tissue (34). In adult tissue, there is constitutive expression of ADAMTS-5 in smooth muscle cells, mesothelium, glomerular mesangial cells, and of particular interest with regard to OA in the dorsal root ganglia, and schwann cells of the peripheral and autonomic nervous system. The findings of this study suggest a wider physiological role for ADAMTS-5 than that of articular cartilage degradation and its intensely investigated role in the development of OA. The lack of evidence of any functional disturbances or abnormalities in ADAMTS-5 KO's suggests that its absence during development in an unchallenged adult null mouse may be compensated by one of several related ADAMTS proteases that may function as less efficient proteoglycanases.

1.1.3.2 Collagen

The most abundant collagen type in AC is type II, making up 90-95% of the collagen mass and playing a critical role in maintaining its integrity, as has been demonstrated in transgenic mice (35). Like aggrecan, type II collagen degradation is a prominent feature of human OA cartilage. Degradation of type II collagen leads to damage of the collagen network and is a critical step in AC erosion in OA (36). It has been demonstrated that type II collagen can only withstand limited degradation before resulting in irreversible cartilage damage in murine models of arthritis (36). A generalised weakening of the collagenous network and subsequent swelling of AC

was initially demonstrated in humans and a number of animal models of OA (37-39). Subsequently, type II collagen degradation was characterised as a localised process in two murine models of spontaneous OA, occurring only in sites adjacent to focal areas of AC degeneration (40).

MMPs play an important role in this process of collagen degradation. *In vitro* studies have demonstrated that cartilage collagenolysis relies on MMP activity (41). MMP-1, MMP-8 and MMP-13 are collagenases secreted by chondrocytes that have the capacity to cleave fibrillar collagens (type II/IX/XI) with resultant fragmentation of fibrils. Of these, MMP-13 has received the greatest attention due to its up regulation in human OA, greater efficiency at type II collagen cleavage (42) and a demonstrated primary role in the release of collagen from human OA cartilage (43).

Much work has been done to characterise the exact role of the collagenases in AC degradation. Postnatal induced over expression of MMP-13 in mice leads to arthritis characterised by cartilage erosion (44). MMP-13 KO mice demonstrate abnormalities in cartilage absorption (45) and fracture healing (46). In a surgical model of OA, MMP-13 KO mice demonstrated chondroprotection that was not associated with any reduction in aggrecanolysis, changes in chondrocyte hypertrophy or osteophyte development (47), confirming that cartilage structural damage depends on MMP-13 activity and suggesting MMP-13 inhibition as a potential therapeutic target for OA.

In addition to the MMP's other proteases, such as cathepsin K, have emerged as important contributors to the cartilage degradation process in OA and along with ADAMTS-5 and MMP-13 are considered major targets for development of future novel therapeutics for OA (48). The exact role these collagenolytic enzymes play in the complex process of AC degradation is still under investigation. In a preclinical anterior cruciate ligament transection (ACLT) model, inhibition of cathepsin K

resulted in protection of SCB integrity, protection against cartilage degradation and a reduction in osteophyte formation (49). There is also evidence cathepsin K degrades AC in naturally occurring equine OA (50). Cathepsin K KO mice are protected against cartilage degradation and SCB changes following surgically induced OA (51). More recently, increased expression and activation of cathepsin K has been identified in human OA cartilage using immunohistochemistry and PCR techniques (52).

1.1.3.3 Tissue inhibitors of metalloproteinase

Tissue inhibitors of metalloproteinases (TIMPs) are specific MMP inhibitors that are involved in the regulation of local MMP activities within tissues (53). Of the 4 mammalian TIMPs, TIMP-3 not only inhibits MMPs but has also been shown to be effective at inhibiting aggrecanases (ADAMTS-4 and 5) (54). Consistent with this, TIMP-3 KO mice have increased spontaneous age-dependent aggrecan loss and OA-like cartilage damage compared with WT mice (55).

1.1.4 Subchondral bone

In addition to articular cartilage changes, subchondral bone remodelling is a significant feature of OA joint pathology that is now recognised as playing an important role in disease progression and pain (56-58).

Bone has the unique capacity to rapidly alter its structural organisation in response to changing mechanical forces, and this has been demonstrated in people with hand and knee OA (59). These alterations are not uniform across all periarticular bone, and occur in two phases – a destructive phase followed by a productive phase (60). The remodelling process commences with the activation of bone resorption that is mediated by osteoclasts. Osteoclasts are a highly specialised lineage of monocyte-

macrophages capable of removing mineralised bone matrix. Bone resorption is followed by bone formation that is mediated by osteoblasts. Under normal physiological settings, these two activities are coupled such that normal bone mass is maintained. Bone modelling occurs when these two processes are not coupled, resulting in a change in bone architecture and volume (increase or decrease), and a modification of the structural properties of cortical and trabecular bone. In addition, periarticular new bone formation can occur via endochondral ossification, where new bone replaces cartilaginous matrix.

Periarticular bone comprises subchondral cortical bone, subchondral trabecular bone, and bone at the joint margins. While varying with disease stage and topographically within the joint, OA is typified by a general net increase in periarticular bone volume with subchondral cortical plate thickening, thinning of vertical trabeculae, a reduction in bone mineral content, focal increased remodelling and resorption, and the development of marginal osteophytes and enthesophytes (61). Imaging (radiography, DXA, MRI) of OA joints reveals various subchondral bone (SCB) changes including sclerosis, cyst formation, bone attrition, and bone marrow lesions (BML). Radiographically, SCB sclerosis appears as an increase in bone density beneath the weight-bearing joint surface. Bone attrition refers to the flattening of the SCB surface in areas of increased loading where remodelling is occurring. BML are a non-specific MRI feature that represents bone marrow necrosis, fibrosis and trabecular abnormalities. They appear to occur in areas of increased bone density (sclerosis) where there is excessive loading (62).

A strong association exists between SCB attrition and BML in the same sub region, suggesting that increased bone stress, as indicated by the presence of BML, leads to increased SCB remodelling and subsequent development of bone attrition (63).

Importantly, in knee OA, articular cartilage loss is evident in areas of bone attrition (64), and the coupling of bone and cartilage turnover in OA may provide a key therapeutic target (61). SCB remodelling and the resolution of SCB cysts has been associated with an improvement in clinical outcomes in patients with advanced post-traumatic OA (65). In a longitudinal multi-centre study of knee OA, enlargement of BML in patients with knee OA lead to an increased risk of cartilage loss in the associated region (66). Animal model studies have also linked SCB changes with disease progression. In mono-iodoacetate (MIA) induced OA, osteoclasts have been implicated in both SCB and calcified cartilage resorption, and early inhibition of osteoclast activity resulted in resolution of joint pathology and pain (67).

1.1.5 Inflammation and the immune system

OA was traditionally viewed as a non-inflammatory arthritis owing to the relatively small white cell populations observed in synovial fluid samples, compared to that seen in rheumatoid arthritis (68). This is despite early observations that synovial inflammation was a component of the disease (69). In the past few years the paradigm has shifted, and it is now widely accepted that inflammation not only exists as part of OA pathology and symptomology but plays a significant role in the pathogenesis (70) with evidence of a relationship between synovitis and the initiation (71) and progression of cartilage erosion (72). Both imaging and histological techniques have been used to characterise synovitis, and a number of studies have now identified a correlation between joint inflammation and disease symptoms such as pain (73, 74), and joint function measures such as walking and stair climbing (75). However, the exact pathogenic mechanisms involved in the development of synovitis and the relationship with other joint tissue changes is still under investigation (76).

A recent review has highlighted the prevalence of increased inflammatory cells in OA synovial tissues, including macrophages, T-cells and mast cells (77). Current evidence suggests that activation of the innate immune system is an essential driver of joint inflammation (especially synovitis) and a central feature of OA. A number of molecules released into the damaged joint can act as damage associated molecular patterns (DAMPs), activating the innate immune response via pattern-recognition receptors such as the toll-like receptors (TLRs) (78). These include ECM breakdown products, for example, hyaluronan (79) and fibronectin (80); as well as plasma DAMPs, for example, α1 microglobulin and α2 macroglobulin (81), that enter the joint subsequent to vascular leakage and exudation. These DAMPs have been shown to induce macrophage production of inflammatory cytokines and growth factors, implicated in both the inflammatory response and cartilage breakdown (81). Although a number of cell types within the joint are capable of responding to DAMPs (including chondrocytes), activation of synovial macrophages and the complement cascade (82), are thought to be the two main drivers for cytokine production, the development of synovitis and propagation of further cartilage damage (83).

Cytokines (such as tumour necrosis factor (TNF)-α, interleukin (IL)-1, and IL-6), and chemokines, such as chemokine ligand (CCL)3 (84), CCL18 (85), CCL19 (86), CCL20 (87), have all been implicated in the pathogenesis of OA (88). Interestingly, these cytokines also have demonstrated pro-algesic effects that could contribute to joint pain. The role of inflammatory cytokines and activation of the innate immune response in OA joint pain pathogenesis is currently under investigation (89).

1.1.6 OA phenotypes

It is clear from the above summary that OA is a disease of the whole joint, and the degree of different tissue involvement and the predominant pathophysiological mechanisms that are active in any individual joint and/or patient may vary. The OARSI FDA OA Initiative defined OA as "a progressive disease of synovial joints that represents failed repair of joint damage that results from stresses that may be initiated by an abnormality in any of the synovial joint tissues, including articular cartilage, subchondral bone, ligaments, menisci, peri-articular muscles, peripheral nerves or synovium", ultimately resulting in "the breakdown of cartilage and bone, leading to symptoms of pain, stiffness and functional disability" (90). This definition articulates the common end point of OA and our current understanding of the disease, but it does not reflect its complexity and the different forms that it can take. Both genetic (91, 92) and environmental factors such as age, gender, obesity, abnormal biomechanical loading (93) and joint injury can contribute to the development of OA (94-97). Each factor contributes differently to the pathobiological profile of the disease (98). OA can be localized to a single joint or generalized, and can be categorized on the basis of numerous disease characteristics including; etiology, pathophysiology, joint/s affected, stage of joint disease, presence of specific symptoms, and rate of progression.

This concept of different subtypes or 'OA phenotypes' has been explored clinically (99) and epidemiologically (100), with a number of phenotype classifications proposed. For example, radiographic imaging can be used to identify clinically relevant OA phenotypes that may represent relevant subgroups for clinical trial selection (101), and distinct phenotypes of multi-joint and knee OA have been identified in population subgroups based on race and gender, which may influence

response to therapy (102-104). There is a move towards stratifying OA patients into sub-types based on different OA phenotypes, to improve clinical trial outcomes and develop a more mechanism based approach to treating OA (105, 106). However, clinicians and researchers are yet to reach consensus on which phenotype classifications are relevant for promoting the translation of preclinical research into effective therapeutics.

1.1.7 OA therapeutic targets

Synovial joints are organs, and therefore OA involves pathology in multiple tissues. Joint pathology changes include articular cartilage damage, subchondral bone sclerosis, joint hypervascularisation, synovial inflammation and fibrosis, osteophyte formation, meniscal and ligament degeneration and injury (70). However, articular cartilage degradation (including proteoglycan loss) remains a key feature of the structural changes that take place in the OA joint. For this reason much research has focused on articular cartilage and the role of chondrocytes in OA (41, 107-114).

Significant progress has been made in our understanding of the pathogenesis of OA (115-121). Researchers believe this knowledge will enable the development of effective disease modifying compounds for the treatment of OA (122-127). This strategy for developing DMOADs is based on the theory that reducing structural joint damage (in particular, reversing articular cartilage degradation) will improve joint mobility and relieve the clinical symptom of pain. Consequently, many compounds that target specific components of OA pathology (SCB, AC, inflammation) have been developed and validated in pre-clinical OA models, and some have progressed to clinical trials (128). However, outcomes from the 13 published clinical trials conducted between 1999 and 2014 have been poor, and there are still no FDA

approved DMOADs (Table 1.1). Interestingly, the pre-clinical studies that informed these clinical trials all demonstrated some improvement in structural damage, but only one study reported on symptomatic outcomes (pain and weight bearing).

This puts into questions the current approach for developing OA therapies. The paradigm shift of thinking about OA as a failure of the joint organ that can manifest as multiple disease phenotypes has not been adopted into the way we use preclinical studies to inform selection of potential future therapeutics. For this to occur, consideration needs to be given to – (a) selecting animal models that replicate a human phenotype of the disease and allow longitudinal evaluation of disease initiation and progression; (b) identifying the tissues that play a role in disease symptomatology (pain and reduced mobility); and (c) mapping structural changes to clinical markers of the disease (pain, gait, weight bearing, mobility). This means that if our aim is to develop DMOADs that treat the disease, not just the pathology that develops in a particular joint tissue, joint structural changes can't be studied in isolation of pain.

The greatest obstacle to this approach is the complex relationship between joint structural pathology and pain, and the huge gaps in our current understanding of the pathophysiology of OA pain.

Table 1.1. Clinical DMOAD trials in knee osteoarthritis*

TRIAL	TARGET	DISEASE MODIFICATION	SYMPTOMATIC OUTCOME (secondary endpoint)	PRECLINICAL VALIDATION IN OA MODEL	STRUCTURAL OUTCOME	SYMPTOMATIC OUTCOME
Oral salmon calcitonin (129)	SCB	JSW: No effect: biochemical markers (CTX-I & CTX-II) effect not significant	WOMAC: no significant effect	Rat MNX and MNX/OVX (130) Dog ACLT (nasal delivery) (131) DMM in mice overexpressing salmon calcitonin (132)	Joint protection, ↓serum CTX-II Joint protection (no effect on osteophytes) OARSI score ↓7 weeks after DMM	N/A N/A N/A
Intra-articular rFGF18 (133)	Cartilage (anabolic)	Primary endpoint not met (↓ cartilage loss in central medial femorotibial compartment MRI)	WOMAC: improved	Rat MMT (134)	Increased thickness of the articular surface (medial tibial plateau). Degeneration scores ↓	N/A
Strontium Ranelate (135)	SCB	JSW: fewer radiographic progressors	Beneficial effects on symptoms at high dose only	Dog ACLT (136) Rat MMT (137)	Cartilage lesions, SCB thickening and Serum CTXII ↓ Cartilage degeneration ↓ SCB remodelling ↓	N/A N/A
SD6010, Oral selective iNOS inhibitor (138)	Cartilage	JSW: no effect	No effect on pain or function	Dog ACLT (139, 140) Collagenase induced arthritis (*Nos2* null mice) (141) Rat MMT model (142)	Cartilage lesions ↓ Osteophytes ↓ Synovitis ↓ Cartilage PG loss ↓ Cartilage lesions ↓ Osteophytes ↓ N/A	N/A N/A Reversal of WBD & allodynia after 3 hours
Zoledronic acid(143)	SCB	Reduction in total BML area on MRI	VAS pain scores ↓ But not KOOS	Rat MIA (144) Rat MMT (145) a) prophylactic b) therapeutic (early or late intervention)	Joint preservation Partial preservation, diminishes with late intervention	Reversal of WBD Partial effect-diminishing with late intervention
Vitamin D3(146)	SCB Cartilage	MRI cartilage volume: no effect	WOMAC: no effect	Rat pMNX (147) Osteochondrosis/OA in pigs (148)	Inconclusive No effect: OA lesion incidence or severity	N/A N/A
Licofelone (5-LOX and COX inh) (149)	Inflammation	JSW: no effect	WOMAC: pain improved	Dog ACLT (150)	MRI cartilage volume ↑ Cartilage damage and osteophytes ↓	N/A
Risedronate(151) Risedronate (152) Risedronate(153)	SCB	JSW: cartilage degradation and bone resorption markers ↓ JSW: no effect uCTXII ↓ Preserved integrity	WOMAC ↓ WOMAC: no effect N/A	DH guinea pig (154) – up to 24 wks NZW rabbits ACLT (155)	OARSI score: no effect, serum CTXII ↓ Loss of cartilage ↓ SCB damage ↓ serum CTXII ↓	N/A
Broad-spectrum MMP inhibitor (156)	Cartilage	JSW: no effect	No effect on pain	Rat MIA (157) STR/Ort mice (158)	Cartilage damage ↓ Cartilage & bone damage ↓	N/A N/A
Doxycycline (159)	Cartilage	JSN: slowed in ipsilateral knee	No effect on pain	Dog ACLT (160) DH guinea pig (161) DMM (mouse) (162)	Femoral condyle damage ↓ Tibial plateau or osteophytes no effect Cartilage volume (MRI) loss ↓ Cartilage loss ↓	N/A N/A N/A

Includes only placebo-controlled, peer-reviewed and published studies since 1999

* Adapted from Malfait, A. M., & Little, C. B. (2015). On the predictive utility of animal models of osteoarthritis. *Arthritis Res Ther*, *17*, 225. doi:10.1186/s13075-015-0747-6

Clinically, a direct relationship between global joint pathology severity and pain intensity has not been demonstrated, and there is no established threshold of joint pathology at which pain starts to develop. There are however, specific joint tissue changes that occur with OA that are associated with pain. These include synovitis and bone marrow lesions (57, 74). But there is no established cause-effect relationship to assist investigations into how different tissues and processes lead to pain.

This lack of association can in part be explained by the multitude of intrinsic patient factors, which determine an individual's pain response. These include genetic (163, 164), psychosocial (165), biomechanical (166) and comorbidity factors (97, 167). The other important consideration is that the relationship between joint pathology and pain is likely to be different for different OA phenotypes, and over the course of the disease. For example, following joint injury, inflammation may be the key driver of pain. As the inflammation resolves and joint disease progresses, other structural changes may take over and alter the characteristics of the pain response. In other words, early phase hypersensitisation may look very different to late phase hypersensitisation at a biomolecular level, but the measured pain outcome (eg allodynia) may look the same. A better understanding of pain mechanisms and the pathophysiological pathways involved in OA pain will bring clarity to the relationship between joint pathology and pain.

In the next section I will review what is known about joint innervation and OA pain, focussing on the knee joint as a dynamic load-bearing joint, which is commonly affected by OA.

1.2 Sensory innervation of the knee joint

1.2.1 Knee joint afferents

Innervation of the rodent knee is derived from the femoral nerve, the sciatic nerve and the obturator nerve. The knee joint is innervated predominately by the medial articular nerve (MAN) and the posterior articular nerve (PAN). The PAN is the larger of the two nerves and originates from the tibial nerve branch of the sciatic (168).

The cell bodies of the afferent neurons innervating the knee joint reside in the lumbar (L1-L5) dorsal root ganglia (DRG), with the majority in L3. In the rat 88% of knee joint afferents are located in L3 and L4 (169). However, knee afferents make up a very small percentage of the total DRG neuron cell bodies.

Researchers have used different methods to identify and characterise the afferent innervation of the mouse knee joint. Ebinger (170) identified the number and distribution of nerve fibre size in the medial and posterior articular nerves of the mouse knee using electron light microscopy. However this histological study did not differentiate between sensory (nociceptor and mechanoreceptor fibres) and sympathetic neurons.

Although the sub population of sensory neurons that innervate the knee joint and transmit nociceptive input to the spinal cord have been mapped and characterised (171-178), including the proteins and neuropeptides that are altered in animals with diseased joints, there is still no clear understanding of the disease mechanisms that drive and modulate these pain signals in the OA joint.

Histological studies demonstrate that articular cartilage is avascular and aneural, so it is assumed that this tissue cannot be directly involved in the generation of pain. However, subchondral bone, periosteum, synovium, ligaments, and the joint capsule

are richly innervated with sensory neurons that have the capacity to transmit nociceptive stimuli.

Sensory stimulation of normal joint tissues does not generate pain, as demonstrated by the ability to move a normal joint through a range of motions without any pain sensation. This suggests that, at least for movement-evoked knee pain, local and central mechanisms alter sensory signals in such a way that a previously benign stimulus (either sub-threshold or non-nociceptive) becomes painful.

1.2.2 Nociceptors

Nociceptors are specialised nerve endings that conduct noxious signals to the dorsal horn of the spinal cord. There are two main types of nociceptors, differentiated by the diameter of their afferent fibres and, the type and magnitude of stimulus required to activate them. High-threshold mechanoreceptors (HTM) are innervated by thinly myelinated, fast conducting (5-30m/s) Aδ fibres that respond to intense mechanical stimulation. Polymodal nociceptors (PMN) are innervated by unmyelinated, slow conducting (0.5-2 m/s) C fibres that respond to intense mechanical stimulation, temperatures exceeding $42^{O}C$ and irritant chemicals. It is thought that Aδ fibres conduct sharp localised pain while C fibres conduct poorly localised, diffuse pain (179). A number of ion channels located in primary afferent nociceptors act as sensory transducers, and are responsible for the detection of physical stimuli. The most important of these are the poly-modal Transient Receptor Potential (TRP) channels (180). These channels are permeable to cations and structurally similar to the superfamily of voltage-gated channels, although not strictly voltage dependent.

1.2.3 Vanilloid 1 receptor

Vanilloid 1 receptor (TRPV1) is a member of the TRP subfamily of cation channels. It is a polymodal receptor activated by three pain-producing stimuli, vanilloid compounds (eg capsaicin), moderate heat (temperatures > 42^{O}C) and low pH (< 5.9). Its highest expression is in sensory neurons where it acts as a polymodal detector of noxious stimuli (181). Sensory neurons from TRPV1 KO mice do not respond to capsaicin and temperatures < 50^{O}C *in vitro*. Mice lacking functional TRPV1 show normal physiological and behavioural responses to noxious mechanical stimuli, however they display an absence of thermal hypersensitivity in the setting of inflammatory pain models such as carrageenan (182). TRPV1 plays an important role in both chemical and thermal hyperalgesia, in models of acute inflammatory pain and neuropathic pain (183). A role in neuropathic pain is further supported by studies reporting increased levels of TRPV1 expression in uninjured DRG following peripheral nerve injury (184, 185). These studies suggest TRPV1 may play a role in the development and maintenance of chronic pain, beyond its thermoreceptor function and contribution to mechanical hyperalgesia. Interestingly, stimulation of the TRPV1 receptor causes an acute neurogenic response that is characterised by vasodilation, plasma extravasation and hypersensitivity; however, there is significantly reduced blood flow in wild type mice compared to TRPV1 KO mice when capsaicin is injected directly into the knee joint (186).

TRPV1 is implicated in arthritis pain but the exact mechanism/s by which it contributes to the pain of OA is not understood. TRPV1 participates in the development of chemical and thermal hyperalgesia in the acute phase, and mechanical hyperalgesia in the chronic phase, of adjuvant induced arthritis; via sensitisation of receptors by inflammatory mediators released in arthritic joints (187). Conversely, an

attenuation of inflammatory arthritis (both inflammation and pain) has been demonstrated in TRPV1 KO mice (188). TRPV1 receptors identified in human synovium provide a target for developing anti-TRPV1 therapeutics, and the efficacy of some of these has been demonstrated in MIA models of OA (189, 190).

Intra articular injection of the axonal tracer Fast Blue and immunohistochemistry techniques have been used to identify the sub population of afferents from mice knee and ankle joints that express TRPV1, with 40% of these afferents expressing the receptor (191). Other investigators have also used Fast Blue to identify the cell bodies of sensory afferents from the rat knee joint, and investigated the expression of calcitonin gene-related peptide (CGRP) and TRPV1 receptors in this sub-population of DRG neurons (192). Using the antigen-induced arthritis (AIA) model in the rat to study the expression of TRPV1 in the lumbar DRG, investigators were unable to demonstrate any up regulation of TRPV1 expression (193), and the proportion of TRPV1 protein-positive lumbar DRG neurons did not increase in the course of acute and chronic AIA in the rat. However, it has been reported that TRPV1 receptor expression in small and medium-sized neurons in DRG is up-regulated during inflammation (194). Other studies have demonstrated an increase in TRPV1 protein-positive neurons with acute inflammation, but not an increase in TRPV1 mRNA levels in DRG neurons (195, 196). In combination these findings support the suggestion that TRPV1 is one mechanism by which peripheral sensitisation develops following inflammation.

A murine adjuvant induced arthritis model was used to investigate the role of extracellular-regulated kinase (ERK) and TRPV1 in primary afferent neurons (197). Preferential activation of ERK in TRPV1-positive neurons innervating the joint was demonstrated and TRPV1 KO mice showed reduced activation of ERK in the sensory

neurons. Changes in p-ERK expression in the sensory neurons correlated with changes in thermal and mechanical hyperalgesia. This study provides evidence that TRPV1 may contribute to the pain of inflammatory arthritis via an ERK-mediated pathway.

The relationship between fibroblast-like synovial (FLS) cells and sensory neurons that innervate the knee joint has been investigated, using a co-culture system of FLS cells from AIA knee joints and DRG neurons (198). The proportion of DRG neurons expressing neurokinin-1 (NK1) receptor-like immunoreactivity was upregulated in the co-culture. Furthermore, the expression of TRPV1 was up regulated when DRG neurons were co-cultured with FLS cells from chronically inflamed joints.

Changes in TRPV1 expression in DRG and the role of this receptor in sensitisation and OA pain have not been studied using a post-traumatic model of OA.

1.2.4 Transient Receptor Potential Ankyrin-1 (TRPA1)

TRPA1, the wasabi receptor, is another member of the transient receptor potential family of ion channels, and a sensor of pungent chemicals and environmental irritants such as mustard oil, garlic, cinnamon oil, clove oil and ginger (199, 200), and also plays a role in acute noxious mechanosensation and cold thermosensation (201, 202). It is specifically expressed in the inner ear (203), and trigeminal and DRG neurons, and is highly co-expressed with TRPV1 in small diameter peptidergic nociceptors. Its role in mechanical nociception remains controversial. TRPA1 has been shown to play a role in nociceptor excitability modulation and neurogenic inflammation at the site of tissue injury, and it may play a role in the transduction of high-threshold mechanical stimuli. TRPA1 KO mice demonstrate a higher mechanical threshold than wild type (WT) mice, and a deficiency in response to acute punctate cutaneous stimuli (202). A

small molecule TRPA1 inhibitor (AP18) has been used to investigate the role of TRPA1 in pain sensitisation. AP18 reverses Complete Freund's Adjuvant (CFA)-induced mechanical hyperalgesia in mice (204). In this same study TRPA1 KO mice did not show significantly increased acute mechanical thresholds, however they did develop CFA-induced hyperalgesia that did not respond to AP18. These findings suggest TRPA1 plays a role in sensitisation, but that a compensatory mechanism may exist in TRPA1 KO mice. It is unclear what molecular or cellular compensation mechanisms may account for these observations. The findings also suggest that TRPA1 may be involved in the maintenance and not the induction of mechanical hyperalgesia. Although TRPA1 and TRPV1 are co-localised and appear to interact functionally, an up regulation of TRPV1 has not been demonstrated in TRPA1 KO mice.

These studies all implicate TRPA1 in mechanical hyperalgesia, despite other investigators failing to demonstrate a difference in mechanical thresholds between TRPA1 KO and WT mice (200). Overall, there is strong evidence that TRPA1 contributes to inflammatory pain, and can be activated by inflammatory mediators such as bradykinin (205). TRPA1 KO mice have an impaired response to bradykinin injection and reduced bradykinin-induced mechanical hyperalgesia (200, 202). However, further investigation is needed into any role it may play in chronic pain states such as OA.

1.2.5 Transient Receptor Potential Vanilloid-2 (TRPV2)

TRPV2 is a structural homologue of TRPV1 that is insensitive to capsaicin but is activated by high temperatures, > 52^{O}C. (206). Interestingly, nociceptors lacking both TRPV1 and TRPV2 have normal heat responses (207). TRPV2 is widely expressed in

neuronal cells, with strong immunolabelling detected in medium-diameter DRG neurons associated with Aδ-fibers (208). The broader distribution of TRPV2 compared to TRPV1, in a diverse range of neurons and non-neuronal tissue, suggests that it may contribute to more than just nociceptive processing (209). TRPV2 KO mice are susceptible to perinatal death but mice that survive do not demonstrate abnormal thermal or mechanical nociception (210). However, there is evidence that TRPV2 does play a role in peripheral sensitisation in inflammatory models (211), and in the development of mechanical hyperalgesia (212). More recent studies have suggested a role for TRPV2 in maintaining cardiac function (213, 214) and controlling cell tumour proliferation (215).

1.2.6 Transient Receptor Potential Vanilloid-4 (TRPV4)

TRPV4 is a polymodal receptor activated by hypotonicity, shear stress, innocuous heat (threshold temperatures >27deg), low pH and arachidonic acid metabolites (216-218). Although widely expressed, its distribution in cochlear hair cells, vibrissal Merkel cells, sensory ganglia, free nerve endings & cutaneous A & C fibre terminals, suggests a primary role as a mechanoreceptor (219).

TRPV4 KO mice show impaired osmotic sensation and sensitivity to acid (220), an increase in mechanical nociceptive threshold and altered thermal selection behaviour, but normal response to low threshold mechanical stimuli (221). TRPV4 agonists promote release of substance P and CGRP from central projections in primary afferents in the spinal cord (222), providing evidence for a role in nociception. TRPV4 mediates mechanical hyperalgesia following exposure to inflammatory mediators (223, 224) suggesting a more specific role for TRPV4 in acute inflammatory pain. The role of TRPV4 in chronic pain has also been investigated

using a neuropathic pain model (225), where it was shown that reduced expression of TRPV4 abolished Taxol-induced mechanical hyperalgesia and attenuated hypotonic hyperalgesia.

1.2.7 The dorsal root ganglia

Joint afferents cannot be differentiated histologically or immunochemically from other afferent populations. In order to study cell bodies in the DRG that innervate the knee joint retrograde labeling techniques have been used to differentiate this sub-group of neurons. Retrograde axonal tracing techniques, where by a dye is injected directly into the stifle joint, can identify the sub population of sensory afferents within the somata of DRG neurons which innervate the structures of the knee joint.

Salo & Tatton (226) identified cells in the DRG which innervate the mouse knee joint using *in vivo* retrograde tracing with Fluoro-Gold. They determined the size, number and distribution of the neurons that innervate the knee joint structures, but did not characterise the cells using immunohistochemical techniques. Salo & Theriault (169) later used retrograde tracing with Fluoro-Gold in combination with immunohistochemistry to characterise the number, distribution and neuropeptide content of cell body neurons in the DRG that innervate the knee joint of the rat. Following from this, retrograde tracing with Fluoro-Gold in combination with immunohistochemistry (labeling for the neuropeptides CGRP and substance P) was used to demonstrate an age-related loss of mechanoreceptors in the mouse knee joint (227).

1.3 Chronic Pain

Although OA is described in terms of structural and biological joint pathology, the magnitude of the disease burden is not linked to these joint changes, but rather to the clinical symptoms (228). The most significant of these is pain, and yet pain is the least well-understood manifestation of this disease (229).

1.3.1 Sensitisation

Pain starts with stimulation of specialised nerve endings (nociceptors) and the subsequent transmission of signals along afferent peripheral sensory nerves to the spinal cord. From the spinal cord this signal is then transmitted via a number of pathways to the higher brain centres for processing into what is perceived as pain (Figure 1.2). But pain is not simply the passive transport of sensory signalling via encoded action potentials from one neuroanatomical location to the next with the eventual processing of such signals in the thalamas and cortex. All along this pathway are opportunities for intrinsic and extrinsic factors to influence the nature, amplitude and perceived location and duration of the original 'pain' signal. This discovery of nervous system plasticity has changed our understanding of pain (230).

The spinal gate theory proposed by Melzack and Wall in 1965 (231) and the subsequent discovery of inhibitory control systems such as endorphins, enkephalins, and transcutaneous nerve stimulation, were early demonstrations of pain signal modulation at the level of the spinal cord and brain (232-242). In addition, others observed the enhanced signalling of peripheral nociceptors following injury, leading to a localised zone of 'primary hyperalgesia' (243-247). At the same time, Mendell and Wall introduced the concept of 'wind-up' in the dorsal horn neurons, by demonstrating that an increase in nociceptor signal frequency resulted in increased

action potential amplitude (248). These phenomena have all contributed to our understanding of pain modulation and hypersensitivity, however they do not fully account for the tactile allodynia (249), secondary hyperalgesia or temporal summation of pain that is observed with chronic pain (250).

The idea of 'central sensitisation' came into play as researchers discovered that the majority of synaptic input to sensory neurons is sub-threshold, and that increasing the strength of this input or reducing inhibition, can result in profound changes to the functional properties of neurons (251-253). But, central sensitisation goes beyond a phenomenon based on activity dependent signal plasticity. Central sensitisation occurs after the period of initial nociceptive transmission, remains autonomous, is sustained beyond the initiating signal, and amplifies the response to non-nociceptor signals as well as nociceptor signals that originate from distant sights. We now know that changes to microglia, astrocytes, gap junctions, membrane excitability and gene transcription at the level of the DRG and spinal cord all contribute to central sensitisation development and the chronic pain state (254-258).

Recent evidence supports the theory that both peripheral and central sensitisation, as well as endogenous inhibitory mechanisms, contributes to the chronic pain of OA. Peripheral sensitisation is thought to be mediated by nerve growth factor **(**NGF) (259) and pro inflammatory cytokines released after cell injury, such as prostaglandins, bradykinin, and TNFα (260). Central sensitisation may be mediated by other inflammatory neuropeptides such as CGRP, Substance P, glutamate and vasoactive intestinal peptide (VIP) (261-264). The endogenous opioid and cannabinoid systems are the main inhibitory mechanisms that play a role in dampening the pain signal in OA (265-267).

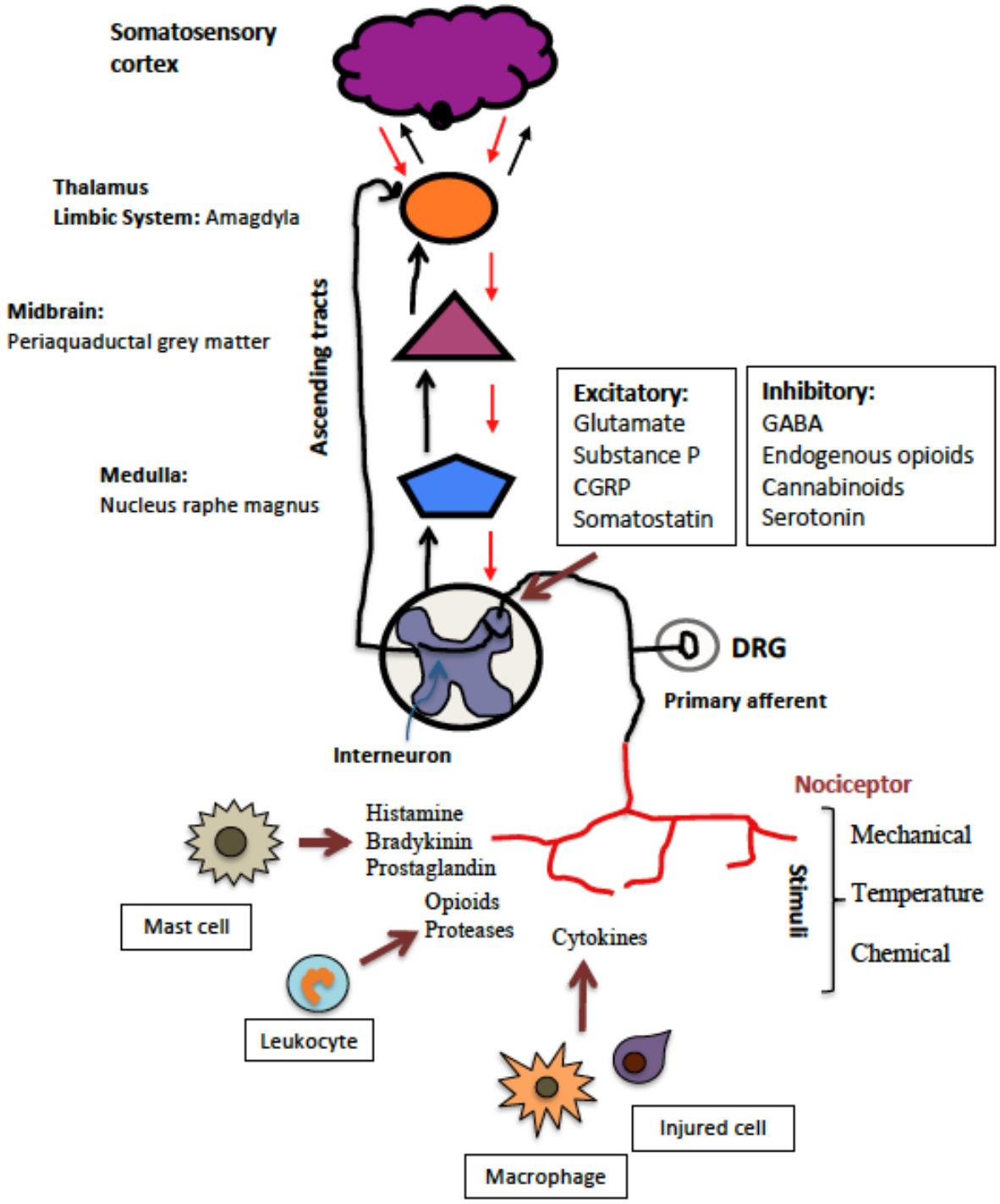

Figure 1.2. Schematic diagram of the Pain Pathway

The Pain Pathway describes the neuronal network that links the sensory inflow generated in peripheral nociceptor terminals with the conscious awareness of a painful stimulus. Tissue injury and inflammation alters the chemical environment of both peripheral and central nociceptor terminals, and heightens the activation threshold of these specialised neurons. In addition, a number of endogenous inhibitory controls exist that act as inhibitory modulators.

1.3.2 OA pain in humans

A number of pain assessment tools have been used to assess pain in OA patients (268), including mechanical and thermal thresholds, range of motion, weight bearing and gait analysis (269). Patient self-reporting questionnaires, such as the Visual Analogue Scale (VAS), the McGill Pain Questionnaire (MPQ), and the Western Ontario and McMaster Universities Index of OA (WOMAC) are also important clinical assessment tools (270).

The development of chronic OA pain is considered a maladaptive process that is both initiated and driven by a number of pathological processes involved in OA (271, 272). For the majority of OA patients, peripheral mechanisms (including inflammation) are thought to play a major role in pain development. In a subgroup of these patients the pain mechanisms are more complex, resulting in a pain syndrome that does not directly correlate with the severity of joint pathology, and that is driven by central processing and neuropathic mechanisms (273-275). These patients respond poorly to conventional therapies such as potent analgesics and joint arthroplasty.

Researchers have yet to unravel these complex molecular pathways and better define the intricate relationship that exists between OA joint pathology and pain. In a multi-center study that looked at the relationship between knee OA and sensitisation, evidence of sensitisation, as measured by mechanical temporal summation (MS) and pressure pain threshold (PPT), was associated with OA related pain severity but not with radiographic OA (276). This finding suggests that intrinsic patient factors, not just joint pathology, determine an individual's OA pain phenotype. The idea that patients with knee OA exhibit increased sensitivity to painful stimuli at distant body sights has been demonstrated in a number of clinical studies. When OA patients were stratified into high versus low symptom severity based on the WOMAC, individuals

in the high group were more sensitive to heat, cold and mechanical (both blunt pressure and punctuate) stimuli, compared to the low symptom group and controls (277). OA patients also demonstrate somatosensory abnormalities that manifest as tactile hypoaesthesia and pressure hyperalgesia (278, 279). The growing evidence for a 'neuropathic' OA phenotype (280-284) has encouraged the development of assessment tools aimed at identifying patients with signs of central sensitisation (285), with the aim of developing a more targeted pain management approach for these patients (286-288).

1.3.3 Mechanisms of OA pain

We know that OA involves global joint pathology that leads to chronic pain and immobility. Historically, it has been assumed that joint pathology drives the pain of OA so the focus has been on understanding the pathobiology of OA and identifying disease-modifying therapeutics that will re-establish a normal joint environment, and thus remove the trigger for development of chronic pain. However, the mechanisms that drive and modulate the pain of OA are poorly understood and the exact biomolecular links between different aspects of joint pathology and pain, and how this may change over the course of the disease are still not known.

Evidence of a co-dependent relationship between joint pathology and OA pain has only really been investigated in the context of inflammatory arthritis models (56, 289-291). Despite the associations that have now been identified using advanced imaging (292-294), there still remains discordance between structural joint pathology and pain severity in people with OA (295). This can in part be explained by the psychosocial, genetic and biomechanical factors, which are also important determinants of the pain phenotype, and ultimately make the identification of any causal effects between

specific joint pathologies and pain, a significant challenge. Further validation of this clinical observation can be found in a naturally occurring model of OA. The relationship between OA pain and joint pathology has been investigated in the Dunkin Hartley guinea pig, which develops spontaneous OA. In this model, both histopathological and micro-CT determinants of joint degeneration correlated well with aging but did not correlate with nociception as measured by electrophysiological recordings (296).

In human OA, strong associations have now been identified between pain and bone marrow lesions (57, 297, 298), synovitis (74, 299), and joint effusion (300, 301); and weaker associations between cartilage damage and pain (75, 302, 303). But, we are yet to identify which processes and joint tissues drive the development of chronic pain, and therefore should be targeted when developing therapeutics. More recently, gene array studies using different animal models have identified thousands of differentially expressed genes (304), suggesting a number of biomolecular mechanisms are working in concert to produce OA pain. It is likely that local, inflammatory and neurogenic mechanisms, as well as psychosocial factors all contribute to the pain of OA (271, 305, 306).

Identifying local (joint specific) and peripheral mechanisms that mediate OA pain will allow for a more targeted approach to developing future therapeutics that are less likely to result in unwanted side effects (307). This strategy has identified a number of TRP channels, including TRPV1, TRPV4 and TRPA1; and the proteinase activated receptors PAR-1, PAR-2 and PAR-4, as potential intra-articular targets.

The endocannabinoid and endogenous opioid systems both play a significant role in immune modulation (308) via a number of mechanisms including T cell signalling (309); and pain modulation (including OA pain) (310), and are emerging as novel,

joint specific therapeutic targets for OA . The antinociceptive activity of cannabinoids has been demonstrated in a number of animal models of arthritis (311-313). Systemic use of opioids is an important part of managing OA pain, however these potent analgesics have significant side effects. Emerging evidence about the complex role that the endogenous opioid system plays in pain (314), at the organ level (266, 315), the DRG (316) and spinal cord (317), suggests a more targeted approach is required (318, 319).

1.3.3.1 Inflammation

It is well established in both human and animal model studies that inflammation, and in particular synovitis, contributes to joint pathology and pain (320). Early electrophysiological studies investigating the effects of intra articular kaolin were able to demonstrate that acute synovitis reduced the activation threshold of Aδ and C fibre sensory afferent neurons (321). A number of joint cells, including chondrocytes and synovial cells, express and respond to cytokines and chemokines that can mediate and amplify nociceptive signally (322). Pro-inflammatory cytokines, including TNFα, IL-1β, and IL-6, are released by joint cells as well as sensory neurons and glial cells in the DRG and microglial cells in the dorsal horn, and have been shown to play an important role in joint pain.

TNFα is a pro-inflammatory cytokine involved in the generation of hyperalgesia associated with both neuropathy and inflammatory processes. TNFα can rapidly alter neuronal excitability, and it can also mediate long-term changes in sensory neuron excitability via transcriptional and protein expression effects. For example, chronic exposure to TNFα significantly increases the proportion of DRG neurons expressing TRPV1 (323). TNFα can act directly on sensory neurons or indirectly via downstream targets such as the chemokine, monocyte chemoattractant protein-1 (MCP-1/CCL2), which is up regulated in sensory neurons following neuronal injury (324).

Interleukins are an important family of cytokines that are reported to produce both rapid and delayed neuronal effects. Interleukin-1β is not only pro-nociceptive, mediating hypersensitivity in inflammatory (260) and arthritis pain models (325), but has also been shown to play a role in articular cartilage degradation, proteoglycan loss

and synovitis, in inflammatory arthritis and mechanical instability models of OA (83, 326-328). *In vitro* studies have demonstrated that interleukin-17 (IL-17) increases DRG expression of TRPV4, and an antibody against IL-17 reduces secondary mechanical hyperalgesia in AIA mice (329). The anti-inflammatory cytokine, interleukin-10 (IL-10) also plays an important role in inflammatory pain, Recently it has been demonstrated that IL-10 producing macrophages mediate resolution of inflammatory hyperalgesia (330).

DRG neurons express a number of chemokine receptors (331) suggesting that chemotactic cytokines also play a role in pain. In particular MCP-1 and its receptor (CCR2) have been implicated in a number of pain models (332-338), including OA where increased MCP-1/CCR2 expression correlated with movement-evoked pain in a post-traumatic model of OA (339). MCP-1 has also been implicated in up-regulating the expression and function of TRPV1 and the voltage-gated sodium channels, Nav1.8 *in vitro* (340). The peripheral voltage gated sodium channels Nav1.7, Nav1.8 and Nav1.9 are all expressed in sensory neurons, with Nav1.8 preferentially expressed in DRG and trigeminal ganglia (341). Maladaptive changes in these channels are pivotal in mediating a number of chronic pain states. Recently, Nav1.7 and Nav1.8 have both been shown to play a role in OA pain pathways in the rat MIA model (342). Angiogenesis has also been investigated as a mediator of OA pain (343). Inflammation is a key driver of angiogenesis, and this has been demonstrated in the synovia (344) and at the osteochondral junction (345) in OA joints.

1.3.3.2 Neuropathic mechanisms

Theories of the neurogenic origins of joint pain are summarized in a review by McDougall (346). Nociceptors respond to algesic chemical substances such as bradykinin, prostaglandins, leukotrienes, IL-1 and serotonin; and chronic excitation of nociceptors is dependent in part on this response, termed neurogenic inflammation. The role of activation of ‘silent nociceptors’ has been demonstrated in the context of joint injury and inflammation, whereby afferent fibers which are quiescent in normal joints are activated (347) and begin transmission of nociceptive signals to the central nervous system. In addition, early studies demonstrated a reduction in the activation

threshold of both C and Aδ afferents in inflamed joints, mediated via inflammatory neuropeptides such as CGRP (348).

Substances released as a consequence of articular cartilage degradation may themselves play an indirect algesic role by influencing the release of neuropeptides from sensory neurons at the level of the dorsal root ganglia, and subsequently enhancing the release of algesic substances in the periphery. Conversely, sensitisation, and the associated release of inflammatory mediators such as substance P and cytokines, may also further contribute to the degenerative processes occurring in OA joints.

Proteinase activated receptors (PARs) are a recently identified group of G-protein-coupled receptors that offer a potential mechanism for linking attenuation of joint disease with alleviation of pain (349, 350). PARs are activated by proteinases released into tissues during inflammation, and demonstrate both pro-inflammatory and anti-inflammatory properties. Currently four members of this family of receptors have been identified, and three of them are implicated in peripheral nociception (PAR-1, PAR-2, PAR-4). PAR-1 is expressed in mouse DRG, and its anti-nociceptive effect has only been observed in association with inflammatory pain (351). PAR-2 has been localized to sensory neurons, and is considered to have a pro-nociceptive effect that is mediated via TRPV1 (352, 353) and TRPV4 (222). PAR-4 expression has been demonstrated in rat DRG (354). PAR-4 is also expressed in rat (355) and mouse knee joints, where a pro-inflammatory and pro-nociceptive role was observed in following intra-articular injection of a PAR-4 agonist (349, 356). This is in contrast to a previous study that showed co-localisation of PAR-4 with the inflammatory neuropeptides substance P and CGRP in the rat DRG, and demonstrated an anti-nociceptive effect for PAR4 in response to thermal and mechanical stimulation (357).

VIP is another inflammatory mediator that may play a role in the link between joint degeneration and pain in OA. Injection of VIP into the knee joints of rats results in synovial hyperaemia and pain (358). Unilateral injection of VIP into normal rat knee joints was demonstrated to cause a shift in weight bearing away from the injected joint as determined by force plate capacitance testing, and a reduction in paw withdrawal threshold of the ipsilateral hindlimb (263). In the MIA model, injection into the affected knee joint of the antagonist VIP6-28, diminished hind limb changes in weight bearing and increased paw withdrawal threshold.

Electrophysiological studies have demonstrated enhanced afferent firing from normal rat knee joints after injection of VIP during normal and hyper-rotation of the joint (359). This VIP mediated sensitization was effectively blocked by pre-administration of VIP6-28. Using the MIA arthritis model the role of VIP and its antagonist VIP6-28 was further investigated. Rats with MIA induced arthritis had significantly reduced afferent firing during normal joint rotation and during hyper-rotation of the affected knee when treated with VIP6-28, suggesting that VIP is released into OA knee joints and may contribute to joint pain. However, the role of VIP in OA pain has not been investigated using a post-traumatic OA model.

Researchers have also attempted to define the relationship between pathology and pain using nerve injury models. These studies may provide some direction for further investigation into the relationship between OA pain mechanisms and OA joint pathology. Neuropathic pain is thought to involve nerve injury-induced specific changes to the DRG and spinal cord, but there is now evidence that neuropathic pain and neuroinflammation share similar mechanisms. The role of MMP-2 and MMP-9 in the pathophysiology of neuropathic pain has been studied using a well-characterised nerve injury model, L5 spinal nerve ligation (SNL) (360). MMP-9 demonstrated a

rapid and transient up-regulation in injured DRG primary sensory neurons with concomitant activation of microglial and pain behaviour, consistent with an early phase of neuropathic pain. In contrast, MMP-2 demonstrated a delayed response to SNL in DRG satellite cells and spinal astrocytes, consistent with a late phase of neuropathic pain. The pro-inflammatory cytokines, TNF-α and IL-1β are rapidly produced after tissue injury, and may play a role in the MMP-9 mediated initiation phase of neuropathic pain. Since both MMP-2 and MMP-9 are up regulated in human OA, the findings of this study highlight the importance of investigating the role of these metalloproteases in the pain of OA.

Neuropathic pain mechanisms in OA have only been investigated in the MIA model. An increase in expression of activating transcription factor 3 (ATF-3) immunoreactivity in L5 DRG associated with early stage disease (day 8 and 14) and no change in L4 DRG was demonstrated in rats with MIA knee arthritis compared to controls (361). At day 8 this corresponded to reduced ipsilateral hind limb weight-bearing and knee joint changes characterised by loss of proteoglycan, ghosting of chondrocytes, degeneration of subchondral bone plates with areas of bone loss and associated activation of osteoclasts and chondroclasts, and hyperplasia of synovial membranes associated with mononuclear inflammatory cell infiltrates. At day 14, increased ATF-3 in DRG also corresponded with reduced ipsilateral hind limb weight-bearing and, focal areas of pronounced ulceration of articular cartilage and superficial subchondral bone development within the affected joints. Since ATF-3 is described as a selective neuronal marker, specifically induced in sensory and motor neurons following nerve injury (362), these findings suggest an early phase neuropathy in the DRG innervating the affected MIA knee joints. However, the results of this study are difficult to interpret since retrograde axonal tracing studies

using fluoro-gold in the adult wistar rat have shown that 88% of knee joint afferents are in fact located in L3 and L4 DRG, with less than 10% residing in L5 (169).

Pain related behaviours have been investigated and described in a number of OA models (363), however little attempt has been made to directly map these behaviours to specific joint histopathology changes or the mechanisms driving these changes.

Fernihough *et al* investigated pain related behaviours in two OA models in the rat; partial medial meniscectomy and MIA injection (364). Histological evaluation of the knee joints in both models demonstrated progressive OA joint pathology development over a 28-day period. No comparison was made between the two models with respect to histological differences at time points before 28 days although the study did report on the initial period of acute inflammation and joint swelling seen with the MIA model up to day 7 post-injection. The study concluded that both OA models induced histological changes and pain related behaviours, (hyperalgesia, allodynia and reduced hind limb weight bearing) characteristic of human OA. However, response to pharmacological interventions (morphine, diclofenac, gabapentin and paracetamol) was only tested in the MIA treated animals because this model induced more robust and reproducible pain related behaviours. The investigators did not consider what impact the initial acute inflammatory response associated with the MIA model might have on later development of pain behaviour such as hyperalgesia and allodynia.

Fast Blue Retrograde labelling was then used to identify cell bodies of primary sensory afferents from the knee joint of rats with MIA induced arthritis, and expression of CGRP and TRPV1 quantified in these labelled neurons (192). The majority of knee joint afferents were found to reside in the L4 DRG. Expression of CGRP and TRPV1 was greater in neurons innervating the knee joint than the general population of neurons across the whole DRG. L4 DRG of MIA mice showed an

increase in expression of both CGRP and TRPV1 compared to control mice, suggesting a potential role for CGRP and TRPV1 in the development of the pain behaviour associated with OA in the knee joint.

The endogenous agonist for TRPA1, 4-hydroxy-2-nonenal (HNE), provides another example of how OA pathogenesis and OA pain mechanisms might share common pathways. HNE is a lipid peroxidation end product that is produced abundantly in OA articular tissue. HNE activates TRPA1, promoting acute pain, neuropeptide release and neurogenic inflammation (365). The formation of HNE is enhanced in synoviocytes from patients with OA (366-369). In addition, HNE induces transcriptional and post translational modifications of type II collagen and MMP-13 in human OA chondrocytes, contributing to cartilage ECM degradation (367). There is also evidence that HNE exerts a number of effects on human OA osteoblasts which alter their metabolic activity (366).

1.3.4 Future therapies for OA pain

Symptomatic OA therapies aimed at managing pain and improving mobility, are inadequate and not without side effects (370). The options for OA sufferers are currently limited to non-steroidal anti-inflammatory drugs (NSAIDs), opioids, corticosteroids, visco-supplements (11), and a suite of nutriceuticals that have largely not been tested for efficacy or safety (371, 372). A number of new compounds that have demonstrated efficacy in animal models have failed to translate into safe and effective OA pain therapies for humans.

NGF is one of the few novel therapeutic targets to emerge from pre-clinical research, which has lead to the development of an effective treatment for chronic OA pain that has entered Phase 3 trials. NGF was first identified as a trophic factor in sensory and

sympathetic neurons of the DRG (373). It is required in early embryonic development for sensory neuron maturation and survival, and plays a major role in the pathophysiology of inflammatory pain (374), including OA pain (375). NGF acts through two distinct types of cell-surface receptors, tropomyosin-related kinase A (TrkA) and p75. Peripheral sensory neurons, central nervous system neurons, as well as non-neuronal cells, such as macrophages and monocytes, all express TrkA. A number of mechanisms of action have been described for NGF. Following tissue injury and inflammation, pro-inflammatory cytokines are released by the damaged tissue and by activated immune cells. These cytokines stimulate the release of NGF from a range of cell types, which acts directly on peripheral sensory neurons via TrkA, to increase the excitability of these cells. In addition, activation of TrkA on non-neuronal cells results in the release of mediators that sensitise sensory neurons and alter the pain threshold (376). Up regulation of NGF in the knee joints of mice with surgically induced OA has previously been demonstrated immediately following surgery and in the chronic phase of disease development (264). More recently regulation of NGF by OA chondrocytes has been demonstrated in mice at the same time that OA-related pain develops (377).

Despite the demonstrated efficacy of anti-NGF therapy in clinical trials, its contribution to OA pain, and the neurophysiological mechanisms involved, is still under investigation. Increased levels of NGF in synovial fluid (378), at the osteochondral junction (345) and in the synovium (379) of OA sufferers, suggests multiple mechanisms are involved, and this is supported by animal model studies that have investigated the role of NGF in knee OA pain. For example, it has been demonstrated that a greater proportion of DRG sensory neurons innervating the subchondral bone of the distal femur express TrkA compared to DRG that house

sensory afferents from the knee joint (380). More recently, the effect of increased knee joint NGF on local as well as remote evoked responses of spinal neurons has been studied to better understand the contribution of knee joint NGF to central (spinal) sensitisation (381).

The complex nature of NGF's role in mediating both inflammatory and neuropathic pain, has given rise to a number of potential applications for anti-NGF therapy (382). Targeting NGF has proven to be an effective strategy for tackling OA pain in pre-clinical animal model studies (264) and in clinical trials (383-385). Phase 3 trials of a humanised anti-NGF antibody have show great promise in alleviating pain and improving mobility in OA sufferers (386-388), however, trials were temporarily suspended by the FDA from 2010 to 2012 due to an increased incidence of joint failure in trial participants. This was initially attributed to increased physical activity in the absence of joint pain leading to accelerated joint damage. Further investigation into possible mechanisms for this hypoalgesic effect, as well as the peripheral nerve safety of anti-NGF therapy, has been undertaken (389, 390).

The story of NGF and its progression through the drug discovery cycle highlights the challenges of progressing pre-clinical research breakthroughs into effective clinical therapies. Many potential therapeutics fail the translation phase due to lack of efficacy or unforeseen side effects in the target species. The reasons for this are complex and reflect the gaps in our current understanding of OA pain (291). A major contributing factor has to be the poorly defined relationship between joint pathology and pain pathophysiology (272). A better understanding of this relationship would allow the classification of OA into phenotypes that reflect differences in clinical presentation as well as disease aetiology, and lead to the development of pain therapies that are

phenotype specific, and that can be trialled in a specific population of OA sufferers and at a specific stage of the disease (391).

This targeted approach to developing and trialling OA pain therapies requires careful selection of pre-clinical animal models that best reflect the pathophysiology of a specific sub-class (phenotype) of the clinical disease. Yet, currently there is a mismatch between the animal models used to study OA joint disease and those used to investigate the mechanisms of OA pain. A review of animal models used to investigate OA joint structural damage as well as OA pain follows.

1.4 Animal models of OA

The use of animal models is a powerful pre-clinical tool that allows more detailed investigation of the observations and associations identified in clinical studies. Information learned from pre-clinical models can then be used to inform better design and conduct of clinical trials. Animal models have advanced our understanding of OA pathobiology and symptomatology (pain), and have led to the development of novel disease modifying OA drugs (DMOAD's). However, despite their efficacy *in vitro* and in pre-clinical models, most DMOAD's have failed to translate into effective and safe treatments for human OA (128). The reasons for this lack of translatability are complex and highlight the need for better animal model selection criteria that are based on more than our current understanding of pathophysiological mechanisms (392, 393).

In the case of preclinical research into OA pain, the animal models used differ with respect to joint pathology, disease progression, pain behaviour and response to therapy; and often do not reflect the human disease. In addition, there is a lack of consistency in two important areas; (1) the pain assays used to investigate pain mechanisms and evaluate potential therapeutics, and (2) the scientific reporting standards. This is despite the availability of numerous guidelines and recommendations (394-396).

Many animal models have been developed to study the pathophysiology of the different arthritic diseases, in particular OA. With over 20 induction methods and at least 10 different species represented in the literature (397), there is no shortage of options for investigating the phenotype and molecular pathways of OA pain. However, there is still no consensus on what constitutes an ideal animal model for OA research (398), in particular the study of OA pain (399).

An ideal animal model is one that induces a consistent and reproducible disease phenotype, which reflects the human disease with respect to etiology and pathology; and is progressive over a suitable time frame to allow the study of different stages of the disease pathophysiology while still allowing a reasonably high throughput. The ideal animal is inexpensive, easy to house, manage and handle; is not dissimilar physiologically from humans (ie a mammal); and is large enough to allow multiple outcome measures to be performed, including those that mimic observed clinical symptoms such as pain (400). Rodents fit these criteria and with the added advantage of enabling the investigation of specific biomolecular pathways through the development of genetically modified strains; the mouse, is an ideal experimental animal (401, 402).

The knee joint is the most commonly utilized joint in animal models of OA. It is readily accessible for both intra-articular injection and surgical intervention. It is also a clinically relevant joint to study, since OA most commonly affects the large weight bearing joints such as the knees and hips (3) as well as the joints of the hand (305).

Animal models used to study OA pain can be broadly categorized into four main types: 1) Spontaneous, 2) Intra-articular injection, 3) Joint Injury (surgical instability, enzymatic instability, non-surgical instability, excessive/abnormal loading), and 4) Genetic modification (399). Spontaneous models mimic both age (296) and obesity (403) associated OA. Intra-articular models utilize irritant substances such as carrageenan and MIA that when injected into the joint elicit a severe inflammatory reaction and/or cellular (chondrocyte) injury or death, and direct tissue damage. Surgical instability models rely on partial or complete transection of one or more ligament of the knee joint, with resultant joint instability, altered biomechanics/loading, tissue degeneration and pain (404-406). These models attempt

to mimic post-traumatic OA, the sub class of human OA patients that acquire the disease following injury to joint structures such as the menisci, the anterior cruciate and collateral ligaments (407). The Collagenase model is a unique instability model that relies on the enzymatic breakdown of ligamentous tissue rather than surgery (408, 409). Joint-injury also includes models where excessive or abnormal loading leads to joint injury over time, such as treadmill running and sub-failure joint loading (410). Examples of genetic modification models that as a result of a specific molecular derangement spontaneously develop OA include IL1-β over-expressing rats (411), and Collagen IXa-1 deficient mice (412).

All of these models differ greatly with respect to disease etiology and time course, joint pathology and pain outcomes, which impacts on their response to therapeutic intervention including genetic modification (as a proof of concept "specific molecular therapy") (399, 413). These differences highlight the need for researchers to report on model specific outcomes and mechanisms, because effects may not be applicable to all OA, rather they may inform specifically on different sub-types of human OA (391).

The investigation of OA pathophysiology has been conducted using a range of these animal models, but more recently there has been a shift towards surgical models that mimic post-traumatic OA and better reflect the human disease with respect to etiology and joint pathology changes (407, 413). In contrast, OA pain mechanisms have largely been studied using intra-articular injection models (291, 414). In addition, findings from inflammatory arthritis models have also been used to better understand the role that inflammation may play in the initiation and modulation of pain signaling in OA (415, 416). This diverse use of animal models highlights the complexities that arise when attempting to extrapolate key findings from pre-clinical studies. As it is

still unclear whether the differences in disease etiology, disease progression and joint pathology, between the models we use to study OA, are relevant to our understanding of OA pain and whether this is contributing to the failure to translate.

Three pre-clinical arthritis models that have been widely used to investigate structural and symptomatic pathophysiology and therapeutic interventions are discussed in greater detail below. Not all of these have typically been considered physiologically relevant models of OA, but in the context of the preceding discussion on disease definition and phenotypes all three models provide some insight into understanding OA pain. Importantly, the different findings from these models highlights the significant gaps in our current understanding of the relationship between joint pathology and pain, and how it changes with initiating cause and disease progression.

1.4.1 Mono-iodoacetate (MIA) induced arthritis

The MIA model (417) is perhaps the most widely used, particularly by pharmaceutical companies, to investigate joint structural damage (histopathology) (418), pain and potential therapeutic targets (419, 420). MIA is an inhibitor of glyceraldehyde-3-phosphate dehydrogenase activity. Following intra-articular injection it induces widespread (depending on dose) chondrocyte degeneration and necrosis as early as day 1, osteoclast and osteoblast proliferation in subchondral bone by day 7, fragmentation and collapse of bony trabeculae by day 28, and large areas of bony remodeling by day 56 (418). Histological changes at day 14 include extensive focal areas of full thickness cartilage damage with complete loss of cellular detail and some loss of proteoglycan matrix, as well as visible marginal changes related to the growth of osteophytes (421).

The pain phenotype of this model is well described (291). Movement provoked pain behaviours have been demonstrated using the knee-bend test and CatWalk™ device (422), as well as mechanical allodynia (364), thermal hyperalgesia (423), reduced hindlimb grip strength (290), and reduced weight bearing (424). This model has also been used to characterize site-specific and time-dependent changes in articular cartilage and synovial tissue gene expression that underlie cartilage injury (425). More recently, investigators have attempted to identify links between joint tissue pathology and the development of chronic pain using this model in the rat (426). However, in this study a systematic evaluation of joint histopathogy using an established scoring system such as the one developed by the OARSI Histology Initiative (427), was not performed. This prevents direct mapping of the reported pain behaviours to joint disease progression in specific tissues. This study also reported on altered gene expression of pro-inflammatory cytokines (IL-1, TNFα) and the neuropeptides CGRP and substance P, in the DRG neurons of L5. The findings are difficult to interpret, as the authors do not include gene expression data for L3 lumbar DRG, where a significant proportion of the sensory neurons that innervate the knee joint reside (169).

MIA-induced arthritis is usually described as a model of OA, largely because of the pathological features particularly in the later stages. However, it is clear that the initiating event with rapid widespread chondrocyte necrosis is not typically seen in any OA phenotype in patients. Some features of the disease pathophysiology, such as the role of ADAMTS and MMPs in aggrecanolysis and collagenolysis respectively, do mimic events in human OA (428). Nevertheless, Barve *et al* (429) demonstrated that there is little transcriptional similarity between rat MIA and human OA cartilage, by characterizing the gene expression profile of diseased cartilage. They identified

less than 4% overlap between rat and human genes that were modulated in the same direction. Similarly, despite the prolific use of this model in pre-clinical OA pain studies, there is growing evidence that the disease mechanisms in MIA induced arthritis are different from those of human OA (128). The MIA model has been shown, depending on dose, to have a substantial component of neuropathic pain (361), that is likely to only be relevant in a subset of human OA patients (430-432). Fundamental differences in the underlying molecular pathophysiology of MIA and human OA, may in part explain the lack of translational progress with novel DMOAD's that demonstrate efficacy when tested in this animal model.

1.4.2 Surgical destabilisation of the medial meniscus (DMM)

Models that surgically induce instability and/or altered joint biomechanics/loading have been widely used to investigate OA (407, 413, 433). These models mimic injuries to key intra-articular structures that are observed in patients and significantly increase the risk of later OA development (434). The knee joint is unique in that fibrocartilagenous menisci within the joint provide stability, proprioception and act as shock absorbers, dissipating the weight bearing load on the underlying cartilage. Loss of meniscal function (tears, maceration, excision) leads to accelerated OA in both humans and animals (435, 436).

While different meniscal injury models have been used in a variety of species to induce OA, showing the universal importance of these structures to knee function, recent years have seen an explosion in use of the surgical destabilization of the medial meniscus (DMM) in mice (407). The DMM model involves transection of the medial menisco-tibial ligament, which acts as the anterior attachment of the medial meniscus to the tibial plateau (437). Loss of this ligament allows the meniscus to be displaced

laterally during ambulation, placing supra-physiological loading on the medial femoro-tibial cartilage and increased joint mobility. DMM produces a reliable and consistent, progressive disease state with all the structural features of OA that is amenable to evaluation of both the acute and chronic phases of OA, compared to more rapidly progressive models that rely on the injection of pro-inflammatory substances into the knee joint. The DMM model has been used to study the structural and biochemical changes associated with loss of articular cartilage and other joint pathology in mice (47, 407, 438, 439). In particular, this model has been used to show pathophysiological mechanisms linking changes in the expression of genes for matrix proteins, MMPs and aggrecanases (ADAMTS-4 and -5) in the meniscus and cartilage (25, 26) to the progression of the OA phenotype in mice. This model has also been used to study sex differences in OA, demonstrating that OA severity is greater in male mice than female mice following DMM surgery (440).

More recently this model has been used to investigate pain mechanisms of OA (264, 316, 363, 441). Although this model does not produce the same robust pain outcomes as the MIA model, it is viewed as perhaps a more clinically relevant model to study pain mechanisms since it represents a common biological trigger of human OA. A recently proposed scoring tool that assesses the translatability of early drug development projects, highlights the importance of this (442). Reliable biomarkers that transfer across from animals to humans, and preclinical studies that use animal models that reflect the disease in humans, have been identified as important translatability factors (443). Nevertheless, the surgery required for OA induction by DMM may introduce non-physiologic inflammation not seen with non-invasive joint injuries (444). As with all instability models, DMM is considered to particularly mimic the post-traumatic OA phenotype (407). However, unlike cruciate and other

ligament failures, meniscal tears and degeneration have been associated with non-traumatic spontaneous age-associated OA in patients (298, 445, 446), suggesting findings from DMM may have wider implications.

1.4.3 Antigen-induced Arthritis (AIA) Model

The AIA model was originally developed as an animal model of rheumatoid arthritis in rabbits (447) and later modified and characterized in mice (448). The model involves immunization with methylated bovine serum albumin (mBSA) in complete Freund's adjuvant, followed by intra articular injection of mBSA. There are strain differences in susceptibility with robust histological knee joint changes demonstrated in C57BL mice. This is a chronic arthritis model persisting for up to 24 weeks in both mice and rabbits (448). It is one of the most widely used models of inflammatory arthritis, exemplifying an exogenously triggered joint immune response that is both T-cell and immune-complex driven (449). At the time points most commonly evaluated in AIA studies (usually up to 3-4 weeks), pathology is typified by profound synovitis with panus formation by 1 week that slowly resolved, progressive cartilage degradation and bone erosion (439, 450, 451).

Although not defined as a model of OA, it is frequently used to study the pain mechanisms of arthritis and has shed some light on the role of inflammation and the immune system that may be relevant in OA pain. Researchers have used this model to demonstrate that inflammatory processes in peripheral tissues such as the knee joint drive macrophage infiltration into the DRG, which in turn correlates with pain related behaviour (452). This model has also been used to characterize the role of pro-nociceptive cytokines such as IL-1β, in the development of thermal hyperalgesia (453), and IL-17 in the development of inflammation evoked mechanical hyperalgesia (329), both features of chronic arthritic knee pain. The role of cytokines in OA pathogenesis (322) and OA pain mechanisms (320) are currently important areas of investigation.

1.5 Literature review summary and research aims

OA is a disease of the entire joint that results in chronic pain and reduced mobility. There are currently no effective therapies for treating or preventing OA. Long-term management of symptoms relies primarily on analgesics that are at best moderately effective, and that have significant side effects when used chronically.

OA is characterised by a pain state that is both initiated and driven by a number of joint specific and systemic pathological processes, with resultant peripheral and central sensitisation of the sensory nervous system. There is growing evidence of a co-dependent relationship between joint pathology and OA pain; and that local, inflammatory and neuropathic mechanisms all contribute to the OA pain phenotype.

Using pre-clinical animal models, researchers have attempted to unravel the molecular pathways involved in OA pain, and better define the complex relationship that exists between joint pathology and pain. Although this has advanced our understanding of the pathophysiology of OA and chronic pain, it has not translated into effective therapeutics. A number of factors have been proposed that may be hindering the translatability of preclinical research in OA pain.

- We are yet to identify which processes and joint tissues drive the development of chronic OA pain, and therefore should be targeted when developing therapeutics.
- There are significant differences between animal model phenotypes with respect to joint pathology and disease progression, pain behaviour and response to therapy.
- Human OA is not all the same, differing between individuals and over time; with genetic and environmental factors contributing to the pathobiological profile of disease that an individual may experience. This suggests that a more

phenotype-based approach to investigating and identifying future therapeutics needs to be adopted. Researchers need to report on model specific outcomes and mechanisms, and relate them back to a specific subtype of human OA.

- The majority of OA pain studies, including those that are testing response to therapeutics, use animal models that don't reflect the human disease with respect to aetiology, disease progression and joint histopathology.
- There is a lack of standardisation of pain assays within the OA pain literature, making it difficult to collectively compare and interpret findings, and producing a plethora of conflicting pain study outcomes that bring us no closer to understanding pain mechanisms and identifying suitable therapeutic targets.

To optimize the use of animal models and inform our understanding of OA pain, we need to know how different pain behaviours correlate with structural changes in different joint tissues. We also need to know if pain and its mechanistic pathways change over time as the disease progresses, and if disease mechanism matters when it comes to understanding OA pain.

Which model we use to study OA is important to our understanding of the disease and its symptoms, and may determine our ability to translate this understanding into effective therapeutics that modify the disease and treat its primary symptom – pain. However, there is currently no consensus on the ideal animal model for OA research, but if OA pain and OA joint pathology do share common pathways, then the study of joint disease and joint pain should be carried out in animal models that are phenotypically similar.

In this thesis I hypothesise that the mechanisms that drive osteoarthritis pain are specific to the pathophysiology of the disease, and differ between different OA phenotypes.

To date, no study has directly compared pain and joint structural change in parallel, longitudinally using two distinct animal models. Therefore, the aim of this research is to map the relationship between joint pathology, pain behaviour and peripheral sensory innervation, over time, comparing a post-traumatic model of OA and an antigen-induced inflammatory model of arthritis.

CHAPTER 2: Methods

The methods described in this chapter were used throughout this thesis. Any exceptions or variations have been noted in the relevant chapter/s. The reagents and equipment used (and the respective suppliers) are listed in Appendix A. Reagent preparation protocols are described in Appendix B. Scoring protocols are outlined in Appendix C.

2.1 Murine models of arthritis: Destabilisation of the medial meniscus (DMM) and Antigen-induced arthritis (AIA)

The C57BL/6 strain of mice is the most common strain used in arthritis research, and is also the background strain from which several knockout strains have been derived to study the role of specific genes identified to be involved in joint disease development and pain transmission.

Male mice develop more severe OA following surgery than female mice (440), and young mice (8 weeks and younger) develop less severe disease than older mice (Little CB unpublished observation). Skeletal maturity in male C57BL/6 mice, defined as cessation of active endochondral ossification and plateauing of long bone growth (although the growth plates do not close), occurs at ~3 months of age (454). For these reasons 10-12 week old male C57BL/6 mice were used to induce arthritis using the DMM model. Since the AIA model requires an initial 3-week period for immunization before arthritis can be induced, 8-10 week old mice were used in this model. This ensured that both models could be studied in parallel using similar aged mice at the actual time of induction of joint disease.

Mice were obtained from a C57BL/6 breeding colony maintained at the Kearns Facility in the Kolling Institute. This colony was established with animals sourced

from Animal Resources Centre (Canning Vale, Perth WA), which maintains a C57BL/6Jax colony (designated C57BL/6JArc). The Kearns Facility colony is refreshed with C57BL/6JArc breeding mice at least every second year to avoid genetic drift from the parent strain. Male littermates are housed in groups (up to 5 per 30x20x18cm cage) to enable timely surgical and subsequent analytical processes to be undertaken, and to avoid the stress associated with solitary caging. Cages are individually ventilated with filter lids, sterilized bedding, environmental enrichment, and maintained at 19-22°C, with a 12-hour light/dark cycle. Animals receive acidified water and complete pelleted food ad libitum. Animal housing, all procedures, and behaviour testing were conducted with the approval of the Royal North Shore Animal Care and Ethics Committee (Protocol numbers 0807-019A, 0911-014A & 1202-003). All animals were housed in the Kearns Facility at the Kolling Institute of Medical Research, St Leonard's, NSW.

2.1.1 Randomisation and blinding

Disease induction (detailed in the following sections) was done such that in any given cage there was a mixture of sham, DMM and control (naïve) mice; or saline injected, mBSA injected and immunized control mice housed together. All animal cages were housed in the same room in the Kearns Facility. Animals within a given cage were allocated to treatment groups in one of two ways. In the case of sham/DMM, animals were randomly selected by one operator (Sanaa Zaki: SZ) who anaesthetized, ear notched and shaved the leg before passing the animal to a second person (Christopher Little: CL) that randomly assigned and performed the sham or DMM surgery keeping SZ blinded. For the saline/AIA model all mice were immunized by a single operator (SZ). Individual syringes containing identical appearing solutions of saline or mBSA

were prepared and then coded and randomly assigned (drawn from a hat) a specific mouse number. These coded/assigned syringes were then intra-articularly injected by a second (SZ). In this way behaviour testing (performed by a single operator SZ) was done blinded to treatment group within the sham/DMM and saline/AIA cohorts, although the skin ulceration and later scar-formation at immunization sites meant it was not possible to blind between the two arthritis models. After sacrifice, samples from individual mice were randomly assigned a code before processing to enable histology scoring (done independently by 2 operators SZ and CL) to also be conducted blinded to arthritis model and time post-induction.

The mixed housing described above was also done to address two additional potential sources of bias in pain behaviour outcomes. The first arises from operator bias if the operator knows that all cage mates have undergone the same intervention. The second arises from the complex effect that conspecifics can have on modulating pain behaviour. It has been demonstrated that mice recognize and respond to overt pain behaviours displayed by conspecifics (455). In both male and female mice these social cues may either enhance or decrease the pain response. For example, exposure to cage mates displaying acute pain behaviour results in an increased sensitivity to noxious stimuli in the observing mouse, and pain behaviour is enhanced after one week of housing with a cage mate exposed to a noxious stimulus (456). These findings suggest the existence of pain 'empathy' amongst cage mates that modulates the pain response. In addition, male mice display reduced pain behaviour in the presence of unaffected stranger male mice, but not familiar male cage mates (457), and this response is testosterone dependent (458). It may represent a form of stress-induced analgesia, since the opposite occurs when male mice are not completely

separated and allowed partial physical contact. The affected mice display hyperalgesia rather than analgesia (458).

The use of mixed housing aimed to reduce any bias towards an enhanced or a reduced pain response resulting from social modulation of pain across different experimental cohorts.

2.1.2 Anaesthesia

All surgeries, sham surgeries, intradermal injections and intra articular injections were performed under general anaesthesia as described here.

Food and water were not withheld prior to anaesthesia. Each mouse was weighed, anaesthetised, and ear notched for identification prior to surgery or injection. Anaesthesia was induced in a Perspex induction chamber containing Isoflurane (2.5%) in a gas mixture of oxygen and nitrous oxide delivered in a 1:2 ratio with flow rates set at 1 and 2 L/min respectively. Gases were delivered via an anaesthetic machine with an out of circuit vaporiser and a Bain breathing system. Anaesthesia was maintained using a nose cone connected to the Bain breathing system and the same gas/anaesthetic mixture. The depth of anaesthesia was monitored and the level of isoflurane (1.5-2%) adjusted to achieve a surgical plane of anaesthesia, as indicated by regular breathing, muscle relaxation and absence of reflexes. No procedure was commenced until the pedal withdrawal reflex was abolished. Body temperature was maintained by ensuring that surgical site preparation and surgery were performed on a towel over a heating pad rather than a cold surface. At the end of the procedure, the animals were disconnected from the anaesthetic machine and allowed to recover in cages on a heating pad to minimize the risk of hypothermia developing. Recovery cages were kept in the operating theatre so that the animals could be visually

inspected every 5 minutes. Animals became conscious and ambulatory within 2-5 minutes from when anaesthetic delivery was stopped. They were visually monitored to ensure they were eating and fully ambulant and weight bearing on the operated leg as they moved about the cage, prior to returning them to their original groups and housing rooms. Animals did not receive any post-operative analgesia. Provisions were included in the ethics protocol for the humane euthanasia of any animal that displayed signs of significant pain or distress. However, this was not deemed necessary for any animal throughout the study.

2.1.3 The DMM model

Surgical instability models are designed to mimic post-traumatic OA in humans, and are the most common laboratory animal models used to study OA (122, 407). However, it is still unclear whether such models also mimic the more common idiopathic form of OA that is seen in humans (399).

The DMM model was chosen because it is a well-established post-traumatic OA model (437) that has been used extensively to study the pathophysiology of OA. It mimics the disease in humans histologically and clinically, since meniscal damage secondary to trauma has been shown to be a high risk factor for development of OA in humans (436, 459, 460). This model reproduces a more slowly progressive disease than other surgical models in mice (437) with a time course suitable for evaluation of both the acute and chronic phases of OA disease.

Following induction of anaesthesia, the right hind limb was prepared for surgery by shaving the skin with a double-sided flexible blade and applying 80% ethanol. Surgery was performed under a surgical microscope. The animal was placed on a sterile, heated towel and the leg draped with sterile paper drape to isolate the surgical

site and minimise contamination. Using micro-surgical scissors, a 3-6 mm lateral para-patella skin incision was made commencing at the level of the distal patella and extending down to the proximal tibial plateau. The femoro-tibial joint capsule was incised just medial to the patella ligament, using a #15 blade (Figure 2.1a). The incision was extended proximally into the vastus medialis muscle using micro iris scissors to enable lateral luxation of the patella. Visualisation of the menisco-tibial ligament of the medial meniscus was facilitated by joint flexion and blunt dissection and proximal elevation of the infra-patella fat pad (without removal of any tissue) (Figure 2.1b). Any subsequent bleeding from the fat pad was controlled by applying pressure over the site with surgical gauze swabs. Articular cartilage surfaces were maintained moist by applying sterile saline. The medial menisco-tibial ligament (MMTL) was identified traversing laterally from the cranial horn of the medial meniscus to the anterior tibial plateau. The MMTL was isolated by passing one arm of curved Dumont #7 tweezers (superfine point dumostar steel) under the ligament at its junction with the anterior pole of the meniscus (Figure 2.1c). The MMTL was then severed using the tweezers, by rotating the tip of the tweezers axial and anterior, which results in tearing of the osseous insertion site. Complete DMM was confirmed by ensuring the meniscus could be manually displaced/luxated medially and the articular surface of the medial tibial plateau visualised (Figure 2.1d).

The joint was flushed with sterile saline, the meniscus and patella manually replaced in their normal anatomical locations, and the incision was then closed in three layers – joint capsule, subcutaneous tissue and skin. Sterile ophthalmic grade 8/0 absorbable suture material (Vicryl) was used to anatomically reconstruct the joint capsule using a continuous suturing pattern, followed by a single subcutaneous mattress suture

(Figure 2.1e). To achieve optimal apposition surgical tissue glue (VetBond, cyanoacrylate) was used to close the skin layer (Figure 2.1f).

Figure 2.1. Destabilisation of the medial meniscus

Surgical transection of the medial tibio-mensical ligament (MMTL): (a) The femoro-tibial joint capsule is incised just medial to the patella ligament; (b) Visualisation of the MMTL is facilitated by joint flexion, blunt dissection and proximal elevation of the infra-patella fat pad; (c) The MMTL is isolated by passing one arm of curved Dumont #7 tweezers under the ligament at its junction with the anterior pole of the meniscus; (d) Complete DMM is confirmed by ensuring the meniscus can be manually displaced/luxated medially and the articular surface of the medial tibial plateau visualised; (e) Anatomical reconstruction of the joint capsule using a continuous suturing pattern, followed by a single subcutaneous mattress suture; (f) Surgical tissue glue is used to close the skin layer and achieve optimal apposition.

2.1.3.1 Sham operated mice

Sham mice were anaesthetised as described for ear notching and surgery. The joint capsule was opened and the MMTL visualised and isolated exactly as for DMM however the ligament was not transected. The joint was lavaged and closed as for DMM.

2.1.3.2 Control mice

Control mice were anaesthetised as described for ear notching but had no surgery.

2.1.4 Antigen induced arthritis model

The AIA model was chosen because it is an established chronic inflammatory arthritis model that induces a cell mediated immune response resulting in a localised single joint inflammatory arthritis. Established as an experimental model for studying human rheumatoid arthritis (448), AIA produces joint changes that are characterised by acute joint inflammation and progressive cartilage damage, fibrosis and bone erosion.

In this model, mice previously immunised with an emulsion of methylated bovine serum albumin (mBSA) in Freund's Complete Adjuvant received an intra articular injection of mBSA in the right knee joint (450).

2.1.4.1 Immunisation:

Antigen preparation

Refer to Appendix B

Antigen loading

Using an 18-gauge needle, emulsion was drawn into a 1ml tuberculin glass syringe and the barrel 'coated' by sliding the plunger up and down, before squirting back the emulsion into the main stock. Approximately 600 μl of emulsion was then loaded

into the syringe. The needle was removed and replaced with a 30-gauge needle and all air expelled from the syringe prior to injection.

Intradermal injection

Mice were anaesthetised as described above and positioned in sternal recumbency with legs splayed. The skin at the base of the tail and dorsum was shaved using a double-sided flexible razor blade and cleaned with 80% ethanol (Figure 2.2a). The skin at the base of the tail was held taught with forceps and the needle was introduced subcutaneously about 5mm at the site where the skin was most taught. The needle was then redirected more superficially into the dermis, so that the tip could be seen through but did not penetrate the skin, and 50 µl of emulsion was slowly injected intradermally resulting in a tight white disc of adjuvant approximately 1cm anterior and 5-10mm medial or lateral to the tail base. A 2nd 50 µl intradermal injection was done adjacent the 1st injection on the opposite side of the midline. (Figure 2.2b)

After 14 days the intradermal injections were repeated as described above approximately 1 cm cranial to the 1st injection sites.

Following immunisation animals were checked daily and handled with care so as not to traumatise the injection sites. Any ulceration that developed at the injection site was treated with topical povidone iodine.

2.1.4.2 Intra articular injection:

7 days after the 2nd intradermal injection, each mouse received an intra articular injection of 10µl mBSA (20mg/ml in sterile 0.15M NaCl) into the right knee joint. This was performed under a dissection microscope.

Mice were anaesthetised as described and positioned in dorsal recumbancy. The right hind limb was prepared by shaving the skin with a flexible razor blade and applying 80% ethanol. A lateral parapatellar skin incision approximately 5mm in length,

extending to the level of the patella tendon, was made by tenting the skin with forceps. By ensuring that the incision did not lie directly over the front of the knee excessive stretching of the wound was minimised when the animal was mobile, and this reduced any interference with wound healing. The leg was held between two fingers and fully extended. The incision was then manipulated to expose the patella tendon. A 31-gauge needle (0.3ml insulin syringe) was inserted with the bevel up just below and lateral to the patella in the patella ligament. The tip of the needle was then manipulated until it rested under the patella along the trochlear groove before injecting 10µl mBSA (20mg/ml). The skin incision was closed with tissue glue.

2.1.4.3 Control mice:

Two sets of control mice were used for the AIA model. Saline injected control mice were immunised as described above and received an intra articular injection of 10µl saline into the right knee joint. Immunised control mice were immunised as described above but did not receive an intra articular injection.

Figure 2.2. Antigen induced arthritis:

(a) skin preparation - the skin at the base of the tail and dorsum is shaved using a double-sided flexible razor blade and cleaned with 80% ethanol; (b) intradermal injections – two 50 µl aliquots of emulsion are slowly injected intradermally resulting in a tight white disc of adjuvant approximately 1cm anterior and 5-10mm medial or lateral to the tail base.

2.1.5 Euthanasia

Euthanasia was performed using three techniques. For harvesting of dorsal root ganglia (DRG) for gene expression, mice were euthanised by CO_2 exposure (animals become unconscious within seconds) followed by decapitation. For harvesting of DRG for immunohistochemistry mice were deeply anaesthetised with 50mg/kg pentobarbitone IP, followed by perfusion (see section 2.5.1) resulting in immediate death. In mice where only knee joints were harvested, euthanasia was performed by anaesthetic overdose with 4% isoflurane (animals become unconscious within seconds) followed by cervical dislocation.

2.2 Histology

In order to better understand the relationship between joint disease and pain, the progressive changes that occurred in different joint tissue structures following induction of OA, were mapped to specific pain related behaviours. Since histology is the gold standard by which to evaluate murine models of knee arthritis, a robust histological scoring system that evaluated both joint structural damage and joint inflammation was utilised for comparing the two animal models in this thesis.

2.2.1 Knee joint processing

Right and left knee joints were harvested following euthanasia (as described in section 2.1.5). The skin and the majority of the muscle were dissected away leaving the joint capsule intact, before the knees (mid tibia to mid femur) were fixed in 10% (v/v) neutral buffered formalin (NBF) for 24 hours. The knee joints were then transferred to 70% v/v ethanol for storage prior to further processing.

The knee joints were decalcified by placing in 10% (v/v) formic acid, in 5% (v/v) formalin for 24 hours at room temperature with gentle agitation. The tissue was then washed for 15 minutes in distilled water to remove the formic acid before been stored in 70% (v/v) ethanol for at least 24 hours prior to processing to paraffin.

The knee joint specimens were dehydrated for one hour each in graded solutions of 70%, 75%, 85% and 95% (v/v) ethanol, and three washes of 1-hour duration in 100% (v/v) ethanol. This was followed by three washes of 2 hours duration in chloroform. Paraffin infiltration of mouse knee joints in cassettes in Paraplast (plain) involved the following: first wax (Paraplast Plain) for 2 hours with vacuum; second wax (Paraplast Plain) for 2 hours with vacuum; third wax (Paraplast Plain) for 2 hours with vacuum; and a final wax (Paraplast Plain) for 6 hours with vacuum.

Knee joints were mounted in blocks with the medial side down for sagittal sections. Blocks were trimmed on the microtome until the very beginning of the articular cartilage was evident and then serial sagittal sections (4µ) were cut across the entire medial femorotibial compartment of the joint. All right knee joints were cut and mounted on superfrost plus slides (three sections per slide). A minimum of six knee joints per treatment group (DMM, Sham, Control, mBSA, Saline, Immunised-control), per time point (day 3, week 1, 2, 4, 8, 12 and 16) were sectioned. For DMM and Sham knee joints where pathology is focal, every 4th slide (i.e. every 36µ) across the width of the medial femoro-tibial joint was stained for scoring to ensure the maximum lesion was evaluated. In the case of the mBSA, saline and immunised-control knee joints where the disease is uniform throughout the joint only one slide containing three sections (at the level of the central load bearing region) was stained for scoring.

Slides were dried at 85°C for 30 min and then overnight at 55^{o}C in an oven to adhere sections to slides.

2.2.2 Histochemical Staining

Slides were stained using toluidine blue and fast green to enable histological evaluation of the articular cartilage (including proteoglycan content), synovium, meniscus and subchondral bone.

Sections were de-parafinised by placing slides in 70% (v/v) ethanol for 15 minutes and draining well. Sections were then stained for 10 minutes in 0.04% (w/v) Toluidine Blue O in 0.1M sodium acetate buffer (pH 4.0), rinsed quickly in running tap water and counterstained for two minutes in 0.1% (w/v) fast green FCF, then quickly rinsed again in running tap water. Finally sections were dehydrated in three changes of isopropyl alcohol and three changes of xylene, before mounting in a resinous mountant (Euckitt).

2.2.3 Histological Scoring system

For evaluation of articular cartilage proteoglycan loss and structural damage, osteophyte formation, and subchondral bone changes, knee joint sections were scored using a modification (461) of previously published guidelines (462). The femur and tibia were scored separately, and on each slide (three sections) the worst score was recorded. Only the slide containing sections of the central weight-bearing region of the joint was evaluated as this coincided with the maximal lesion in DMM (see Methods Validation Chapter 3). Details of the scoring method used are outlined in Appendix C.

Synovial inflammation was evaluated using a newly developed scoring system that included assessment of the synovial lining, the sub-synovium, synovial exudate, panus formation and cortical bone erosion,(461). Again only the central weight-bearing region of the joint was evaluated. Details of this scoring method are also outlined in Appendix C.

The histological scoring was performed by two independent observers (SZ, CL) blinded to treatment and time, and the average of the two scores calculated and used for analysis (refer to Chapter 3, Figure3.7b for inter-observer variability).

2.3 Pain behaviour testing

Pain behaviour tests used in this thesis were selected based on what is currently known about the clinical characteristics of OA pain in human patients. People with chronic OA modify their physical activity, and adjust their weight distribution and gait (463). Patients with OA have reduced thresholds to repeated mechanical stimulation (evoked temporal summation), and reduced pressure pain thresholds (localised mechanical hyperalgesia) compared to normal subjects (276, 284, 464). Human OA patients also demonstrate thermal hyperalgesia (277).

Mice were acclimatised to all the test equipment in the week prior to baseline testing. Acclimatisation involved placing the mouse in the different test chambers for a short period of time (1-3 minute in forceplate and hotplate chambers, and 30 minutes in von Frey chamber) to allow them to explore the environment without any intervention. This was done on at least two occasions. For tests that involved manual restraint, mice were briefly restrained to simulate testing and then released back into their cage. Again this was done on at least two occasions.

2.3.1 Von Frey filament testing

Von Frey filaments were used to test for mechanical allodynia (465). Baseline withdrawal thresholds were assessed up to 1 week prior to induction of arthritis. Testing was then performed at day 3, week 1, 2, 4, 8, 12 and 16, after arthritis induction

Mice were placed in individual transparent plastic chambers sitting on a wire mesh floor (Figure 2.3a), and allowed to acclimatise for up to 30 minutes prior to each test period until exploratory and grooming behaviours decreased. A 3-second stimulus was then applied by touching the plantar surface of the hind paw with a von Frey filament presented perpendicularly and exerting enough force to bend the filament (Figure 2.3a). A positive withdrawal was defined as biting, licking, shaking and/or withdrawal of the paw during or immediately following the 3-second stimulus. The stimulus was applied twice before confirming a positive or negative response. A series of von Frey filaments were used for testing, starting with filament 3.61 (0.4 g force). The size of filament was incrementally increased or decreased following a positive or negative response respectively, using the "up and down method" described by Chaplan (465). This up-down procedure was applied 6 times to calculate the 50% withdrawal response threshold using the algorithm described by Dixon (466).Up to 6 mice were tested at any one time. The contralateral (left) hind paw was tested in all mice followed by the ipsilateral (right) hind paw. Each paw was tested twice to obtain an average. If mice were displaying grooming behaviour, urinating, defecating, moving around the cage excessively or attempting to climb the walls of the chamber, they were not tested at that time point.

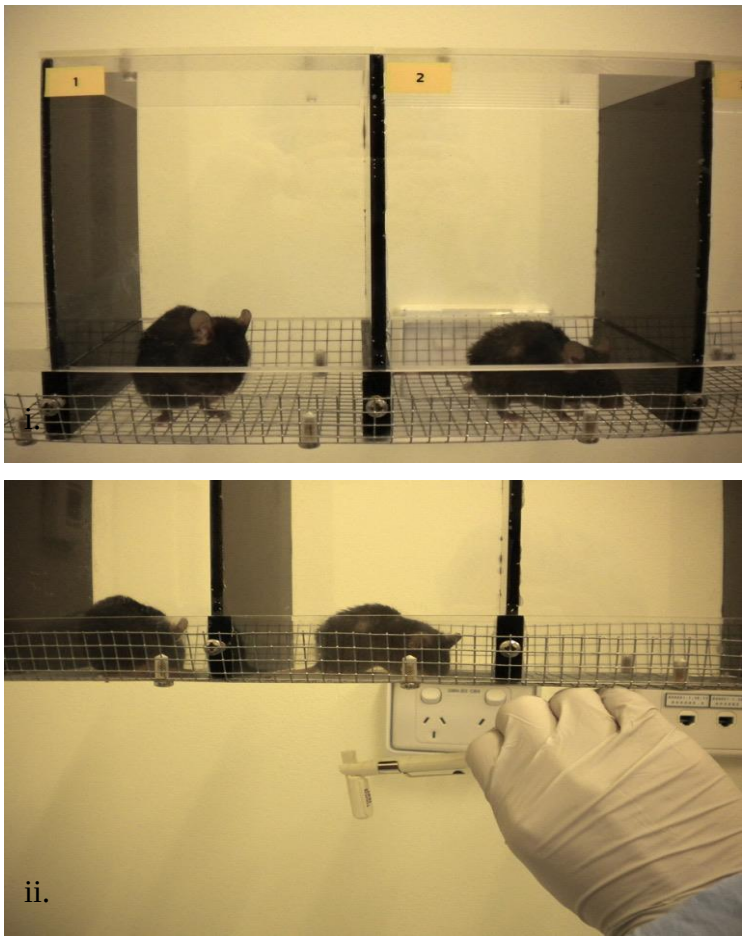

Figure 2.3a: Von Frey testing chambers and application of filament.

(i) Mice are placed in individual transparent plastic chambers sitting on a wire mesh floor; (ii) A 3-second stimulus is then applied by touching the plantar surface of the hind paw with a von Frey filament presented perpendicularly and exerting enough force to bend the filament.

2.3.2 Hotplate test

Thermal hyperalgesia was measured using a hotplate device. Baseline response latency was determined up to 1 week before induction of arthritis. Test measurements were taken at day 3, week 1, 2, 4, 8, 12 and 16, after arthritis induction.

The hotplate was set at 52 degrees Celsius. The mouse was placed on the hotplate, inside a transparent plastic cylindrical chamber (Figure 2.3b). The response latency was determined by observing for shaking & licking of the left or right hind paw. Each mouse was tested twice and response times averaged. Mice were given a 10 to 15 minute rest period between each test. A maximum exposure time of 60 seconds was set to ensure tissue trauma to the plantar surface of the paws did not occur. Testing was also stopped if the mouse attempted to jump out of the chamber.

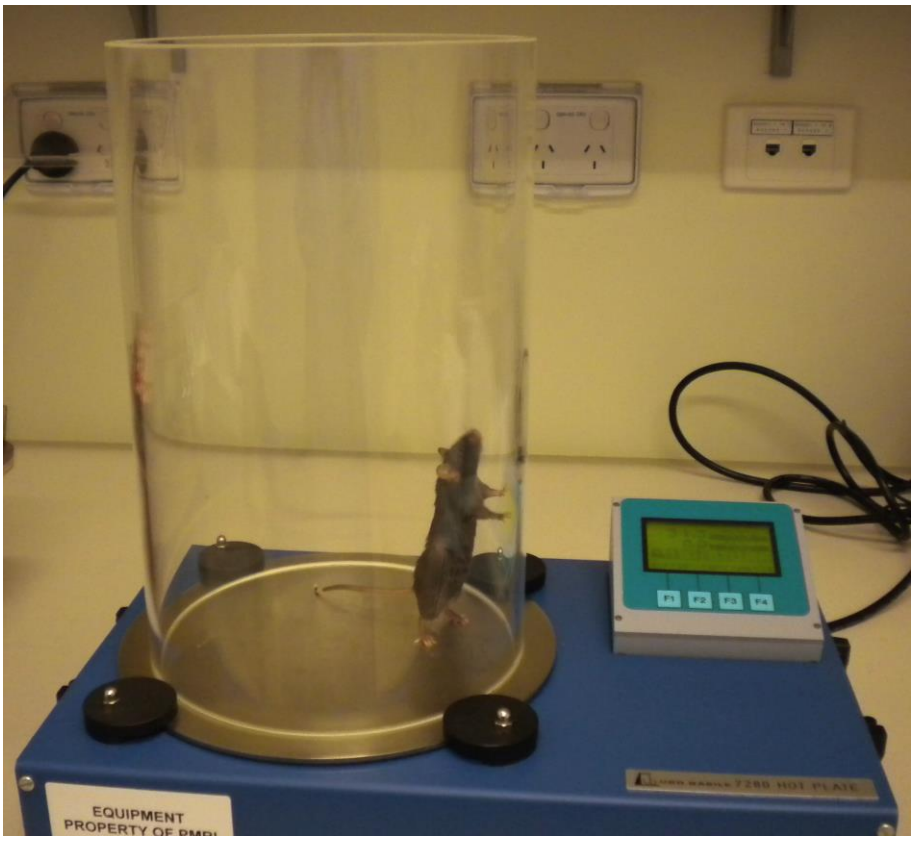

Figure2.3b. Hotplate device

Mice are placed on the hotplate, inside a transparent plastic cylindrical chamber with the plate set at 52 degrees Celsius.

2.3.3 Pressure Application Measurement

Mechanical hyperalgesia of the knee was assessed using a Pressure Application Measurement (PAM) device. Baseline withdrawal thresholds were assessed up to one week prior to induction of arthritis. Testing was then performed at day 3, week 1, 2, 4, 8, 12 and 16, after arthritis induction.

Mice were manually restrained in the right hand and the PAM device was held in the left hand for testing. The device was held between the thumb and index finger, and used to squeeze the knee joint with increasing force until the mouse responded. Left and right knees were tested, and two measurements were taken for each knee, one with the transducer applied to the medial side and one with the transducer applied to the lateral side of the joint (Figure 2.3c). Two attempts were recorded for each measurement to obtain an average and ensure consistency in response. Mice that displayed large discrepancies between the two attempts were retested at the end of the test period.

The rate of force applied was guided by the PAM software to ensure an increasing amount of force was applied at a constant rate (30g/s), up to a maximum of 450g. A positive response was defined as an attempt to withdraw the limb. The force at which the mouse withdrew was recorded as the withdrawal threshold. The maximum force (450g) was assigned if the mouse did not withdraw. If a mouse struggled and attempted withdrawal following manual restraint or when the PAM device was gently placed against the knee, the mouse was returned to his cage and allowed to settle for 5 minutes before testing was attempted again.

Figure 2.3c. Pressure Application Measurement device

Mouse is restrained and the transducer is applied to the medial side of the knee joint; (ii) followed by the lateral side of the knee joint. The device is held between the thumb and index finger, and used to squeeze the knee joint with increasing force until the mouse responds.

2.3.4 Forceplate

An in-house developed electronic forceplate (National Instruments-DAQmx hardware driver) and LabVIEW Run-Time Engine 2009 Software (National Instruments Australia) were used to measure hind limb weight distribution. Baseline hind limb weight distribution was assessed up to 1 week prior to induction of arthritis. Weight distribution was then tested at day 3, week 1, 2, 4, 8, 12 and 16, after arthritis induction.

This test involved placing a mouse in a small transparent plastic chamber with each hind paw resting on a separate transducer plate (Figure 2.3d). The mouse was allowed to settle in the chamber for up to 1 minute prior to recording. Continuous recordings were taken for a total period of 30 seconds to obtain an average force in grams for each hind limb. Recordings occurred when the mouse was observed to be positioned as follows: (1) front paws resting on the front vertical panel of the chamber; (2) the mouse was not leaning/resting on either of the lateral vertical panels of the chamber; (3) the tail was positioned outside of the test chamber and held slightly raised to ensure testicles and tail base were not in contact with the transducer plates; and (4) the hind paws were each placed on the respective left and right plate. If the mouse moved during the 30-second test period, recording was paused and then recommenced once correct positioning was observed. Results were expressed as mean weight distribution ratio (right/left hind limb).

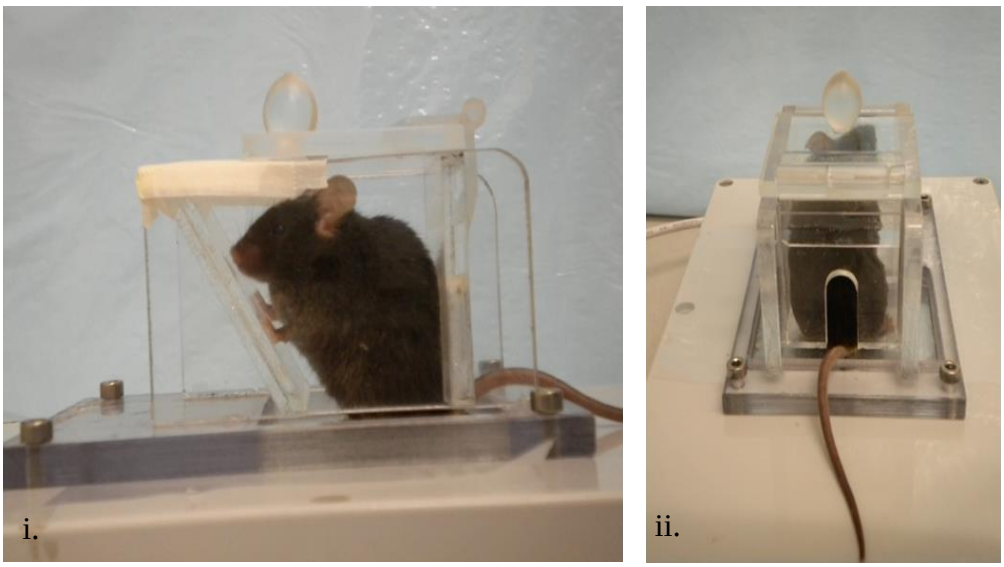

Figure 2.3d. Forceplate device

(i) The mouse is placed in a small transparent Perspex chamber with the front paws resting on the front vertical panel of the chamber and the hind paws were each placed on the respective left and right plate; (ii) the tail is positioned outside of the test chamber and held slightly raised to ensure testicles and tail base are not in contact with the transducer plates.

2.3.5 Stride length

Baseline measurements were taken up to 1 week before induction of arthritis. Test measurements were taken at day 3, week 1, 2, 4, 8, 12 and 16, after arthritis induction. Individual mice were physically restrained to enable dipping of their hind paws in non-toxic water based paint (Figure 2.3e(i)). They were then quickly released into a transparent plastic run (50mm x 100cm) in which the floor was lined with printing roll paper (Figure 2.3e(ii)). The sides and end of the run were covered to create darkness and encourage the mice to run to the end. Once the mouse reached the end they were removed from the run to ensure the trail of footprints they had created on the paper were not smudged or superimposed if the mouse attempted to run in the opposite direction. If the mouse paused to groom, defecate, urinate or explore, this was noted on the recording paper with an asterix (*) (Chapter 3, Figure 3.5b).

The feet of the mouse were cleaned with moist tissues prior to returning the mouse to his cage. The floor of the run was lined with fresh printing paper for each mouse.

Stride length was then determined based on the footprints created on the printing paper. The mean stride length when supporting the affected limb (right to left) and the unaffected limb (left to right) was calculated by averaging out 5 consecutive right-to-left strides and 5 consecutive left-to-right strides respectively. The mean complete stride length for the left and right hind limb was also calculated by averaging out 5 left-to-left strides and 5 right-to-right strides. Sections of the recorded footprints that included a pause period (*) as described above, were not used to calculate stride length. For each mouse, measurements were taken from the same footprint location to ensure consistency (Figure 2.3e(iii)).

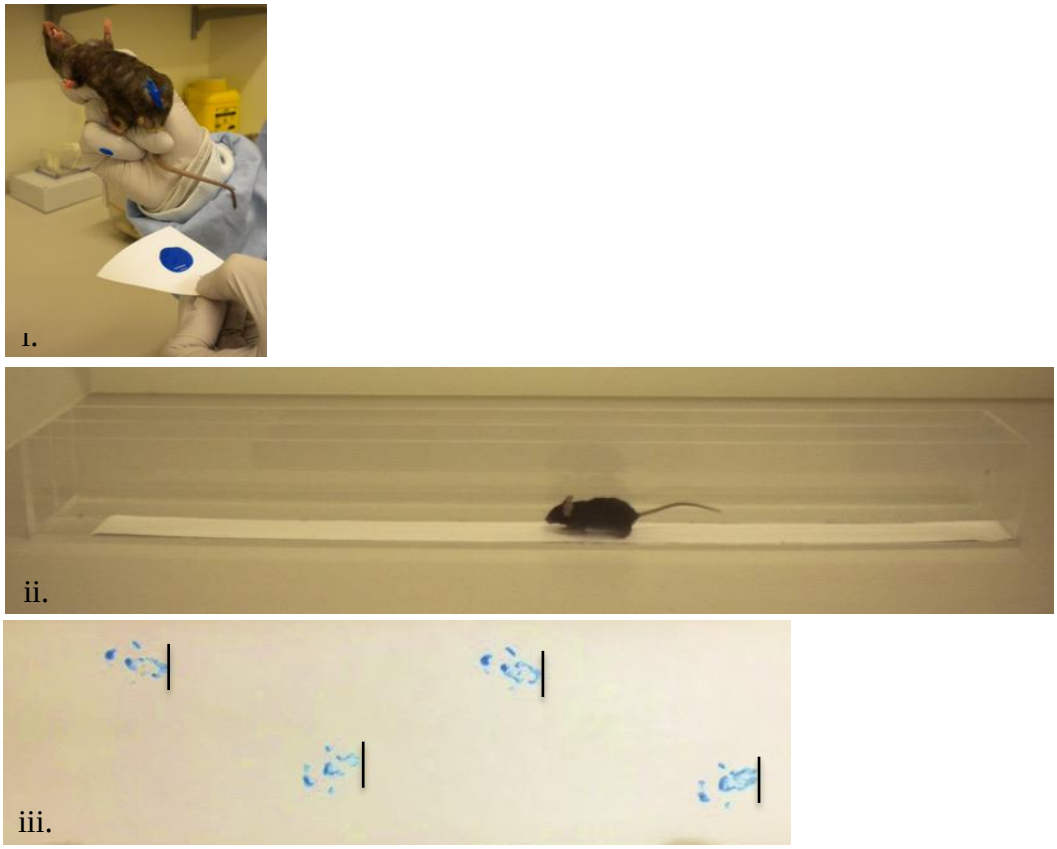

Figure 2.3e. Stride length measurement

The mouse is physically restrained to enable dipping of the hind paws in non-toxic water based paint; (ii) the mouse is then quickly released into a transparent plastic run (50mm x 100cm) in which the floor has been lined with printing roll paper; (iii) measurements were then taken from the same footprint location to ensure consistency.

2.4 DRG gene expression using real time Reverse Transcription-Polymerase Chain Reaction (RT-PCR)

Based on previous studies that used retrograde tracing techniques to label and characterise knee joint afferents (169, 226, 227), the cell bodies of the afferent neurons innervating the knee joint reside in the lumbar dorsal root ganglia (DRG) (L1 – L5), with the majority in L3. In the rat 88% of knee joint afferents are located in L3 and L4. However, knee joint afferents make up a small proportion of the total neuron cell body population in these DRG (less than 15%), and only about half of these are small, myelinated and unmyelinated nociceptors. Knee joint afferents also comprise the large, low threshold mechanoreceptors that are required for normal joint movement. Therefore, to optimize the ability to identify changes in gene expression in nociceptor neurons in the innervating DRG, only L3 and L4 DRG were harvested for real time RT-PCR.

A number of inflammatory neuropeptides including Substance P (Tac-1) and CGRP, and inflammatory cytokines such as IL-1β have been demonstrated to play a role in chronic pain and sensitisation (467-470). TRPV1, TRPV2, TRPV4 and TRPA1 are all part of the Transient Receptor Potential (TRP) family of cation channels and have been described in the DRG. Numerous studies suggest all 4 TRP channels play a role in the development of chronic pain, and in particular mechanical hypersensitivity (471-474). The role of both the endogenous opioid and cannabinoid systems in pain modulation has been studied extensively (265, 266, 291, 308, 311, 475). However, the exact role that they play in pain modulation in diseases such as OA is still not known. There is growing evidence that supports a neurogenic component to OA pain (361, 476, 477), highlighting the importance of investigating markers of neuronal injury (ATF3) in OA.

Based on this current understanding of chronic pain and sensitisation, the following genes were selected for investigation using real time RT-PCR: Tac-1, CGRP, IL-1β, Oprm1, CNR1, TRPV1, TRPV2, TRPV4, TRPA1 and ATF3 (Table 2.1).

In an attempt to investigate potential links between the mechanisms involved in cartilage degradation and peripheral pain mechanisms, gene expression of the principle aggrecanases implicated in cartilage degradation in OA (ADAMTS-4 and ADAMTS-5) was also measured using real time RT-PCR. While ADAMTS-4 expression relies on induction by pro-inflammatory cytokines, ADAMTS-5 is expressed constitutively in a number of adult tissues including DRG (34). ADAMTS-4 has not previously been investigated in the DRG, but it is the most highly expressed ADAMTS in the central nervous system (CNS) and is thought to play a role in controlling synaptic plasticity during CNS development (478). It has been demonstrated that ADAMTS-5 knock out mice are protected from OA and do not develop mechanical allodynia at 8 weeks after surgical induction of OA (441). To date, no one has investigated regulation of ADAMTS-4 or ADAMTS-5 in the DRG and how it changes over the course of OA disease development.

Gene symbol	Name	Evidence for potential role in chronic OA pain
Tac-1	Substance P Tachykinin-1	Mechanical hyperalgesia is significantly reduced in NK1 receptor deficient mice in CFA-induced inflammatory arthritis model (479). Tac-1 expression in the DRG is down-regulated in the peak inflammatory phase of Collagen-induced arthritis. Systemic administration of NK1 receptor antagonist inhibits joint swelling but not mechanical allodynia (480). The density of Sub P immune-reactive nerve fibres in the hip joint is increased in humans with painful OA but not in patients with failed total hip arthroplasties that are non-painful (481).
Calcitonin (CGRP)	Calcitonin gene related peptide	CGRP deficient mice do not develop thermal hyperalgesia in carrageen induced inflammatory arthritis (468). CGRP promotes mechanical hyperalgesia in MIA and meniscal transection induced OA (469). The density of CGRP immune-reactive nerve fibres in the hip joint is increased in humans with painful OA but not in patients with failed total hip arthroplasties that are non-painful (481).
IL-1β	Interleukin-1β	Intra-articular induction of IL-1β contributes to joint pathology and pain (325).
Oprm1	Mu opioid receptor	Temporal induction of the endogenous opioid system delays onset of pain in the DMM model of OA (316). Opioid induced analgesia for neuropathic pain is achieved at higher doses than inflammatory pain. Opioid receptor expression in the DRG is down-regulated in neuropathic pain (chronic nerve constriction model) and unaltered in CFA-induced inflammatory pain (314).
CNR1	Cannabinoid receptor 1	Peripheral CNR1 activation results in a greater reduction in mechanosensitivity in MIA induced OA knee joints compared to controls (475). CNR1 inhibits NGF induced sensitisation of TRPV1 (482).
TRPV1	Transient Receptor Potential Vanilloid-1	Joint inflammation and pain are attenuated in TRPV1 deficient mice in CFA-induced inflammatory arthritis (188). Increased TRPV1-immunoreactivity present in human OA synovium. Intra-articular administration of TRPV1 antagonist reverses knee joint mechanical sensitisation in mice with MIA induced OA (190). Mechanical hyperalgesia observed in models of polyneuropathy develops earlier and with greater intensity in TRPV1 deficient mice (183).
TRPV2	Transient Receptor Potential Vanilloid-2	TRPV2 expression in DRG is up regulated following CFA-induced inflammation and is associated with onset of thermal hyperalgesia (211).
TRVP4	Transient Receptor Potential Vanilloid-4	Development of mechanical allodynia in a neuronal injury model of chronic pain is in part driven by TRPV4 (483).
TRPA1	Transient Receptor Potential Ankyrin-1	TRPA1 modulates low intensity mechanical stimulation following CFA induced inflammation (474). Activation of TRPA1 plays a role in inducing and sustaining mechanical hyperalgesia in CFA induced inflammatory arthritis (484). TRPA1 inhibitor reverses CFA-induced mechanical hyperalgesia in wild type mice but not in TRPA1 deficient mice (204). TRPA1 deficient mice display less reduction in ipsilateral hindlimb weight bearing compared to wildtypes in MIA-induced arthritis (485).
ATF3	Activating Transcription Factor-3	Lumbar DRG ATF3-immunoreactivity is increased in mice with MIA induced knee OA and reduced ipsilateral weight bearing (361). Intra articular injection of 2mg MIA induces expression of ATF3 in DRG innervating the knee joint and surrounding tissues (486).
ADAMTS4	Aggrecanase 1	Mechanical strain of articular chondrocytes drives the release of inflammatory and neurotrophic factors associated with joint degeneration (ADAMTS4) and pain (NGF, TNFa) (487).
ADAMTS5	Aggrecanase 2	ADAMTS5 deficient mice are resistant to OA-like joint pathology and do not develop mechanical allodynia in the DMM OA model (441).

Table 2.1. Genes selected for RT-PCR analysis and evidence for role in chronic pain states including OA pain

2.4.1 DRG harvesting

Lumbar 3 and 4 DRG were harvested at day 3, week 1, 2, 4, 8, 12 and 16, after arthritis induction, from DMM, Sham, mBSA injected, and Saline injected mice. DRG were also harvested at week 4, 12 and 16 from age matched control mice.

Mice were euthanized using CO_2 inhalation followed by decapitation. Decapitation was performed to facilitate exsanguination and minimise blood contamination during dissection and DRG harvest. The coat was sprayed liberally with 70% ethanol to minimize contamination. The skin covering the dorsum was dissected away to expose the underlying muscle layers and allow visualisation of the vertebral column (Figure 2.4a). Harvesting of DRG was done under a dissection microscope and each mouse was completed in ~15 minutes. A size-11 scalpel blade was used to score the muscles overlying the dorsal vertebral column. The muscles were then dissected off the vertebral column using a Friedman Rongeur (Figure 2.4b), exposing the dorsal spinous processes (Figure 2.4c). Laminectomy forceps (#2) were then used to remove the dorsal vertebral column, exposing the spinal cord (Figure 2.4d). The spinal cord was gently elevated to enable visualisation of the DRG using fine Dumont (#5) forceps and micro spring scissors to cut nerve roots and free up the cord, starting at the sacrum and working towards the thoracolumbar junction (Figure 2.4e). Left and right DRG (L3 and L4) were lifted with fine Dumont (#5) forceps and dissected out by cutting the attaching nerve roots with micro spring scissors. L3 and L4 DRG from each side were immediately transferred to separate 1.5ml polypropylene (Eppendorf) tubes, homogenised in 50µl TRIzol® reagent using a motorized pestle, and then placed in dry ice. Samples remained in dry ice until all DRG were harvested (up to 6 hours), and then transferred to a freezer and stored at -80^{o}C.

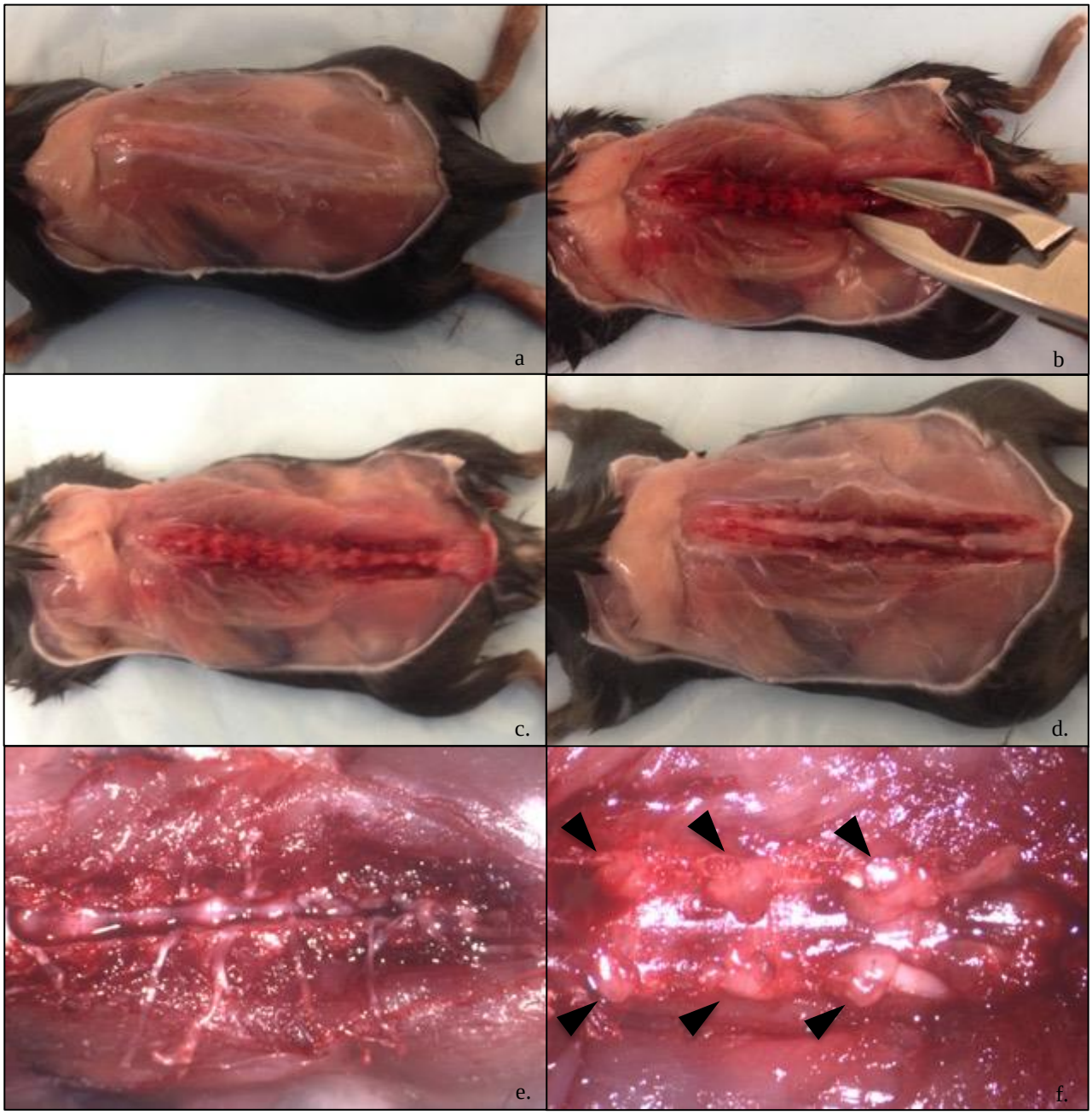

Figure 2.4. DRG harvesting

(a) Removal of the overlying skin to expose the vertebral column; (b) dissection of the lumbar muscles using rongeurs; (c) exposure of the dorsal spinous processes; (d) removal of dorsal spinous processes to expose the spinal cord; (e) lumbar DRG and nerve roots following dissection of the spinal cord; (f) left and right L2 – L4 DRG in situ (solid arrows).

2.4.2 RNA extraction

Total RNA was extracted from L3-4 DRG using the Qiagen RNeasy kits as described by the manufacturer. Previously homogenized samples were thawed at room temperature. Samples were done in batches due to the limitations of the centrifuge required for the extraction process, which held a maximum of 30 samples. Left and right DRG samples from the same animal were done at the same time, and each batch included samples from each treatment group to ensure consistency within individuals and between treatment groups in the extraction process. An additional 950µl TRIzol® reagent was added to each sample, followed by Chloroform (300µl). Samples were vigorously vortexed for 15 seconds, and incubated at room temperature for 5 minutes, followed by centrifugation for 15 minutes at 12,000 rpm to stratify the aqueous and organic phases. The aqueous phase, containing RNA, was carefully transferred to new micro-tubes in 100µl aliquots using a 200µl pipette, and then combined with an equal volume of 70% ethanol. Samples were gently mixed by inversion before loading onto RNeasy spin-columns in 600µl aliquots followed by centrifuging at 12,000 rpm for 20 seconds. RWI buffer (350µl) was then added to each spin column, incubated at room temperature for 5 minutes and centrifuged at 12,000 rpm for 20 seconds. The collection tubes were discarded and new collection tubes placed under the spin columns. 80µl of DNase in RDD buffer was applied to each spin column, centrifuged for 20 seconds at 12,000 rpm, and reapplied. Samples were then incubated at 37^{o}C for 1 hour. After incubation the spin columns were washed with 350µl RWI, followed by two washes with 500µl RPE buffer. Spin columns were centrifuged for 20 seconds at 12,000 rpm after each wash. An additional 2-minute centrifugation was done to evaporate any traces of ethanol and dry the spin columns. Finally, RNA was eluted

from spin columns by loading 32µl RNase free water and centrifuging for 1 minute at 12,000 rpm.

2.4.3 RNA quantification

RNA was quantified using a Nanodrop spectrophotometer (ThermoScientific). DNA contamination was detected by running a no-RT quantitative RT-PCR on 0.3µg of the total RNA using the Rotor-Gene 6000 (Corbett Life Science, Australia) and the housekeeping gene GAPDH.

2.4.4 Reverse Transcription

Due to the large number of samples (multiple treatment groups and multiple time points) reverse transcription could not be performed on all samples at once, and still ensure each sample received equal exposure time to the master mix and incubation. Instead reverse transcription was done in batches based on harvest time point. Variability in RNA yield from the DRG of individual mice prevented reverse transcription of 1µg RNA for each sample. Instead, an equal amount of total RNA (0.5 to 1 µg), based on the smallest total yield from any given sample in a batch, was reverse transcribed into cDNA using the Omniscript RT kit (Bioline).

The reverse transcription (RT) master mix was made up as described in Appendix B. All RNA samples were denatured prior to performing RT by placing on a heating block, set at 70^{o}C, for 5 minutes. To each calculated amount of RNA was added enough RNase-free water to make a total volume of 30µl. 10µl of master mix was then added to the side of each tube. Samples were then spun down quickly in the centrifuge and incubated for 3 hours at 37^{o}C, followed by 5 minutes incubation in a

heating block set at 93^{o}C. The samples were then cooled quickly by placing in ice for 5 minutes. The cDNA samples were diluted with RNase-free water to a total volume of 150μL per 1μg of original RNA. The cDNA samples were stored at 4^{o}C until used.

2.4.5 Primer design

Murine primer sets were designed using MacVector 11.1 primer design software. Primers were purchased from Sigma Genosys and full details are provided in Appendix A. Primer specificity was confirmed by performing a melt curve analysis and demonstrating a single amplicon of appropriate size.

2.4.6 Quantitative real-time RT-PCR

qRT-PCR was performed using the Rotor-Gene 6000 (Corbett Life Science, Australia) and analysis software (Corbett Research Pty Ltd, copyright 2004). cDNA standards were prepared by combining aliquots of multiple samples of cDNA from different treatment conditions (i.e control, sham, DMM, saline, AIA) and post-induction times, and making serial 4-fold dilutions to provide four standards (1:1, 1:4, 1:16, 1:64) that were used as "in-run standards". Standards were run in duplicate along with 2 negative controls (RNase free water), with each primer pair that was tested. A master mix was made up comprising 1x Immomix, 10μM forward and 10μM reverse primer and 1x SYBR Green 1 dye made up to a total of 20μl per reaction, in RNase free water. 20 μl of master mix was added to each reaction tube followed by 5μl of cDNA sample or standard. The following thermal profile was used for each reaction: 10 minutes denaturation at 95^{o}C; 45 cycles of 95^{o}C for 10 seconds;

a primer specific (see Appendix A) annealing temperature for 15 seconds; and extension for 20 seconds at 72^{o}C.

A melt curve analysis was performed for each reaction to confirm that a single product was produced for each amplicon. Quantitative analysis was then performed and RNA values for each gene were normalised to total RNA, and expressed as fold change relative to mean sham-operated and saline-injected respectively.

Glyceraldehyde-3-phosphate dehydrogenase (GAPDH) was initially trialled for normalisation of RNA values for genes of interest, as this has previously been widely used as a housekeeping gene, including for studies of DRG gene expression (488, 489). However, analysis of data revealed that GAPDH demonstrated significant variation in expression between sham and treatment mice DRG, at some of the measured time points. Unfortunately, insufficient RNA sample remained from many of the measured time points, to allow identification of a more suitable housekeeping gene that displayed stability in expression in DRG tissue, across the different treatment groups and the different time points. For this reason, RNA values were not normalized against a housekeeping gene, but instead normalised to total RNA and expressed as fold change relative to the respective sham-operated or saline-injected, control as previously recommended (490-492).

2.5 Immunohistochemistry

DRG (lumbar 3-5) samples harvested for immunostaining were collected at key time points (day 7, week 4, 8 and 16) and stored initially as fixed-frozen blocks at -80^{o}C. To maximize the preservation of DRG tissue architecture and cell morphology, and allow multiple sectioning of individual DRG over the lengthy period it took to stain for the different antibodies, samples were subsequently embedded in paraffin for long term storage.

Immunostaining of DRG was then performed in batches, the size of which was limited by the number of Sequenza trays (Thermo Scientific) available. Each batch contained sections from each treatment group and two time points. This allowed qualitative analysis of relative protein expression in the DRG between treatment groups and over time.

2.5.1 Perfusion of mice with paraformaldehyde

Mice were anaesthetised with an intraperitoneal injection of 50mg/kg pentobarbitone. Once deeply anaesthetised (loss of pedal reflex and slow breathing) mice were placed in a fume hood and positioned in dorsal recumbency on a tray. The limbs were held out in an extended position using adhesive tape. The coat was sprayed with 70% (v/v) ethanol and the skin overlying the ventral thorax was lifted with forceps to allow a large skin incision to be made with tissue scissors. The xiphoid process was then elevated and an incision made through the diaphragm to facilitate complete sectioning of the ribcage, to expose the heart.

A small incision was made in the right auricle and a short 25-gauge needle (attached via minimum volume tubing to a 50ml syringe) was inserted into the left ventricle.

Flush solution (approximately 15ml) was then run through the animal until clear fluid was coming from the right auricle and the abdominal organs were pale. Fixative solution (approximately 50ml) was then run through the animal until the animal became rigid. Details of the composition of the flush and fixative solution are listed in Appendix B.

The DRG were then dissected out as described in 2.4.1 and post fixed in 4% PFA for 90 minutes. Isolated DRG were then placed in 30% sucrose at 4^{o}C for 24 hours before mounting into Base Molds (Tissue Path, Fischer Scientific) in a water-soluble specimen matrix (Tissue-Tek O.C.T). The specimen blocks were placed immediately in dry ice for snap freezing and then transferred to the freezer for storage at -80^{o}C until further processing.

2.5.2 DRG Processing

Following the harvesting of all time points, DRG stored at -80^{o}C were brought to room temperature and transferred to 70% (v/v) ethanol prior to paraffin embedding. Individual DRG specimens were wrapped in Kimwipes™ to ensure they were not lost during processing.

All DRG specimens were dehydrated for 30 minutes each in graded solutions of 70%, 75%, 85% and 95% (v/v) ethanol, and three washes of 30 minutes duration in 100% (v/v) ethanol. This was followed by three changes of 30 minutes duration in chloroform. DRG were then put through three 30-minute cycles in wax (Paraplast Plain) without vacuum. DRG were embedded in Paraplast Plain in cassettes using magnification to ensure a consistent orientation. DRG tissue was embedded flat along

their longitudinal access. In this orientation the neurons were centered with nerve roots extending from either side.

Blocks were trimmed on the microtome until neurons were first visualised (microscopically), before serial sections (4μ) were cut and mounted onto superfrost plus slides (one sections per slide). The 1st and 10th slide were stained with Haematoxylin and Eosin (H&E) to enable evaluation of DRG cellular morphology prior to immunohistochemical staining of slides 2-9. If the number of neurons on these sections was sparse a further 10 sections were cut and mounted on slides, and the H&E staining repeated on slide 20 to evaluate the quality of the section prior to immunohistochemical staining of slides 11-19.

To de-paraffinise, slides were immersed in xylene for two changes of 5 minutes duration each. The sections were then immersed in graded solutions of 100%, 100%, 95% and 70% (v/v) ethanol for three minutes each. The slides were then rinsed in a container of running tap water and drained well before been stained for 10-12 seconds in Mayer's Haematoxylin. Sections were then rinsed quickly in running tap water and placed in Scott's blueing solution for one minute, and again rinsed quickly in running tap water. Sections were then counterstained in Eosin for 1 minute and rinsed immediately under running water. Finally sections were dehydrated in three changes of isopropyl alcohol and three changes of xylene, before mounted in a resinous mountant (Euckitt®).

2.5.3 Antibody staining

2.5.3.1 Deparaffinisation

Slides were immersed in xylene for two changes of 5 minutes duration each. The sections were then immersed in graded solutions of 100%, 100%, 95% and 70% (v/v) ethanol for three minutes each. The slides were then rinsed in a container of running tap water and drained well.

2.5.3.2 Primary antibody incubation

Slides were assembled in Sequenza trays (Thermo Scientific). Wash buffer (Tris Buffered Saline and Tween-20) was added to the top of each slide chamber and incubated at room temperature for 6 minutes. 100µl of Dako Protein Block (serum free) was then added to each slide chamber, and incubated at room temperature for 10 minutes. 100µl of diluted primary antibody or appropriate negative control antibody was added to each slide chamber followed by incubation at 4^{o}C overnight. Details of antibodies are available in Appendix A.

2.5.3.3 Detection

Wash buffer (TBST) was added to each slide chamber and incubated at room temperature for 6 minutes. Three drops of Envision+ polymer (dual link) were added to each chamber and incubated for 30 minutes, followed by wash buffer (TBST) for 6 minutes. Slides were then removed from the Sequenza tray and placed in a humid chamber. 200ml of substrate chromogen (NovaRED) was applied to each slide, making sure the section was covered with reagent, and incubated for 15 minutes at room temperature. Slides were then placed in rack and washed in running tap water for five minutes.

2.5.3.4 Counterstain

Slides were placed into Mayer's Haematoxylin for 10 seconds and washed until clear. Slides were then placed in Scott's Blue for 1 minute and washed until clear.

2.5.3.5 Mounting

Slides were put through four changes of 100% (v/v) ethanol with 10-second agitation in each container. Slides were then put through three changes in xylene with 20-second agitation in each container. Slides were left in xylene in preparation for mounting. Slides were drained, mounted in a resinous mountant (Euckitt®) and a coverslip applied, and then allowed to dry in the fume hood.

CHAPTER 3: Development and validation of methods

The methods for induction of post-traumatic OA by DMM and inflammatory arthritis using AIA are well established in the host laboratories (439, 450, 461). In contrast, our laboratories had not previously evaluated pain outcomes in these mouse models. This chapter outlines how the pain assays were selected, and the protocol for conducting them was developed, modified and optimised.

Furthermore, different histopathological scoring systems have previously been used to quantify arthritis progression in DMM (47) and AIA (439). Histopathological scoring in the DMM model is focused on quantifying articular cartilage damage (462). In contrast, histopathological scoring in the AIA model is aimed primarily at quantifying the inflammatory changes (448, 452, 493). This chapter therefore also describes experiments to validate the use of a single histological scoring system to enable direct comparison between the two arthritis models for subsequent correlation with pain outcomes.

3.1 Pain assessment

The International Association for the Study of Pain (IASP) defines pain as "An unpleasant sensory and emotional experience associated with actual or potential tissue damage, or described in terms of such damage" (494). This definition, adopted by pain experts to also describe pain in animals, highlights the challenge that researchers face when attempting to accurately and consistently quantify pain in preclinical studies. Nociception refers to the processing of information about the internal and external environment by the peripheral and central nervous system. This commences with the activation of peripheral nociceptors (specialised nerve endings that detect noxious stimuli). Transmission of nociceptive input to the cerebral cortex results in

the perception of pain. However, pain can also be perceived in the absence of any nociceptive signalling.

Like humans, animals experience pain as a complex physiological, somatosensory, emotional and cognitive phenomenon, however they cannot verbally express or describe the emotional component that is unique to every individual. The challenge for researchers is to identify pain assays that accurately mimic the pain observed with human disease, and develop outcome measures that are consistent and can be validated.

Changes in behaviour, posture and even facial expression provide valuable clues about an animal's pain experience. Burrowing and nesting behaviours are also now recognised as an indicator of health and wellbeing in laboratory mice (495, 496), and has been validated as a marker of acute post-surgical pain (497, 498). However, there is currently no report of its validation as a marker of chronic pain, such as that which develops in both humans and animals with OA. Similarly, facial expression markers have been validated in mouse, rat and rabbit models of acute pain (499-503), but have proven unreliable as markers of chronic pain.

Chronic pain assessment in humans relies principally on self-reporting assessment tools such as the WOMAC questionnaire (504). The use of questionnaires assists clinicians and researchers with quantifying the chronic pain state in an individual (505, 506). More recently attempts have been made to develop qualitative pain assessment tools that allow for the phenotyping of chronic OA pain and therefore, a more targeted approach to pain management (430, 507, 508).

Chronic OA pain in human patients is characterised by movement evoked joint pain, locomotor restriction, spontaneous pain at rest, and poor sleep (509). Some of these features have also been demonstrated in preclinical models of arthritis, inflammatory

pain and chronic musculoskeletal pain. For example, fragmented sleep has been demonstrated in mice with chronic muscular pain (510).

Somatosensory testing has also been used to characterise chronic OA pain. Researchers have demonstrated that patients who present with high levels of clinical pain, but only mild to moderate radiographic evidence of knee joint pathology, demonstrate reduced thermal and mechanical thresholds in quantitative sensory tests of central sensitisation (511). On the other hand, patients with mild knee OA pain experience knee joint mechanical hyperalgesia, as demonstrated by an increase in the pressure pain threshold (PPT), but not thermal hyperalgesia (512). In a cohort of patients with different degrees of knee OA, pain intensity (as reported by the patient) correlated significantly with knee PPT, temporal summation (TS) and conditioning pain modulation (CPM) (513). These three quantitative sensory tests are used to assess changes in central pain mechanisms, and reflect the development of central sensitisation.

Chronic OA is also characterised by changes in gait. For example, patients with medial compartment knee OA demonstrate altered foot kinematics (514). Gait disturbances are also observed in pre-clinical models of OA. In the Collagen-induced arthritis model, mice demonstrate an increased stride frequency and shorter stride length (515). However, these gait modifications may reflect progression of joint pathology and subsequent changes in joint mechanical function and/or range of motion, rather than indicating joint pain severity (516).

The pain assays selected for evaluation in this thesis can be used to assess the development of central sensitisation (as is observed in a sub group of chronic OA patients), and represent features of the pain state in pre-clinical models that reflect the clinical features observed in chronic OA patients.

Three stimulus evoked pain tests were investigated:

1. The von Frey fibre test for tactile allodynia
2. The hotplate test for thermal hyperalgesia
3. The PAM (pressure application device) test for mechanical hyperalgesia

Three motor function based behaviour tests were also investigated:

1. Hind-limb weight distribution using a force plate (incapacitance)
2. Gait analysis using hind-limb stride length measurements
3. Motor coordination using a rotarod

All six tests have been validated as outcome measures of pain through ablation of response following the administration of established analgesics such as non-steroidal anti-inflammatory drugs and opioids (316, 406, 423, 517, 518).

However, despite the validation of these pain tests, it is apparent from the literature that there is tremendous variability in the outcome measures that define a positive response and subtle differences in the exact method used to measure these outcomes. This absence of standardisation means that outcomes do not translate across research laboratories, and result in many inconsistencies in the published data from apparently the same experiments. The interpretation of many of the behavioural outcomes, and in particular, what constitutes a "response" can be very subjective and operator/observer dependent, which leads to a significant amount of irreproducibility in the field.

The purpose of the experiments described in this chapter, therefore, was to optimise the methods used and determine which pain outcome measures could detect pain/disability in mouse OA, and that would therefore be used in subsequent longitudinal studies.

Twelve naïve 8-week-old male C57BL/6 mice were used to evaluate the suitability of 5 of the six pain-related behaviour tests (von Frey, Hotplate, Rotarod, Forceplate and Gait). A separate group of 12 naïve 8-week-old male C57BL/6 mice were used to evaluate the PAM device. This was done because the PAM testing required significant restraint of the mice (see section 3.1.3), and it was thought that imposing this additional stress on the mice might confound the results of the other pain tests.

The aim of using naïve mice was to establish a repeatable method for each pain behaviour assay that achieved consistent baseline values. Where modifications were made to a particular assay, the modified method was trialled on six new mice. Once consistent baselines were established, the pain behaviour tests were used to investigate pain using the AIA model. This model was used because it produces a more severe inflammatory response in the knee joint. Based on the current literature (420, 519, 520), an inflammatory arthritis such as AIA should provide a more robust model for demonstrating difference in pain behaviour between treatment mice and saline injected mice with no joint pathology. AIA was established in six mice, as described in Chapter 2 (section 2.1.4), and six mice served as immunised, saline injected, controls. Joint inflammation peaks early in the AIA model (521) and so for the experiments described in this chapter, testing was conducted day 0 (prior to immunisation), day 3, day 7 and day 14 (von Frey and PAM). Table 3.1 outlines the testing schedule and how many times individual mice were tested using the different pain assays.

Table 3.1. Testing schedule for optimisation of pain behaviour assays

Pain test	Baseline testing*				AIA testing**		
	Trial 1	Trial 2	Trial 3	Trial 4	Day 3	Day 7	Day 14
Von Frey	A (12)	A (12)	B (12)	C (12)	C (12)		C (12)
Hotplate 42	A (12)						
Hotplate 50	A (12)	A (12)	A (12)		A (12)	A (12)	
Hotplate 52	B (12)	B (12)			B (12)	B (12)	
Hotplate 55	B (12)	B (12)					
PAM	D (12)	E (12)	E (12)			E (12)	E (12)
Force plate	A (12)	C (12)			C (12)	C (12)	
Stride length	A (6)	A (12)			A (12)	A (12)	
Rotarod	A (12)	A (12)	A (12)		A (12)	A (12)	

A, B C, D and E denote different mice cohorts. The number of mice tested is indicated in brackets. * Animals that were used to establish baselines for more than one pain test were rested for at least 24 hours before performing the next test. Baseline testing was done over a 2-week period prior to administering the first immunisation. ** Animals that underwent more than one pain test were rested for at least two hours before performing the next pain test.

A single assessor (SZ) performed all behaviour testing described in this thesis. The assessor was blinded to treatment group until the completion of testing at all time points. Blinding is a crucial aspect of conducting pain behaviour experiments, as it reduces detection bias in a study. It is done because the assessor may be influenced by the knowledge about treatment assignment (for example, an animal with osteoarthritis should demonstrate a lower pain response threshold than a control animal) and this can induce a systematic detection bias. Overestimation of treatment effect due to unblinded assessors in randomised clinical trials has been estimated to range from 17 - 50% (522, 523). There is an even greater risk of observer bias in animal model experiments where the outcome measure is subjective, as in the case of behaviour

testing and scoring of histological preparations (524). Recently the impact of unblinded assessors in animal model experiments on observer bias was evaluated (525). Ten experiments (2450 animals) were included in the meta-analysis, and an average exaggeration of 59% of the odds ratio (OR) from non-blinded assessments, was calculated. This implies a considerable high risk of observer bias if an assessor is not adequately blinded.

Despite the recent publication of guidelines for the reporting of in vivo animal experiments (ARRIVE Guidelines) (395), many publications do not include proper reporting, especially details of the blinding. Care must be taken when interpreting results from studies that simply state the experiment was blinded without clarification of the blinding. For example, are there any visible differences (e.g. surgical incision) between treatment groups that would unblind the assessor? Does the assessor remain blinded until the conclusion of the experiment when all data has been collected? Is the order that testing or scoring occurs random? Or do all animals in one treatment group get tested followed by the other treatment group? Are different treatment groups housed in mixed cages to avoid any bias associated with testing cage mates?

For the experiments described in this Chapter, there were no visible differences between mice from the two treatment groups (Saline vs. AIA). Mice were housed in mixed treatment group cages, and tested in a random order each time.

3.1.1 Mechanical allodynia

Quantitative assessment of mechanical allodynia was done using von Frey filaments (Stoelting Touch Test Sensory Evaluator Kit, USA) and the 'up-down' method described by Dixon (466). Details of the method used are outlined in Chapter 2 (section 2.3.1). The use of a monofilament device to perform sensory testing was first reported in humans in 1922 (526) and subsequently standardised in the form of a set of calibrated nylon monofilaments by Semmes and Weinstein (527). These same monofilaments are now used by researchers to measure mechanical withdrawal thresholds and draw conclusions about the development of sensitisation in neuropathic, acute and chronic pain models. However, there is still no established consensus on what normal thresholds are in mice or rats. In addition there are a number of limitations of using nylon monofilaments to measure mechanical sensory thresholds in animal models of disease which require further consideration (528).

Although the nylon monofilaments are calibrated, application parameters such as bend rate and the tip geometry influence the amount of vertical force generated by each fibre. In addition, the degree of bending can affect the non-vertical loading and therefore alter the total vertical force generated (528). Other confounders include, the application time, which can vary from less than a second to more than 10 seconds; and the site of application, which is difficult to accurately control. The significance of these application parameters is user dependent, and highlights the need for individuals to learn and practice the technique to ensure consistency and repeatability of results. It also suggests a reason for why there is such variability between individuals and highlights the challenge of yielding reproducible results across two or more different laboratories.

There are currently no published guidelines on how to train an experimenter to perform the test, and there is no standardised protocol for conducting the test, or method for the analysis and reporting of results. The method of analysis used in this thesis (465) is frequently reported, but is by no means universally accepted.

The following test method was used:

1. Six mice were placed in individual transparent plastic chambers with wire mesh flooring, and left undisturbed for one hour to acclimatise. A one second stimulus was applied to the plantar surface of the hind paw with a von Frey filament presented perpendicularly and exerting enough force to bend the filament.
2. A positive response was defined as shaking, licking, biting and/or withdrawal of the tested paw.
3. A series of von Frey filaments were used, starting with filament 3.61 (0.4 g force)
4. The left hind paw was tested in all six mice followed by the right hind paw in all animals.

To establish baseline paw withdrawal threshold (PWT) using von Frey filaments, the same mice were tested on two separate occasions with a five-day rest period in between. This initial baseline data (Trial 1 and 2) collected from naïve mice was highly variable and inconsistent both within (right vs. left paw) and between individual animals (Figure 3.1a and 3.1b). To rule out the effect of stress due to over handling and testing, the von Frey test was repeated using the same method on a different group of naïve mice (n=12) (Trial 3). This group of mice demonstrated a similar withdrawal threshold (Figure 3.1b).

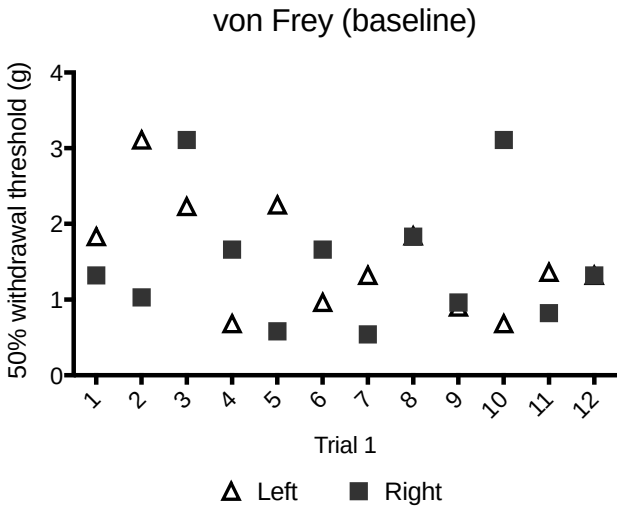

Figure 3.1a. Baseline 50% paw withdrawal threshold (PWT)

Using von Frey filaments, naïve C57BL mice were tested (n=12) on the left and right hind paw. Graph demonstrates the observed within animal variability (left vs. right paw) in baseline 50% PWT.

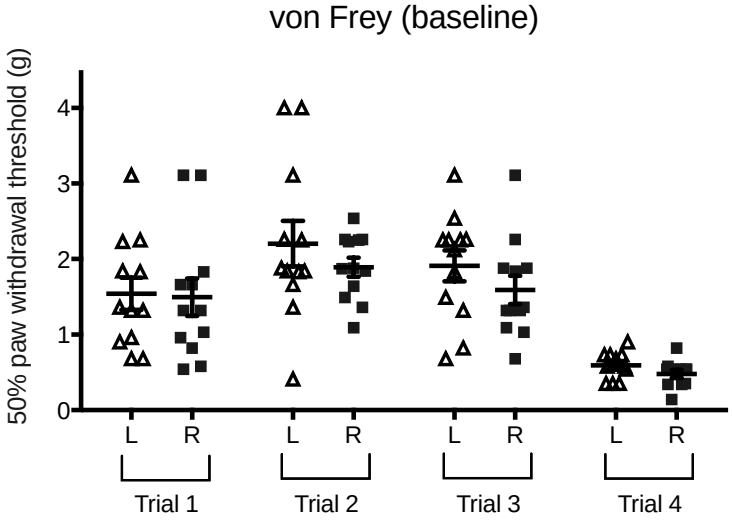

Figure 3.1b. Baseline 50% PWT using von Frey filaments

Trial 1 and 2 represent the same cohort of naïve mice (n=12) tested on two occasions with a five-day rest period in between. Trial 3 is a second cohort of C57BL mice tested using the same method as trial 1 and 2. These mice demonstrated similar within and between animal variability in baseline 50% PWT. Trial 4 represents a third cohort of C57BL mice tested using a modified method. The results are presented graphically as a scatter plot, with mean and SEM marked.

A number of factors were attributed to this inconsistency:

- Operator error in interpreting mouse response
- The length of acclimatisation time
- Use of a wire mesh floor surface

In addition, these initial baseline 50% withdrawal thresholds in naïve mice were higher than that reported in the literature by other pain research groups (406, 441).

As a naïve operator, I was unfamiliar with basic behaviour characteristics of mice. For example, mice are highly driven when it comes to basic activities such as voiding and grooming. This translated to a higher withdrawal threshold if mice were tested while they were performing these activities. The mice also displayed a quiescent state where they appeared unresponsive, but their eyes remained fully open. In this state, the response to a tactile stimulus was unpredictable. For any given stimulus, the response was either exaggerated or they did not respond at all. Mice that were asleep in the chamber at the time of testing were hypoalgesic and did not respond even when the largest von Frey fibres were used.

In addition, I observed that there was variability in how quickly mice acclimatised after being placed in the test chambers, and that they did not remain settled indefinitely. In fact, following this period of reduced activity, the mice entered a state of heightened arousal where they demonstrated excessive grooming, excitatory exploratory behaviour, and attempts at escape from the chamber. In this state mice were very difficult to test. It was also observed that after a period of time mice began to shift their weight from one limb to the other. In contrast, some mice fell asleep after being in the chamber for only 30 minutes.

It has been demonstrated in rats that the type of floor surface used influences the withdrawal threshold for the von Frey test and that wire mesh floors are associated

with a large variability in withdrawal threshold between control animals (529). Exposure to a wire mesh floor may itself induce a hyper aesthetic state resulting in an artificially reduced withdrawal threshold. Rodents do experience anxiety from being elevated (530), and so the mesh floor may act as a stressor because the mice can see through it. Physiological stress will influence an animal's sensory processing. In addition, the mesh floor allows mice to receive visual cues as the operator's hand approaches the mouse and raises the von Frey filament. This phenomenon was observed during testing and resulted in movement and a state of alertness before the filament was even applied to the paw.

The stress of elevation because the surface is not opaque, the influence of visual signalling, and the effect of sensory stimulation due to standing on the mesh floor, could all in part explain the failure of some mice to settle in the chambers, and also why longer acclimatisation periods resulted in heightened activity levels.

The state of arousal and attentiveness is an important modulator of pain sensitivity in humans (531, 532). The modulatory effect of equivalent behavioural states on mechanical and thermal nociception has also been examined in mice using a nerve injury model in three different mouse strains including the C57BL strain (533). Researchers reported six behavioural states; deep sleep, light sleep, resting, alert, grooming and exploring. They concluded that nociceptive sensitivity was influenced by activities such as grooming, alertness, light sleep and deep sleep (533).

To address these confounding factors, the following caveats were added to the testing method. Mice were not tested when asleep, grooming, urinating, defecating or highly active and frequently rearing on their hind limbs. Mice that remained stationary in a hunched position, but with eyes open, for an extended period of time, were deemed to be asleep and therefore were lightly stimulated (light tap on Perspex wall) prior to

testing. Testing was not done while a mouse was observing the operator through the mesh floor. Mice were tested twice on each paw with a minimum 15-minute break between testing, and the two scores were averaged to obtain a mean 50% withdrawal threshold. Where the two scores differed by more than the equivalent of two von Frey filaments, mice were tested a third time and the three scores averaged. Acclimatisation time was reduced from one hour to 30 minutes. If after 30 minutes the mice were still very active, testing was incrementally delayed by 10 minutes until a point when the mice appeared settled in their cages. Acclimatisation time was capped at one hour because after this point, mice either became further agitated or started to fall asleep. Both of these states increased the variability and potentially reduced the accuracy of testing.

With the adoption of these modifications to the method, subsequent von Frey testing achieved more consistent baseline 50% withdrawal thresholds, both within and between individual mice (Figure 3.1b: Trial 4).

Following the establishment of consistent and repeatable 50% withdrawal threshold measurements from naïve mice, AIA was induced and testing repeated on Day 3 and day 14, post arthritis induction (Figure 3.1c). This demonstrated little change in left and right 50% PWT in saline injected mice at day 3 and 14. In AIA mice there was no change in the 50% PWT of the left hind limb, but a significant reduction in the 50% PWT of the right hind limb at day 3 ($p = 0.007$) that persisted to day 14 ($p = 0.012$). This confirmed the ability to detect reduction in PWT using the von Frey method described above, following the induction of arthritis.

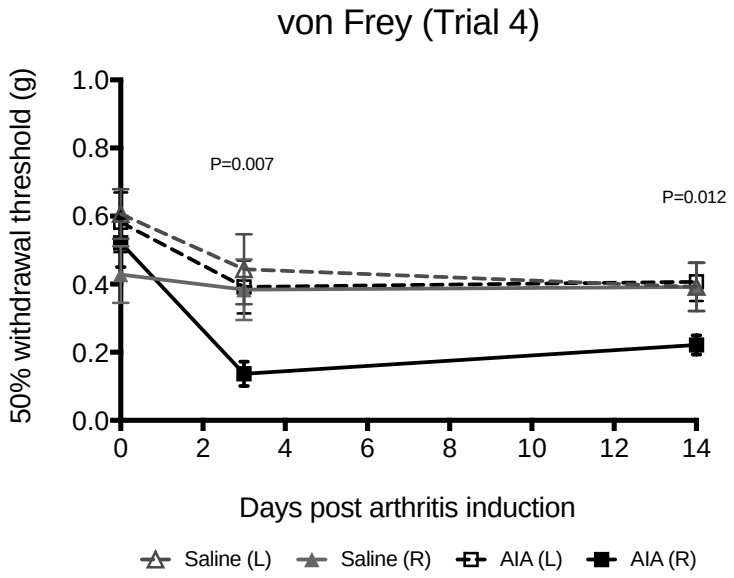

Figure 3.1c. Development of von Frey test protocol

50% PWT at day 0, day 3 and day 14 following induction of AIA in C57BL mice (n=6), in the right knee joint. Sham group (n=6) were immunised and received an intra articular saline injection. At day 3 (P=0.007) and 14 (P=0.012) 50% PWT in the right limb was significantly reduced compared to baseline in AIA mice. The results are presented graphically as a line graph of the means with SEM marked.

3.1.2 Thermal hyperalgesia

Quantitative assessment of thermal hyperalgesia was performed using a hotplate device (Ugo Basile, Italy). The hotplate assay was first reported by Woolfe and MacDonald in 1944 (534), and later modified by Eddy and Leimbach (535). Eddy and Leimbach used a 55-degree hotplate to test a number of novel new compounds for their analgesic properties in comparison to morphine and methadone. They tested 2000 naïve mice and calculated a mean reaction time of 9.51 seconds +/- 1.02 seconds.

Pain researchers have used the hotplate assay extensively. However, there is still no consensus on the optimal test temperature, the effect of acclimatisation and habituation, or which response behaviours best correlate with pain. The literature suggests that a lower intensity stimulus (≤ 50 degrees Celsius) is more sensitive at detecting an effect, but produces greater variability in the response latency (517, 536). There are conflicting reports about the effect of habituation, with some researchers demonstrating a significant decrease in response latency (from 20 to 12 seconds) across trials when using a 50 degrees hotplate, but no change in sensitivity to the analgesic effects of morphine (517). Other researchers have demonstrated a significant repeated testing effect in mice tested 6 times at 30-minute intervals over a three-hour test period using a 59-degree hotplate, with a trend of decreasing latency with each test trial (537). In contrast, response latency was unaffected by repeated testing when a 55-degree hotplate was used with a short maximum exposure (20 seconds) (538).

A decrease in response latency represents an increased sensitivity to a noxious heat stimulus. This may be due to the influence of stress-induced anti-nociception (SIA), which in part is mediated via the endogenous opioid system (539). A novel test

environment, restraint or other physical stressors can all induce SIA (540). Repeated exposure to a noxious stimulus, whether during habituation or repeated test measures, will potentially reduce the effect of SIA and therefore result in an increase in sensitivity. This could be explained by the idea that different temperatures will recruit different populations of sensory afferents, some of which can be modulated by opioids (including endogenous opioids) and others that can't.

Prior to testing, mice were acclimatised by placing them in the Perspex cylindrical chamber for brief intervals of time (30 to 60 seconds), on four separate occasions over a one-week period. Two temperature settings, 42 degrees and 50 degrees Celsius, were used to optimise the test. These temperatures were selected for the following reasons:

- Exposure to temperatures greater than 42 degrees Celsius represents a shift in perception from innocuous warmth to noxious heat (541).
- There are a number of nociceptors that detect heat and have been implicated in the development of inflammation driven thermal hyperalgesia. The role of the TRPV1 receptor is the best characterised of these and this receptor is activated by noxious temperatures greater than 42 degrees Celsius (541).
- The literature suggests that a low intensity stimulus (≤ 50 degrees Celsius) is more sensitive at detecting a treatment effect.

Initially the hotplate was set to 42 degrees Celsius. Individual mice were placed in a cylindrical Perspex chamber, which lay over the hotplate and prevented escape. A lap timer was used to record the time at which the following observations first occurred:

- Shaking of front paw
- Licking/chewing of front paw
- Shaking of hind paw
- Licking/chewing of hind paw
- Jumping

Exposure to the hotplate did not exceed 60 seconds to avoid thermal injury to the ventral paw skin. Mice were then returned to their cage mates. After a 15-minute period of recovery the test was repeated with the hotplate temperature set at 50 degrees Celsius. Exposure to the hotplate for the second time did not exceed 30 seconds to avoid thermal injury to the ventral paw skin. Baseline measurements were taken on three separate occasions in the same 12 mice over a one-week period.

When the hotplate was set at 42 degrees Celsius only 2 out of 12 mice responded before the 60-second cut off. One mouse responded on only one occasion and one mouse responded for two out of three baseline tests. When the hotplate was set at 50 degrees Celsius all mice responded in less that 60 seconds, but there was significant within-mouse variability across the three baseline trials (Figure 3.2a), and significant between-mouse variability for any given baseline test [(mean ± SD (10.0 ± 3.0)]. This finding supported what other investigators have reported about the use of a low intensity stimulus (517, 536).

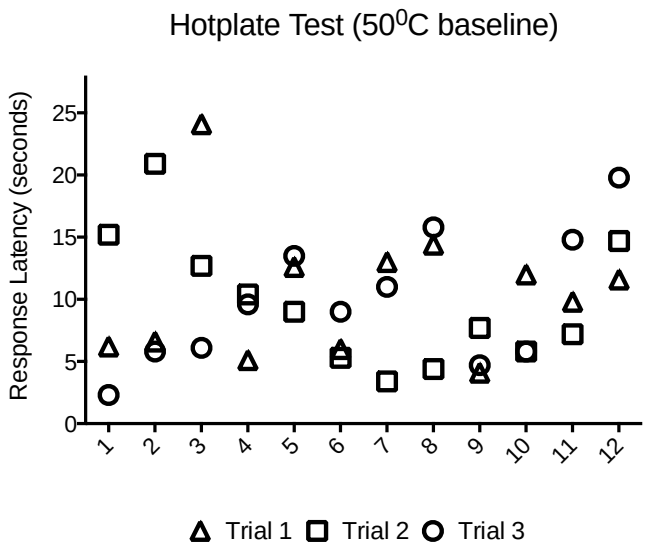

Figure 3.2a. Baseline paw withdrawal latency (PWL)

Hotplate set at 50°C. Graph demonstrates the variability in baseline PWL in naïve C57BL mice (n=12) tested three times over a one-week period (trial 1 – 3). The PWL endpoint was defined as either front limb or hind limb response.

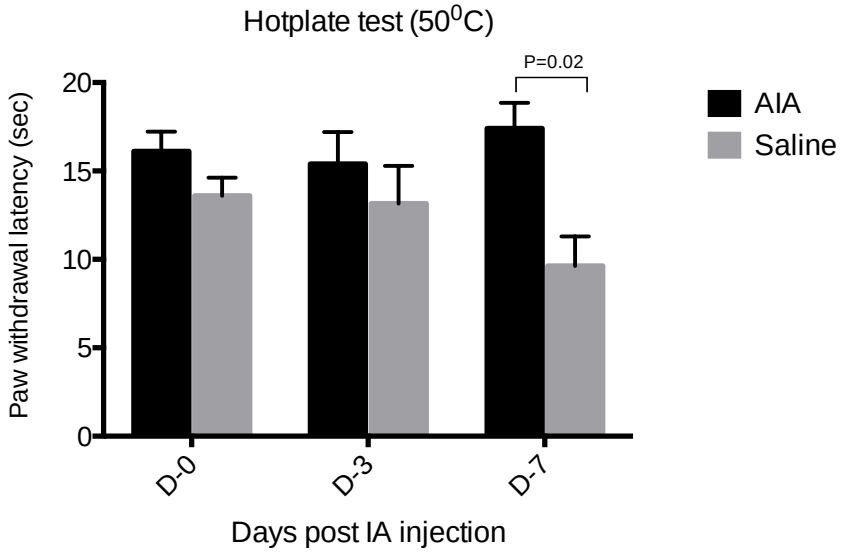

Figure 3.2b. Development of Hotplate test protocol

Baseline hind limb PWL when hotplate set at 50°C in C57BL mice (n=12). PWL endpoint defined as time to first attempt at shaking or licking hind paw. Testing was then repeated day 3 and day 7 following induction of AIA. At day 7, PWL in AIA was significantly increased compared to saline injected mice (P=0.02). The results are presented graphically as a bar graph of the means with SEM's marked.

Licking behaviour of the front paws was displayed when mice were grooming as well as in response to the noxious heat stimulus. Therefore, in some mice the time to first licking their front paw was very short and did not represent a withdrawal response to a noxious stimulus. It was also difficult to interpret jumping behaviour. Jumping behaviour was observed in many mice during acclimatization when the hotplate was in fact not turned on (room temperature). Therefore, jumping is an escape behaviour and not specifically related to pain. So mice that displayed jumping behaviour may have been attempting escape from the confinement of the chamber, or the noxious heat stimulus, or both. Despite acclimatisation, some mice had an aversion to being in the Perspex chamber and almost immediately attempted to escape by jumping.

Based on these observations, the following changes were made to the hotplate test protocol:

- Mice whose first response was to jump were eliminated from the study.
- The paw withdrawal latency (PWL) was redefined as time to first attempt at shaking or licking a hind limb. This avoided misinterpretation of grooming behaviour (licking the front paws) as a positive response to the thermal stimulus.

This protocol was then used to compare AIA mice and immunised saline injected mice at day 3 and day 7 (Figure 3.2b).

There was no significant difference in PWL between treatment groups at D0 or D3. At D7 there was a significant difference between treatment groups ($p=0.02$). However, this corresponded to a decrease in PWL in the saline group rather than the AIA group. There was no significant difference within each treatment group when comparing baseline (D0) to D3 or D7 post treatment (Table 3.2).

Table 3.2: Hotplate Test

Plate set at 50°C. End point described as hind limb paw withdrawal latency (PWL). (*) Paired data analysis using Wilcoxon signed-rank test (significance $p<0.05$). (**) Unpaired data analysis using Mann-Whitney test (significance $p<0.05$).

Treatment		**Baseline vs. D3**	**Baseline vs. D7**
Saline		0.35*	0.21*
AIA		0.60*	0.60*
	Baseline	**Day 3**	**Day 7**
AIA vs. Saline	0.26**	0.26**	0.02**

Therefore, development of thermal hyperalgesia could not be demonstrated in the AIA model when mice were exposed to a 50 degrees Celsius heat stimulus. Based on this finding the protocol for the hotplate test was revised further and tested on 12 additional mice. The TRPV2 channel is activated following exposure to temperatures greater than 52 degrees Celsius (206), and may also play a role in the development of inflammation driven thermal hyperalgesia (211). The hotplate settings were therefore increased to 52 and 55 degrees Celsius and mice were exposed to the stimulus for a maximum of 60 seconds. Two measures were taken for each temperature setting and the values averaged. Mice were rested for at least 15 minutes prior to retesting. At 55 degrees 10 out of the 12 mice displayed jumping behaviour on at least one of the trials. At 52 degrees only two mice displayed jumping behaviour on one of the trials, and the PWL was less variable within individual mice (Figure 3.2c).

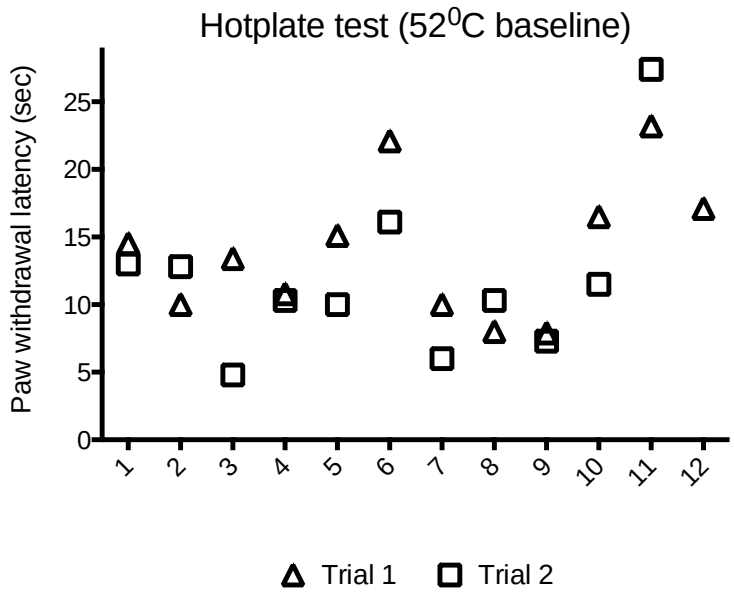

Figure 3.2c. Development of Hotplate test protocol

Baseline hind limb PWL when hotplate set at 52°C in C57BL mice (n=12). PWL endpoint defined as time to first attempt at shaking or licking hind paw. The higher temperature resulted in less variability in baseline PWL in mice (P = 0.42; trial 1 vs. trial 2)

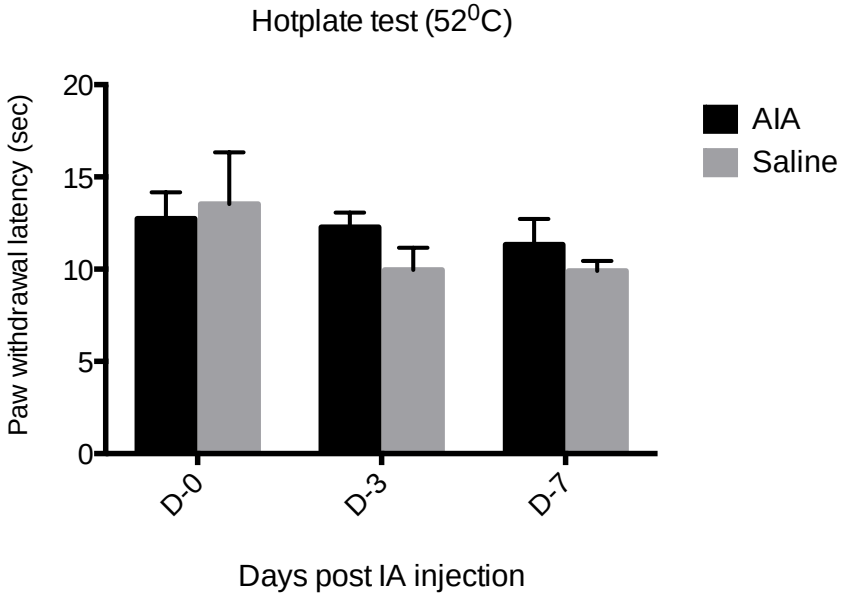

Figure 3.2d. Development of Hotplate test protocol

Hind limb PWL at day 0, day 3 and day 7 following induction of AIA in C57BL mice (n=6), in the right knee joint. Sham group (n=6) were immunised and received an intra articular saline injection. At day 3 and 7 PWL was decreased compared to baseline in both saline and AIA mice. The results are presented graphically as a bar graph of the means with SEM's marked.

Following the establishment of less variable hind limb withdrawal latency measurements from naïve mice, AIA was induced and testing repeated on Day 3 and day 7, post arthritis induction.

At 52 degrees Celsius the PWL was decreased at day 7 relative to baseline in both AIA and Saline groups, but the decrease was not statistically significant (AIA p=0.92; Saline p=0.25) (Figure 3.2d). There was no significant difference between AIA and saline at any of the test time points (Day 3 p=0.82; Day 7 p=0.12). While this experiment failed to demonstrate a significant change in hotplate hind limb latency with AIA up to 7 days post induction, the test itself was robust and repeatable.

3.1.3 Mechanical hyperalgesia

Knee joint hypersensitivity is measured clinically in OA patients to assess pain. This is usually done by directly squeezing the joint with a pressure-measuring device such as a pressure dolorimeter (542). Electronic devices such as these have been shown to produce less between-observer variability compared to manual techniques (543). However, it is only moderately reliable at differentiating OA patients from healthy controls, and is poorly correlated with other measures of pain intensity such as the McGill Pain Questionnaire (544).

The use of a commercial digital pressure application measurement (PAM) device (Ugo Basile, Italy) has the advantage of delivering a quantifiable force that can be directly applied to the knee joint. Baseline withdrawal thresholds (WT) are reported in rat models of inflammatory arthritis (518). The PAM device has been validated in both mice and rats (545), however, the majority of studies reporting the use of the PAM device were conducted in rats (453, 546, 547). The device's software produces a graphical readout of the pressure being applied in real time and this allows the rate

of increase in pressure to be controlled. Increasing the pressure applied at a consistent rate produces greater inter-operator agreement (545). It has been demonstrated that the ramp speed of a stimulus increase affects the response threshold, with an increased steepness resulting in increased thresholds (548). An optimal increase rate of 30g/s is recommended for mice when using the PAM device, and this translates to a maximum test time of 15 seconds when the maximum applied force is set at 450g (Figure3.3a).

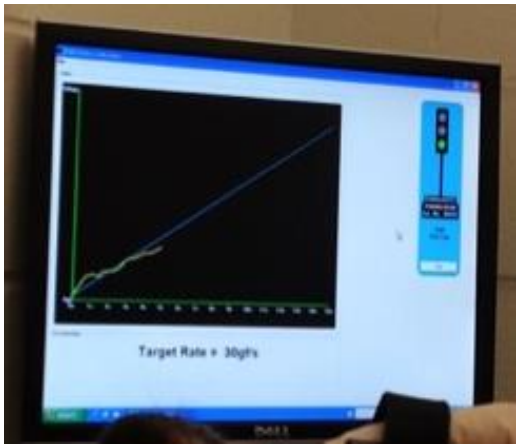

Figure 3.3a. Pressure Application Measurement (PAM) device

Screen shot of force/time graph with optimal rate of increase set at the recommended 30g/sec. Maximum test time = 15 seconds and maximum force = 450g.

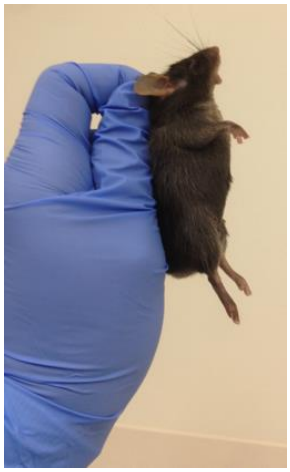

Figure 3.3b. PAM protocol restraint method

The mouse is cradled in the palm of the right hand while grasping the loose skin along the neck and back, with the tail secured between the palm of the hand and the last digit.

For mice a 5 mm circular probe is recommended to limit the size of the stimulus area. Unlike rats, mice require significant restraint to enable application of the circular probe over the area of the knee joint. Initially mice were removed from their home cage by grasping them at the base of the tail. They were then placed on the top of the wire lid, and while the left hand continued to gently hold the base of the tail, the right hand pinched the loose skin at the back of the neck. The tail was then released and the mouse cradled in the palm of the right hand while grasping the loose skin right along the neck and back, with the tail secured between the palm of the hand and the last digit (Figure 3.3b). The WT was determined for the right and left knee in naïve mice, by squeezing the knee between the thumb (with probe attached) and the index finger. There was considerable variability between the left and right limb in the majority of individual mice (Figure 3.3c).

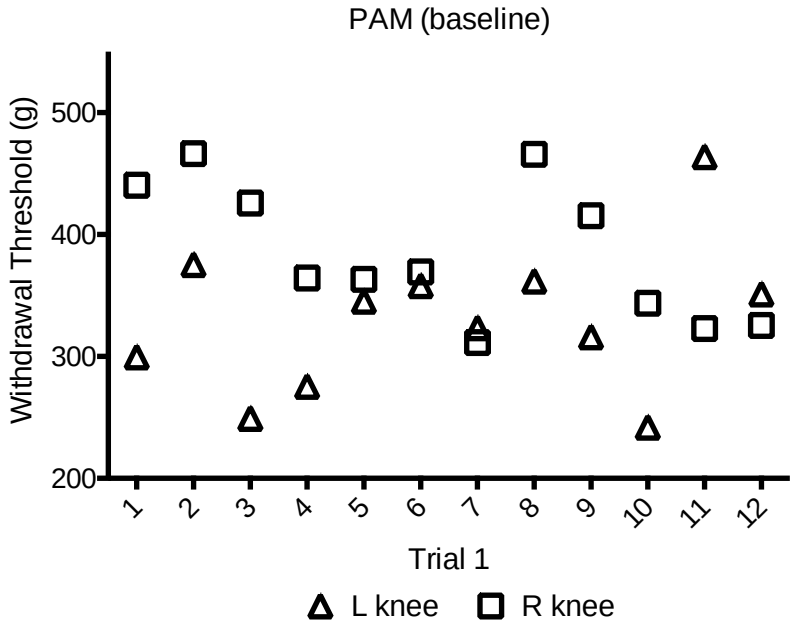

Figure 3.3c. Development of PAM device protocol

Baseline testing of naïve C57BL mice (n=12). Trial 1 graph illustrates considerable variability between left and right hind limb withdrawal threshold (WT) in the majority of mice (P = 0.033; right vs left WT).

A number of observations were made during baseline testing that may have contributed to the variability in PAM outcome. Some mice resisted restraint and vocalised when restrained prior to the application of the probe. These mice were released, allowed to recover and then restrained again. Other mice became very still and unresponsive when restrained, displaying a catalepsy-like state. Manipulation-induced behavioural arrest in response to restraint such as pinching the skin of the neck has been demonstrated in a number of prey species including mice and rabbits (549, 550). The response to having pressure applied to the knee varied between individuals; some simply turned and looked at their knee, some vocalised, some retracted their limb and struggled in an attempted to release themselves, and some displayed both of these behaviours.

The variability in baseline thresholds was attributed to the following:

- Differences in response behaviour between mice.
- Confounding effect of distress caused by the actual restraint method
- Confounding effect of manipulation-induced behavioural arrest (catalepsy)
- Variability in the exact anatomical location where the probe made contact with the knee, ie. medial vs. lateral joint compartment, patella-femoral vs femoro-tibial joint compartment.

To reduce this variability in baseline WT both within and between mice, the following modifications were made to the PAM protocol, and baseline testing was then performed on a new set of 12 mice.

- Each mouse was tested at four sites; medial and lateral knee joints on both left and right knees. The medial and lateral measurements from each side were combined and averaged to obtain a single WT value for the left and right knee.
- Mice who struggled and vocalised immediately following restraint were released and given time to recover before testing was attempted again.
- In mice that demonstrated catalepsy, mild head movement in the direction of the knee was considered a positive response.
- In mice that did not demonstrate catalepsy, purposeful limb withdrawal, struggling and/or vocalisation were all considered a positive response.

Mice were tested twice at each location to obtain an average withdrawal response.

Following these adjustments and with continued practice of the technique, baseline testing became less variable (Figure3.3d). AIA was then induced and testing repeated on day 7 and day 14, post arthritis induction (Figure 3.3e). This demonstrated a small decrease in left and right WT in both saline injected and AIA mice at day 7. This decrease reverted at day 14 except in the right hind limb of AIA mice. In AIA mice there was a significant decrease ($p = 0.035$) in right hind limb WT compared to the left hind limb at day 14. This confirmed the ability to detect a reduction in WT using the PAM device as described above, following the induction of arthritis.

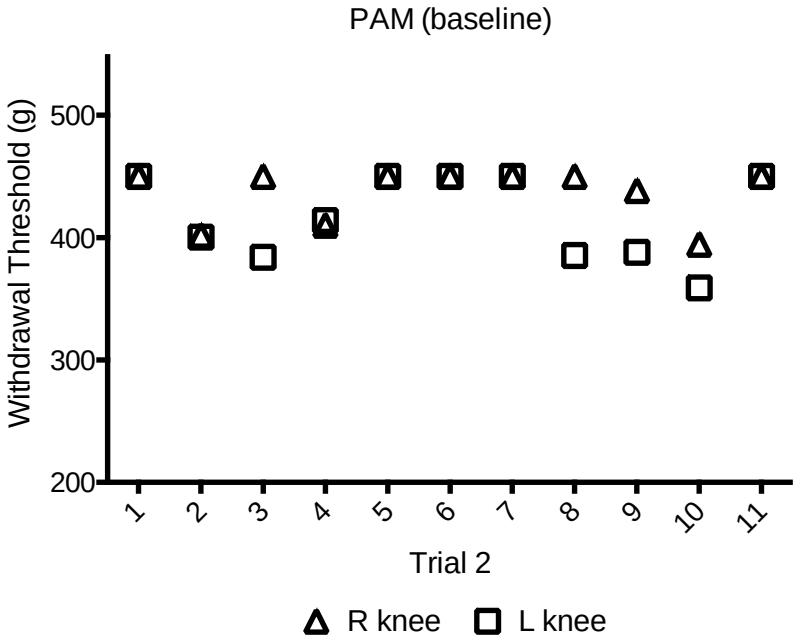

Figure 3.3d. Development of PAM device protocol

Baseline testing of naïve C57BL mice (n=12). Trial 2 graph illustrates reduced variability between left and right hind limb WT in all mice, following modifications to the testing protocol (as described in section 3.1.3).

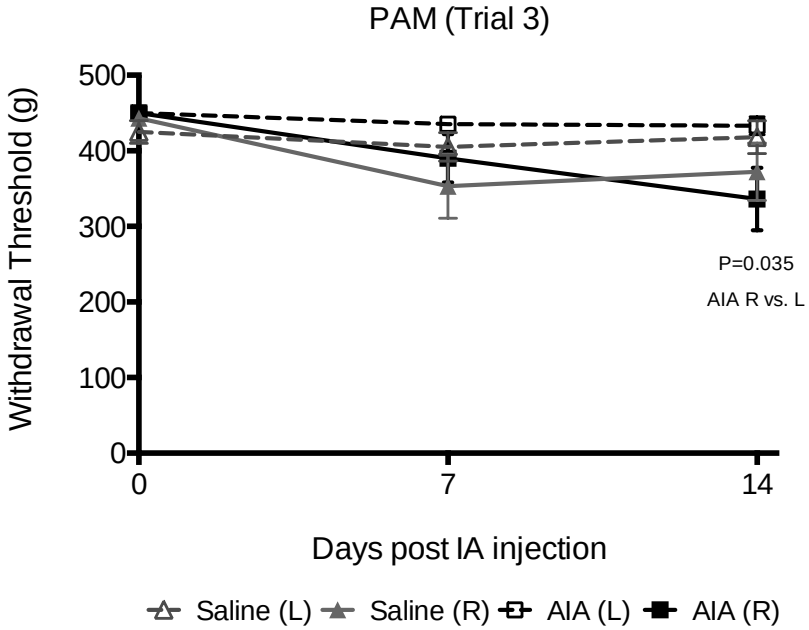

Figure 3.3e. Development of PAM device protocol

WT at day 0, day 7 and day 14 following induction of AIA in C57BL mice (n=6), in the right knee joint. Sham group (n=6) were immunised and received an intra articular saline injection. At day 14 (P=0.035) WT in the right knee was significantly decreased compared to the left knee in AIA mice. The results are presented graphically as a line graph of the means with SEM's marked.

3.1.4 Weight distribution

Hind limb weight distribution is considered a clinically relevant measure of OA pain (551). It mimics the clinical observation of pain on standing that is reported by OA patients.

A purpose built incapacitance tester was used to measure hind limb weight distribution (Figure 3.4a). This device quantifies the force applied to two precision force transducers over which lie metal plates where the hind paws of the test mouse are placed. A special Perspex chamber was also made, to restrain the mouse and enable visualisation of correct positioning. The transducers were linked to LabVIEW Run-Time Engine 2009 software (National Instruments, Australia) and a National Instruments-DAQmx hardware driver that enabled continuous data acquisition and graphical readout (Figure 3.4b), as well as the easy conversion of data to excel format for later viewing and analysis. Commercially available incapacitance testers such as the Columbus Instruments InCap do not provide a continuous readout, but rather give a single readout based on the average force applied over a pre set time interval, usually no more than a few seconds.

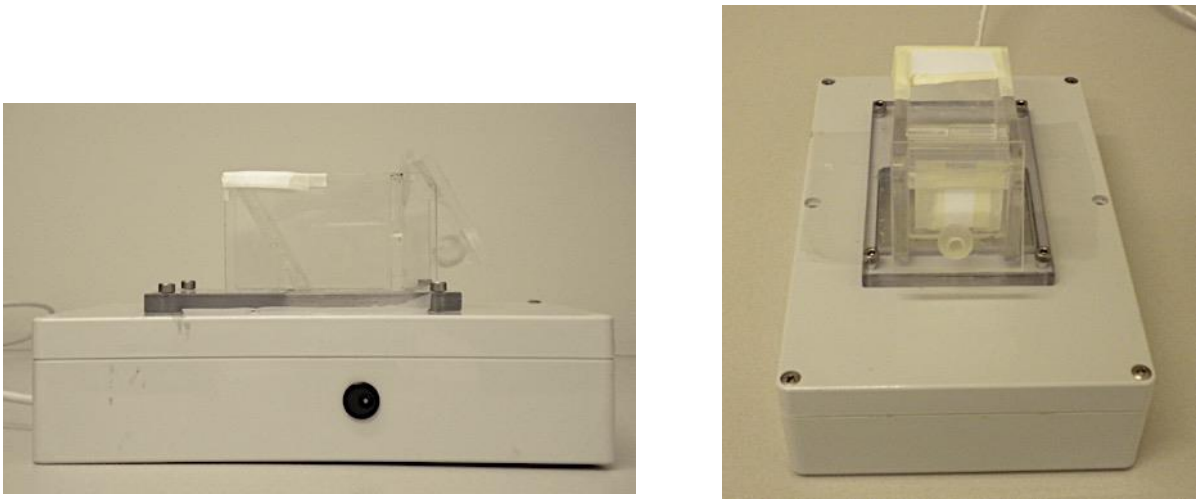

Figure 3.4a. Incapacitance device used to measure hind limb weight distribution.

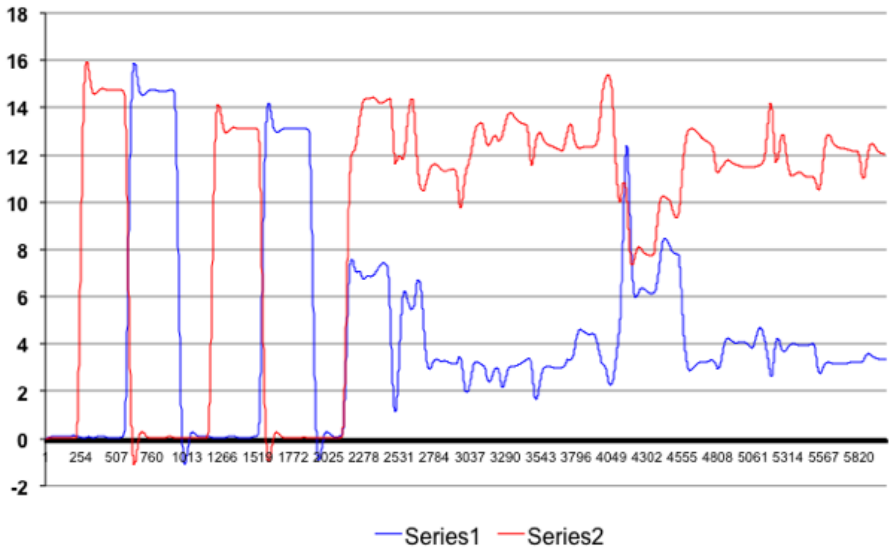

Figure 3.4b. Hind limb weight distribution

Graphical continuous readout of applied force of the right (series 1) and left (series 2) hind limb. Each 30-second test trial was preceded by 2 standard weight measurements (13.0g and 14.6g) to zero the instrument.

Mice were acclimatised prior to baseline testing by placing them in the chamber for 3-minute intervals on alternate days, the week before testing commenced. The continuous graphical readout enabled a number of observations to be made during this acclimatisation period.

- Even when mice appear to be still, they will shift their weight from limb to limb periodically.
- When male mice position their forelimbs on the front vertical wall of the Perspex chamber, their scrotum remains in contact with the force plates and this contributes to the force applied to each plate.
- Naïve mice with no prior musculoskeletal pathology will preferentially weight-bear on one particular hind limb and intermittently shift their weight.
- Subtle movements like turning the head to the left or right results in significant changes in hind limb weight distribution.

Based on these observations, it was evident that a single time point measurement would reflect an animal's weight distribution patterns less accurately than averaging the weight distribution measurements over a set time interval. A 30 second test period was selected. It was observed that mice become very agitated if confined in the test chamber for longer periods.

After placing the mouse in the test chamber, the tail was exteriorised and supported to ensure the base of the tail and the testicles were elevated off the force plates. The mouse was then allowed to settle in the chamber and get into the correct position, before testing commenced. This modification reduced the variability in baseline weight distribution in naïve mice (Figure 3.4c: Trial 1 vs. Trial 2). AIA was then induced and testing repeated on day 3 and day 7, post arthritis induction (Figure 3.4d). This demonstrated no change in hind limb weight distribution in saline injected mice

at day 3 or day 7. In AIA mice there was a significant change in hind limb weight distribution at day 3 ($p = 0.001$) and day 7 ($p < 0.001$). In fact, the right to left weight distribution ratio decreased from 1 to less than 0.5. This confirmed the ability to detect a change in R to L hind limb weight distribution using an incapacitance device as described above, following the induction of arthritis.

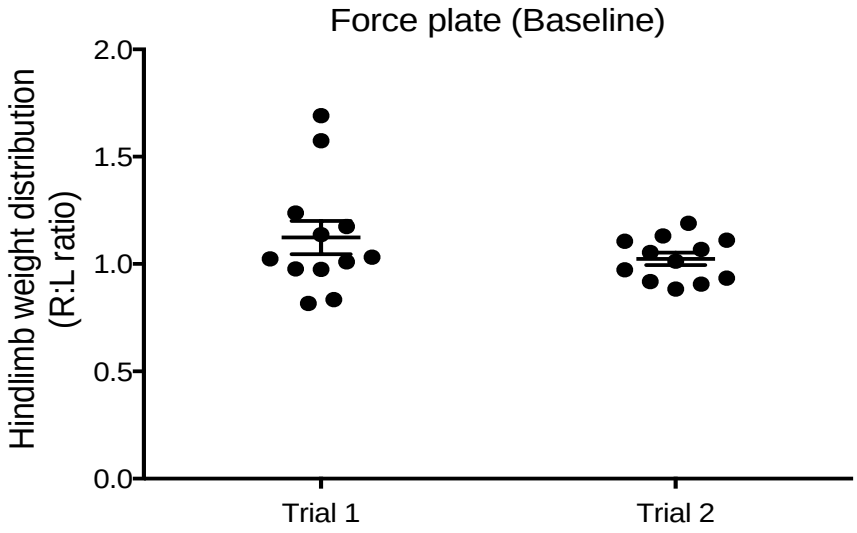

Figure 3.4c. Development of hind limb weight distribution test protocol

Baseline hind limb weight distribution in naïve C57BL mice (n=12). Trial-1 measurements are a single point in time measurement of applied force (right/left) in grams, recorded once the mouse was correctly positioned in the test chamber. Trial-2 measurements are the average of a 30 second continuous measurement of applied force (right/left) in grams, recorded during periods when the mouse was correctly positioned in the test chamber. The results are presented graphically as a scatter plot with means and SEM's marked.

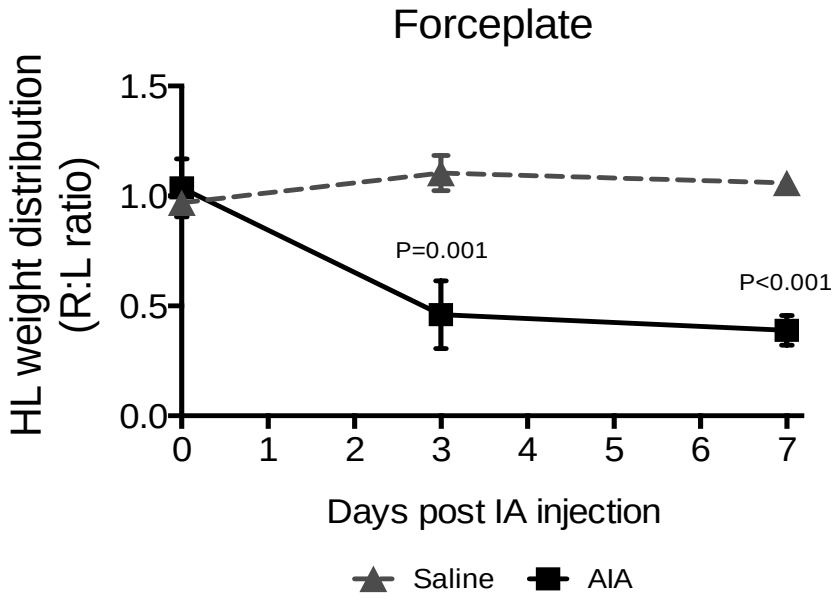

Figure 3.4d. Development of hind limb weight distribution test protocol

Hind limb weight distribution (R/L ratio) at day 0, day 3 and day 7 following induction of AIA in C57BL mice (n=6). Sham group (n=6) were immunised and received an intra articular saline injection. In AIA mice there was a significant decrease in the R/L weight distribution ratio at day 3 (P=0.001) and day 7 (P<0.001). The results are presented graphically as a line graph of the means with SEM's marked.

3.1.5 Stride length

The relationship between pain, disability and kinematics has been investigated extensively in humans with OA (552) however, the clinical significance of gait analysis as a tool for investigating the relationship between knee angles and moment, and pain and disability is still not clearly defined. It has been demonstrated that people with OA have a shorter stride length and walk more slowly than disease free adults (553). Stride length has also been measured in numerous animal models of arthritis using manual video recordings (554), video-based automated gait analysis systems (eg Catwalk™, Noldus Information Technology) (555), automated treadmills (556), digital imaging systems (e.g. DigiGait, Mouse Specifics, Inc.)(515), and paw print measurements (493).

For this study a one-metre-long clear Perspex tunnel was used (Figure 2.3e). The base of the run was lined with white thermal paper Each mouse was restrained by pinching the dorsal skin of the neck and non-toxic paint (Crayola, Australia Pty Ltd) applied to the ventral surface of the hind paws (Figure 2.3e). The mouse was then released into the tunnel, leaving its paw prints on the paper as it made its way to the end of the tunnel. The paper was removed and allowed to dry. The paw prints were then used to measure the distance between consecutive footprints from opposite limbs (right-to-left and left-to-right distance) and from the same limb (left-to-left and right-to-right distance) (Figure 3.5a).

After an initial test trial it was observed that many mice were hesitant to walk along the tunnel. In subsequent trials the sides and last third of the top of the tunnel were covered with black paper. This created a dark environment and encouraged mice to run to the end of the tunnel.

It was also observed that some mice stopped along the run to groom and/or urinate/defecate. Paw prints made during these activities were noted on the paper and not used to measure stride length, as this artificially reduced the average stride length (Figure 3.5b). Measurements were taken from a section where at least 5 consecutive, uninterrupted strides occurred.

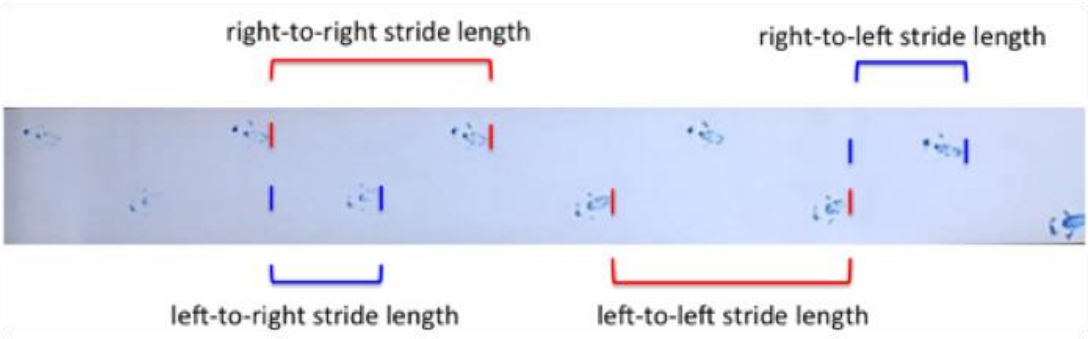

Figure 3.5a. Hind limb paw print trace for stride length measurement

The right-to-left and left-to-right stride lengths are labelled in blue. The right-to-right and left-to-left stride lengths are labelled in red.

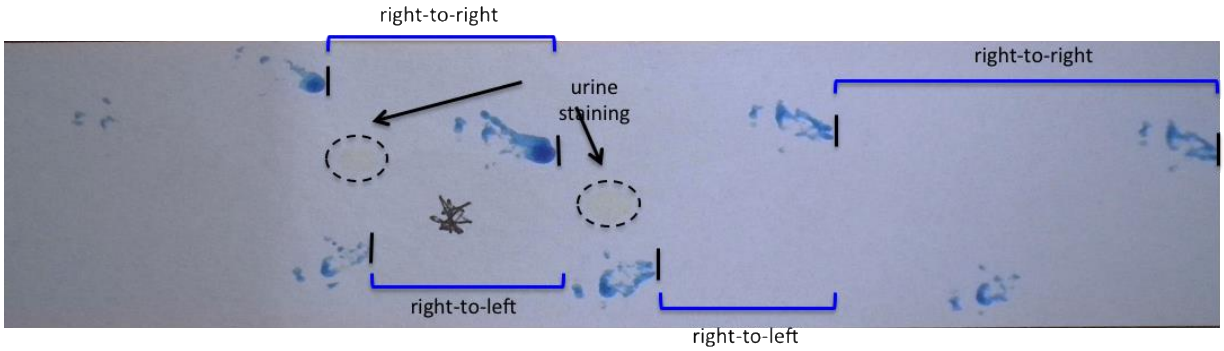

Figure 3.5b. Development of stride length measurement protocol

Hind limb paw print trace with urine stains marked (black dotted line). This trace illustrates the decrease in stride length (right-to-right) that occurs when mice stop to urinate or defecate. These artificially shortened strides were not used to calculate the average stride lengths

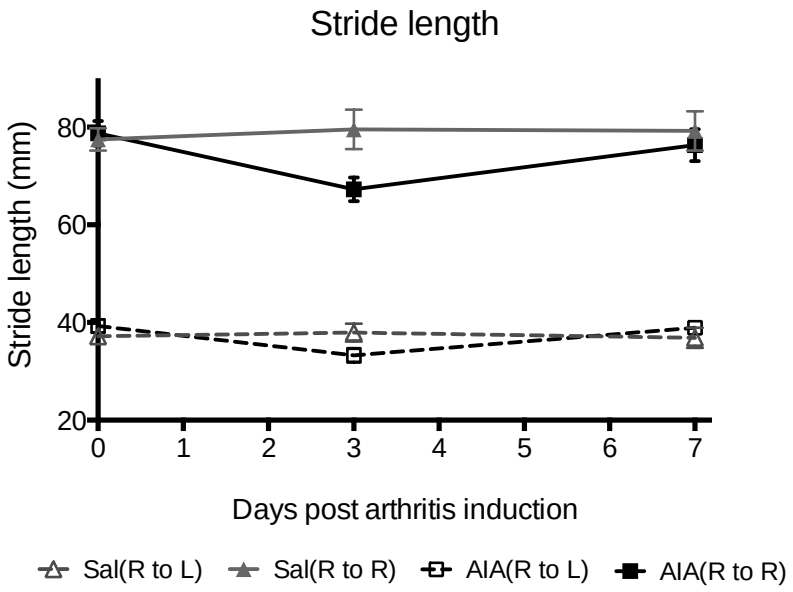

Figure 3.5c. Development of stride length measurement protocol

Hind limb paw print traces recorded at day 0, day 3 and day 7 following induction of AIA in C57BL mice (n=6). Sham group (n=6) were immunised and received an intra articular saline injection. Both stride length (right-to-left) and complete stride length (right-to-right) were reduced in AIA mice at day 3 compared to baseline. The results are presented graphically as a line graph of the means with SEM's marked.

Speed was not measured in this study, but it was apparent simply through visual observation that mice moved at different speeds along the run. Speed alters stride length (557) and so in many studies walking velocity is adjusted for when determining changes in stride length (515). However, speed itself changes with disease state and pain, and so adjusting for differences in walking speed may mask changes in gait that are in fact due to joint disease and/or pain. For example, Complete Freund's adjuvant (CFA) induced arthritis in rats results in both reduced velocity and a dramatic reduction in stride length (558).

In this study relative stride length was also determined by calculating stride length when supporting the affected limb (right-to-left) relative to complete stride length (right-to-right) as previously described (493, 559).

Following acquisition of baseline stride length data, AIA was induced and testing repeated on Day 3 and day 7, post arthritis induction. This showed firstly that both stride length measurements (right-to-left and right-to-right) were consistent pre-arthritis induction (Figure 3.5c day 0). Both stride length (right-to-left) and complete stride length (right-to-right) were reduced in the AIA mice at day 3 (Figure 3.5c) but then returned to baseline by day 7. This is similar to other studies that used the AIA model, where a decrease in stride length was only observed in the early acute phase of the disease (493).

3.1.6 Rotarod

The rotarod is an automated rotating rod that forces motor activity once a mouse or rat is placed on it. It has been used to test sensorimotor skills (balance and coordination) in a number of different animal models, including arthritis models in rats and mice (412, 560, 561).

In this experiment an accelerating rotarod was used (Ugo Basile, Italy) (Figure 3.6a), commencing at a speed of 4 rpm and accelerating to 40 rpm over a 300 second interval, and continuing for a total of 6 minutes (or until the mouse fell off the rod). To condition mice to the rotarod four training trials were conducted the week prior to commencing baseline testing. These involved 2 trials with a 15-minute rest interval between testing. As previously reported (520), latency to fall (LTF) was defined as time to fall or passive rotation, with passive rotation occurring when a mouse freely rotated on the rod for two consecutive revolutions.

To determine baseline and subsequent LTF values, one training trial was conducted followed by two test trials. The two test trials were used to determine the mean LTF. Mice were rested for 15 minutes between each test.

Despite conditioning the mice, there was considerable variability in baseline LTF between mice (range 198 – 400) (Figure 3.6b), with some mice displaying the ability to remain on the rotarod for much longer than the maximum 6 minutes. A ceiling value of 400 seconds did not truly reflect the LTF for those mice. During testing it was observed that mice developed different strategies for staying on the rod. For example, some mice used the side panel to lean on for support. This enabled them to take weight off the contralateral limb and still use the ipsilateral limb to walk and not fall off the rod. Other mice performed single passive revolutions at regular intervals to rest their hind limbs and therefore prevent falling.

Changes in LTF have best been demonstrated in animal models where arthritis is induced in both hind limbs (560) or in multiple limbs (412). This may be due to the fact that when multiple joints are affected it is difficult to compensate by shifting weight distribution to an unaffected limb and minimise the work done by the affected limb.

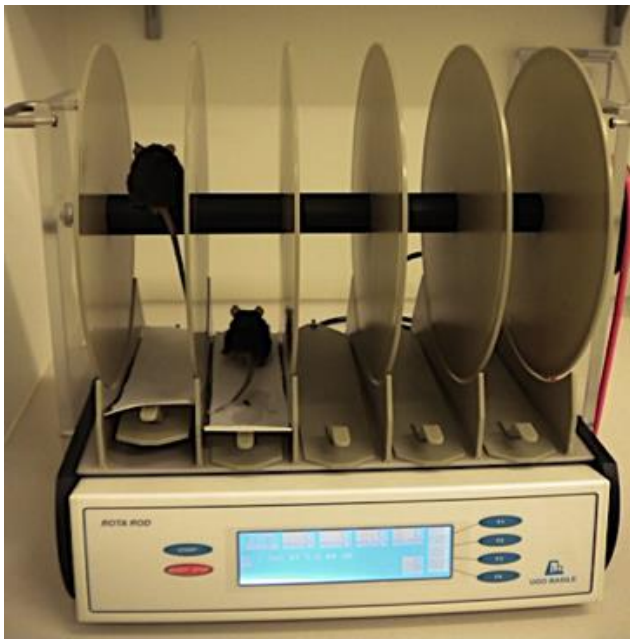

Figure 3.6a. Development of rotarod test protocol

The mouse in the first chamber is moving while the device is rotating and maintaining his balance. The mouse in the second chamber has lost balance and fallen off the rod.

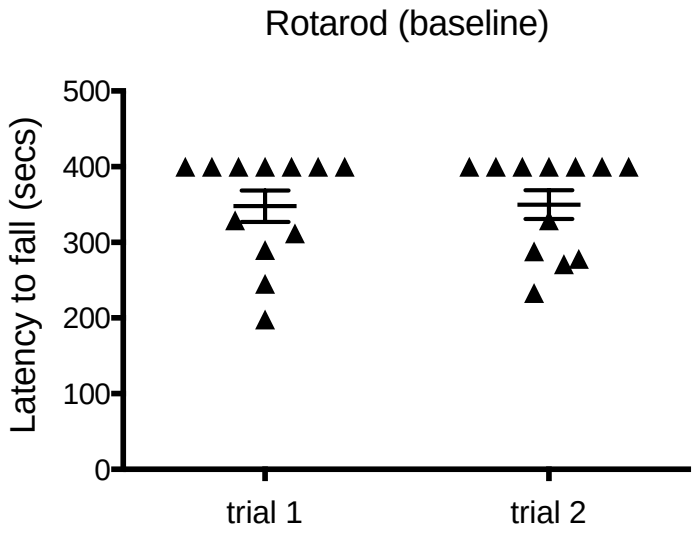

Figure 3.6b. Development of rotarod test protocol

Baseline latency to fall (LTF) measurements recorded in seconds. The rotarod commences rotating at a speed of 4 rpm, accelerates to 40 rpm over 300 seconds and continues for a total of 6 minutes. The graph illustrates the variability in baseline LTF in naïve C57BL mice (n=12) and how the number of animals that remained on the rotarod after 6 minutes skews the data. The results are presented graphically as a scatter plot with means and SEM's marked.

The decision was made not to continue with rotarod testing for the following reasons:

- The adaptive behaviours that were observed confounded any changes (or lack thereof) in LTF observed following induction of AIA.
- In subsequent experiments arthritis would be induced in only one knee joint, allowing for adaptive compensatory behaviours to develop.
- The ability of individual mice to stay on the rod for times that far exceeded 6 minutes meant that a maximum LTF of 400 seconds masked the extent of variability in LTF between individual animals.

3.1.7 Pain testing Conclusions

After conducting these preliminary pain behaviour experiments and testing the modified pain behaviour test protocols in the AIA model, the following tests were selected to conduct subsequent experiments in this thesis.

1. Von Frey
2. Hotplate 52°C
3. PAM – medial and lateral averaged for each knee joint
4. Forceplate – 30 second continuous reading averaged
5. Stride length – right-to-left and right-to-right stride

These pain behaviour tests were then used to define the pain phenotype in both arthritis models and investigating how this changes over time, and how it maps to knee joint pathology.

3.2 Histology scoring

Pathology in all joint tissues can be a feature of OA in humans. Synovitis, cartilage proteoglycan loss, loss of cartilage integrity and erosion, alterations in chondrocyte morphology, subchondral bone remodelling leading to erosion, increased vascularisation and thickening, and formation of marginal osteophytes and enthesiophytes, are features of knee joint histology changes in patients with symptomatic OA presenting for total knee replacement (TKR) (379). Different aspects of joint pathology feature in different OA phenotypes and at different stages of the disease; and only some have been associated with pain. Most patients with knee OA have medial compartment tibio-femoral joint (TFJ) OA, femora-patella joint (FPJ) OA, or a combination (562, 563). In this thesis, histological evaluation of TFJ pathology focused on the pattern of change observed in human patients. A method of evaluation was required to define and quantify the knee joint histopathology that developed in the two distinct mouse models that were used.

Reporting of OA joint pathology in mouse models has previously focused predominantly on the changes that occur in cartilage, and published recommendations such as The OARSI Histopathology Initiative (462) are aimed at standardising how histological sections are assessed. An additional challenge when it comes to assessing and reporting joint histopathology is that joint injury can result in both focal and diffuse joint pathology. In the case of the DMM model, pathology develops primarily in the medial compartment of the joint. Therefore, evaluating a pt-OA model requires scoring multiple sections of the joint in order to identify maximum and cumulative (total in all sections of the TFJ) pathology scores (462).

In contrast, histological evaluation of inflammatory arthritis models such as AIA has previously been determined on a single 6μm sagittal section corresponding to the

central weight-bearing region of the medial TFJ (439). This assumes inflammation is a global joint change. There are multiple scoring systems reported (452, 493, 521) and all focus on synovial changes (including cellular infiltration) and the degree of joint space inflammatory cell effusion.

A detailed scoring system (Appendix C) was developed to evaluate TFJ pathology in the two mouse models used in this study. It combined the evaluation of joint structural damage (articular cartilage and subchondral bone changes) using a similar scoring system to that described in the OARSI Histopathology Initiative (462), and the evaluation of joint changes associated with inflammation (synovitis, synovial hypertrophy and joint cellular infiltration). To enable comparison between the two arthritis models, histological evaluation of knee joints was done on a single 6μm sagittal section that corresponded to the central weight-bearing region of the medial TFJ.

The following validations were performed before adopting the scoring system to compare the two arthritis models over time, and investigate the relationship between specific joint pathology features and pain outcome measures.

1. Serial sagittal sections across the width of the medial TFJ from DMM, Sham, AIA and Saline injected control mice at day 7 and day 28 following induction of arthritis (n=6 mice per treatment group), were scored using the measures of joint inflammation defined in Appendix C. Two (2) independent observers who were blinded with regard to treatment, joint region and time performed the scoring. The maximum score for each of the joint inflammation parameters irrespective of the slide was recorded. The scoring system demonstrated a significant and repeatable difference between treatment groups and within treatment group (AIA, DMM, Sham) over time (day 7 vs. day 28) (Figure 3.7a). The differences over time for

DMM and Sham demonstrated the sensitivity of the scoring system, as it was able to quantify post-surgical inflammation (evident in DMM and Sham groups at day 7), and inflammation associated with OA disease (evident in DMM only at day 28). The scoring system also demonstrated low inter-observer variability of individual scores and total scores (Figure 3.7b).

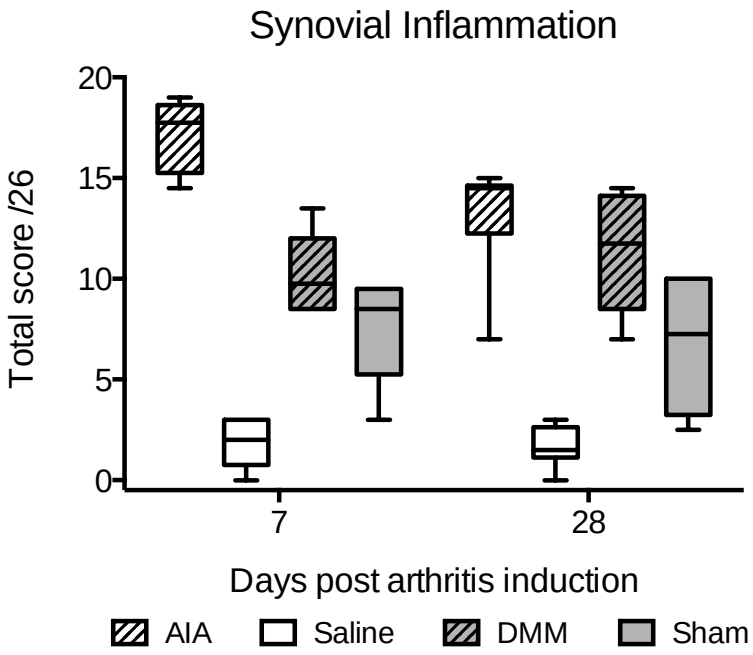

Figure 3.7a. Synovial inflammation

This graph represents the maximum score for each of the joint inflammation parameters irrespective of the slide. Serial sagittal sections across the width of the medial tibio-femoral joint from DMM, Sham, AIA and saline injected mice (n=6 per treatment group) at day 7 and day 28 following induction of arthritis, were scored using the measures of inflammation defined in Appendix C. The results are presented graphically as box plots, with medians marked, 95% (upper bounds) and 5% (lower bounds) percentiles hinged, and whiskers depicting upper and lower limits of dataset.

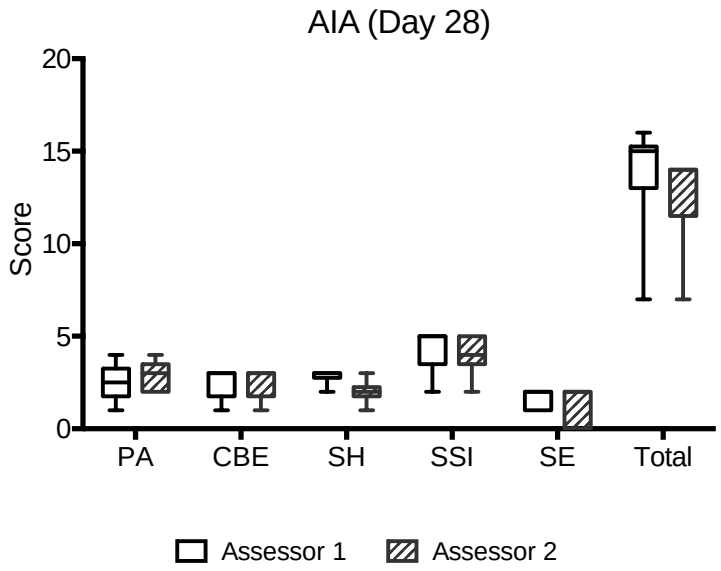

Figure 3.7b. Inter-observer variability

This graph represents the inter-observer variability for both individual (panus-PA, cortical bone erosion-CBE, synovial hyperplasia-SH, sub-synovial inflammation-SSI, synovial exudate-SE) and total inflammation scores of AIA mice (n=6) at day 28 following induction of arthritis. Scoring was performed by two independent observers blinded with regard to treatment, joint region and time, The results are presented graphically as box plots, with medians marked, 95% (upper bounds) and 5% (lower bounds) percentiles hinged, and whiskers depicting upper and lower limits of dataset.

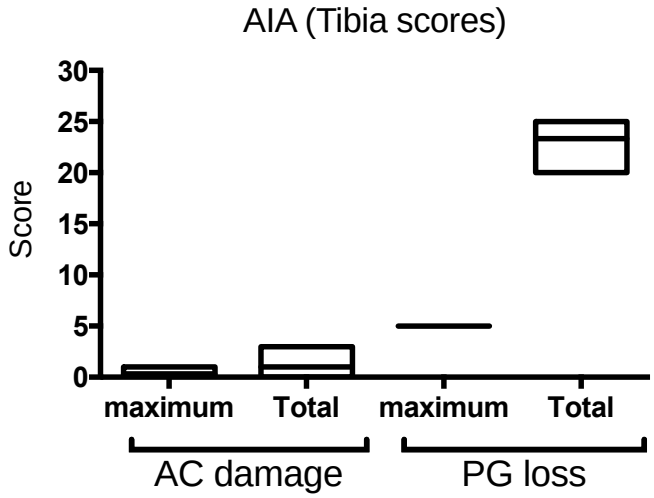

Figure 3.7c. Serial sagittal section scores

This graph represents the combined scores of serial sagittal sections across the width of the medial TFJ for tibial articular cartilage (AC) damage (mean = 0.33, SEM = 0.33) and tibial proteoglycan (PG) loss (mean = 5.0, SEM = 0.0) for AIA mice (n=4). Scores were similar across all sections of the medial compartment indicating the central weight-bearing region is a suitable site for scoring maximum joint damage. The results are presented graphically as floating bars (minimum and maximum) and a line at the mean.

2. In AIA mice (n=4), serial sagittal sections of the medial TFJ were scored by two independent observers blinded to joint region, to determine if structural joint changes were similar across the entire medial compartment of the joint and therefore whether the central weight-bearing section reflected the maximum cartilage damage score. Scores were similar across all sections of the joint (Figure 3.7c), indicating that the central weight-bearing region was a site of maximum joint damage.
3. In DMM mice, serial sagittal sections of the medial TFJ were scored by two independent observers, blinded to joint region, to determine the maximum cartilage damage score based on serial sections and compare with scores from the central weight-bearing section. There was no significant difference between the central weight-bearing region score and the maximum articular cartilage damage score when determined by scoring serial sections (Figure 3.7d).
4. In DMM mice, sagittal sections corresponding to the site of maximum inflammation score, the maximum articular cartilage damage score and the central weight-bearing region of the medial compartment of the TFJ were scored (n=3) at seven time points (day 3, week 1, 2, 4, 8, 12, 16), by two independent observers who were blinded to joint region and time (Figure 3.7e). At all time points the inflammation score was not significantly different between the central weight-bearing section and the maximum articular cartilage structural damage section. At week1, 4, 12 and 16 these two sections both reflected the maximum joint inflammation score.

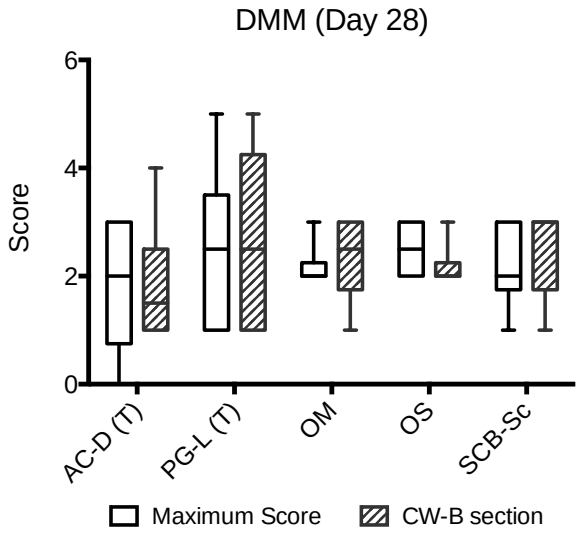

Figure 3.7d. Maximum score vs. central weight bearing section

This graph represents the maximum scores determined by scoring serial sagittal sections across the width of the medial compartment of the TFJ and the central weight-bearing (CW-B) section scores for each measured parameter: tibial articular cartilage damage (AC-D (T)); tibial proteoglycan loss (PG-L (T)); osteophyte maturity (OM); osteophyte size (OS) and subchondral bone sclerosis (SCB-Sc); from DMM mice (n=6) 28 days after induction of arthritis. The results are presented graphically as box plots, with medians marked, 95% (upper bounds) and 5% (lower bounds) percentiles hinged, and whiskers depicting upper and lower limits of dataset.

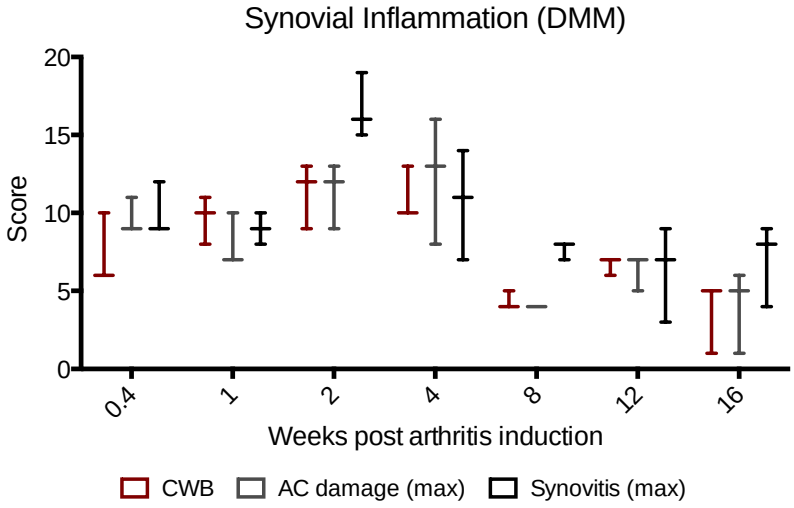

Figure 3.7e. Synovial inflammation comparative scores

This graph represents histology scores for sagittal sections corresponding to the site of maximum inflammation score (synovitis max.), maximum articular cartilage damage score (AC damage max.) and the central weight-bearing region (CWB) of the medial compartment of the TFJ from DMM mice (n=3) day 3, week 1, 2, 4, 8, 12 and 16 after induction of arthritis. The results are presented graphically as box plots, with medians marked and whiskers depicting upper and lower limits of dataset.

Taken together, these findings indicated that both maximum articular cartilage damage and global joint inflammation can be reliably quantified, and compared between treatment groups, by evaluating a single histological section at the level of the central weight-bearing region of the medial TFJ, using the scoring system described in this thesis (Appendix C).

CHAPTER 4: Knee joint histopathology following destabilization of the medial meniscus (DMM) and antigen-induced arthritis (AIA) in mice

4.1 Introduction and aims

In this current chapter, the progressive histopathological changes that occurred in different knee joint tissue structures, following induction of arthritis using two distinct arthritis models are evaluated and compared.

The knee joint is a complex organ comprising cartilage, subchondral bone, synovium, capsule, ligaments, tendons and muscles; and pathology of all joint tissue structures is a feature of OA in humans (70). Inflammation is a major feature of animal models such as AIA, and inflammation also plays a significant role in the pathogenesis of OA in humans (70). In fact, joint inflammation (synovitis) is one of the few joint pathologies of OA that has been shown to correlate with disease symptoms (74, 75).

Histopathology is the gold standard by which to measure joint pathology in animal models of arthritis. However, different methods and scoring systems have been reported for the two animal models used in this thesis (25, 26, 439, 448). In order to better compare joint pathology changes over time in the two models, the same processing methods and scoring system were used. The scoring system used quantifies all aspects of OA joint pathology, allowing further investigation into whether different stages of disease and different disease phenotypes (inflammatory vs. post-traumatic) demonstrate different patterns of joint pathology. The scoring system also provides scope for investigating the relationship between pain and specific joint pathologies at different stages of OA disease.

The aims of chapter 4 are:

1. To characterize the histopathology changes that develop in the knee joint following induction of arthritis using two murine models (AIA and DMM), including the temporal pattern of these changes.
2. To identify any associations between the different tissue pathologies that develop over time, and compare these associations between the two murine models to identify key features that might link the models to different human OA phenotypes.

4.2 Methods, statistical analysis and data presentation

Details of the methods used to induce the two models of arthritis, DMM and AIA, are described in chapter 2, section 2.1. The methods used for histological processing, sectioning and staining are described in chapter 2, section 2.2. The scoring system used is outlined in Appendix C. Development and validation of this scoring system is described in chapter 3, section 3.2.

Comparison of histopathology scores between treatment groups and time points were analysed using the nonparametric ranked Kruskal-Wallis analysis for multiple groups and, where there was significance, the Mann Whitney U-test (for unpaired data) was performed for between group comparisons (StataSE software, Stata corporation, TX, USA). The Benjamini-Hochberg correction (564) was applied to the *P* values of the histology scores. The resulting *P* values for each histology score, when the alpha level was set at 0.05, are summarized in Table 4.1a and 4.1b. The results are presented graphically as box plots, with medians marked, 95% (upper bounds) and 5% (lower bounds) percentiles hinged, and whiskers depicting upper and lower limits of the dataset.

Associations between the different histology scores were determined by generating partial correlation coefficients, using Kendall's tau-b (565). This nonparametric process uses pairwise ranked data values between the two variables under study (ordinal scores) and thus does not require data to be normally distributed or the relationship between the variables to be linear. The Benjamini-Hochberg correction was applied to the *P* values of the histology associations for each score, resulting in $P < 0.022$ being considered significant when the alpha value was set at 0.05.

Ordinal logistic regression was used to determine whether the histology outcome variables changed over time; and correcting for time, whether there was a difference between treatments. The Benjamini-Hochberg correction was applied to the *P* values of the time and treatment effects for each score, resulting in $P < 0.035$ being considered significant when the alpha value was set at 0.05.

Since AC damage is the hallmark of human OA and radiographic joint space narrowing is still used to diagnose and grade the disease; AC damage was assigned as the dependent variable and odds ratios were calculated to determine what factors increase the risk of joint disease developing in the two arthritis models. In human OA, synovitis is more strongly associated with pain than AC damage (74), and so in separate analyses synovitis was also assigned as a dependent variable and odds ratios were calculated to determine what factors increased the risk of synovitis developing in the two arthritis models.

In the results, 'significance' refers to statistical significance, with *P* values included in the results tables.

4.3 Results

Representative histological sections of the knees of mice day 3, week 1, 2, 4, 8, 12 and 16 after induction of arthritis (DMM and AIA), and age matched control mouse joints are presented in Figures 4.1a to 4.1c. Marked differences in joint histological features were observed between treatment groups and many histopathological features demonstrated a model-specific temporal pattern of change. These differences between models and with time, are readily apparent in outcomes of quantitative scoring of arthritis pathology.

4.3.1 Effect of AIA and DMM on inflammation following induction of arthritis

Joint inflammation was defined as synovitis. Synovial inflammation was evident in AIA, DMM and sham surgery mice from day 3 following induction of arthritis. In both models it peaked at week 2 and then decreased gradually until week 16 (Figures 4.2c). Synovitis was significantly increased in AIA mice compared to saline injected mice at all time points (Figure 4.2a). Synovitis was significantly increased in DMM mice compared to sham surgery mice at day 3, week 1 and week 16, and significantly increased compared to age matched controls at week 4, 8, 12 and 16 (Figure 4.2b). Sham surgery resulted in less synovitis than DMM at all time points. After week 4, there was no significant difference between sham surgery mice and age match controls. AIA mice developed significantly greater synovitis compared to DMM mice at week 1, 2, 4, 8 and 12 (Figure 4.2c).

Table 4.1a Joint histopathology scores in AIA and DMM

Score	Time (W)	DMM vs Sham	DMM vs AIA	AIA vs saline
Synovitis[1]	0.4	**0.019**	0.053	**0.004**
	1	**0.006**	**0.005**	**0.002**
	2	0.198	**0.004**	**0.004**
	4	0.053	**<0.001**	**<0.001**
	8	0.084	**<0.001**	**<0.001**
	12	0.060	**<0.001**	**<0.001**
	16	**0.008**	0.025	**<0.001**
PG loss[2]	0.4	0.794	0.048	**0.026**
	1	0.433	**0.002**	**0.001**
	2	**0.004**	**0.002**	**0.002**
	4	**<0.001**	**0.005**	**<0.001**
	8	**<0.001**	**<0.001**	**<0.001**
	12	**0.004**	**<0.001**	**<0.001**
	16	**<0.001**	**<0.001**	**<0.001**
AC damage[3]	0.4	0.800	0.040	0.140
	1	0.101	0.320	**0.022**
	2	**0.004**	0.070	**0.016**
	4	**<0.001**	**0.017**	**<0.001**
	8	**<0.001**	0.423	**<0.001**
	12	**0.004**	**<0.001**	**<0.001**
	16	**<0.001**	0.054	**<0.001**
Osteophyte maturity[4]	0.4	-	-	-
	1	0.058	**0.009**	-
	2	**0.002**	**0.002**	-
	4	**<0.001**	**<0.001**	-
	8	**<0.001**	**0.020**	**0.020**
	12	**0.003**	**0.011**	**0.003**
	16	**<0.001**	**<0.001**	**<0.001**
Osteophyte size[5]	0.4	-	-	-
	1	0.058	**0.009**	-
	2	**0.002**	**0.002**	-
	4	**<0.001**	**<0.001**	-
	8	**<0.001**	0.051	**0.020**
	12	**0.003**	**0.003**	**0.003**
	16	**<0.001**	0.291	**<0.001**
SCB sclerosis[6]	0.4	0.935	0.317	0.390
	1	0.342	**0.008**	**0.003**
	2	0.031	**0.002**	**0.022**
	4	**0.002**	**<0.001**	0.045

	8	**0.002**	0.738	0.277
	12	0.145	**0.002**	**<0.001**
	16	0.028	**<0.001**	**0.002**
SCB vascularity[7]	0.4	0.794	**0.005**	0.065
	1	0.338	**0.009**	**0.015**
	2	**0.012**	**0.002**	**0.002**
	4	0.107	**0.004**	**0.003**
	8	0.459	0.858	0.299
	12	0.332	0.862	0.125
	16	0.393	0.072	0.050
Chondrocyte hypertrophy (cell death)[8]	0.4	**0.002**	0.326	**0.002**
	1	**0.007**	0.053	**<0.001**
	2	**0.003**	1.000	**0.002**
	4	**<0.001**	**0.033**	**<0.001**
	8	**<0.001**	**0.004**	**<0.001**
	12	**0.007**	**<0.001**	**<0.001**
	16	**<0.001**	**<0.001**	**<0.001**

Knee joint histopathology scores between treatment groups (DMM vs. Sham, DMM vs. AIA, and AIA vs. Saline) comparisons using Kruskal-Wallis analysis followed by Mann-Whitney U-test. After Benjamini-Hochberg correction, 5% confidence level is $P < 0.025^{(1)}$, $P < 0.026^{(2)}$, $P < 0.022^{(3)}$, $P < 0.02^{(4)}$, $P < 0.02^{(5)}$, $P < 0.022^{(6)}$, $P < 0.015^{(7)}$, $P< 0.033^{(8)}$. P-values shown in bold typeface are significant below after correcting for multiple comparisons.

Table 4.1b Synovitis histolopathology scores in DMM and AIA

Time (weeks)	Panus[1]	Cortical bone erosion[2]	Synovial hyperplasia[3]	Sub synovial inflammation[4]	Synovial exudate[5]
0.4	0.371	0.089	0.224	0.053	0.150
1	0.392	**0.004**	0.231	**0.004**	**0.011**
2	**0.005**	**0.003**	**0.005**	**0.005**	**0.005**
4	**0.013**	**<0.001**	**0.005**	**<0.001**	**<0.001**
8	0.140	**0.023**	**0.002**	**0.001**	**<0.001**
12	**0.003**	**0.008**	**0.001**	**<0.001**	**0.002**
16	0.271	0.163	0.242	**0.002**	**0.001**

Knee joint histopathology synovitis scores, DMM vs. AIA, comparisons using Kruskal-Wallis analysis followed by Mann-Whitney U-test. After Benjamini-Hochberg correction, 5% confidence level is $P < 0.013^{(1)}$, $P < 0.023^{(2)}$, $P < 0.005^{(3)}$, $P < 0.005^{(4)}$, $P < 0.011^{(5)}$. P-values shown in bold typeface are significant below after correcting for multiple comparisons.

Figure 4.1a. OA knee joint histopathology – Acute inflammatory phase

Representative sections of knee joint day 3, week 1 and 2 post induction of arthritis in DMM, Sham surgery, AIA and Saline injected mice. Images are toluidine blue stained saggital sections near the central weight-bearing region of the joint. X5 magnification

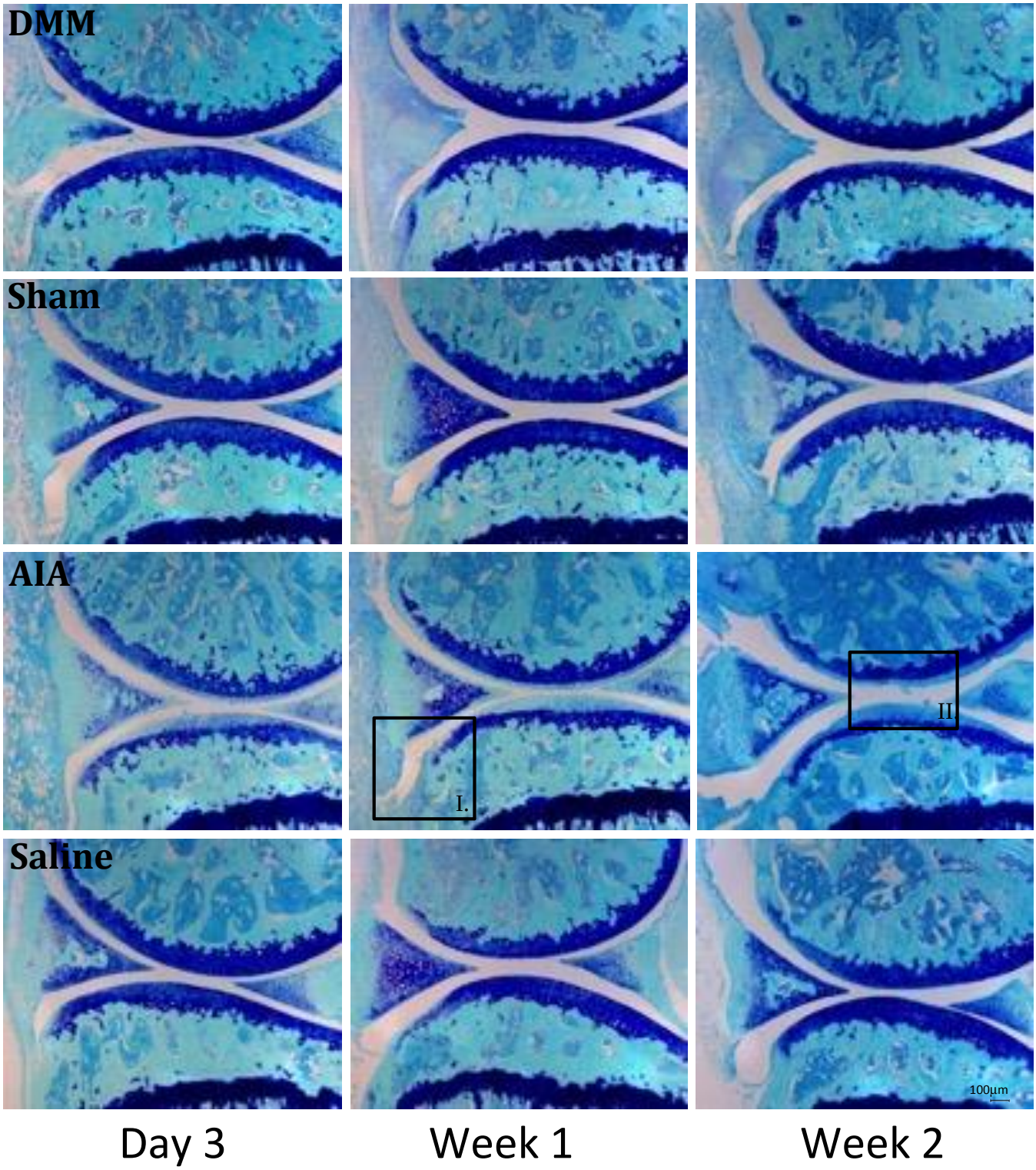

Insert I = Synovitis at week 1

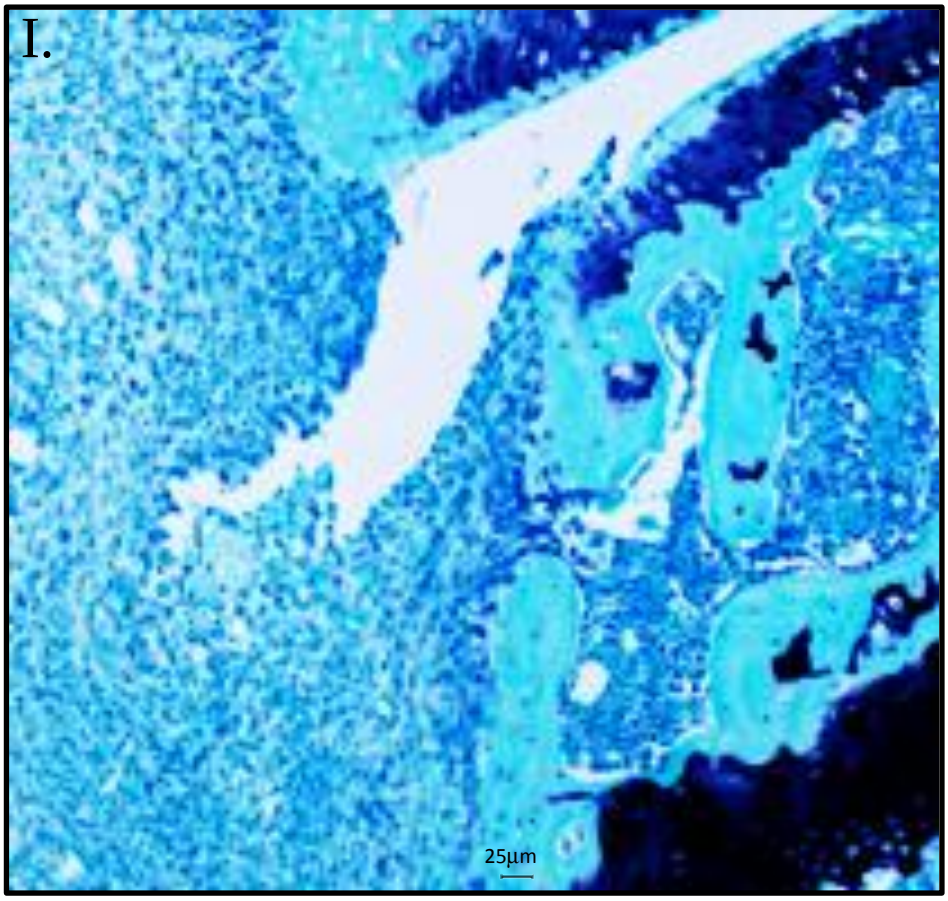

Insert II = PG loss and SCB vascular invasion at week 2.

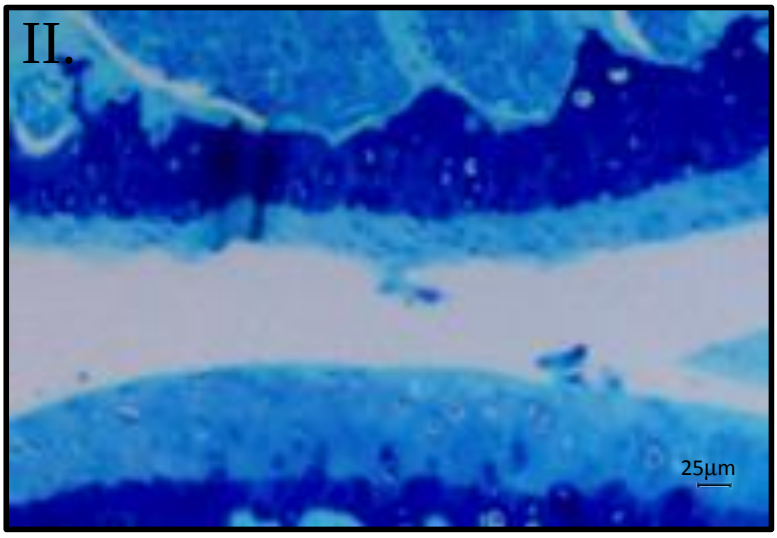

Figure 4.1b. = OA knee joint histopathology – Early progressive OA

Representative sections of knee joint week 4 and 8 post induction of arthritis in DMM and AIA mice. Sham surgery and Saline injected mice included for comparison. Images are toluidine blue stained saggital sections near the central weight-bearing region of the joint. X5 magnification
Insert III = osteophyte formation at week 8

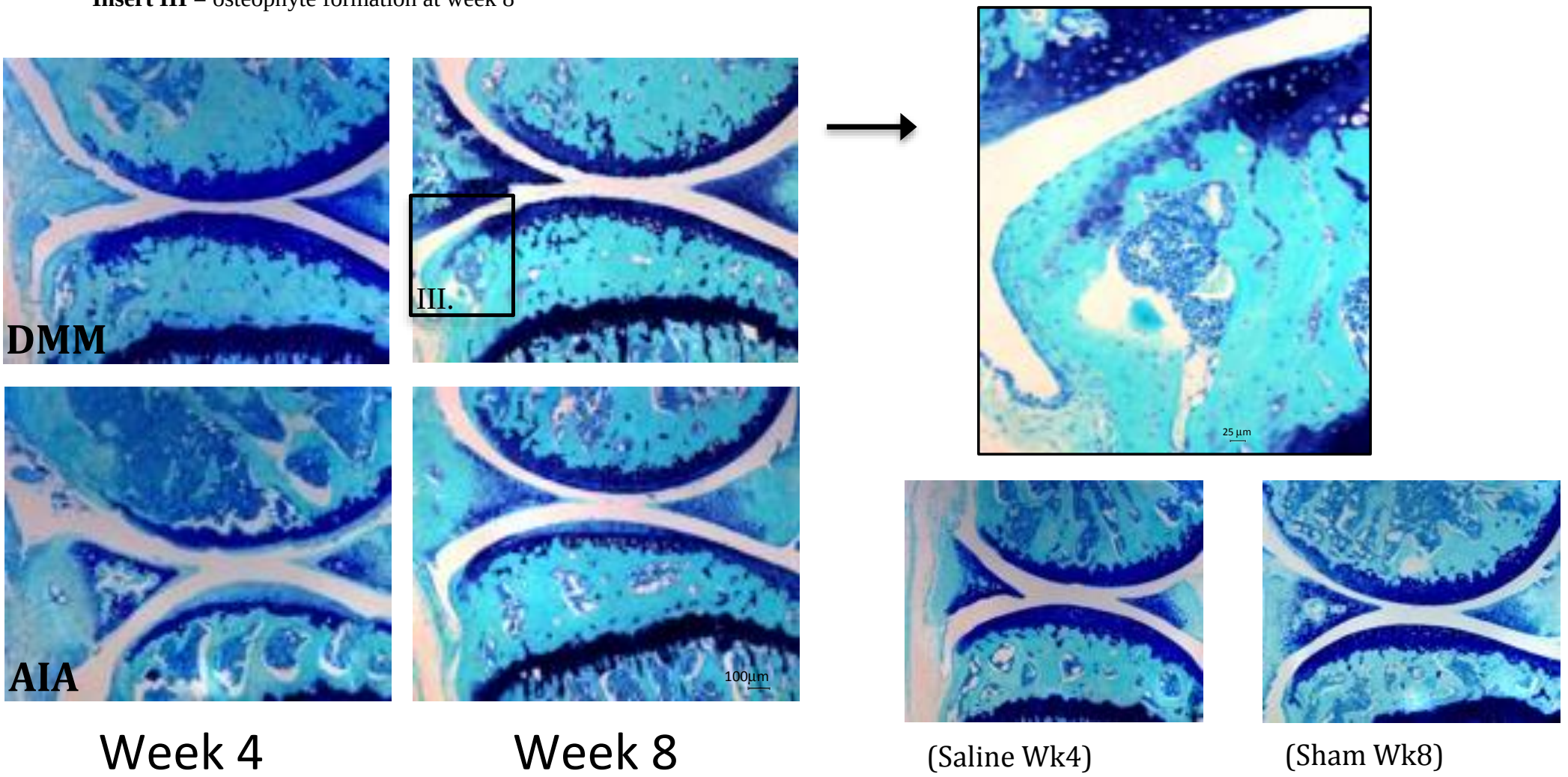

Figure 4.1c. = OA knee joint histopathology – Late chronic OA

Representative sections of knee joint week 12 and 16 post induction of arthritis in DMM and AIA mice. Sham surgery and Saline injected mice included for comparison. Images are toluidine blue stained saggital sections near the central weight-bearing region of the joint. X5 magnification **Insert IV** = SCB sclerosis at week 12; **Insert V** = AC damage and joint space narrowing at week 16.

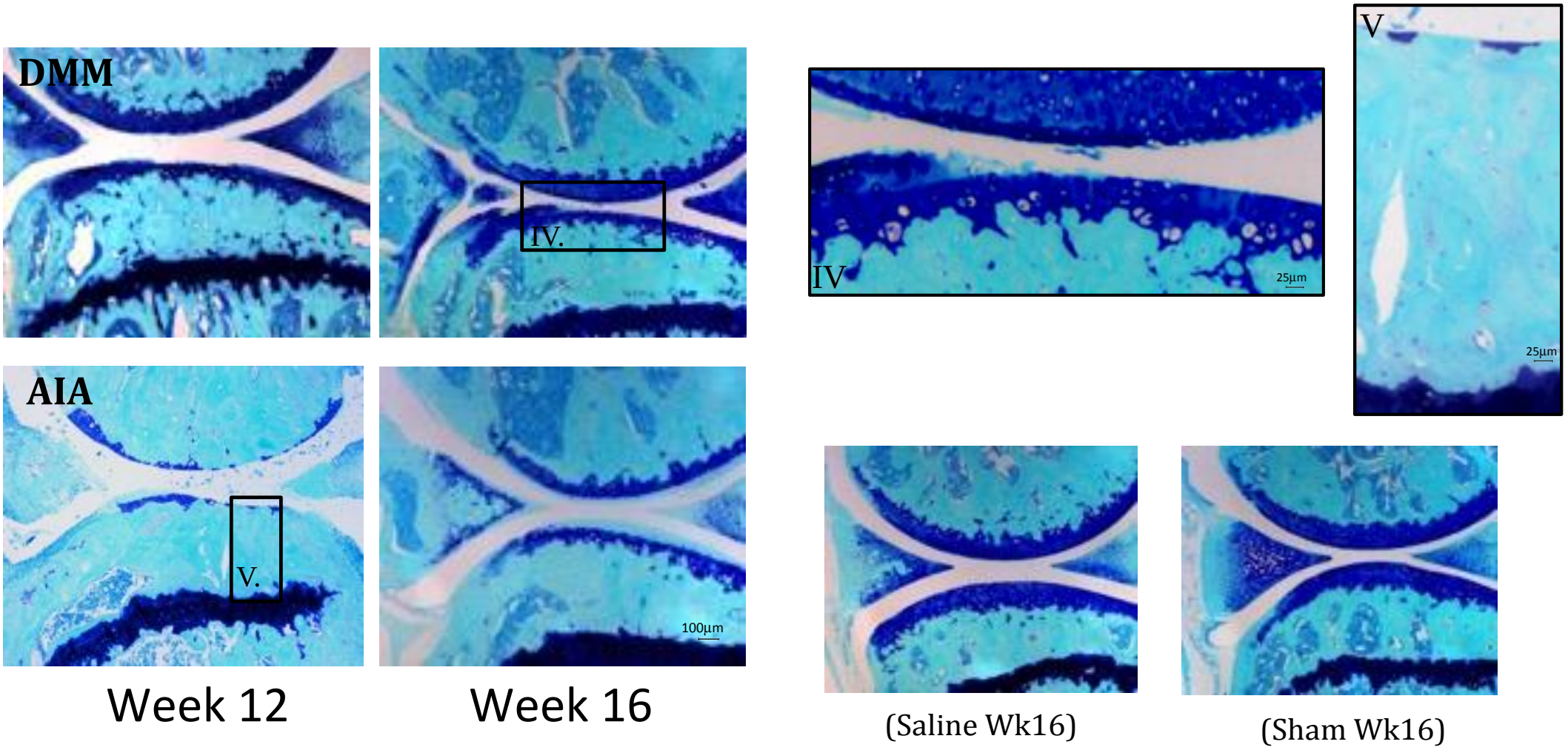

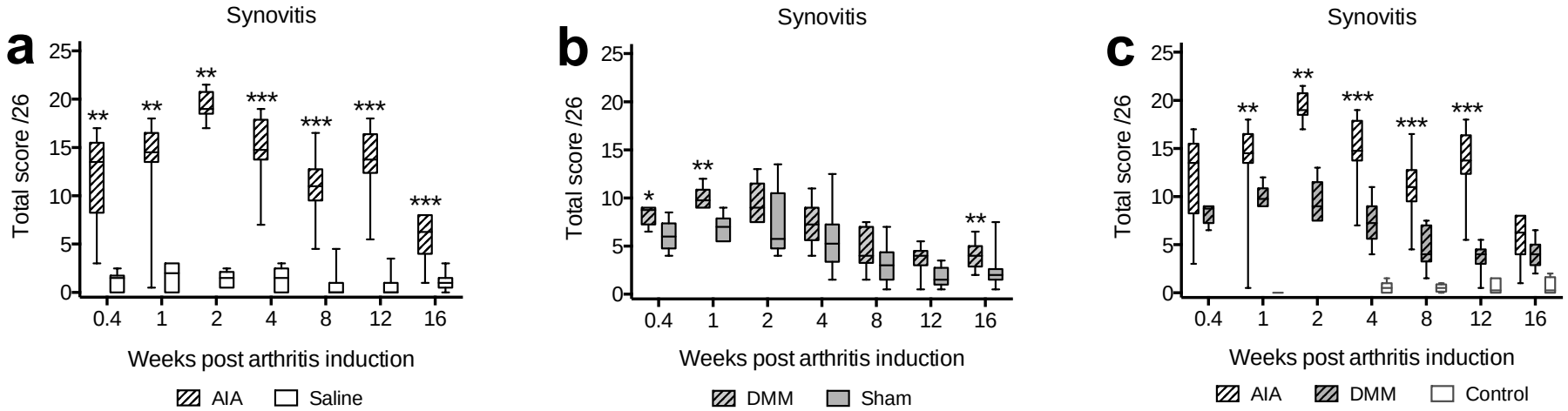

Figure 4.2. Knee joint inflammation histopathology I

Joint inflammation (defined as synovitis) in AIA vs. saline injected (a); DMM vs. sham surgery (b); and DMM vs. AIA (c) mice, at day 3, week 1, 2, 4, 8, 12 and 16 following induction of arthritis. The results are presented graphically as box plots, with medians marked, 95% (upper bounds) and 5% (lower bounds) percentiles hinged, and whiskers depicting upper and lower limits of dataset. Significance = $P<0.05$ (*); $P<0.01$ (**); and $P<0.001$ (***).

The total synovitis score depicted in Figure 4.2 was arrived at by sum of scores of five individual parameters: panus, cortical bone erosion associated with panus, synovial lining cell hyperplasia, sub-synovial inflammation and synovial exudate. Overall, the temporal pattern of development and the degree of severity of these five measures of synovitis differed between the two models.

4.3.1.1 Panus

The appearance of panus occurred in both models immediately following induction of arthritis, with severity peaking at week 2 (Figure 4.3a). Panus was significantly worse in the AIA compared with DMM at week 2, 4 and 12.

4.3.1.2 Bone erosion

The degree of cortical bone erosion associated with panus increased in the AIA model immediately following induction of arthritis (Figure 4.3b). This peaked at week 2 and did not decline substantially until week 8, although it was still significantly increased compared to DMM mice up until week 12. This was in contrast to the DMM model, which demonstrated a low and consistent level of bone erosion throughout the course of the disease. Cortical bone erosion was significantly greater in AIA compared with DMM at week 1, 2, 4, 8 and 12.

4.3.1.3 Synovial hyperplasia

Synovial hyperplasia occurred in both models following induction of arthritis with no significant difference between AIA and DMM until week 2 when synovial hyperplasia peaked in AIA mice (Figure 4.3c). Synovial hyperplasia remained significantly greater in AIA until week 16, when it declined to a level similar to DMM mice.

4.3.1.4 Sub-synovial inflammation

Immediately following induction of arthritis sub-synovial inflammation was severe in the AIA model and did not start to resolve until week 8 (Figure 4.3d). In contrast sub-synovial inflammation developed more gradually and was not as severe in the DMM model. Sub-synovial inflammation remained significantly more severe in AIA mice compared to DMM from week 1 until week 16, despite the decrease observed in AIA mice from week 8.

4.3.1.5 Synovial exudate

Synovial exudate was a consistent feature in the AIA model until week 16 when the proportion of mice with joint exudate declined (Figure 4.3e). In contrast, synovial exudate was only observed consistently in the first week following induction of arthritis in DMM mice and declined up until week 4. Beyond week 4 there was no synovial exudate observed in any DMM mice. Synovial exudate was significantly more severe in AIA mice compared to DMM from week 1 until week 16.

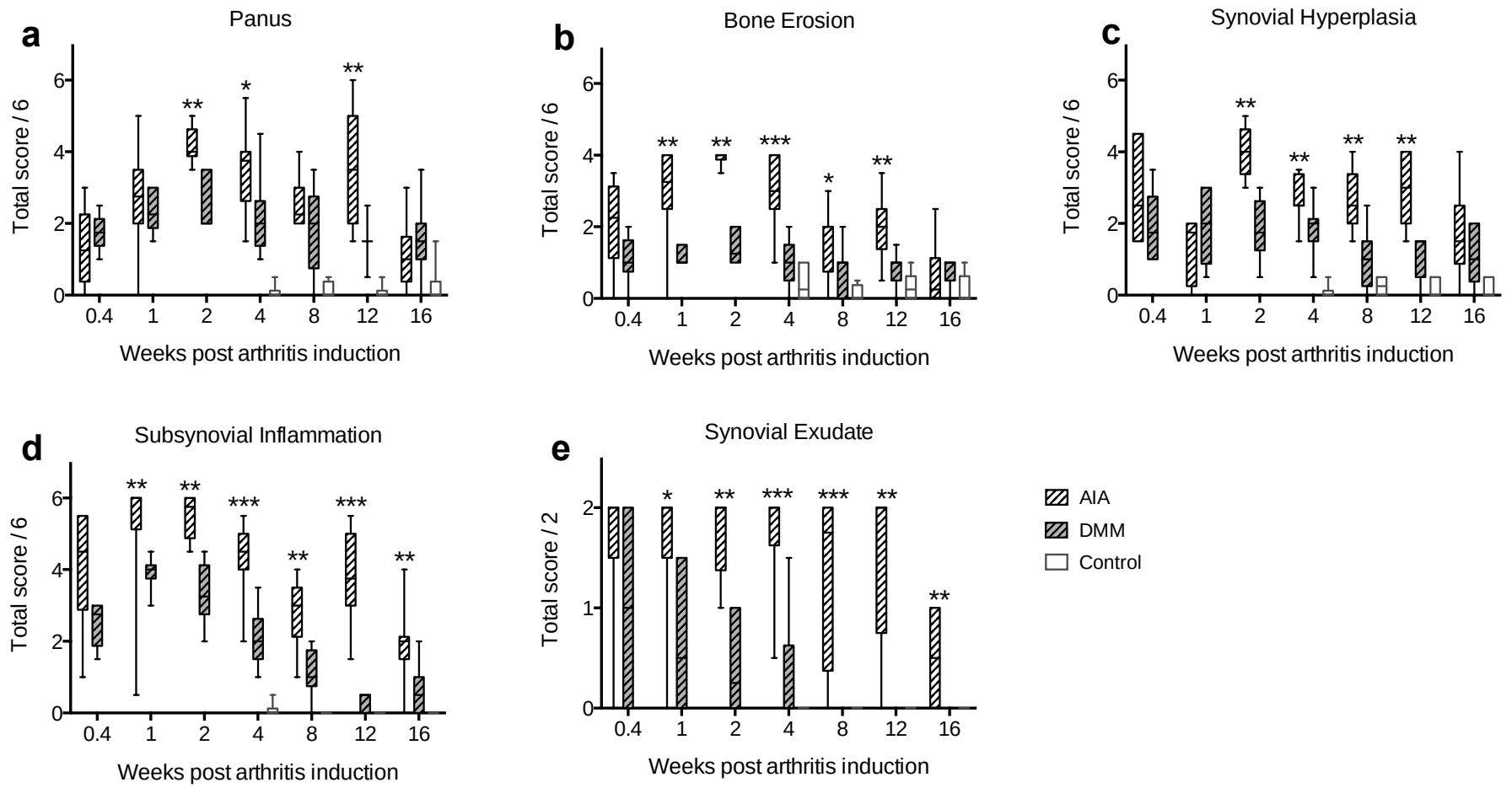

Figure 4.3. Knee joint inflammation histopathology II

Panus (a); Cortical bone erosion (b); Synovial hyperplasia (c); Sub-synovial inflammation (d); and Synovial exudate (e), in DMM vs AIA mice at day 3, week 1, 2, 4, 8, 12 and 16 following induction of arthritis. The results are presented graphically as box plots, with medians marked, 95% (upper bounds) and 5% (lower bounds) percentiles hinged, and whiskers depicting upper and lower limits of dataset. Significance = $P<0.05$ (*); $P<0.01$ (**); and $P<0.001$ (***).

4.3.2 Effect of AIA and DMM on articular cartilage degradation following induction of arthritis

Articular cartilage (AC) histopathology was measured in terms of the combined score of maximum tibial and femoral AC proteoglycan loss, AC structural damage and chondrocyte hypertrophy/apoptosis.

4.3.2.1 Proteogylcan loss

Maximum proteoglycan loss peaked at week 1 in AIA and was significantly greater than saline injected mice at all time points (Figure 4.4a). Maximum proteoglycan loss was significantly greater in DMM mice than in sham surgery mice from week 2 (Figure 4.4b). AIA mice had significantly greater proteoglycan loss than DMM mice at weeks 1 to16 (Figure 4.4c).

4.3.2.2 AC structural damage

In AIA mice, maximum AC structural damage was very mild up to week 4, and then increased dramatically from week 8 to 16 (Figure 4.5a). The difference between AIA and saline injected mice was significant at weeks 1 to 16. At no time point was structural damage in saline injected mice significantly different to age-matched controls. Maximum AC structural damage observed in DMM mice was mild at day 3 post surgery, and did not become significantly greater than sham surgery or age-matched control mice until week 2, and increased progressively until week 16 (Figure 4.5b). Structural damage was mild and transient in sham surgery mice, and there was no significant difference between sham surgery and age-matched controls at any of the time points that were scored. There was little difference between the two arthritis models in AC structural damage scores over the time course of the study; DMM >

AIA at week 4 and AIA > DMM at week 12. By week 16 there was no significant difference in structural damage between DMM and AIA mice (Figure 4.5c).

4.3.2.3 Chondrocyte hypertrophy

Chondrocyte hypertrophy in non-calcified cartilage developed early and persisted in both AIA and DMM mice (Figure 4.6a and b), and was significantly greater than in saline injected and sham surgery, respectively. There was a significant difference between the two models from week 4 to 16, when chondrocyte hypertrophy was greater in AIA (Figure 4.6c).

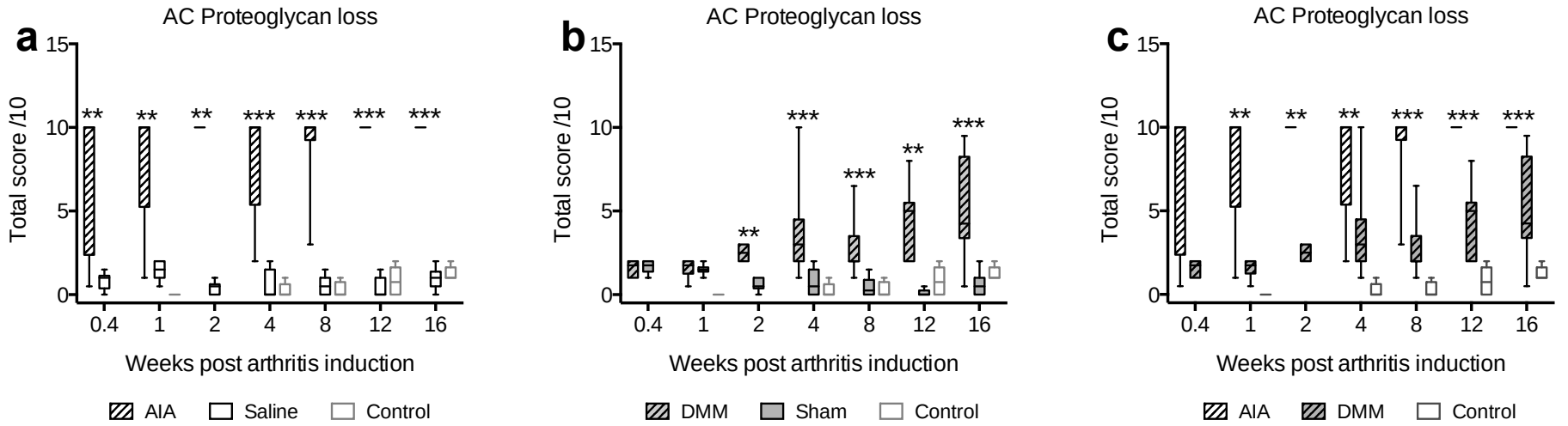

Figure 4.4. Knee joint articular cartilage histopathology I

Proteoglycan loss in AIA vs. saline injected (a); DMM vs. sham surgery (b); and DMM vs. AIA (c) mice, at day 3, week 1, 2, 4, 8, 12 and 16 following induction of arthritis. The results are presented graphically as box plots, with medians marked, 95% (upper bounds) and 5% (lower bounds) percentiles hinged, and whiskers depicting upper and lower limits of dataset. Significance = $P<0.05$ (*); $P<0.01$ (**); and $P<0.001$ (***).

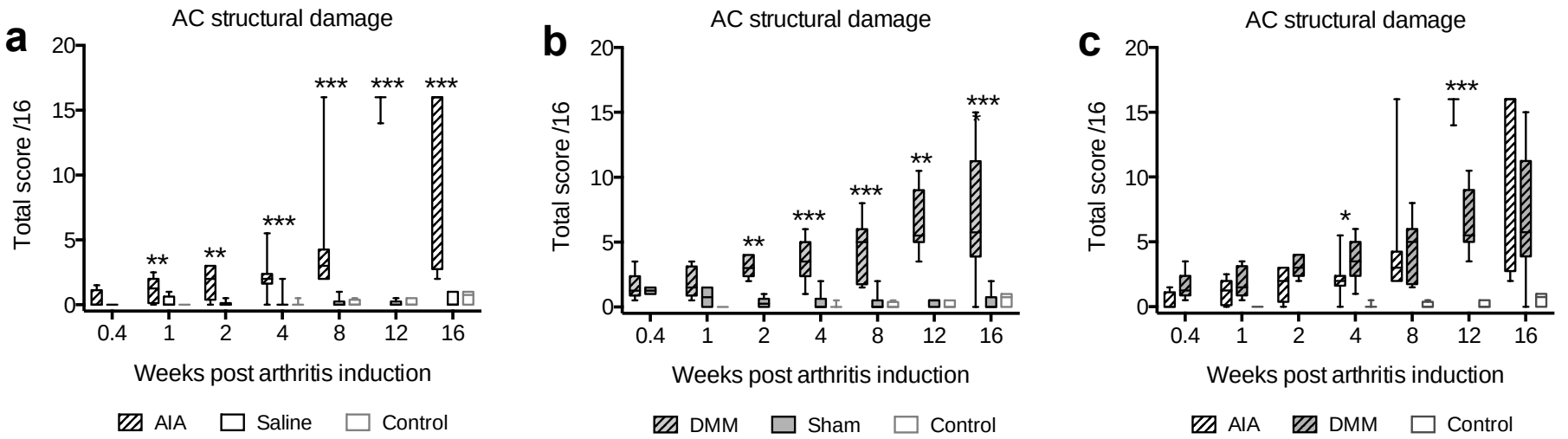

Figure 4.5. Knee joint articular cartilage histopathology II

Articular cartilage structural damage in AIA vs. saline injected (a); DMM vs. sham surgery (b); and DMM vs. AIA (c) mice, at day 3, week 1, 2, 4, 8, 12 and 16 following induction of arthritis. The results are presented graphically as box plots, with medians marked, 95% (upper bounds) and 5% (lower bounds) percentiles hinged, and whiskers depicting upper and lower limits of dataset. Significance = $P<0.05$ (*); $P<0.01$ (**); and $P<0.001$ (***).

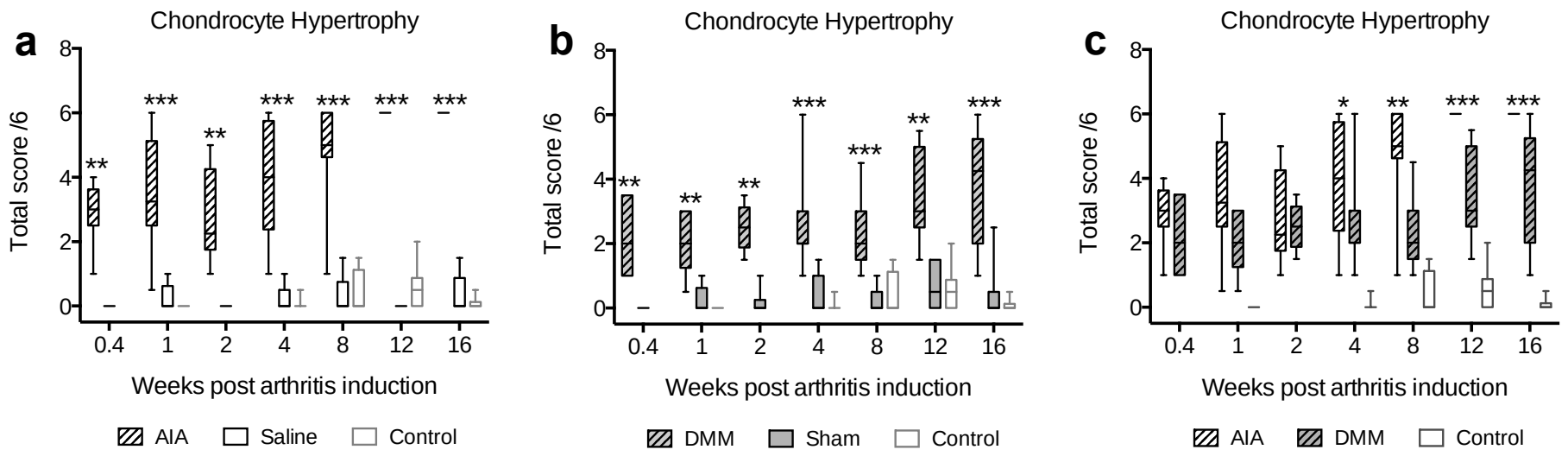

Figure 4.6. Knee joint articular cartilage histopathology III

Chondrocyte hypertrophy in non-calcified cartilage in AIA vs. saline injected (a); DMM vs. sham surgery (b); and DMM vs. AIA (c) mice, at day 3, week 1, 2, 4, 8, 12 and 16 following induction of arthritis. The results are presented graphically as box plots, with medians marked, 95% (upper bounds) and 5% (lower bounds) percentiles hinged, and whiskers depicting upper and lower limits of dataset. Significance = $P<0.05$ (*); $P<0.01$ (**); and $P<0.001$ (***).

4.3.3 Effect of AIA and DMM on bone following induction of arthritis

Bone histopathology changes were defined in terms of osteophyte development (maturation and size), and subchondral bone (SCB) vascularisation and sclerosis or thickening.

4.3.3.1 Osteophytes

Osteophytes developed in both DMM and AIA mice, but not in sham surgery or saline injected mice. In AIA, osteophytes only developed late (week 8) and reached peak size and maturity at week 16 (Figures 4.7a and 4.8a). In the DMM model in contrast, osteophytes developed early (week 1), initially as neo-cartilage and then maturing to bone through endochondral ossification, reaching peak size and maturity by week 4 (Figures 4.7b and 4.8b). Osteophyte size was significantly greater in DMM mice compared to AIA at week 1, 2, 4 and 12. Osteophyte maturity was significantly greater in DMM compared to AIA from week 1 to 16. By week 16 there was no significant difference in osteophyte size between the two models although those in the AIA model had not fully ossified (Figures 4.7c and 4.8c).

Unique to the AIA model was the development of enthesophytes. These were observed from week 1, increasing in size and maturity up to week 16. The enthesophytes were observed on the anterior, medial margin of the tibia, at the level of the growth plate, adjacent the site of insertion of the patella ligament. This novel pathology has not previously been described in the AIA model.

4.3.3.2 Subchondral bone

Subchondral bone sclerosis displayed two phases of change in both AIA and DMM. In control mice SCB sclerosis increased with age, reaching a median score of 2 by week 16. In the AIA model SCB sclerosis was absent at weeks 1 and 2, and was observed from week 4. At week 12 and 16 it was significantly increased compared to saline injected mice (Figure 4.9a). Saline injected mice displayed greater SCB sclerosis than controls in the first two weeks following injection, and then demonstrated a similar pattern of increase with age after week 4. Both DMM and sham surgery mice displayed increased SCB sclerosis compared to age matched controls in the first two weeks following surgery (Figure 4.9b). From week 4, sham surgery joints displayed a similar increase over time as age matched controls. In contrast, SCB sclerosis increased more rapidly in the DMM after week 2, exceeding the score of sham surgery and control mice. The difference between the groups was significant at week 4 and 8. SCB sclerosis was greater in DMM than AIA in the early stages of disease, and this difference was significant at weeks 1, 2 and 4. SCB sclerosis in AIA then exceeded DMM following week 8, and was significantly different again at week 12 and 16 (Figure 4.9c).

SCB vascularisation remained similar to age matched controls at all time points in saline injected mice but was significantly increased in AIA compared to saline injected mice from week 1 to week 4 (Figure 4.10a). SCB vascularisation remained similar to age matched controls at all time points in DMM and sham surgery (Figure 4.10b). SCB vascularisation was significantly increased in AIA compared to DMM in the early stages of disease (day 3 to week 4), and then decreased at week 8 to levels comparable to the other treatment groups (Figure 4.10c).

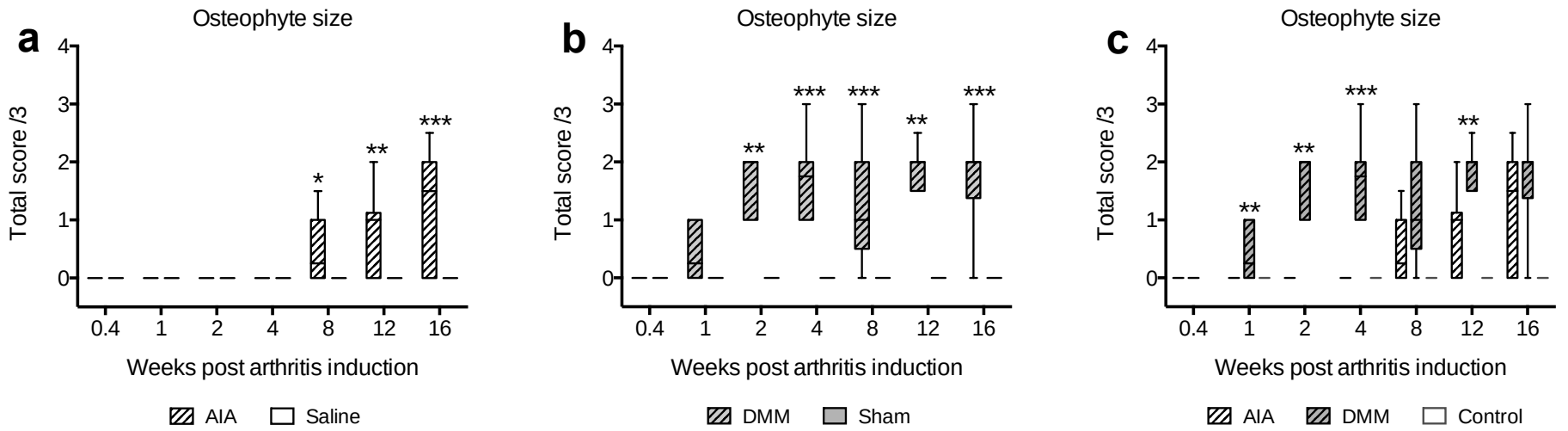

Figure 4.7. Knee joint osteophyte histopathology I

Osteophyte size in AIA vs. saline injected (a); DMM vs. sham surgery (b); and DMM vs. AIA (c) mice, at day 3, week 1, 2, 4, 8, 12 and 16 following induction of arthritis. The results are presented graphically as box plots, with medians marked, 95% (upper bounds) and 5% (lower bounds) percentiles hinged, and whiskers depicting upper and lower limits of dataset. Significance = $P<0.05$ (*); $P<0.01$ (**); and $P<0.001$ (***).

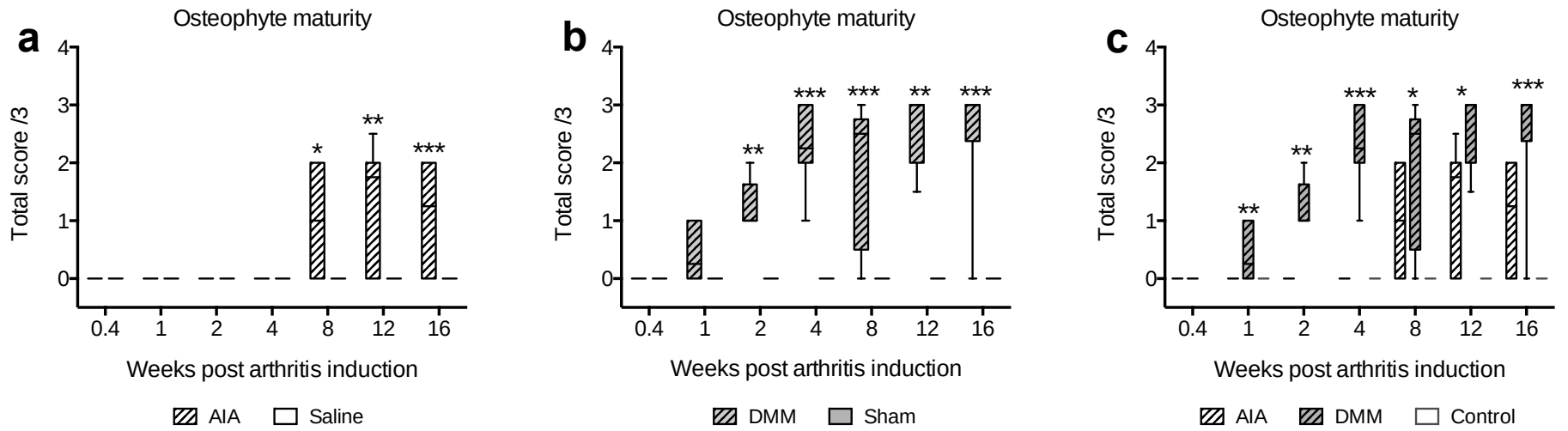

Figure 4.8. Knee joint osteophyte histopathology II

Osteophyte maturity in AIA vs. saline injected (a); DMM vs. sham surgery (b); and DMM vs. AIA (c) mice, at day 3, week 1, 2, 4, 8, 12 and 16 following induction of arthritis. The results are presented graphically as box plots, with medians marked, 95% (upper bounds) and 5% (lower bounds) percentiles hinged, and whiskers depicting upper and lower limits of dataset. Significance = $P<0.05$ (*); $P<0.01$ (**); and $P<0.001$ (***).

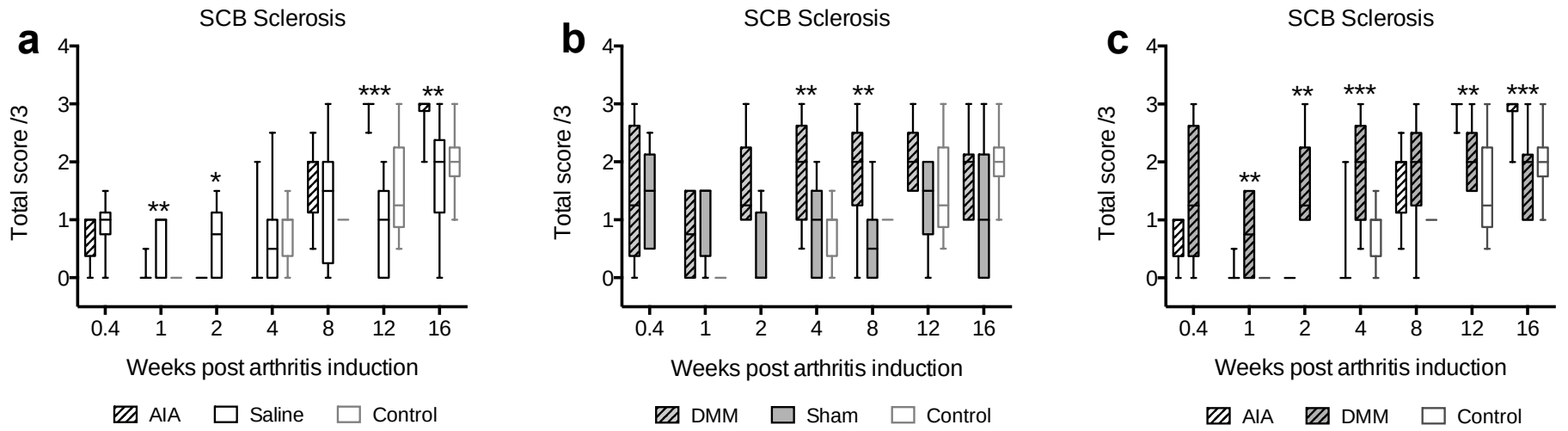

Figure 4.9. Knee joint subchondral bone histopathology I

SCB sclerosis in AIA vs. saline injected (a); DMM vs. sham surgery (b); and DMM vs. AIA (c) mice, at day 3, week 1, 2, 4, 8, 12 and 16 following induction of arthritis. The results are presented graphically as box plots, with medians marked, 95% (upper bounds) and 5% (lower bounds) percentiles hinged, and whiskers depicting upper and lower limits of dataset. Significance = $P<0.05$ (*); $P<0.01$ (**); and $P<0.001$ (***).

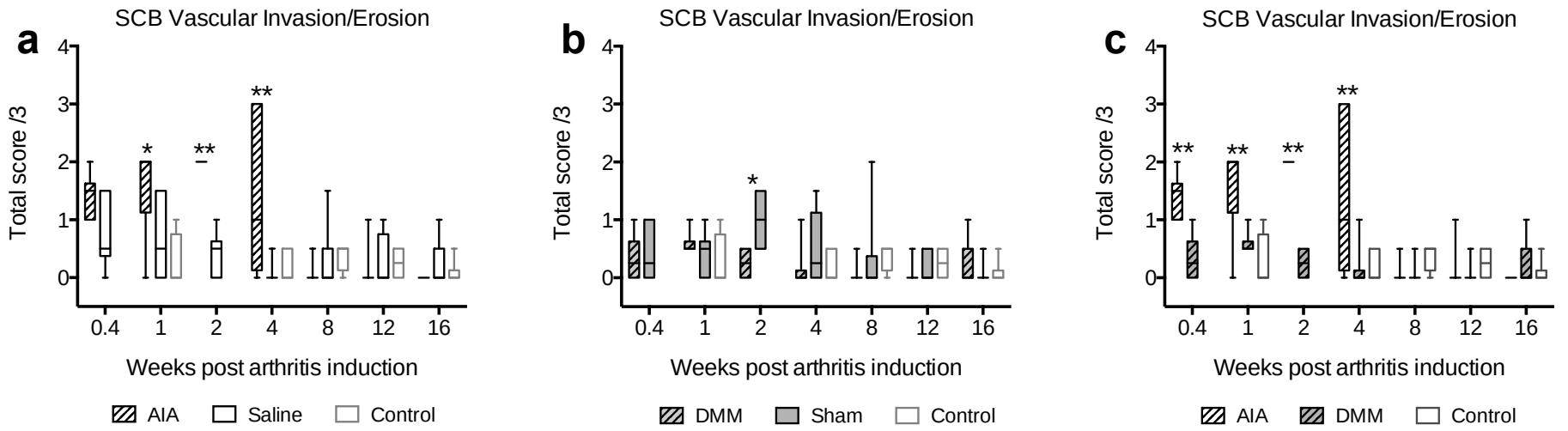

Figure 4.10. Knee joint subchondral bone histopathology II

SCB vascularisation in AIA vs. saline injected (a); DMM vs. sham surgery (b); and DMM vs. AIA (c) mice, at day 3, week 1, 2, 4, 8, 12 and 16 following induction of arthritis. The results are presented graphically as box plots, with medians marked, 95% (upper bounds) and 5% (lower bounds) percentiles hinged, and whiskers depicting upper and lower limits of dataset. Significance = $P<0.05$ (*); $P<0.01$ (**); and $P<0.001$ (***).

4.3.4 Time and Treatment effect on joint pathology

Logistic regression analysis was used to interrogate the pattern of change over time for each histology outcome variable, and also within the two arthritis models (Table 4.2). This provides a more robust evaluation of the effect of the two arthritis induction methods on the different joint pathologies, by taking time into account and allowing all the data to be included in the analyses rather than individual time points.

When corrected for treatment group (sham, saline, DMM, AIA), synovial inflammation increased over time up to week 2, and thereafter decreased significantly. Articular cartilage structural damage and chondrocyte hypertrophy progressively and significantly increased over time, however there was no significant time effect for AC proteoglycan loss. Osteophyte size and maturity both increased significantly with time post arthritis induction. Both SCB sclerosis and vascularity also demonstrated a significant temporal effect, SCB sclerosis increasing while SCB vascularity decreased over time.

When time was corrected for, a significant treatment effect was observed for a number of the histology outcomes, in some cases differing between the two arthritis models. Synovitis was significantly increased in AIA and DMM relative to saline and sham respectively, and increased in AIA relative to DMM, regardless of which stage of the disease process. This treatment effect was also evident in four of the individual parameters (panus, bone erosion, synovial hypertrophy and sub-synovial inflammation) that combine to make up the synovitis score. Synovial exudate was only increased in AIA relative to saline and DMM. AC structural damage, AC proteoglycan loss and chondrocyte hypertrophy were all increased in AIA and DMM relative to their saline and sham controls. Only AC proteoglycan loss and chondrocyte hypertrophy were significantly increased in AIA relative to DMM. Osteophyte size

and maturity were increased in AIA and DMM relative to saline and sham, but decreased in AIA relative to DMM. SCB sclerosis was increased in DMM relative to sham but not in AIA relative to saline. SCB vascularity was increased in AIA and DMM relative to saline and sham.

Table 4.2. Joint histopathology logistic regression analysis

Score	Period(w)	Time[1]	Time (P)	Treatment[2]		Cf tx[3]	Tx (P)
Synovitis	0 - 2	Increased	0.010	Sham	Increased	Saline	<0.001
				AIA	Increased	Saline	<0.001
				DMM	Increased	Sham	0.002
				AIA	Increased	DMM	<0.001
Synovitis	2 - 16	Decreased	<0.001	Sham	Increased	Saline	< 0.001
				AIA	Increased	Saline	<0.001
				DMM	Increased	Sham	<0.001
				AIA	Increased	DMM	<0.001
AC damage	0 - 16	Increased	<0.001	Sham	Increased	Saline	0.003
				AIA	Increased	Saline	<0.001
				DMM	Increased	Sham	<0.001
				AIA	-	DMM	0.330
AC PG loss	0 - 16	-	0.110	Sham	-	Saline	0.820
				AIA	Increased	Saline	<0.001
				DMM	Increased	Sham	<0.001
				AIA	Increased	DMM	<0.001
Chondrocyte hypertrophy	0 - 16	Increased	<0.001	Sham	-	Saline	0.370
				AIA	Increased	Saline	<0.001
				DMM	Increased	Sham	<0.001
				AIA	Increased	DMM	<0.001
Osteophyte maturity	0 - 16	Increased	<0.001	Sham	-	Saline	0.910
				AIA	Increased	Saline	<0.001
				DMM	Increased	Sham	<0.001
				AIA	Decreased	DMM	<0.001
Osteophyte size	0 - 16	Increased	<0.001	Sham	-	Saline	0.820
				AIA	Increased	Saline	<0.001
				DMM	Increased	Sham	<0.001
				AIA	Decreased	DMM	<0.001
Subchondral bone sclerosis	0 - 16	Increased	<0.001	Sham	-	Saline	0.350
				AIA	-	Saline	0.350
				DMM	Increased	Sham	<0.001
				AIA	-	DMM	0.048

Subchondral bone vascularity	0 - 16	Decreased	<0.001	Sham	-	Saline	0.960
				AIA	Increased	Saline	0.004
				DMM	Decreased	Sham	0.010
				AIA	Increased	DMM	<0.001
Panus	0 -16	Decreased	<0.001	Sham	Increased	Saline	<0.001
				AIA	Increased	Saline	<0.001
				DMM	Increased	Sham	<0.001
				AIA	Increased	DMM	<0.001
Bone erosion	0 -16	Decreased	<0.001	Sham	Increased	Saline	<0.001
				AIA	Increased	Saline	<0.001
				DMM	Increased	Sham	0.031
				AIA	Increased	DMM	<0.001
Synovial hypertrophy	0 -16	Decreased	<0.001	Sham	-	Saline	0.230
				AIA	Increased	Saline	<0.001
				DMM	Increased	Sham	<0.001
				AIA	Increased	DMM	<0.001
Subsynovial inflammation	0 - 16	Decreased	<0.001	Sham	Increased	Saline	<0.001
				AIA	Increased	Saline	<0.001
				DMM	Increased	Sham	0.003
				AIA	Increased	DMM	<0.001
Synovial exudate	0 -16	Decreased	<0.001	Sham	Increased	Saline	0.008
				AIA	Increased	Saline	<0.001
				DMM	-	Sham	0.370
				AIA	Increased	DMM	<0.001

Logistic regression on joint histology scores in AIA and DMM was used to determine whether histology outcome variables changed over time, and then when correcting for time whether there was a difference between treatments. Where the direction (i.e. increase vs decrease) and/or significance of the temporal change for a particular histological feature differed with time after arthritis induction, the periods are reported separately. (1) Change over time when corrected for treatment, (2) Change between treatments when corrected for time, (3) Comparator treatment.

4.3.5 Correlation between pathological change in different joint tissues in AIA and DMM when corrected for time

The knee joint functions as a biomechanical organ comprising numerous tissues. Since OA is a failure of the entire joint organ, understanding how the pathological changes that occur in different joint tissues are associated provides important information on changes in pathophysiology in different arthritis phenotypes and with time. The preceding regression analysis provided information on the change in joint pathology measures with time, and in the two models, but not how the changes in the different joint tissues are interrelated. These associations were determined by calculating partial correlation coefficients for the various joint tissue pathologies in the different treatments (AIA, Saline, DMM, Sham) when corrected for time (Table 4.3). The significant associations in the two arthritis models and those common to both models are also represented schematically in Figures 4.11a-c, with positive correlations shown in solid lines and negative correlations in dashed lines, the weight of the line reflecting the strength of the correlation.

4.3.5.1 Articular cartilage histopathology partial correlations

In AIA mice AC structural damage correlated positively with chondrocyte hypertrophy but not proteoglycan loss. In addition, AC structural damage in this model correlated with all measured bone pathologies other than vascularity (positively with osteophyte maturity, osteophyte size and SCB sclerosis). Proteoglycan loss in AIA on the other hand, only correlated with SCB vascularity and chondrocyte hypertrophy, all being positive associations. Chondrocyte hypertrophy also correlated positively with SCB sclerosis and negatively with vascularity.

In DMM mice AC structural damage correlated with cartilage and bone related pathologies (positively with proteoglycan loss, chondrocyte hypertrophy, osteophyte

size, osteophyte maturity and SCB sclerosis; negatively with SCB vascularity). AC proteoglycan loss also correlated positively with chondrocyte hypertrophy, and bone related pathologies (osteophyte maturity and osteophyte size, and SCB sclerosis). In addition, chondrocyte hypertrophy positively correlated with osteophyte size and maturity.

4.3.5.2 Joint inflammation partial correlations

In AIA mice synovitis scores correlated positively with SCB vascularity, negatively with SCB sclerosis, as well as the previously stated positive association with AC structural damage. In DMM mice however, synovitis scores only correlated with SCB vascularity, no significant correlations found with any articular cartilage or other bone related pathologies.

4.3.5.3 Bone histopathology partial correlations

In AIA mice SCB sclerosis correlated strongly with osteophyte size and maturity, and there was a strong negative correlation with both synovitis and SCB vascularity. SCB vascularity also strongly negatively correlated with osteophyte size and maturity. In DMM mice SCB sclerosis was positively correlated with osteophyte maturity but not size, and there was a negative correlation with SCB vascularity but not synovitis. In both AIA and DMM mice, there was a positive correlation between osteophyte size and maturity, strongest in AIA.

Table 4.3. Cartilage pathology, bone pathology and joint inflammation partial correlations in AIA and DMM

a. Articular cartilage structural damage	**Treatment**	**r**	***P***
AC PG loss	AIA	0.176	0.082
	Saline	**0.289**	**0.004**
	DMM	**0.561**	**<0.001**
	Sham	**0.314**	**0.001**
Chondrocyte hypertrophy	AIA	**0.414**	**<0.001**
	Saline	0.108	0.520
	DMM	**0.513**	**<0.001**
	Sham	0.109	0.350
Osteophyte maturity	AIA	**0.343**	**<0.001**
	Saline	-	-
	DMM	**0.325**	**0.001**
	Sham	-	-
Osteophyte size	AIA	**0.313**	**<0.001**
	Saline	-	-
	DMM	**0.393**	**<0.001**
	Sham	-	-
SCB sclerosis	AIA	**0.265**	**0.018**
	Saline	0.120	0.093
	DMM	**0.387**	**<0.001**
	Sham	0.221	0.089
SCB vascularity	AIA	-0.190	0.027
	Saline	-0.028	0.860
	DMM	**-0.313**	**0.004**
	Sham	-0.058	0.610
Synovitis	AIA	**0.179**	**0.008**
	Saline	0.151	0.190
	DMM	-0.178	0.077
	Sham	0.169	0.037
b. Articular cartilage proteoglycan loss	**Treatment**	**r**	***P***
Chondrocyte hypertrophy	AIA	**0.369**	**0.001**
	Saline	0.182	0.170
	DMM	**0.588**	**<0.001**
	Sham	0.133	0.230
Osteophyte maturity	AIA	0.010	0.920
	Saline	-	-
	DMM	**0.492**	**<0.001**
	Sham	-	-
Osteophyte size	AIA	0.009	0.910
	Saline	-	-
	DMM	**0.450**	**<0.001**
	Sham	-	-

SCB sclerosis	AIA	-0.045	0.730
	Saline	0.070	0.630
	DMM	**0.280**	**0.007**
	Sham	-0.001	0.990
SCB vascularity	AIA	**0.230**	**<0.001**
	Saline	-0.032	0.830
	DMM	-0.178	0.077
	Sham	0.020	0.860
Synovitis	AIA	0.213	0.066
	Saline	0.117	0.300
	DMM	-0.063	0.420
	Sham	0.075	0.370
c. Chondrocyte hypertrophy	**Treatment**	**r**	***P***
Osteophyte maturity	AIA	0.170	0.074
	Saline	-	-
	DMM	**0.358**	**<0.001**
	Sham	-	-
Osteophyte size	AIA	0.144	0.088
	Saline	-	-
	DMM	**0.349**	**<0.001**
	Sham	-	-
SCB sclerosis	AIA	**0.400**	**<0.001**
	Saline	-0.246	0.036
	DMM	0.242	0.042
	Sham	0.042	0.770
SCB vascularity	AIA	**-0.285**	**0.008**
	Saline	0.020	0.900
	DMM	-0.103	0.410
	Sham	-0.038	0.800
Synovitis	AIA	0.086	0.400
	Saline	0.135	0.270
	DMM	-0.057	0.420
	Sham	0.095	0.330
d. Subchondral bone sclerosis	**Treatment**	**r**	***P***
Osteophyte maturity	AIA	**0.393**	**<0.001**
	Saline	-	-
	DMM	**0.261**	**0.012**
	Sham	-	-
Osteophyte size	AIA	**0.370**	**<0.001**
	Saline	-	-
	DMM	0.086	0.460
	Sham	-	-
Synovitis	AIA	**-0.342**	**0.004**
	Saline	-0.079	0.460
	DMM	-0.168	0.073
	Sham	-0.081	0.390

SCB vascularity	AIA	**-0.700**	**<0.001**
	Saline	-0.160	0.240
	DMM	**-0.495**	**<0.001**
	Sham	**-0.406**	**<0.001**
e. Osteophyte maturity	**Treatment**	**r**	***P***
Osteophyte size	AIA	**0.865**	**<0.001**
	Saline	-	-
	DMM	**0.429**	**<0.001**
	Sham	-	-
Synovitis	AIA	-0.167	0.067
	Saline	-	-
	DMM	-0.127	0.110
	Sham	-	-
SCB vascularity	AIA	**-0.351**	**<0.001**
	Saline	-	-
	DMM	-0.167	0.038
	Sham	-	-
f. Osteophyte size	**Treatment**	**r**	***P***
Synovitis	AIA	-0.209	0.014
	Saline	-	-
	DMM	0.042	0.550
	Sham	-	-
SCB vascularity	AIA	**-0.319**	**<0.001**
	Saline	-	-
	DMM	-0.192	0.190
	Sham	-	-
g. Synovitis	**Treatment**	**r**	***P***
SCB vascularity	AIA	**0.305**	**<0.001**
	Saline	-0.195	0.140
	DMM	**0.255**	**0.011**
	Sham	0.152	0.180

Cartilage pathology, bone pathology and joint inflammation partial correlations in AIA and DMM when corrected for time. P-values shown in bold typeface are significant below after Benjamini-Hochberg correction for multiple comparisons, 5% confidence level is $P < 0.022$.

Figure 4.11. Knee joint histopathology associations

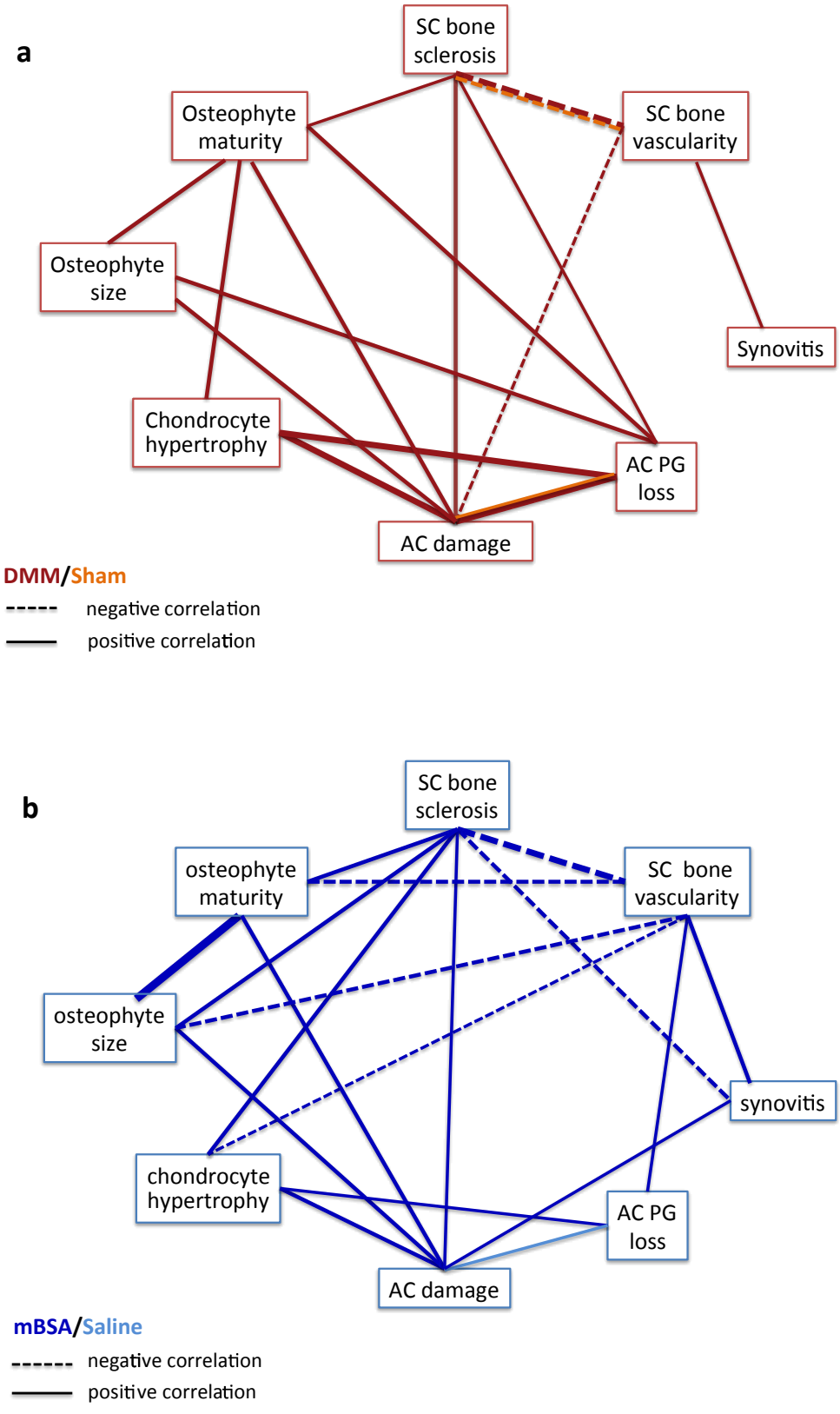

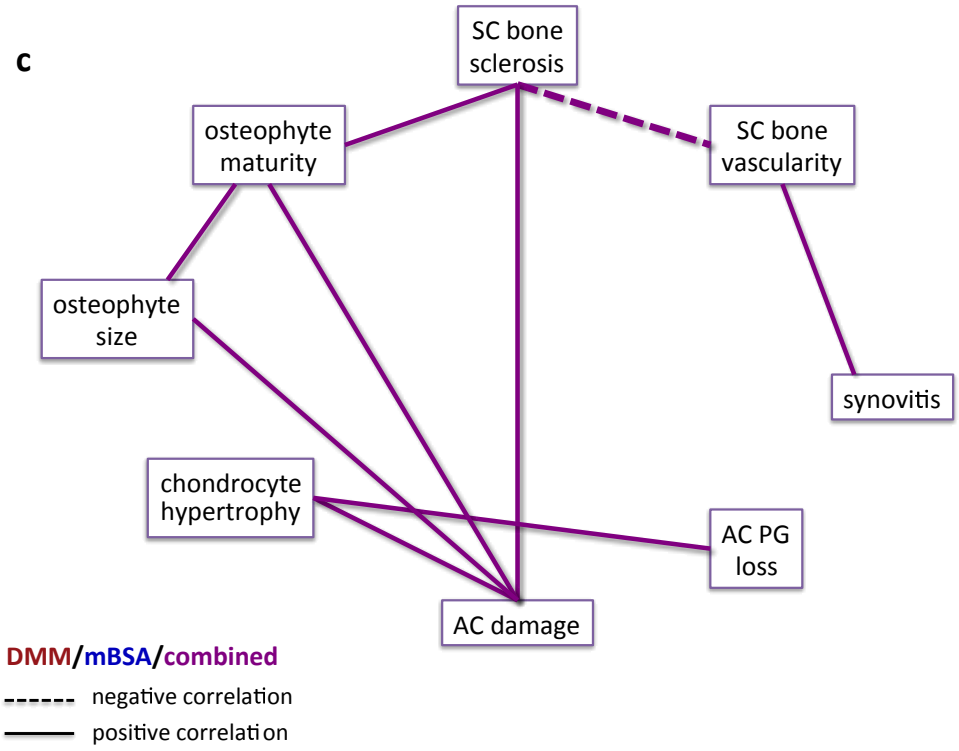

Significant associations between pathological changes in different knee joint tissues (cartilage, bone, and joint inflammation) in AIA model (a); DMM model (b); DMM and AIA models combined (c); as determined by calculation of partial correlation coefficients when corrected for time. After Benjamini-Hochberg correction, 5% confidence level is $P < 0.022$.

4.3.6 Comparison of joint tissue pathology relationships in AIA versus DMM

Finally, ordinal logistic regression models were developed that described the variables that were significantly and independently associated with OA progression as measured by cartilage structural damage (Table 4.4) and OA joint inflammation as measured by synovitis (Table 4.5). These models were highly significant but revealed very different independent risk factors with significant odds ratios for the two arthritis models (Table 4.4 and 4.5). The risk of cartilage damage in the DMM model was increased 1.7 fold in association with joint injury (surgery), 2.4 fold with increased AC proteoglycan loss, 2.3 fold with increased osteophyte size, 2.0 fold with increased chondrocyte hypertrophy and 1.7 fold with increased SCB sclerosis. In contrast, the risk of cartilage damage in the AIA model was increased in association with time after disease induction (1.2 fold), increased synovitis (1.2 fold), increased chondrocyte hypertrophy/cell death (2.0 fold), and increased osteophyte size (13 fold).

The risk of joint inflammation in the DMM model was increased 3.5 fold in association with joint injury (surgery) and 4 fold with increased vascular invasion. However, in DMM the risk of joint inflammation was decreased with time post-surgery and increased SCB sclerosis (0.77 fold and 0.63 fold, respectively). In the AIA model the risk of joint inflammation was increased 9.4 fold in association with treatment (mBSA injection) and 1.4 fold with increased AC PG loss. The risk of joint inflammation in AIA was decreased in association with increases in osteophyte size and SCB sclerosis (0.21 fold and 0.43 fold, respectively).

Table 4.4. Risk factors for OA (cartilage damage)

Best ordinal logistic regression models defining the variables significantly associated with increased risk of OA development (defined as AC damage) in the AIA and DMM models. The included variables in both models are corrected for all others i.e. they are independently significant risk factors for cartilage erosion

Model	Risk factor	OR (95% CI)	P (variable)	P (model)
DMM/Sham	Surgery/joint injury	1.7 (1.0 – 2.9)	0.047	<0.001
	AC PG loss	2.4 (1.5 – 3.9)	<0.001	
	Chond. Hyp./cell death	2.0 (1.2 – 3.2)	0.005	
	OP size	2.3 (1.3 – 4.1)	0.010	
	SCB sclerosis	1.7 (1.1 – 2.7)	0.023	
AIA/Saline	Time	1.2 (1.1 – 1.4)	0.003	<0.001
	Synovitis	1.2 (1.0 – 1.4)	0.019	
	Chond. Hyp./cell death	2.0 (1.3 – 3.0)	0.002	
	OP size	13 (3.3 – 50)	<0.001	

Table 4.5. Risk factors for OA (joint inflammation)

Best ordinal logistic regression models defining the variables significantly associated with increased risk of joint inflammation (defined as synovitis) in the DMM and AIA models. The included variables in both models are corrected for all others i.e. they are independently significant risk factors for joint inflammation.

Model	Risk factor	OR (95% CI)	P (variable)	P (model)
DMM/Sham	Surgery/joint injury	3.5 (2.4 – 5.1)	<0.001	<0.001
	Time	0.77 (0.72 – 0.82)	<0.001	
	SCB vascular invasion	4.0 (1.9 – 8.3)	<0.001	
	SCB sclerosis	0.63 (0.43 – 0.92)	0.016	
AIA/Saline	mBSA/saline	9.4 (2.4 – 36)	0.001	<0.001
	AC damage	1.2 (1.0 – 1.3)	0.003	
	AC PG loss	1.4 (1.1 – 1.7)	0.008	
	OP size	0.21 (0.11 – 0.40)	<0.001	
	SCB sclerosis	0.43 (0.29 – 0.64)	<0.001	

4.4 Discussion

In this chapter, knee joint sections from DMM and AIA mice were histologically scored for the purpose of evaluating the histopathological changes that occur in the two models over time. Sham surgery, saline injected and age matched control knee joints were also scored for comparison. The focus of this chapter was to identify the temporal pattern of joint pathology and any associations between the different joint tissue changes that could distinguish the models as unique joint disease phenotypes. How these different histopathological changes in joint tissue relate to pain is investigated in subsequent chapters.

Knee joint pathology in the DMM model was characterised by moderate early phase synovial inflammation that increased and peaked at week 2 and despite declining thereafter, low-grade inflammation persisted. Regression analysis revealed this low-grade inflammation was greater than that of sham surgery and age matched control mice. Although the early phase of synovial inflammation was attributed to surgical trauma and tissue disruption since it also developed in sham surgery mice, it was also significantly greater in DMM suggesting an acute additive effect of OA-inducing joint injury. In contrast, the AIA model was characterised by severe synovial inflammation that while also peaking at week 2 persisted for longer (12 weeks) before decreasing to levels that were comparable to the DMM model at week 16.

The idea that AIA is an inflammation driven model of arthritis and DMM is a post-traumatic model of OA with trauma associated mild inflammation is not new (413, 437, 521); however, this is the first time that an attempt has been made to not only quantify the degree of inflammation that occurs in the two models in terms of the different joint tissue changes that are involved in the inflammatory process (synovial hyperplasia, sub-synovial infiltration, synovial exudate, panus formation and cortical

bone erosion)(461), but also determine any associations between joint inflammation and the development of OA-like joint pathologies.

Despite the presence of significant synovitis in both models, a direct association between synovitis and AC damage was only identified in AIA. In the AIA model there was an association between synovitis and subchondral bone pathology (both vascularisation and sclerosis). In contrast, synovitis was only associated with SCB vascularity in the DMM model. In combination with the fact that synovitis is a significant risk factor for development of AC damage in the AIA model but not in DMM, these associations suggest that inflammation, at least as measured by histological scoring of synovitis, is a more direct driver of joint pathology in this model than in the DMM.

The correlation differences between the two models also suggests that the severity of inflammation and the type of inflammation, rather than its absolute presence, may determine the role it plays in the development of OA joint pathology. This study did not evaluate differences in inflammatory cell populations or the presence of specific cytokines in the inflammatory 'soup' that developed in the two models. However, evidence of the existence of these differences can be drawn from the type of histopathological inflammation observed in each model. For example, panus, sub-synovial inflammation and synovial exudate were a feature of both early and late phase AIA inflammation. While panus was also present in both early and late phase DMM inflammation, synovial hyperplasia rather than sub-synovial inflammation was an early and persistent feature in this post-traumatic OA model.

Human OA, both its presence and severity, is still defined by radiographic changes of joint space narrowing and the presence of osteophytes (566, 567). These radiographic hallmarks of human OA are reflected histologically in the DMM model as AC

proteoglycan loss and structural damage (joint space narrowing), and osteophyte maturation to calcified cartilage and bone (such that they would be detected on radiographs). AC proteoglycan loss and structural damage appeared early (week 1-2) and were both progressive thereafter. In contrast, these 2 aspects of cartilage pathology were not temporally associated in the AIA model where there was immediate and complete proteoglycan loss (day 3) that persisted, and a more delayed development of AC structural damage (week 8). Temporally the formation of mature/boney osteophytes (potentially visible radiographically) was quite distinct in the two models; 2-4 weeks in DMM and 12-16 weeks in AIA. Nevertheless, by 16 weeks both arthritis models had pathology that would be consistent with the current radiographic diagnostic criteria for OA in patients.

Although osteophyte formation occurred in both models, there were distinct differences and specific tissue pathology associations. In the DMM model there was a moderate association ($r = 0.429$) between osteophyte size and maturity, reflecting initial formation of cartilaginous outgrowths that then underwent endochondral ossification to form mature osteophytes. In AIA there was a very strong association between osteophyte size and maturity ($r = 0.865$), perhaps suggesting some subtle difference in pathophysiology of their formation in the two models. This may be further supported by the fact that osteophyte size and maturity were significantly correlated with AC structural damage but not AC PG loss or chondrocyte hypertrophy in the AIA model. In contrast, osteophyte size and maturity were significantly correlated with all three components of articular cartilage pathology (AC PG loss, AC structural damage and chondrocyte hypertrophy) in the DMM model. Yet in both models osteophyte size was associated with an increased risk of OA progression as

measured by cartilage structural damage, although in AIA the risk was much greater (OR = 13).

In human OA patients, osteophyte size is also associated with a moderate increased risk of OA disease progression (568). However, this increased risk is largely accounted for when adjustments are made for the effect of joint malalignment on disease progression, due to the strong association between large osteophytes and joint malalignment.

The factors that drive osteophyte formation are incompletely understood, but likely involve mechanical and soluble/growth factor signaling to activate mesenchymal stem cells (MSC) in the periosteum and synovial membrane, and potentially also macrophage-like cells [reviewed in (569)]. The relative contribution of biomechanics and soluble mediators to osteophyte development may differ with arthritis phenotype as previously demonstrated comparing the more inflammatory collagenase-induced OA (ciOA) with the less inflammatory DMM model of post-traumatic OA (570, 571). The osteophyte development in AIA may reflect a stronger role for growth factors such as TGFβ and BMPs-2 and -9 rather than biomechanics as previously reported in ciOA (572-576), while in DMM, joint instability may be more critical with osteophytes potentially acting to stabilise the joint (577). Osteophyte development in AIA occurred when synovitis was resolving but cartilage erosion was maximal, potentially implicating a role for increasing micro-instability with loss of cartilage volume in the late stages of this model. However, there was significant negative correlation between subchondral bone vascularity and both osteophyte size and maturation in AIA but not DMM. This is consistent with the greater joint inflammation and associated bone resorption in early AIA, and late osteophyte formation may be indicative of the need to resolve specific pro-inflammatory signals

to allow bone formation. This phenomenon was recently described in TNF-transgenic mice where blocking the key Wnt inhibitor Dikkopf-1, reversed the bone-destructive pattern typical of rheumatoid arthritis to one of bone formation, and particularly osteophyte formation, typical of osteoarthritis (578).

In addition to osteophyte formation the AIA model also resulted in the formation of enthesophytes. This histopathological finding has not been reported previously in the AIA model. Enthesophytes differ from osteophytes with respect to anatomical location, tissue derivation and most likely pathogenesis. Unlike osteophytes, enthesophytes do not develop from the margins of the articular surface, but rather from the site of insertion of tendons, ligaments or articular capsule and they extend in the direction of pull of their tendon or ligament of origin (579). Based on location, the enthesophytes observed in the AIA mice most likely originated from the attachment site of the patella tendon/ligament. In contrast to osteophytes, which developed late in AIA, the enthesophytes developed early (week 1) and this would suggest that inflammation and not joint instability is a key factor in driving their formation in the AIA model.

In humans the formation of enthesophytes and osteophytes are strongly correlated following correction for age and gender (580). This association has been further investigated in individuals with high bone mass in an attempt to identify a subset of OA patients with an OA phenotype that is characterised by excess bone formation (581).

Our ‘tissue’ definition of OA has broadened from describing it as a disease of articular cartilage to a disease of multiple tissues that make up the joint organ (62, 122). This study identified different model-specific associations between the three major tissue structures in the joint (articular cartilage, synovium and subchondral

bone). While providing further support to the clinical relevance of the "joint organ" definition, it also highlights how the pathological interaction between joints tissues is dependent on the arthritis phenotype. The subchondral bone is one tissue that is reshaping our understanding of OA pathogenesis (62, 73, 582, 583). In the DMM model SCB sclerosis was consistently greater than sham surgery and age matched controls, despite the observed age-related increase in SCB thickening. The only decrease in SCB sclerosis that was observed in DMM occurred in week 1, when joint inflammation peaked and the SCB was characterised by increased vascularity. A similar pattern of change from SCB resorption to bone formation was observed in the AIA model, however, the decrease in SCB persisted for longer (week 4), reflecting the differences in joint inflammation severity and the degree of SCB vascularisation in the two models. SCB vascularisation was significantly associated with synovitis in AIA and DMM, indicating that it is part of the "whole joint inflammation" that occurs in the early stages of disease in both models.

Despite the temporal differences described, by 16 weeks the two models were not significantly different with respect to inflammation (synovitis and SCB vascularisation), AC structural damage or osteophyte size. By all accounts at week 16 histopathologically both models are OA-like. However, model specific tissue pathology associations were identified that confirm the unique disease phenotypes that these models represent (Figure 4.10). While it must be remembered that no causal relationships can be established from the data presented in this chapter, the different associations between joint pathologies in the two models may have implications when considering the potential of therapeutic intervention targeting one tissue to treat the global joint pathology of OA. In other words, the "OA phenotype" matters.

In the DMM model there was a strong positive relationship between cartilage structural damage and both PG loss and chondrocyte hypertrophy/apoptosis. This is consistent with the known role of both aggrecanolysis and the chondrocyte differentiation in OA cartilage degradation, and that genetic modifications targeting these molecular pathways can reduce OA cartilage damage in mice [reviewed in (407)]. Interestingly while AC structural damage in AIA was associated with chondrocyte hypertrophy and this with PG loss, there was no significant association between PG loss and cartilage erosion in this model. In the final OLR analysis of the two models the subtle differences in the cellular and molecular regulation of cartilage degradation are evident in PG loss and chondrocyte hypertrophy/apoptosis being the significant risk factors in DMM, while it was only chondrocyte hypertrophy/apoptosis in AIA. This is consistent with previous observation using genetically modified mice, demonstrating that the molecular regulation and/or enzymes involved in the sustained PG loss in AIA are distinct from those in DMM (439). However, it also confirms the importance of hypertrophic differentiation and chondrocyte death in cartilage structural damage (584-586), and that modulating this is an important therapeutic target that may cross different osteoarthritis phenotypes.

That the relationships observed between different histopathological aspects of cartilage pathology align with current understanding of the pathophysiological mechanisms in this tissue provides confidence in the current analyses. We therefore explored the associations between different joint tissues in the two models. Consistent with the associations observed in human knee OA (63, 66, 570, 587) AC structural damage in the DMM model was significantly associated with increased SCB thickening and osteophyte formation (size), these two variables being significant independent risk factors in the logistic regression model describing AC damage in the

DMM model. This suggests that in the DMM induced post-traumatic OA the tissue specific mechanisms driving cartilage damage, SCB sclerosis and osteophyte formation are co-dependent. This is supported by data from genetically modified mice where targeting molecular mechanisms expected to specifically modulate bone turnover can significantly reduce cartilage damage in models of post-traumatic OA (407).

In the AIA model however, despite some evidence for a correlation, SCB sclerosis did not remain in the final analysis as an independent risk factor for AC structural damage. Instead when corrected for all other variables, synovitis and osteophyte size were significant predictors of increasing AC structural damage in AIA. The factors that control association between osteophyte formation and cartilage damage as discussed above, appear to be acting in both arthritis models although at different times in disease progression. The negative correlation between synovial inflammation and SCB sclerosis observed in both models could in part account for the delayed AC structural damage observed in AIA model as synovitis persists at a greater level for longer, and supports the idea that the reduced SCB thickening is chondroprotective (583, 588). However, the complex relationship between SCB and cartilage damage in OA is evident from recent therapeutic studies in mice (589, 590). Administration of bisphosphonates to reduce bone resorption had no effect on cartilage damage following meniscectomy-induced OA, however if the mice were first made osteopaenic or "bone-resorbers" by ovariectomy or Runx-2 overexpression, then bisphosphonates significantly reduced AC structural damage. This data suggests that excessive bone resorption may contribute to rather than protect against cartilage damage in OA. While no significant association was found between SCB vascularisation (the histological marker of bone resorption) and cartilage damage in

the AIA model, it would be interesting to determine if bisphosphonates had a chondroprotective effect in this model.

It is perhaps also not surprising that in a model initiated by inducing an acute intra-articular immune/inflammatory response to a foreign antigen (AIA), that synovitis would be a significant risk factor for cartilage damage. Interestingly however, no direct association could be demonstrated between synovial inflammation and the development of articular cartilage pathology in the DMM model. This is somewhat surprising given that genetic modulation of various immune/inflammatory pathways has been shown to significantly inhibit cartilage degradation in mouse models of post-traumatic OA (reviewed in (407)). This may reflect that the histopathological scoring method used for synovitis does not discriminate between different cellular or molecular phenotypes of inflammation. Thus while deficiency of complement factor 5 (82), IL-1 (591), and IL-6 (592) for example have been shown to be chondroprotective in mouse post-traumatic OA, mice lacking complement regulatory protein 59a (82) or deficient in toll-like-receptors (TLRs)1-4 or their primary response gene Myd88 (593) show no change in OA cartilage damage. Thus there are specific inflammatory pathways and molecules that may be up-regulated and play critical roles in OA, and importantly in different stages and/or phenotypes of OA. This has been demonstrated previously for S100A9, which plays a central role in cartilage degradation in the more inflammatory ciOA, but not DMM (571). Whether it is simply the severity and prolonged time course of the synovial inflammation in AIA that drives the association between synovitis and AC damage in this model compared with DMM; or that more of the individual pathways that show association in DMM are up regulated in AIA; or that different, or more-potent pathways are regulated, is not clear.

Despite both models resulting in OA-like joint pathology, the different tissue associations observed in the two models suggest that different tissue specific mechanisms may be driving the joint pathology changes that ultimately lead to OA. The data presented in this chapter demonstrates that even when the long-term global joint pathology is the same, the relationship between the different tissue pathologies and the risk factors for developing OA, are likely determined by the initiating cause, and this is different for each animal model. This highlights the importance of defining animal model phenotypes in terms of initiating mechanisms and temporal joint tissue pathology, as well as end-stage joint disease characteristics. While most would agree that DMM is a model of post-traumatic (pt)-OA, the idea that AIA may also be an OA model would not be widely accepted. Acutely AIA is clearly a model of inflammatory arthritis, but at least from a pathological viewpoint, at some stage it "becomes OA". With time long-term AIA could be considered a model of "post-inflammatory (pi)-OA".

Although the two models eventually show all the hallmark pathological features of human OA (AC erosion, SCB sclerosis, marginal osteophytes), the time course of how this is arrived at and the relationship between the joint pathologies are very different. This suggests that even if both models are ultimately definable as different OA phenotypes, how one might plan to target or treat the disease has to be different. Furthermore, if despite ultimately similar OA pathology, the disease pathophysiology (tissue relationships and time course) differs between the models, does this mean the pathology/pain relationship and pain pathophysiology/molecular mechanisms will also differ? The relationship between pathology and pain in DMM versus AIA will be explored in the following chapters.

CHAPTER 5: Pain behaviour outcomes following destabilization of the medial meniscus (DMM) and antigen-induced arthritis (AIA) in mice

5.1 Introduction and aims

In the previous chapter, the progressive histopathological changes that occur in different knee joint tissue structures following induction of arthritis using the DMM and the AIA models were evaluated, and different tissue pathology associations identified for each model. Interestingly, these joint pathology associations were not time dependent, and in contrast to the indistinguishable OA-like pathology observed in both models at week 16, were very much model-specific.

In this chapter, activity-based and evoked pain-response behaviours were measured following induction of arthritis using DMM and AIA. This enabled further differentiation between the two models through evaluation of different pain related behaviours at key stages of disease development, as well as characterization of the temporal pattern of behaviour demonstrated in the two arthritis models. Associations between different pain behaviour outcomes were also investigated.

Animal models are a useful pre-clinical research tool that are used to understand disease pathophysiology and facilitate the development and testing of new therapeutic agents (128). In the case of OA, the focus of pre-clinical research is to develop and test therapeutic agents that not only demonstrate efficacy with respect to halting joint disease progression and initiating joint pathology repair, but also that target the most clinically relevant disease symptom – pain (391).

The challenge then becomes to identify animal models that mimic OA joint disease pathophysiology and symptomatology (399). This challenge is made even greater

because of the complex nature of pain as both a symptom and a disease. Defining and quantifying pain in a pre-clinical setting is difficult (363). This in part explains why pre-clinical OA models remain unreliable predictors of disease response in humans and why favorable outcomes in animal models do not readily translate to effective human therapies (128).

To address this current impediment to translation in OA research, pain outcomes in this thesis were defined (in terms that reflect what has been observed clinically in human OA), standardized (by developing detailed protocols on how tests are conducted to minimize operator variability), and then measured simultaneously in two animal models over a defined time period that reflected joint disease progression. The two models were specifically selected because; one has been used extensively to investigate OA specific pathophysiology (DMM) (28, 47, 407, 439) and one has been used to investigate arthritis pain and inflammatory pain mechanisms more broadly (AIA) (198, 453, 519, 594, 595).

The aims of chapter 5 are:

1. To characterize and compare the pain related behaviours that develop with knee joint arthritis induced by DMM and AIA.
2. To track, in parallel, how each pain related behaviour changes temporally with disease progression in the two models of arthritis.
3. To identify any associations between different pain-related behaviours in the two models of arthritis.

5.2 Methods, statistical analysis and data presentation

Details of the methods used to induce the two models of arthritis, DMM and AIA, are described in chapter 2, section 2.1. The pain assays used in this chapter have previously been reported and validated (316, 465, 493, 517, 545), and the exact methods used for carrying out the pain tests were developed by the researcher (chapter 3, section 3.1) and described in chapter 2, section 2.3.

Comparison of pain data between treatment groups and time points were analysed using the nonparametric ranked Kruskal-Wallis analysis for multiple groups and, where there was significance, post hoc analysis using the Mann Whitney U-test (for unpaired data) was performed for between group comparisons. Within treatment group comparisons relative to baseline were conducted using the Wilcoxon signed-rank test (StataSE software, Stata corporation, TX, USA). The results are presented graphically as means with error bars depicting the standard error of each data set.

The experiments reported in this chapter were designed to be hypothesis generating due to the variable nature of pain behaviour data and the fact that pain testing as described in this thesis (refer to Chapters 2 and 3) has not previously been conducted in two distinct arthritis models, tested longitudinally at the same time points over a 16 week period of joint disease progression. For this reason, the alpha value was set at 0.05 and the Benjamini-Hochberg correction was not applied to the *P* values to correct for repeated measures.

Associations between the different pain related behaviours were determined by generating partial correlation coefficients, using Kendall's tau-b (565). This nonparametric process uses pairwise ranked data values between the two variables under study (ordinal scores) and thus does not require data to be normally distributed or the relationship between the variables to be linear. Linear regression was used to

determine whether the pain-related behavior outcome variables changed over time; and when correcting for time, whether there was a difference between treatments.
In the results, 'significance' refers to statistical significance, with *p* values included in the relevant results tables (Tables 5.1 – 5.7).

5.3 Results

Changes from baseline were observed in both AIA and DMM mice at different time points for the different pain related behaviours. These changes followed a similar trend in both animal models. However, a model-specific temporal pattern was observed for individual pain-related behaviours. These model-specific temporal changes are readily visible in figures 5.1c, 5.3c, 5.4c, 5.5c and 5.5i and are discussed in the following sections.

5.3.1 Effect of AIA and DMM on tactile allodynia following induction of arthritis

Paw withdrawal, evoked by von Frey filament stimulation was used to calculate the 50% paw withdrawal threshold (PWT) as a measure of tactile allodynia. Following the establishment of a consistent method for measuring PWT evoked by von Frey filament stimulation, this pain assay was used to test for tactile allodynia in four separate experiments. The results reported in this section are the combined data from four cohorts of mice. Not all time points were captured for each mouse for several reasons. Firstly, a proportion of mice were culled at predetermined time points for the purpose of knee joint (see chapter 4) and DRG (see chapter 6) tissue harvesting. Secondly, we wished to avoid excessive testing and any confounding effect the associated stress of frequent testing would have on response thresholds. Any mice that

demonstrated extreme agitation and did not settle following the acclimatisation period were excluded from that test period, but were not excluded completely from the study. The decision to exclude an animal during a particular test period was made by the operator blinded to treatment. No particular treatment or sham group was excluded with any greater frequency. A total of 154 mice were used for testing. Ipsilateral 50% PWT's for DMM, AIA, sham and saline groups are summarised graphically in figure 5.1a-c and *P* values listed in Table 5.1. Contralateral 50% PWT's are summarized in figure 5.1d-f.

Table 5.1. Von Frey (ipsilateral 50% PWT)

Between treatment comparisons and within treatment changes compared to baseline. P-values shown in bold typeface are significant ($P<0.05$).

Time	Treatments	P – value (T1 vs. T2)*	Treatment	P – value (vs. D0)*
Day 0	DMM vs. Sham	0.582	DMM	-
	DMM vs. Control	0.373	Sham	-
	DMM vs. AIA	**0.022**	AIA	-
	AIA vs. Saline	0.536	Saline	-
	AIA vs. ImControl	0.065	Control	-
	AIA vs. Control	0.088	Im Control	-
Day 3	DMM vs. Sham	0.321	DMM	0.527
	DMM vs. Control	-	Sham	0.052
	DMM vs. AIA	**0.042**	AIA	**0.027**
	AIA vs. Saline	**0.013**	Saline	0.685
	AIA vs. ImControl	-	Control	-
	AIA vs. Control	-	Im Control	-
Week 1	DMM vs. Sham	-	DMM	-
	DMM vs. Control	-	Sham	-
	DMM vs. AIA	-	AIA	**<0.001**
	AIA vs. Saline	**<0.001**	Saline	**0.003**
	AIA vs. ImControl	**0.011**	Control	-
	AIA vs. Control	-	Im Control	**0.028**
Week 2	DMM vs. Sham	0.692	DMM	0.065
	DMM vs. Control	**0.005**	Sham	0.077
	DMM vs. AIA	1.000	AIA	**0.003**
	AIA vs. Saline	**0.002**	Saline	0.056
	AIA vs. ImControl	0.838	Control	0.249
	AIA vs. Control	**<0.001**	Im Control	**0.028**
Week 4	DMM vs. Sham	0.931	DMM	**0.017**
	DMM vs. Control	**0.001**	Sham	**0.013**
	DMM vs. AIA	0.150	AIA	**<0.001**
	AIA vs. Saline	0.784	Saline	**0.008**
	AIA vs. ImControl	0.878	Control	0.753
	AIA vs. Control	**0.003**	Im Control	**0.028**
Week 8	DMM vs. Sham	0.593	DMM	0.108
	DMM vs. Control	0.066	Sham	0.224
	DMM vs. AIA	0.915	AIA	**<0.001**
	AIA vs. Saline	0.621	Saline	**<0.001**
	AIA vs. ImControl	0.655	Control	0.116
	AIA vs. Control	**0.007**	Im Control	**0.028**
Week 12	DMM vs. Sham	**0.035**	DMM	0.117
	DMM vs. Control	**0.038**	Sham	0.272
	DMM vs. AIA	0.654	AIA	0.333
	AIA vs. Saline	0.234	Saline	0.056
	AIA vs. ImControl	0.417	Control	0.115
	AIA vs. Control	**0.020**	Im Control	**0.046**
Week 16	DMM vs. Sham	0.175	DMM	**0.041**
	DMM vs. Control	**0.002**	Sham	0.783
	DMM vs. AIA	0.305	AIA	**0.019**
	AIA vs. Saline	0.067	Saline	**0.016**
	AIA vs. ImControl	0.092	Control	0.345
	AIA vs. Control	**0.017**	Im Control	**0.028**

* T1 and T2 = 1st and 2nd treatment, D0 = baseline

Baseline ipsilateral PWT in DMM and AIA mice was not significantly different from the respective control groups or age matched naïve mice (P = 0.582). Baseline contralateral PWT in DMM and AIA mice was also not significantly different from the respective control groups or age matched naïve mice (P = 0.355).

Ipsilateral PWT decreased significantly compared to age matched naïve mice in both the AIA and DMM model. In the AIA model, both saline-injected and mBSA-injected mice developed early (day 3) ipsilateral tactile allodynia. However, the decrease in PWT was significantly greater in AIA mice compared to saline-injected mice at day 3 (P = 0.013), week 1 (P < 0.001), and week 2 (P = 0.002). Immunised control mice that did not receive an intra-articular injection also developed persistent ipsilateral tactile allodynia (figure 5.1g).

In the DMM model, both sham and DMM mice developed early ipsilateral tactile allodynia by day 3. This began to resolve in sham mice after week 8 testing, and returned to baseline levels by week 12. In contrast, the tactile allodynia that developed in DMM mice persisted over the 16-week time course.

In the contralateral limb, significant differences in PWT between the six treatment and control groups were only observed at week 1 (P = 0.014) and week 16 (P = 0.034) following induction of arthritis. In general, there was greater variability in PWT within treatment groups and between treatment groups over time, on the contralateral side (figure 5.1f and 5.1h).

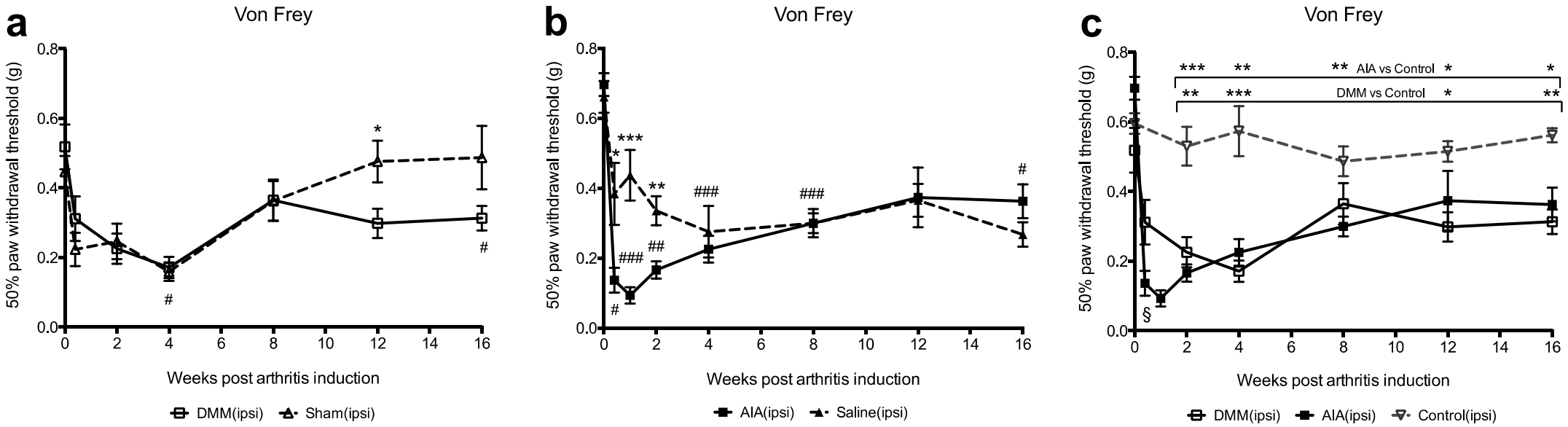

Figure 5.1a-c. Ipsilateral 50% Paw Withdrawal Threshold (PWT)

Using von Frey filament stimulation of the hind paws, as a measure of tactile allodynia in DMM vs. sham (a); AIA vs. saline (b); and DMM vs. AIA (c) mice at day 3, week 1, 2, 4, 8, 12 and 16 following induction of arthritis. The results are presented graphically as a line graph of the means with SEM's marked. Significance for Treatment vs. sham/saline/control = $P<0.05$ (*); $P<0.01$ (**); and $P<0.001$ (***). Significance for Treatment vs. baseline (day 0) = $P<0.05$ (#); $P<0.01$ (##); and $P<0.001$ (###).

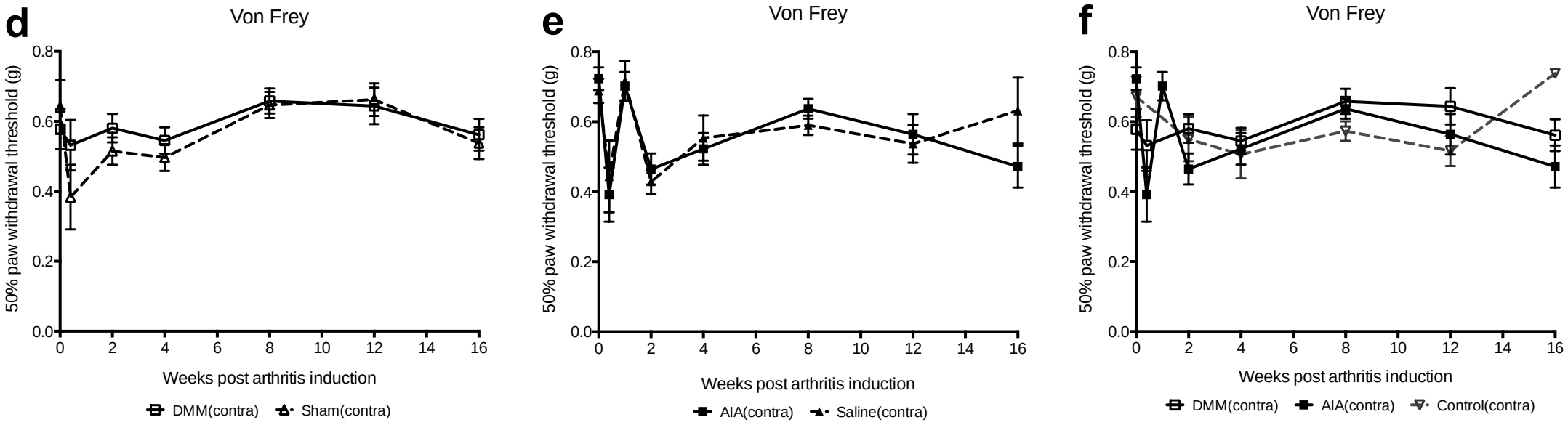

Figure 5.1d-f. Contralateral 50% Paw Withdrawal Threshold (PWT)

Using von Frey filament stimulation of the hind paws, as a measure of tactile allodynia in DMM vs. sham (d); AIA vs. saline (e); and DMM vs. AIA (f) mice at day 3, week 1, 2, 4, 8, 12 and 16 following induction of arthritis. The results are presented graphically as a line graph of the means with SEM's marked.

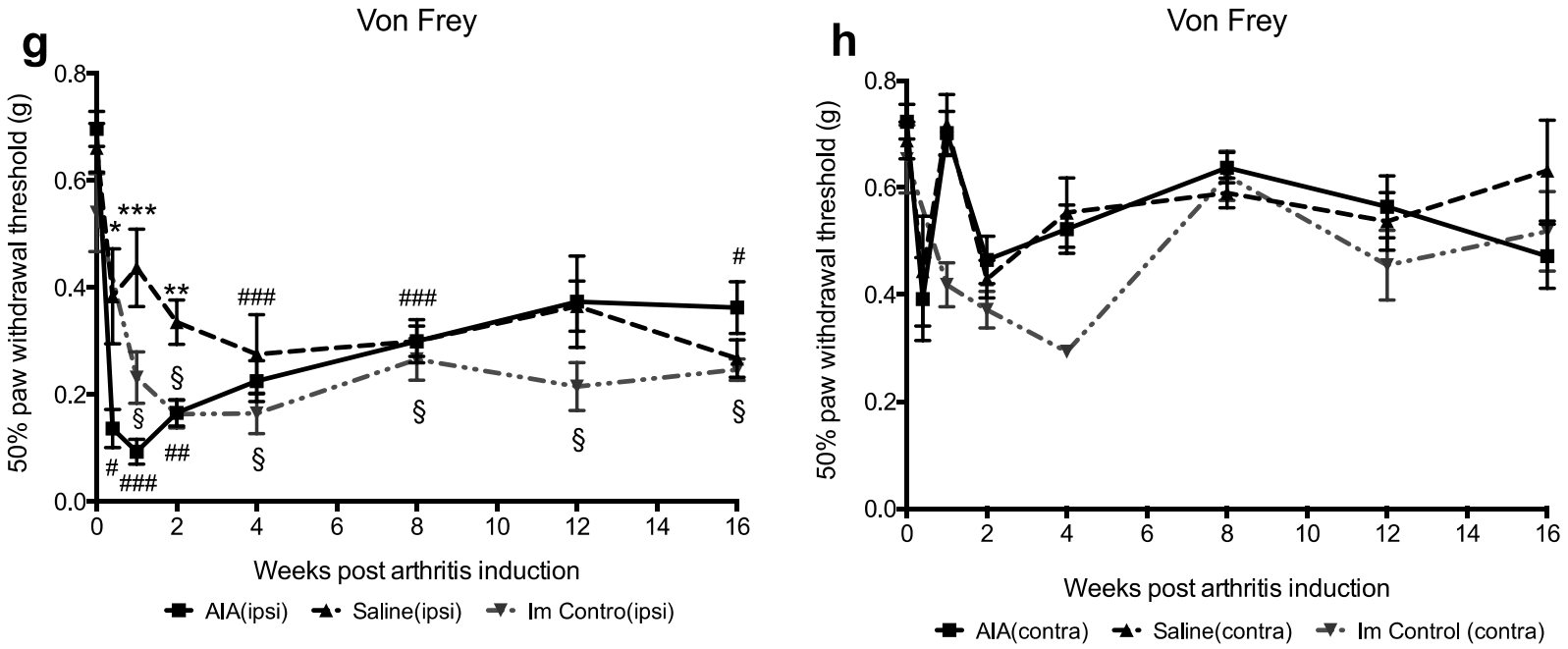

Figure 5.1g-h. 50% PWT in immunised only mice

Ipsilateral (g) and contralateral (h) 50% Paw Withdrawal Threshold (PWT) using von Frey filament stimulation of the hind paws, as a measure of tactile allodynia in immunised only (Im Control) mice and compared with AIA mice at day 3, week 1, 2, 4, 8, 12 and 16 following induction of arthritis. The results are presented graphically as a line graph of the means with SEM's marked. Significance for AIA vs. saline = $P<0.05$ (*); $P<0.01$ (**); and $P<0.001$ (***). Significance for AIA vs. baseline (day 0) = $P<0.05$ (#); $P<0.01$ (##); and $P<0.001$ (###). Significance for ImControl vs baseline (day 0) = $P< 0.05$ (§)

5.3.2 Effect of AIA and DMM on thermal hyperalgesia following induction of arthritis

Paw withdrawal latency (PWL) evoked by placing individual mice on a metal hotplate set at 52 degrees C, was used as a measure of thermal hyperalgesia. This pain assay was used to test for thermal hyperalgesia in five separate experiments. The results reported in this section are the combined data from five cohorts of mice. Not all time points were captured for each mouse because a proportion of mice were culled at predetermined time points for the purpose of knee joint and DRG tissue harvesting. Not all time points were captured in each cohort because of the confounding issue of conditioning when mice are tested too frequently on a hotplate (refer to Chapter 3).

Any mice that demonstrated extreme agitation and/or attempted to escape from the chamber by jumping as soon as they were placed on the hotplate even when it was set to room temperature, were excluded from testing. A total of 178 mice were used for testing. PWL's for AIA, DMM, saline, sham and control groups are summarised graphically in figure 5.2a-e and *P* values listed in Table 5.2.

Baseline PWL (figure 5.2a) was significantly different between the six treatment and control groups ($P = 0.027$). Post-hoc analysis identified a significant difference between saline injected and immunized control mice ($P = 0.023$). Baseline PWL for all other treatment and control/sham group combinations was not significantly different.

In all mice there was a temporal effect in the first week of testing with a decrease in PWL. This was followed by an increase in PWL at week 2. This decrease in PWL between baseline and the first test period only reached significance in the age matched control group ($P = 0.012$).

In AIA and saline injected mice there was a mild but significant decrease in PWL compared to baseline at week 8 (P = 0.041 and P = 0.017). In AIA mice this decrease in PWL was persistent and reached significance again at week 16 (P = 0.046). In saline injected mice PWL returned to above baseline levels by week 12. To investigate if immunisation alone had an effect on PWL, immunized non-injected mice were also tested (Figure 5.2e). In immunized control mice there was no significant difference between baseline and any of the other measured time points (week 1, 4 and 8). Baseline and week 1 PWLs were significantly lower in saline injected mice compared to immunised non-injected mice (P = 0.023 and 0.026).

In DMM mice PWL decreased from week 4 (P = 0.028) to week 16, compared to baseline. PWL was decreased in DMM mice compared to Shams from week 4 to week 16, but the difference between the groups was not significant. PWL was also decreased in DMM compared to AIA, reaching significance at week 4 only (P = 0.018).

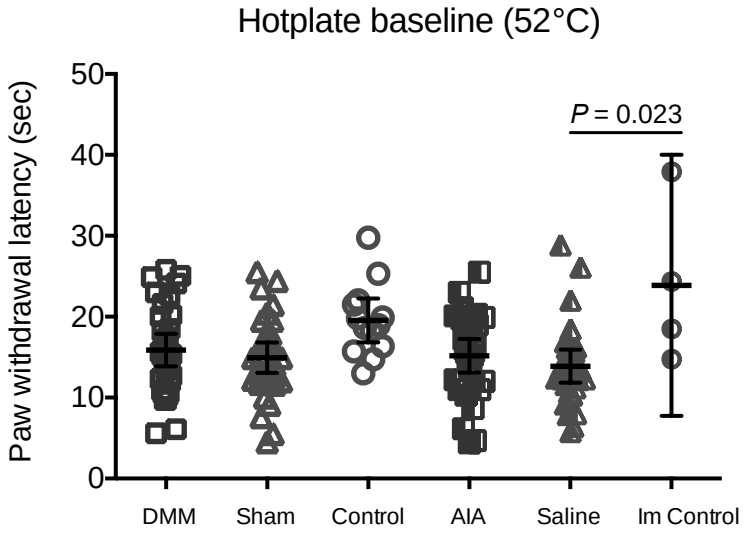

Figure 5.2a. Hotplate paw withdrawal latency (PWL) baseline

Evoked by placing individual mice on a metal hotplate set at 52^0C, was used as a measure of thermal hyperalgesia. The baseline values are presented graphically as a scatter plot (mean and 95% CI).

Table 5.2. Hotplate (52^0C PWL)
Between treatment comparisons and within treatment changes compared to baseline. P-values shown in bold typeface are significant (P<0.05). * T1 and T2 = 1st and 2nd treatment, D0 = baseline.

Time	Treatments	P – value (T1 vs. T2)*	Treatment	P – value (vs. D0)*
Day 0	DMM vs. Sham	0.582	DMM	-
	DMM vs. Control	0.125	Sham	-
	DMM vs. AIA	0.836	AIA	-
	AIA vs. Saline	0.179	Saline	-
	AIA vs. Im Control	0.098	Control	-
	AIA vs. Control	0.106	Im Control	-
Day 3	DMM vs. Sham	0.599	DMM	0.775
	DMM vs. Control	-	Sham	0.493
	DMM vs. AIA	0.789	AIA	0.909
	AIA vs. Saline	0.536	Saline	0.265
	AIA vs. Im Control	-	Control	-
	AIA vs. Control	-	Im Control	-
Week 1	DMM vs. Sham	0.641	DMM	0.347
	DMM vs. Control	0.194	Sham	0.454
	DMM vs. AIA	0.500	AIA	0.314
	AIA vs. Saline	0.120	Saline	0.230
	AIA vs. Im Control	0.171	Control	**0.012**
	AIA vs. Control	0.077	Im Control	0.465
Week 2	DMM vs. Sham	0.166	DMM	0.077
	DMM vs. Control	0.061	Sham	0.530
	DMM vs. AIA	0.564	AIA	0.388
	AIA vs. Saline	0.817	Saline	0.060
	AIA vs. Im Control	-	Control	-
	AIA vs. Control	0.261	Im Control	-
Week 4	DMM vs. Sham	0.140	DMM	**0.028**
	DMM vs. Control	0.159	Sham	0.093
	DMM vs. AIA	**0.018**	AIA	0.203
	AIA vs. Saline	0.388	Saline	0.241
	AIA vs. Im Control	0.580	Control	**0.028**
	AIA vs. Control	0.768	Im Control	0.273
Week 8	DMM vs. Sham	0.108	DMM	0.600
	DMM vs. Control	0.502	Sham	0.753
	DMM vs. AIA	0.063	AIA	**0.041**
	AIA vs. Saline	0.753	Saline	**0.017**
	AIA vs. Im Control	**0.040**	Control	0.655
	AIA vs. Control	0.909	Im Control	0.068
Week 12	DMM vs. Sham	0.465	DMM	0.225
	DMM vs. Control	0.053	Sham	0.345
	DMM vs. AIA	0.063	AIA	0.116
	AIA vs. Saline	0.214	Saline	0.292
	AIA vs. Im Control	0.077	Control	-
	AIA vs. Control	0.117	Im Control	-
Week 16	DMM vs. Sham	0.234	DMM	0.686
	DMM vs. Control	**0.028**	Sham	0.917
	DMM vs. AIA	0.462	AIA	**0.046**
	AIA vs. Saline	0.137	Saline	0.753
	AIA vs. Im Control	0.066	Control	-
	AIA vs. Control	**0.007**	Im Control	-

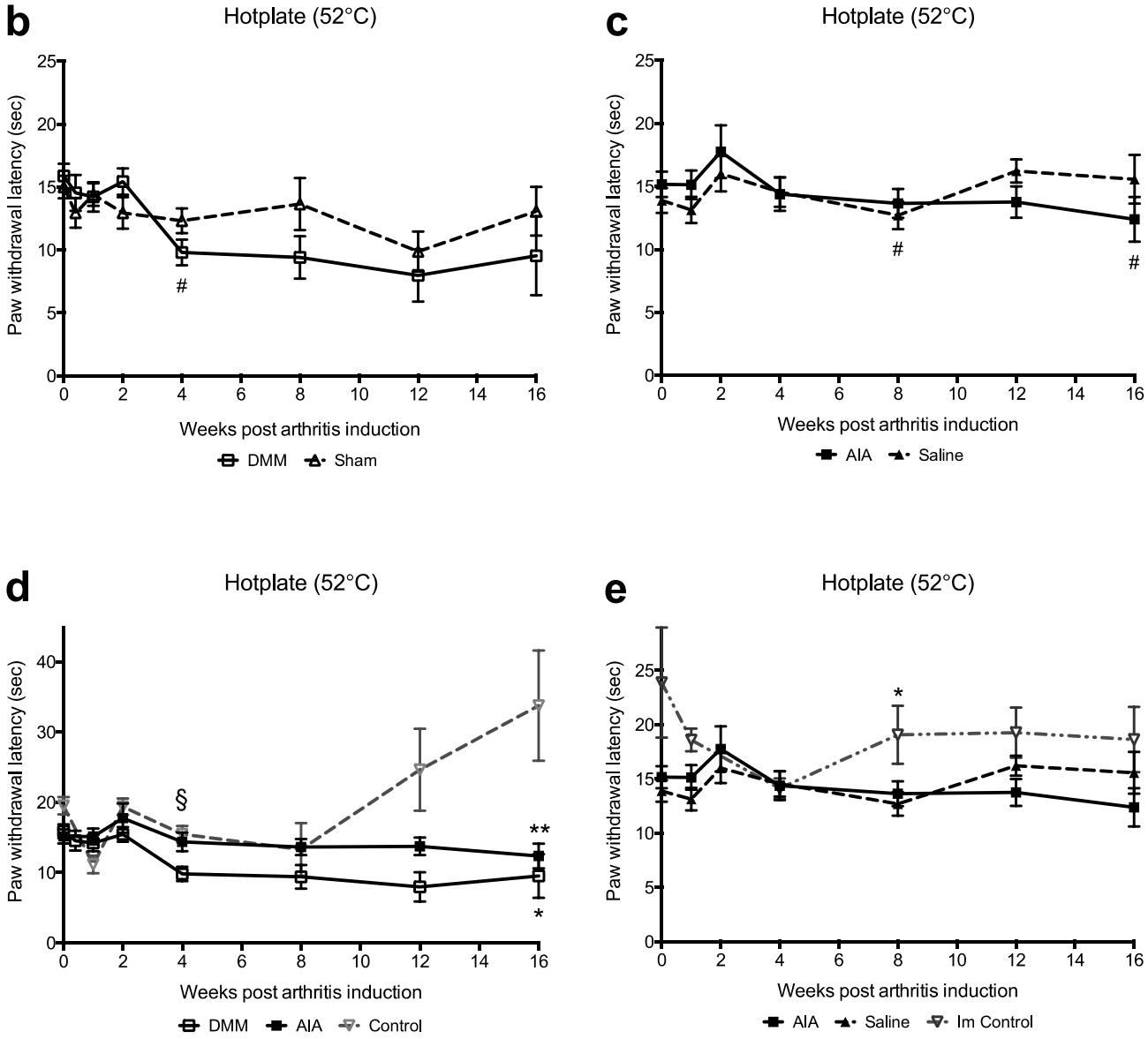

Figure 5.2b-e. Hotplate PWL

Evoked by placing individual mice on a metal hotplate set at 52 degrees C, was used as a measure of thermal hyperalgesia in DMM vs. sham (b); AIA vs. saline (c); DMM vs. AIA (d); and Immunised-control (e) mice at day 3, week 1, 2, 4, 8, 12 and 16 following induction of arthritis. The results are presented graphically as a line graph of the means with SEM's marked. Significance for Treatment vs. Control/ImControl = $P<0.05$ (*) and $P<0.01$ (**). Significance for Treatment vs. baseline (day 0) = $P<0.05$ (#); Significance for AIA vs DMM = $P< 0.05$ (§).

5.3.3 Effect of AIA and DMM on mechanical hyperalgesia following induction of arthritis

Paw withdrawal, evoked by applying digital pressure across the knee joint of individual mice, was used as a measure of mechanical hyperalgesia. This pain assay was used to test for mechanical hyperalgesia in two separate experiments. The results reported in this section are the combined data from two cohorts of mice. Not all time points were captured for each mouse because a proportion of mice were culled at predetermined time points for the purpose of knee joint and DRG tissue harvesting. Not all time points were captured in each cohort to avoid excessive testing and any confounding affect the associated stress of frequent restraint and testing would have on response thresholds (refer to Chapter 3). If an individual mouse could not be restrained appropriately for testing without exerting excessive force the measurement was excluded for that time point but the mouse was not excluded from the study. A total of 131 mice were used for testing. PWT for AIA, DMM, saline, sham and control groups are summarised graphically in figure 5.3a-h and *P* values listed in Table 5.3.

Table 5.3. PAM device (right knee PWT)
Between treatment comparisons and within treatment changes compared to baseline. P-values shown in bold typeface are significant (P<0.05). * T1 and T2 = 1st and 2nd treatment, D0 = baseline.

Time	Treatments	P – value (T1 vs. T2)*	Treatment	P – value (vs. D0)*
Day 0	DMM vs. Sham	0.317	DMM	-
	DMM vs. Control	0.317	Sham	-
	DMM vs. AIA	-	AIA	-
	AIA vs. Saline	0.289	Saline	-
	AIA vs. Control	0.480	Control	-
	AIA vs. Im Control	0.242	Im Control	
Day 3	DMM vs. Sham	-	DMM	-
	DMM vs. Control	-	Sham	-
	DMM vs. AIA	-	AIA	-
	AIA vs. Saline	-	Saline	-
	AIA vs. Control	-	Control	-
	AIA vs. Im Control	-	Im Control	
Week 1	DMM vs. Sham	-	DMM	-
	DMM vs. Control	-	Sham	-
	DMM vs. AIA	-	AIA	0.109
	AIA vs. Saline	0.788	Saline	0.317
	AIA vs. Control	-	Control	-
	AIA vs. Im Control	0.708	Im Control	**0.007**
Week 2	DMM vs. Sham	0.091	DMM	-
	DMM vs. Control	**0.047**	Sham	-
	DMM vs. AIA	0.563	AIA	-
	AIA vs. Saline	0.648	Saline	-
	AIA vs. Control	**0.026**	Control	-
	AIA vs. Im Control	-	Im Control	-
Week 4	DMM vs. Sham	-	DMM	-
	DMM vs. Control	-	Sham	-
	DMM vs. AIA	-	AIA	-
	AIA vs. Saline	0.725	Saline	0.317
	AIA vs. Control	-	Control	-
	AIA vs. Im Control	0.845	Im Control	0.578
Week 6	DMM vs. Sham	0.169	DMM	0.052
	DMM vs. Control	0.209	Sham	0.425
	DMM vs. AIA	0.112	AIA	-
	AIA vs. Saline	0.565	Saline	-
	AIA vs. Control	0.887	Control	0.388
	AIA vs. Im Control	-	Im Control	-
Week 8	DMM vs. Sham	-	DMM	-
	DMM vs. Control	-	Sham	-
	DMM vs. AIA	-	AIA	-
	AIA vs. Saline	0.150	Saline	-
	AIA vs. Control	-	Control	-
	AIA vs. Im Control	0.156	Im Control	-
Week 12	DMM vs. Sham	0.652	DMM	-
	DMM vs. Control	-	Sham	-
	DMM vs. AIA	0.385	AIA	-
	AIA vs. Saline	0.107	Saline	-
	AIA vs. Control	-	Control	-
	AIA vs. Im Control	-	Im Control	-

Week 14	DMM vs. Sham	0.740	DMM	**0.035**
	DMM vs. Control	-	Sham	0.087
	DMM vs. AIA	-	AIA	-
	AIA vs. Saline	-	Saline	-
	AIA vs. Control	-	Control	-
	AIA vs. Im Control	-	Im Control	-
Week 16	DMM vs. Sham	0.149	DMM	**0.028**
	DMM vs. Control	**0.002**	Sham	0.140
	DMM vs. AIA	**0.010**	AIA	-
	AIA vs. Saline	0.600	Saline	-
	AIA vs. Control	0.221	Control	0.317
	AIA vs. Im Control	0.180	Im Control	-

There was no significant difference between baseline PWT for the six different treatment and control groups in either the right (P = 0.518) or left (P = 0.192) knee joint.

In the AIA model ipsilateral PWT decreased at two weeks following induction of arthritis and at two weeks there was a significant difference in ipsilateral PWT between AIA and aged matched control mice (P = 0.026). By week 16 ipsilateral PWL returned to baseline levels. A similar pattern of change was observed in both saline-injected and immunized control mice. But, there were no significant differences observed in the saline injected or immunized control mice compared with age-matched control mice, at any of the measured time points.

In the DMM model ipsilateral PWT also decreased at two weeks following induction of arthritis and remained decreased until week 16. In DMM ipsilateral PWT was significantly lower than age-matched controls at week 2 (P = 0.047) and week 16 (P = 0.002). It was also significantly lower than baseline measurements in DMM mice at week 6 (P = 0.052), week 14 (P = 0.035) and week 16 (P = 0.028). The decrease in ipsilateral PWT in sham mice followed a similar temporal pattern but the decrease was of a much smaller magnitude and was not significantly different from baseline or compared to age matched controls at any measured time points.

Contralateral PWT conformed to a similar temporal pattern of change in both AIA and DMM mice, however the decreases were minimal and not significant.

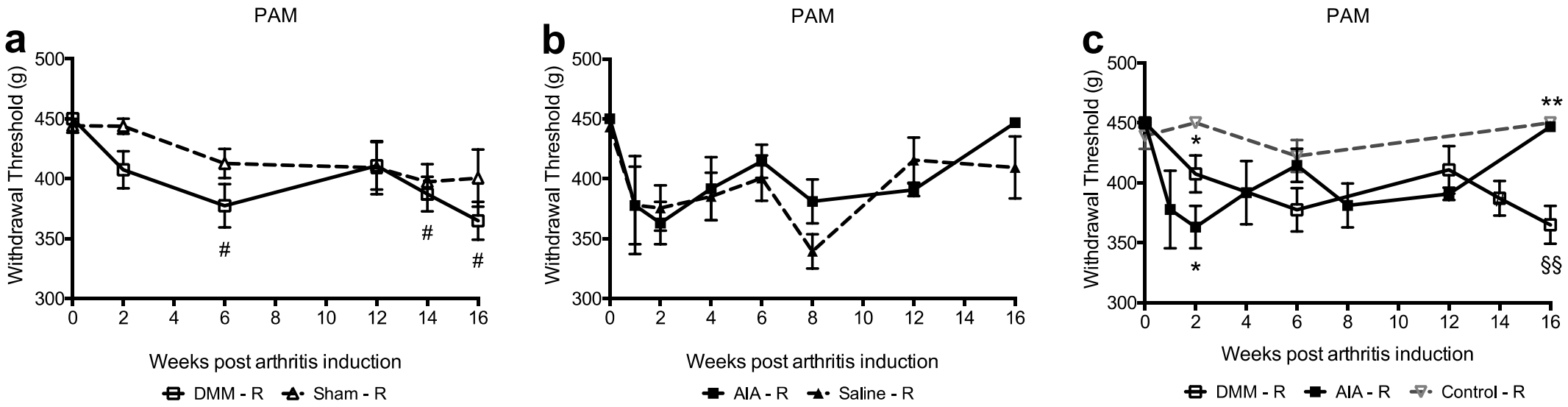

Figure 5.3a-c. Ipsilateral paw withdrawal threshold (PWT)

Using the PAM device across the knee joint, as a measure of mechanical hyperalgesia in DMM vs. sham (a); AIA vs. saline (b); and DMM vs. AIA (c) mice at day 3, week 1, 2, 4, 8, 12, 14 and 16 following induction of arthritis. The results are presented graphically as a line graph of the means with SEM's marked. Significance for Treatment vs. control = $P<0.05$(*); and $P<0.01$(**). Significance for Treatment vs. baseline (day 0) = $P<0.05$(#). Significance for AIA vs. DMM =$P< 0.01$(§§).

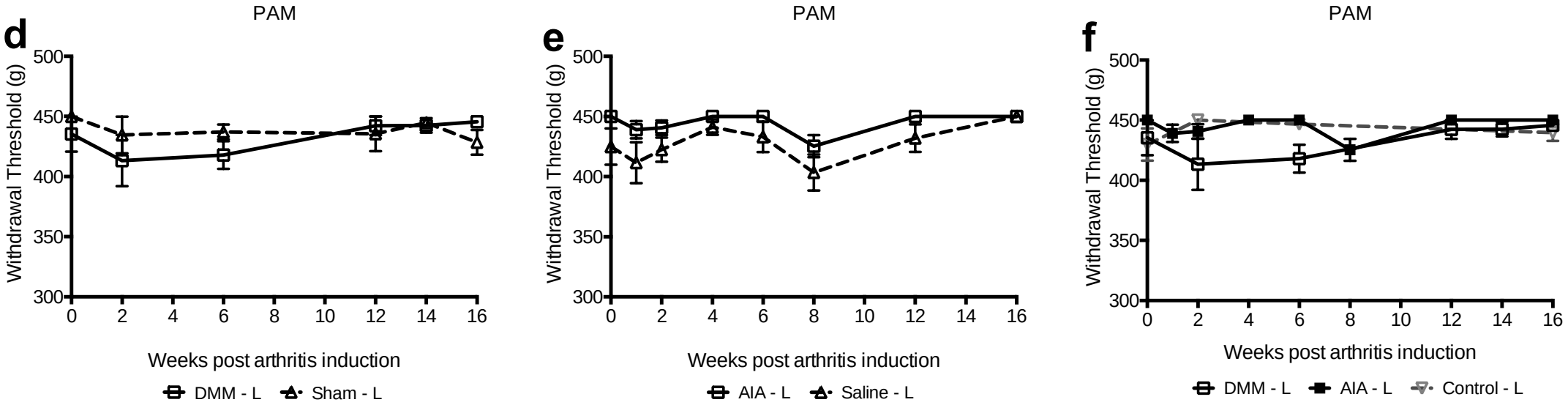

Figure 5.3d-f. Contralateral paw withdrawal threshold (PWT)

Using the PAM device across the knee joint, as a measure of mechanical hyperalgesia in DMM vs. sham (a); AIA vs. saline (b); and DMM vs. AIA (c) mice at day 3, week 1, 2, 4, 8, 12, 14 and 16 following induction of arthritis. The results are presented graphically as a line graph of the means with SEM's marked.

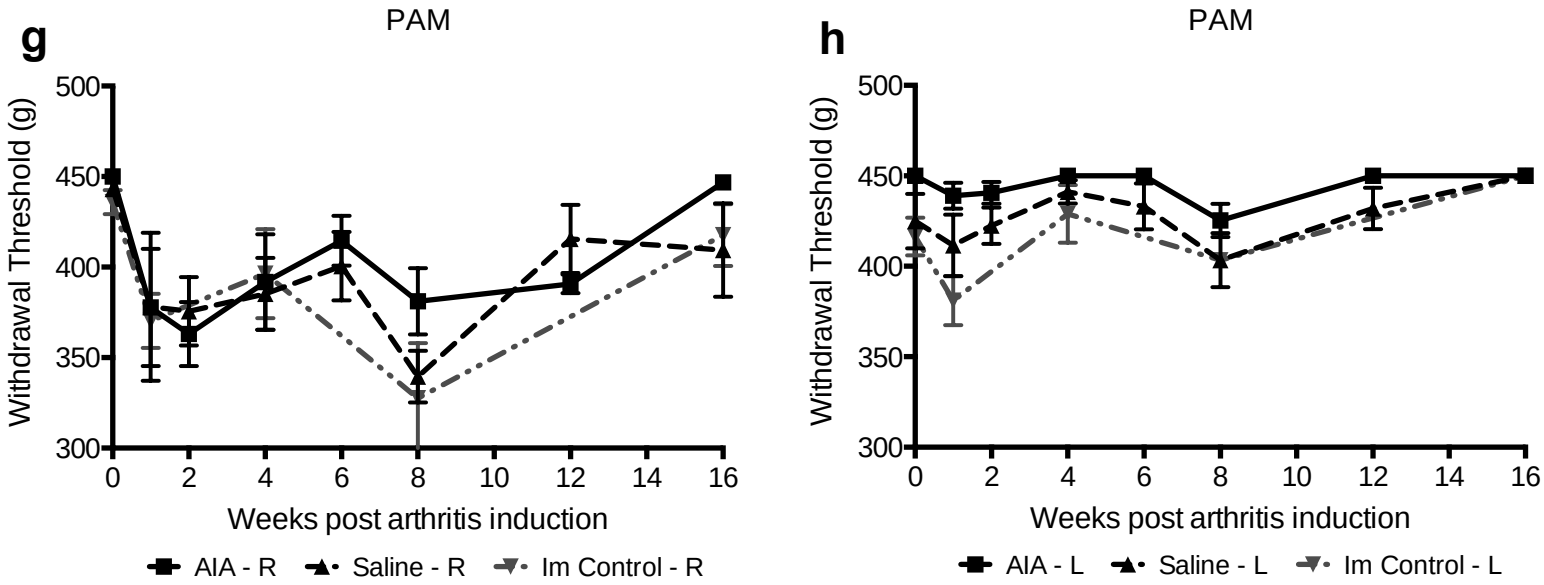

Figure 5.3g-h. PWT in immunised only mice

Ipsilateral (g) and contralateral (h) PWT using the PAM device across the knee joint, as a measure of mechanical hyperalgesia in Immunised only (Im-control) and compared with AIA mice at day 3, week 1, 2, 4, 8, 12 and 16 following induction of arthritis. The results are presented graphically as a line graph of the means with SEM's marked.

5.3.4 Effect of AIA and DMM on hind limb weight distribution following induction of arthritis

Hind limb (HL) weight distribution was measured in mice across six experiments, and the results reported in this section are the combined data from six cohorts of mice. Not all time points were captured for each mouse because a proportion of mice were culled at predetermined time points for the purpose of knee joint and DRG tissue harvesting. Not all time points were captured in each cohort to avoid excessive testing and any confounding affect the associated stress of frequent restraint and confinement in a small test chamber would have on stress induced analgesia (refer to Chapter 3). If an individual mouse was unable to settle in the test chamber the measurement was excluded for that time point but the mouse was not excluded from the study. A total of 229 mice were used for testing. HL weight distribution, expressed as the ratio of right to left HL weight bearing force in grams, for AIA, DMM, saline, sham and control groups are summarised graphically in figure 5.4a-d and *P* values listed in Table 5.4.

Table 5.4. Forceplate (hindlimb weight distribution)
Between treatment comparisons and within treatment changes compared to baseline. P-values shown in bold typeface are significant (P<0.05). * T1 and T2 = 1st and 2nd treatment, D0 = baseline.

Time	Treatments	P – value (T1 vs. T2)*	Treatment	P – value (vs. D0)*
Day 0	DMM vs. Sham	0.255	DMM	-
	DMM vs. Control	0.086	Sham	-
	DMM vs. AIA	0.542	AIA	-
	AIA vs. Saline	0.452	Saline	-
	AIA vs. ImControl	-	Control	-
	AIA vs. Control	0.180		
Day 3	DMM vs. Sham	0.097	DMM	< **0.001**
	DMM vs. Control	-	Sham	< **0.001**
	DMM vs. AIA	<**0.001**	AIA	< **0.001**
	AIA vs. Saline	<**0.001**	Saline	0.116
	AIA vs. ImControl	-	Control	-
	AIA vs. Control	-		
Week 1	DMM vs. Sham	0.379	DMM	**0.005**
	DMM vs. Control	-	Sham	**0.019**
	DMM vs. AIA	<**0.001**	AIA	<**0.001**
	AIA vs. Saline	<**0.001**	Saline	0.732
	AIA vs. ImControl	**0.001**	Control	-
	AIA vs. Control	-		
Week 2	DMM vs. Sham	0.177	DMM	**0.040**
	DMM vs. Control	0.152	Sham	0.082
	DMM vs. AIA	<**0.001**	AIA	<**0.001**
	AIA vs. Saline	<**0.001**	Saline	0.254
	AIA vs. ImControl	-	Control	-
	AIA vs. Control	**0.012**		
Week 4	DMM vs. Sham	0.120	DMM	0.469
	DMM vs. Control	0.549	Sham	**0.026**
	DMM vs. AIA	**0.003**	AIA	**0.016**
	AIA vs. Saline	**0.008**	Saline	0.124
	AIA vs. ImControl	0.477	Control	0.075
	AIA vs. Control	**0.004**		
Week 8	DMM vs. Sham	0.949	DMM	0.117
	DMM vs. Control	0.127	Sham	0.148
	DMM vs. AIA	0.670	AIA	0.215
	AIA vs. Saline	0.942	Saline	0.210
	AIA vs. ImControl	0.055	Control	0.345
	AIA vs. Control	0.423		
Week 12	DMM vs. Sham	0.322	DMM	0.913
	DMM vs. Control	0.641	Sham	**0.011**
	DMM vs. AIA	0.093	AIA	0.200
	AIA vs. Saline	0.784	Saline	0.093
	AIA vs. ImControl	0.162	Control	0.463
	AIA vs. Control	0.067		
Week 16	DMM vs. Sham	0.676	DMM	**0.018**
	DMM vs. Control	0.108	Sham	**0.017**
	DMM vs. AIA	0.615	AIA	0.100
	AIA vs. Saline	0.249	Saline	0.859
	AIA vs. ImControl	0.363	Control	0.116
	AIA vs. Control	0.059		

Baseline hind limb weight distribution in AIA and DMM mice was not significantly different from the respective control groups or age matched naïve mice ($P = 0.235$). There was no significant change in HL weight distribution at any of the measured time points (Figure 5.4d) in control, saline injected or immunized non-injected mice.

A similar temporal pattern of change in HL weight distribution was observed in both AIA and DMM mice, with a decrease in right HL weight bearing in the early stages of the disease (week 1 – 4) following induction of arthritis. This decrease was not detected consistently in the chronic phase of the disease in either arthritis models. The changes in HL weight distribution were greater in magnitude and lasted longer in AIA mice.

In AIA mice right to left HL weight distribution decreased significantly at day 3 ($P < 0.005$), week 1 ($P < 0.005$), week 2 ($P < 0.005$) and week 4 ($P = 0.016$), after induction of arthritis compared to baseline (Figure 5.4a).

In DMM mice right to left HL weight distribution decreased significantly at day 3 ($P < 0.005$), week 1 ($P = 0.005$), week 2 ($P = 0.040$) and then again at week 16 ($P = 0.018$) after induction of arthritis. In sham mice the initial decrease in HL weight distribution was less and was only significant at day 3 ($P < 0.005$) and week 1 ($P = 0.019$). Interestingly, sham mice also demonstrated a second phase of reduced HL weight distribution, that was significantly reduced compared to baseline at week 4 ($P = 0.026$), week 12 ($P = 0.011$) and 16 ($P = 0.017$).

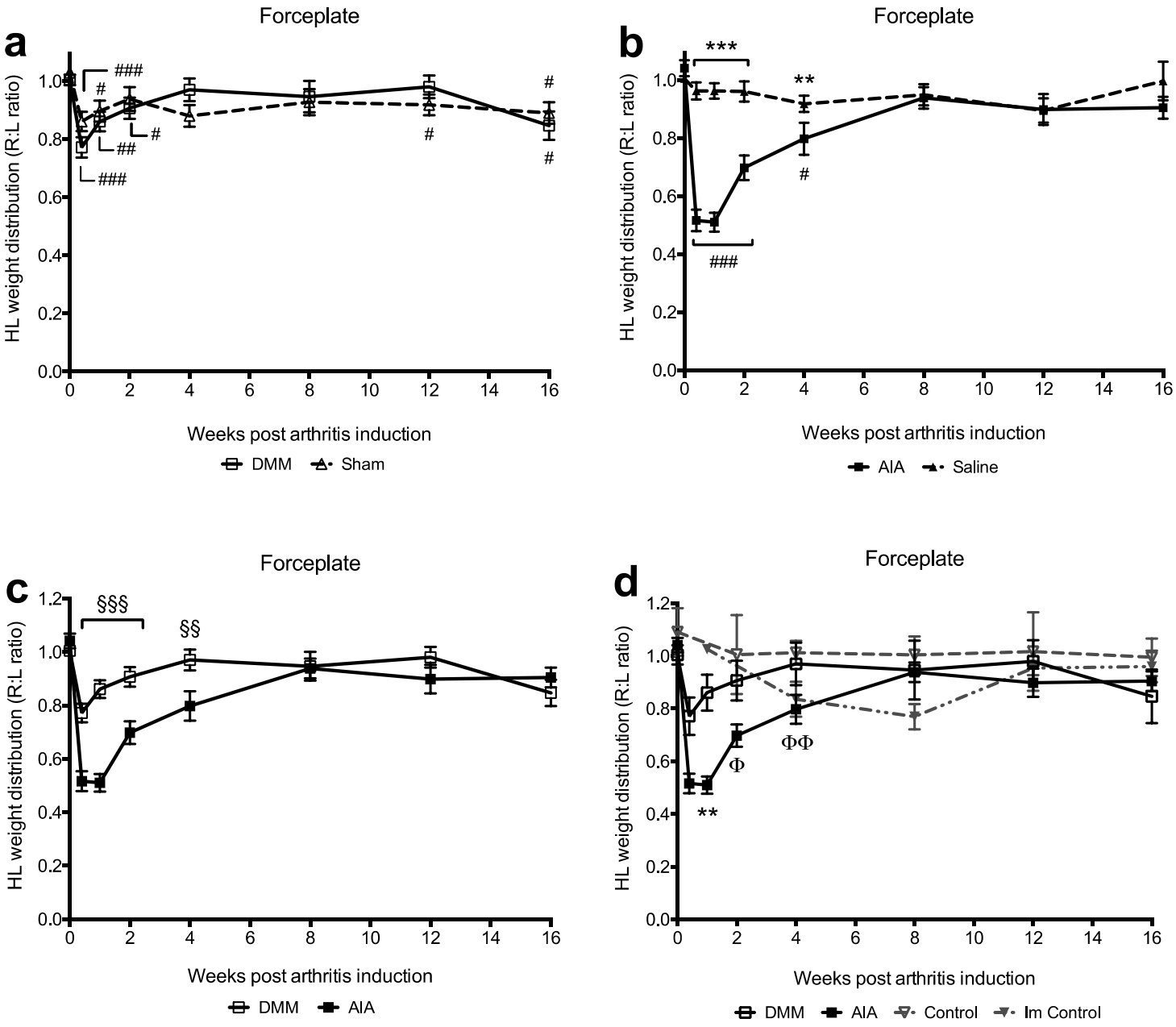

Figure 5.4a-d. Hind limb (HL) weight distribution

Measured using a Forceplate, and expressed as right to left (R:L) HL ratio, in DMM vs. sham (a); AIA vs. saline (b); DMM vs. AIA (c); and Immunised-control (d) mice at day 3, week 1, 2, 4, 8, 12 and 16 following induction of arthritis. The results are presented graphically as a line graph of the means with SEM's marked. Significance for AIA vs. Saline/ImControl = $P<0.01$ (**); and $P<0.001$ (***). Significance for Treatment vs. baseline (day 0) = $P<0.05$ (#); $P<0.01$ (##); and $P<0.001$ (###). Significance for AIA vs DMM = $P< 0.01$ (§§); and $P< 0.001$ (§§§). Significance for AIA vs. Control = $P<0.05$ (Φ); and $P<0.01$ (ΦΦ)

5.3.5 Effect of AIA and DMM on stride length following induction of arthritis

Gait was characterised by measuring changes in stride length. Stride length was determined by measuring the distance between the right and left HL paw print (right-to-left stride length; RLS), the left and right HL paw print (left-to-right stride length; LRS), and the distance from one right HL paw print to the next (full stride length right; FSLR), and one left HL paw print to the next (full stride length left; FSLL). Five consecutive measurements were averaged to determine a final value for each stride length parameter. Results for RLS, LRS, FSLR and FSLL are depicted graphically in figures 5.5a – 5.5l and *P* values listed in Table 5.5a – 5.5d.

The stride measurements were also used to calculate the right relative step (LRS:FSLL ratio) when weight bearing on the unaffected limb, and the left relative step (RLS:FSLR ratio) when weight bearing on the affected limb. FSL is closely associated with walking speed and so normalising stride length to a complete walk cycle (FSL) eliminates speed (493, 557) as a confounding factor when interpreting changes in stride length following induction of arthritis in the two models. Results for right and left relative step are depicted graphically in figures 5.5m and 5.5n.

Measurements were performed across two experiments, and the results reported in this section are the combined data from three cohorts of mice. Not all time points were captured for each mouse because a proportion of mice were culled at predetermined time points for the purpose of knee joint and DRG tissue harvesting. Also, during some test periods individual mice stopped too frequently to allow measurement of at least 5 consecutive uninterrupted strides. The most common behaviour displayed during stopping was grooming and urination. These mice were excluded from that single test period but were used for subsequent testing at later time points. A total of 84 mice were used for testing.

Table 5.5a. Stride length (right to left stride - RLS)
Between treatment comparisons and within treatment changes compared to baseline. P-values shown in bold typeface are significant (P<0.05). * T1 and T2 = 1st and 2nd treatment, D0 = baseline.

Time	Treatments	P – value (T1 vs. T2)*	Treatment	P – value (vs. D0)*
Day 0	DMM vs. Sham	0.874	DMM	-
	DMM vs. AIA	0.199	Sham	-
	AIA vs. Saline	0.180	AIA	-
			Saline	-
Day 3	DMM vs. Sham	0.505	DMM	0.615
	DMM vs. AIA	0.115	Sham	0.258
	AIA vs. Saline	0.058	AIA	**0.006**
			Saline	0.093
Week 1	DMM vs. Sham	0.773	DMM	0.308
	DMM vs. AIA	0.882	Sham	0.638
	AIA vs. Saline	0.467	AIA	0.446
			Saline	0.078
Week 2	DMM vs. Sham	0.326	DMM	0.814
	DMM vs. AIA	**0.051**	Sham	0.875
	AIA vs. Saline	0.537	AIA	0.828
			Saline	0.184
Week 4	DMM vs. Sham	0.749	DMM	0.462
	DMM vs. AIA	0.631	Sham	0.173
	AIA vs. Saline	1.000	AIA	0.753
			Saline	0.249
Week 8	DMM vs. Sham	0.873	DMM	0.345
	DMM vs. AIA	1.000	Sham	**0.028**
	AIA vs. Saline	0.631	AIA	**0.035**
			Saline	0.917
Week 12	DMM vs. Sham	0.100	DMM	0.138
	DMM vs. AIA	0.144	Sham	0.293
	AIA vs. Saline	0.295	AIA	0.345
			Saline	0.207
Week 16	DMM vs. Sham	0.715	DMM	0.893
	DMM vs. AIA	1.000	Sham	0.075
	AIA vs. Saline	1.000	AIA	0.600
			Saline	0.249

Table 5.5b. Stride length (left to right stride - LRS)
Between treatment comparisons and within treatment changes compared to baseline. P-values shown in bold typeface are significant ($P<0.05$). * T1 and T2 = 1st and 2nd treatment, D0 = baseline.

Time	Treatments	P – value (T1 vs. T2)*	Treatment	P – value (vs. D0)*
Day 0	DMM vs. Sham	0.658	DMM	-
	DMM vs. AIA	0.374	Sham	-
	AIA vs. Saline	0.800	AIA	-
			Saline	-
Day 3	DMM vs. Sham	0.783	DMM	0.754
	DMM vs. AIA	0.612	Sham	0.900
	AIA vs. Saline	0.636	AIA	0.113
			Saline	0.263
Week 1	DMM vs. Sham	0.236	DMM	0.433
	DMM vs. AIA	0.767	Sham	0.388
	AIA vs. Saline	0.669	AIA	0.744
			Saline	0.601
Week 2	DMM vs. Sham	0.141	DMM	0.158
	DMM vs. AIA	0.300	Sham	0.326
	AIA vs. Saline	0.613	AIA	0.349
			Saline	0.811
Week 4	DMM vs. Sham	0.065	DMM	0.075
	DMM vs. AIA	**0.055**	Sham	0.917
	AIA vs. Saline	0.262	AIA	0.753
			Saline	0.400
Week 8	DMM vs. Sham	0.262	DMM	0.600
	DMM vs. AIA	0.296	Sham	0.753
	AIA vs. Saline	0.149	AIA	0.753
			Saline	0.075
Week 12	DMM vs. Sham	1.000	DMM	0.686
	DMM vs. AIA	1.000	Sham	0.345
	AIA vs. Saline	0.150	AIA	0.917
			Saline	0.400
Week 16	DMM vs. Sham	0.068	DMM	0.138
	DMM vs. AIA	0.582	Sham	0.600
	AIA vs. Saline	0.873	AIA	**0.028**
			Saline	0.116

Table 5.5c. Stride length (full stride length right - FSLR)
Between treatment comparisons and within treatment changes compared to baseline. P-values shown in bold typeface are significant (P<0.05). * T1 and T2 = 1st and 2nd treatment, D0 = baseline.

Time	Treatments	P – value (T1 vs. T2)*	Treatment	P – value (vs. D0)*
Day 0	DMM vs. Sham	0.624	DMM	-
	DMM vs. AIA	0.237	Sham	-
	AIA vs. Saline	0.458	AIA	-
			Saline	-
Day 3	DMM vs. Sham	0.383	DMM	0.875
	DMM vs. AIA	0.354	Sham	0.730
	AIA vs. Saline	0.304	AIA	**0.015**
			Saline	0.985
Week 1	DMM vs. Sham	0.175	DMM	0.100
	DMM vs. AIA	0.751	Sham	0.754
	AIA vs. Saline	0.448	AIA	0.446
			Saline	**0.018**
Week 2	DMM vs. Sham	0.106	DMM	0.209
	DMM vs. AIA	0.117	Sham	0.255
	AIA vs. Saline	0.874	AIA	0.777
			Saline	0.231
Week 4	DMM vs. Sham	0.092	DMM	**0.046**
	DMM vs. AIA	0.078	Sham	0.462
	AIA vs. Saline	0.297	AIA	0.292
			Saline	0.141
Week 8	DMM vs. Sham	0.522	DMM	0.116
	DMM vs. AIA	0.337	Sham	0.600
	AIA vs. Saline	**0.045**	AIA	0.173
			Saline	0.116
Week 12	DMM vs. Sham	0.465	DMM	0.080
	DMM vs. AIA	0.144	Sham	0.345
	AIA vs. Saline	0.378	AIA	0.173
			Saline	0.917
Week 16	DMM vs. Sham	0.082	DMM	0.225
	DMM vs. AIA	0.715	Sham	0.917
	AIA vs. Saline	0.873	AIA	**0.027**
			Saline	0.917

Table 5.5d. Stride length (full stride length left - FSLL)
Between treatment comparisons and within treatment changes compared to baseline. P-values shown in bold typeface are significant (P<0.05). * T1 and T2 = 1st and 2nd treatment, D0 = baseline.

Time	Treatments	P – value (T1 vs. T2)*	Treatment	P – value (vs. D0)*
Day 0	DMM vs. Sham	0.887	DMM	-
	DMM vs. AIA	0.274	Sham	-
	AIA vs. Saline	0.445	AIA	-
			Saline	-
Day 3	DMM vs. Sham	0.581	DMM	0.730
	DMM vs. AIA	0.441	Sham	0.551
	AIA vs. Saline	0.245	AIA	**0.029**
			Saline	0.588
Week 1	DMM vs. Sham	0.237	DMM	0.182
	DMM vs. AIA	0.933	Sham	0.530
	AIA vs. Saline	0.537	AIA	0.744
			Saline	**0.026**
Week 2	DMM vs. Sham	0.248	DMM	0.071
	DMM vs. AIA	0.138	Sham	0.410
	AIA vs. Saline	0.849	AIA	0.879
			Saline	0.276
Week 4	DMM vs. Sham	0.109	DMM	**0.046**
	DMM vs. AIA	0.065	Sham	0.463
	AIA vs. Saline	0.262	AIA	0.463
			Saline	0.249
Week 8	DMM vs. Sham	0.337	DMM	0.074
	DMM vs. AIA	0.149	Sham	0.345
	AIA vs. Saline	0.199	AIA	0.249
			Saline	0.293
Week 12	DMM vs. Sham	0.201	DMM	0.080
	DMM vs. AIA	0.120	Sham	0.173
	AIA vs. Saline	0.575	AIA	0.075
			Saline	0.917
Week 16	DMM vs. Sham	0.359	DMM	0.174
	DMM vs. AIA	0.855	Sham	0.753
	AIA vs. Saline	0.748	AIA	**0.046**
			Saline	0.753

There was no significant difference for baseline RLS (P = 0.490), LRS (P = 0.758), FSLR (P = 0.567) or FSLL (P = 0.655) measurements between the four treatment groups. The mean baseline RLS, LRS, FSLR and FSLL were 31.6mm, 32.6mm, 63.5mm and 63.9mm respectively.

Changes in LRS followed a different temporal pattern in AIA and saline injected mice even though by week 16 LRS was the same for both groups (5.5b). In AIA mice LRS remained similar to baseline and only decreased significantly at week 16 (P = 0.028). In saline mice LRS was decreased week 4 to week 16 but this did not reach significance compared to day 0 or compared to AIA at any of the measured time points. In contrast, changes in RLS followed a similar temporal pattern in AIA and saline injected mice. In AIA and saline injected mice RLS was decreased at day 3 and week 8 but was only significant in AIA mice (P = 0.006 and P = 0.035 respectively). FSLR and FSLL were both significantly decreased at day 3 in AIA mice (P = 0.015 and 0.029) and increased at week 1 in saline injected mice (P = 0.018 and 0.026). FSLR and FSLL decreased further week 4 to week 16 in both AIA and saline injected mice, reaching significance in AIA mice at week 16 (P = 0.027 and 0.046).

The changes in stride length observed in DMM mice followed a different trend to AIA. LRS was decreased from week 4 to week 16 following induction of arthritis. In contrast RLS did not decrease until week 12. Both FSLR and FSLL increased initially at week 1 and then decreased, reaching significance at week 4 (P = 0.046 and 0.046). In sham mice RLS decreased significantly (P = 0.028) at week 8. The differences observed between DMM and sham mice for LRS and FSL measurements were not significant at any time point.

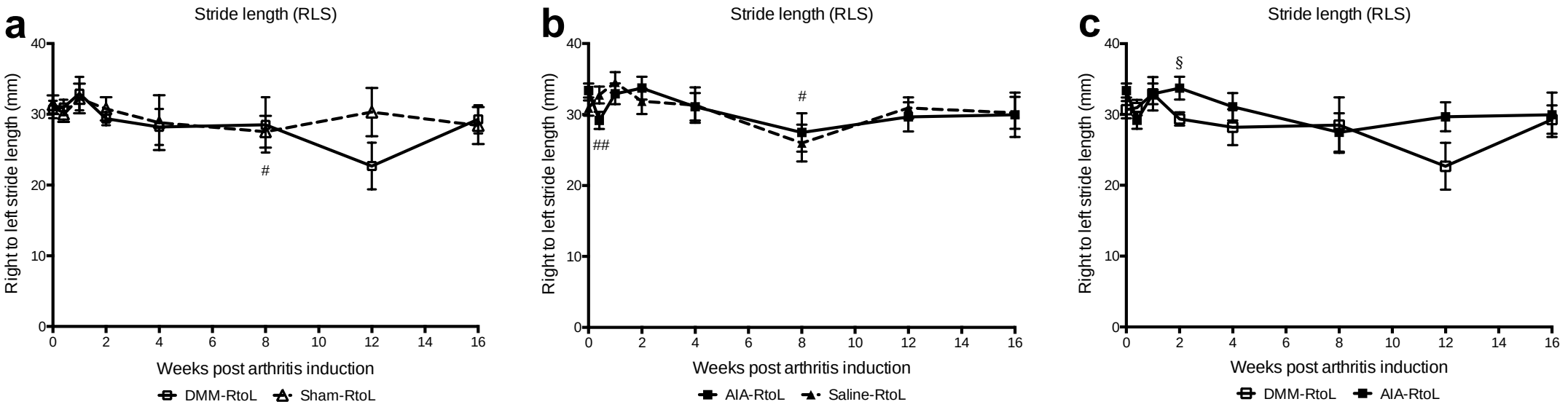

Figure 5.5a-c. Stride length I

Stride length measured as hind limb right to left stride (RLS) length, in DMM vs. sham (a); AIA vs. saline (b); and DMM vs. AIA (c) mice at day 3, week 1, 2, 4, 8, 12 and 16 following induction of arthritis. The results are presented graphically as a line graph of the means with SEM's marked. Significance for Treatment vs. baseline (day 0) = $P<0.05$ (#); and $P<0.01$ (##). Significance for AIA vs DMM = $P< 0.05$ (§).

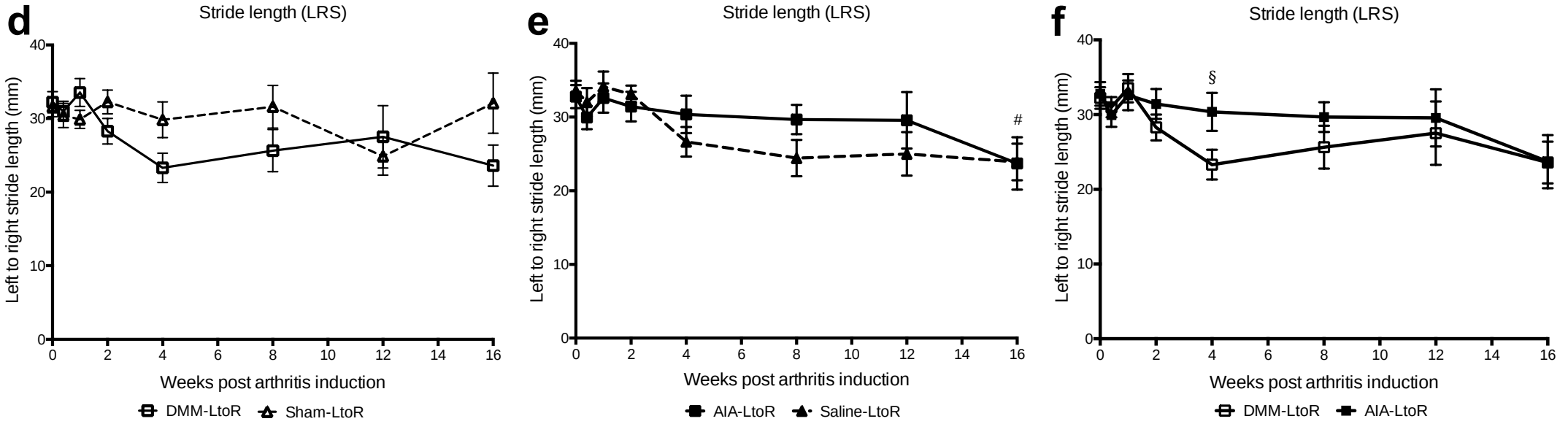

Figure 5.5d-f. Stride length II

Stride length measured as hind limb left to right stride (LRS) length, in DMM vs. sham (a); AIA vs. saline (b); and DMM vs. AIA (c) mice at day 3, week 1, 2, 4, 8, 12 and 16 following induction of arthritis. The results are presented graphically as a line graph of the means with SEM's marked. Significance for Treatment vs. baseline (day 0) = $P<0.05$ (#). Significance for AIA vs DMM = $P< 0.05$ (§).

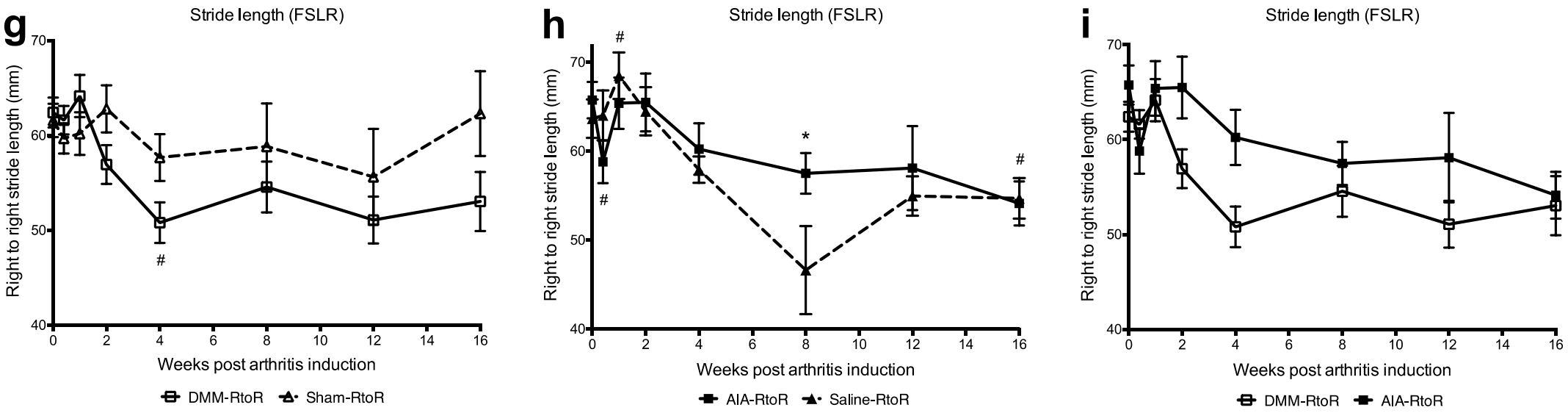

Figure 5.5g-i. Stride length III

Stride length measured as hind limb right to right full stride length (FSLR), in DMM vs. sham (a); AIA vs. saline (b); and DMM vs. AIA (c) mice at day 3, week 1, 2, 4, 8, 12 and 16 following induction of arthritis. The results are presented graphically as a line graph of the means with SEM's marked. Significance for AIA vs. Saline = $P<0.05$ (*). Significance for Treatment vs. baseline (day 0) = $P<0.05$ (#).

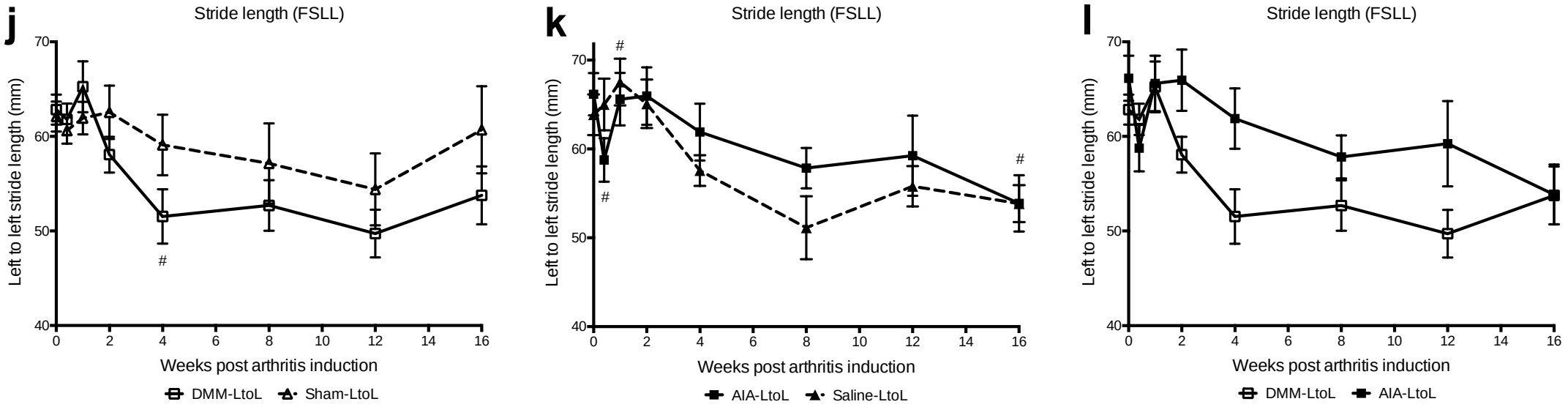

Figure 5.5j-l. Stride length IV

Stride length measured as hind limb left to left full stride length (FSLL), in DMM vs. sham (a); AIA vs. saline (b); and DMM vs. AIA (c) mice at day 3, week 1, 2, 4, 8, 12 and 16 following induction of arthritis. The results are presented graphically as a line graph of the means with SEM's marked. Significance for Treatment vs. baseline (day 0) = $P<0.05$ (#).

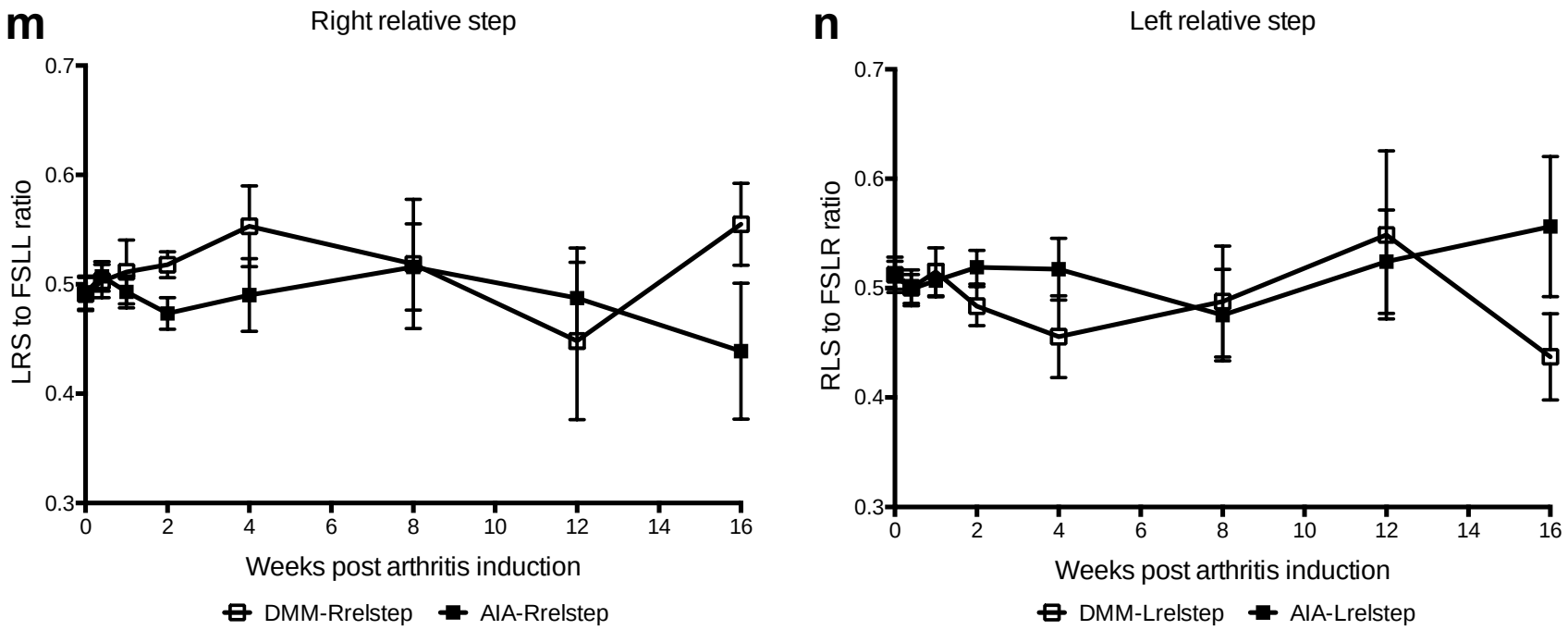

Figure 5.5m-n. Stride length V

Stride length expressed as relative step in DMM vs. AIA mice at day 3, week 1, 2, 4, 8, 12 and 16 following induction of arthritis. Right relative step (m) is defined as the relative stride length when supporting weight on the unaffected limb, and calculated as the LRS:FSLL ratio. Left relative step (n) is defined as the relative stride length when supporting weight on the affected limb, and calculated as the RLS to FSLR ratio. The results are presented graphically as a line graph of the means with SEM's marked.

The observed differences in LRS, RLS and FSLR between AIA and DMM demonstrated interesting trends although these differences were not significant. Right and left relative step displayed a similar pattern of change to LRS and RLS, in AIA mice. However, DMM displayed the reverse pattern of change to LRS and RLS, with an increased R relative step and decreased L relative step at week 16. So for DMM mice at week 16, when speed is accounted for, stride length is decreased when weight bearing on the affected limb and increased when weight bearing on the unaffected limb. The changes from baseline and the differences between treatment and sham groups were not significant.

5.3.6 Time and treatment effect on pain-related behaviours

Linear regression analysis was used to investigate the pattern of change over time for each pain-related behaviour outcome variable, and also within the two arthritis models (Table 5.6). This provides a more robust evaluation of the effect of the two arthritis models on pain- outcomes, by taking time into account and allowing all the data to be included in the analyses rather than individual time points.

When corrected for treatment group (sham, saline, DMM, AIA), Forceplate measurements decreased significantly up to day 3, before increasing significantly over time. Von Frey measurements decreased significantly over time up to week 4, and thereafter increased significantly with time. PAM measurements decreased significantly over time up to week 2. Hotplate and Stride length (FSLL) measurements progressively and significantly decreased over time.

When time was corrected for, a significant treatment effect was observed for a number of the pain-related behaviour outcomes. Forceplate HL weight distribution was significantly decreased in AIA relative to both saline and DMM regardless of which stage of the disease process. Von Frey PWT was significantly decreased in sham relative to saline and in AIA relative to saline in the acute phase of the disease process (0 – 4 weeks). There were no treatment effects in the later stages of disease, beyond week 4. No significant treatment effect was demonstrated in PAM when time was corrected for. There was also no significant treatment effect when time was corrected for in hotplate measurements. Stride length did demonstrate a treatment effect: FSLL was decreased in DMM relative to sham and increased in AIA relative to DMM.

Table 5.6. Time and treatment effect on pain behaviour

Linear regression on separate pain parameters in AIA and DMM was used to determine whether pain outcome variables changed over time (1), and when corrected for time whether there was a difference between treatment (2) and comparator treatments (3). Where the direction (increase vs decrease) and/or significance of the temporal change for a particular pain outcome differed with time after arthritis induction, the periods are reported separately. Forceplate, PAM and stride length data was normally distributed, Von Frey and Hotplate data was normalised using log transformation.

Score	Period (w)	Time[1]	Time (P)	Treatment[2]		Cf tx[3]	Tx (P)
Forceplate	0 – 0.4	Decreased	<0.001	Sham	-	Saline	0.320
				AIA	Decreased	Saline	**<0.001**
				DMM	-	Sham	0.072
				AIA	Decreased	DMM	**0.001**
Forceplate	0.4 - 16	Increased	<0.001	Sham	-	Saline	0.12
				AIA	Decreased	Saline	**<0.001**
				DMM	-	Sham	0.62
				AIA	Decreased	DMM	**0.001**
Von Frey	0 - 4	Decreased	<0.001	Sham	Decreased	Saline	**0.004**
				AIA	Decreased	Saline	**<0.001**
				DMM	-	Sham	0.63
				AIA	-	DMM	0.19
Von Frey	4 - 16	Increased	0.001	Sham	-	Saline	0.99
				AIA	-	Saline	0.75
				DMM	-	Sham	0.21
				AIA	-	DMM	0.36
PAM	0 - 2	Decreased	0.037	Sham	-	Saline	0.100
				AIA	-	Saline	0.720
				DMM	-	Sham	0.730
				AIA	-	DMM	0.140
PAM	2 - 16		0.650	Sham	-	Saline	0.180
				AIA	-	Saline	0.340
				DMM	-	Sham	0.091
				AIA	-	DMM	0.210
Hotplate	0 - 16	Decreased	0.007	Sham	-	Saline	0. 210
				AIA	-	Saline	0.450
				DMM	-	Sham	0.860
				AIA	-	DMM	0.080
Stride length (FSLL)	0 - 16	Decreased	<0.001	Sham	-	Saline	0.23
				AIA	-	Saline	0.86
				DMM	Decreased	Sham	**0.019**
				AIA	Increased	DMM	**0.012**

5.3.7 Correlation between different pain-related behaviours in AIA and DMM when corrected for time

Each individual perceives the experience of pain differently, and each pain outcome measure may reflect a different aspect of the pain experience. Yet in pre-clinical pain research we attempt to define it in terms of a series of basic observations or responses to a specific stimulus. Understanding how the different pain-related behaviours that can be observed in pre-clinical studies are associated could provide important nuanced information about the pain phenotype of the different animal models that are used to study OA. The existence of any associations was investigated by calculating partial correlation coefficients for the different pain-related behaviours in the different treatments (AIA, Saline, DMM, Sham) when corrected for time (Table 5.7). Interestingly, when time was corrected for, there were no significant associations between the different pain-related behaviours in either of the arthritis models. In the saline group there was a weak association between PAM and hotplate, which was lost when correction for repeated measures was performed.

Table 5.7. Pain related behaviour partial ranked correlations in AIA and DMM when corrected for time.

a. HL weight distribution	Treatment	r	*P*
Von Frey	AIA	0.163	0.089
	Saline	0.123	0.440
	DMM	0.118	0.260
	Sham	0.028	0.860
PAM	AIA	0.091	0.560
	Saline	0.001	0.930
	DMM	0.277	0.250
	Sham	0.120	0.310
Hotplate	AIA	0.057	0.470
	Saline	0.017	0.790
	DMM	0.030	0.680
	Sham	0.031	0.610
Stride length	AIA	0.043	0.600
	Saline	0.065	0.320
	DMM	0.017	0.840
	Sham	0.061	0.380
b. Von Frey			
PAM	AIA	0.032	0.830
	Saline	0.123	0.460
	DMM	0.023	0.850
	Sham	0.053	0.750
Hotplate	AIA	-	-
	Saline	0.081	0.580
	DMM	-	-
	Sham	0.149	0.260
Stride length	AIA	-	-
	Saline	-	-
	DMM	-	-
	Sham	-	-
c. PAM			
Hotplate	AIA	-	-
	Saline	0.237	**0.016**
	DMM	-	-
	Sham	0.125	0.300
Stride length	AIA	-	-
	Saline	-	-
	DMM	-	-
	Sham	-	-
d. Hotplate			
Stride length	AIA	0.044	0.580
	Saline	0.092	0.280
	DMM	0.088	0.300
	Sham	0.118	0.160

5.4 Discussion

In this chapter, pain-related behaviours were measured following induction of arthritis in DMM and AIA mice. Sham surgery and saline injected mice were also tested for comparison. The focus of this chapter was to characterise the pain that develops in these two distinct animal models and track how the pain-related behaviours change over time. Time and treatment effects were investigated, and associations between the different pain-related behaviours were also investigated in the two models of arthritis.

Pain in both the DMM and AIA models was characterised by tactile allodynia, knee joint mechanical hyperalgesia, reduced weight bearing of the affected HL, thermal hyperalgesia and changes in stride length, at different points of disease progression. For all of the pain-related behaviours there were differences between the two models with respect to the degree of severity of the pain behaviour that developed and/or the pattern of change over time that was observed.

There was little variability in baseline readings for the behaviour tests conducted, with the exception of the hotplate test. However, all pain related behaviours demonstrated greater variability in subsequent measurements following induction of arthritis, despite clearly defined endpoints and a single operator performing the testing. This suggests that the pain experience for each individual mouse is different, as it is for individual humans (596). This variability also means that many of the experiments conducted in this chapter were underpowered and so the conclusions that are drawn from these experiments are in part based on the patterns and trends that were observed, rather than statistically significant findings. As stated previously these were hypothesis generating experiments as the methods used to conduct the behaviour tests were modified from what has previously been published and have not been previously described or tested in two distinct models of arthritis.

5.4.1 Tactile allodynia

Tactile allodynia on the ipsilateral hind paw developed early in treatment and sham groups but not in control mice. Allodynia was observed before the time point at which bona fide OA like joint pathology changes start to develop in the two models (refer to chapter 4). This suggests that the early phase tactile allodynia is driven by the trauma and inflammation caused by surgery, immunisation and knee joint injection. Further support of this is the fact that allodynia resolved completely in sham surgery mice at the time when OA was well established in DMM mice.

Interestingly in the AIA model, allodynia developed in both mBSA and saline injected mice. Allodynia is a hallmark sign of central sensitisation. Central sensitisation is a manifestation of both activity dependent (early phase) and independent (late phase) sensory signal plasticity that can be transient or long lasting. It occurs after a period of initial nociceptive transmission and is sustained beyond the initiating signal. Immediate changes involve alteration of the distribution and function (increased excitability) of ion channels and receptors in response to high-level nociceptor input. On going noxious input and inflammation then lead to transcriptional changes at the level of the DRG and spinal cord (dorsal horn) (255). Since it is unlikely that a minor interference (ie saline injection) could trigger the type of changes in the sensory nervous system that are needed for central sensitisation to develop (597), von Frey testing was also performed on immunised mice that had no knee joint intervention. As predicted, a similar degree of allodynia was observed in immunised-only mice. This novel finding has not been reported before in the AIA model and highlights the limitations of using models that have both a systemic and local joint effect.

Tactile allodynia in the contralateral hind paw could not be demonstrated consistently in either model. Interpretation of results from the contralateral side is difficult because a response to von Frey fibres requires movement of the contralateral limb, which may result in greater weight bearing on the ipsilateral knee joint and a worsening of the pain in that joint. In other words, pain in the ipsilateral knee joint may indirectly increase the threshold at which an animal responds to a noxious stimulus on the contralateral side. However, the differences between the ipsilateral and contralateral 50% PWT in each treatment group cannot be fully explained by this, especially in the saline injected and immunised-only mice. For consistency, animals were tested first on the left hind paw and then the right hind paw. The effect of testing order cannot be excluded as another contributing factor to the observed difference in 50% PWT between the ipsilateral and contralateral limbs.

5.4.2 Mechanical hyperalgesia

In DMM mice development of ipsilateral knee joint mechanical hyperalgesia displayed an early (week 6) and late (week 16) phase, which corresponds to the acute and chronic stage of OA disease development and pathology in this model (refer to chapter 4). In contrast, AIA mice displayed greater pain pressure sensitivity earlier on in the disease when joint inflammation was at a peak and less sensitivity in the late phase when OA joint pathology was well established (refer to chapter 4). As occurred with tactile allodynia, a similar pattern of mechanical hyperalgesia was observed in saline injected and immunized-only mice. These observations again highlight the confounding effect of measuring pain outcomes in an animal model that induces systemic and local joint effects. Changes in pressure pain sensitivity in the contralateral knee were very mild but followed a similar temporal pattern to the ipsilateral knee in both AIA and DMM mice.

Reduced pressure-pain threshold is a clinically relevant measure of OA pain as it mimics what has been observed in patients with knee OA pain (268). Patients with mild knee pain display greater sensitivity to pressure applied to the lateral side of the joint. While patients with severe knee pain display greater sensitivity to pressure applied to the medial side of the joint (284). In addition, these patients display increased evoked temporal summation, in response to repeated pressure application. Both of these are measures of central sensitisation. Interestingly, the degree of localized sensitisation as measured by pressure application tests and evoked temporal summation correlate with clinical pain ratings reported by OA patients. This is in contrast to the lack of correlation between standard radiological findings and clinical or experimental pain measures in OA patients. It highlights the need for similar investigations to better define the relationships that may exist between experimental measures of pain and specific joint pathologies in pre-clinical animal models.

It must be noted that the level of physical restraint required when testing mice for knee joint sensitivity to a mechanical stimulus made it challenging to differentiate between mice that were responding to the applied stimulus and those that were demonstrating escape behaviour due to the restraint method. In addition, the stress associated with restraint may also have induced activation of the endogenous opioid system and other mechanisms involved in stress-induced analgesia, which in turn would influence the response threshold in individual mice. These added complexities reinforce the importance of blinding and testing control and sham mice in parallel throughout the experiment.

5.4.3 Hind Limb Weight distribution

Hind limb weight distribution in DMM and AIA mice was evaluated as a measure of pain using a force plate. The average right to left HL weight bearing ratio pre-

treatment ranged from 1.0 – 1.1 in AIA, DMM, sham and naïve control mice. Both models induce a mono-articular arthritis and so any shift in weight distribution that favours the non-treated HL is assumed to be an avoidance response secondary to pain. However, in the DMM model it can't be ruled out that changes in weight distribution are also due to biomechanical changes arising from joint instability. The fact that two aspects of OA could be at play in the DMM model (pain and biomechanical instability) may in part explain the conflicting results published by researchers using DMM and other joint destabilisation models (316, 406, 598).

Reduced weight bearing on the ipsilateral HL was observed early in AIA, DMM and sham surgery mice. Unlike the pain-related behaviour tests that indicate central sensitisation, changes in HL weight distribution were not observed in saline injected and immunized-only mice. This suggests that HL weight distribution is a measure of pain driven primarily by local joint pathology and not by systemic mechanisms.

The pattern of change in HL weight distribution was similar in both models. However, the peak reduction in ipsilateral HL weight bearing was greater in the AIA mice (50% vs. 30%) and persisted for longer (4 weeks vs 2 weeks) in this early phase of change. This suggests that the early changes in weight bearing may reflect the inflammation and trauma caused by the methods used to induce arthritis and not the direct effect of OA on weight bearing. Interestingly, a late phase (week 16) reduction in ipsilateral HL weight bearing was only observed in DMM and sham mice despite significant OA joint pathology in AIA mice and the absence of joint pathology in sham mice at this stage (refer to chapter 4). This late reduction in ipsilateral HL weight bearing was observed more consistently in DMM mice, with decreased ipsilateral HL weight bearing observed in 3 of the 4 DMM cohorts that were tested at week 16 and in only 2 of the 4 sham cohorts. The fact that changes in HL weight

distribution was observed in AIA, DMM and sham surgery mice indicate that altered weight distribution is not simply a biomechanical phenomenon following the creation of joint instability. However, the reasons why reduced weight bearing in the ipsilateral HL persisted in some sham surgery mice long after post-surgical joint pathology had resolved is still not known.

5.4.4 Stride length

In DMM mice gait was characterised by a small increase in FSLL, FSLR, LRS and RLS in the immediate post-surgical period (week 1) followed by a sustained decrease in LRS, FSLL and FSLR from week 4, that persisted until week 16. This is similar to what has been observed in patients with knee OA where both stride length and walking velocity (reflected in full stride data) are reduced (553); and what has been reported in arthritis animal model studies using digital gait analysis systems (515). These changes can in part be explained by the reduced range of motion and increased joint stiffness that also occurs in patients with chronic knee OA. Despite these known associations from what has been observed in patients with knee OA, changes in stride length have not previously been investigated in the DMM model, as a potential marker of disease progression or indicator of response to novel therapies.

In AIA mice a significant decrease in LRS, FSLL and FSLR occurred immediately following mBSA injection into the joint (day 3). This acute response to mBSA injection coincided with visible swelling of the knee joint, significant synovial exudate, sub synovial inflammation and synovial hyperplasia (refer to chapter 4). AIA mice recovered partially following this initial decrease in stride length before displaying a more gradual 2nd phase of decrease in LRS, FSLL and FSLR, reaching DMM values by week 16. Also important to note is the fact that Relative Step

followed a similar pattern to the changes in stride length, suggesting that the decrease in FSLL and LRS is not simply due to a slower gait speed in the AIA model.

The temporal changes in stride length support previous study findings, which demonstrated a similar pattern of change in the AIA model (493). The failure to demonstrate an association between stride length and any other pain-related behaviours is also supported by this study, where it was demonstrated that stride length correlates with other pain related measures (mechanical and thermal hyperalgesia) in the acute phase, at day 3, but not in the chronic phase (after week 3) of arthritis development (493).

However, it is important to note that in this thesis multiple behaviour tests were not conducted on the same individual mice and so the ability to make any conclusions about potential pain-relate behaviour associations is limited. In addition, the study referred to here defines three weeks post joint injection as 'chronic', whereas the histological findings in this thesis would suggest that at three weeks the joint pathology is still characterized by acute inflammation and significant articular cartilage damage has not developed at this relatively early time point.

The differences in the temporal pattern of change in stride length between the two models reflect some of the differences in onset of OA specific joint pathology development. Combined with the histology data from chapter 4, the temporal differences between the two models appear to reflect the early onset of OA joint pathology from week 4 (AC damage, osteophytes and SCB sclerosis) observed in the DMM model compared to AIA mice that developed characteristic OA joint pathology more gradually (refer to chapter 4) with significant AC damage occurring later than in DMM mice.

Overall, DMM and AIA mice displayed different temporal patterns of change for all stride measurements. However, the low animal numbers in each treatment group at these time points and the variability within each animal group meant that these changes were not statistical significant.

5.4.5 Thermal hyperalgesia

PWL decreased over time in AIA, DMM and sham mice. Thermal hyperalgesia developed in DMM mice from week 4. Significant decreases in PWL were observed in AIA and saline-injected mice but these changes were less than what was observed in DMM mice. In DMM mice the decrease in PWL over time was only significant at week 4. This is most likely due to the small sample size of paired data at each time point ($n \leq 5$).

Therefore, interpreting the observed changes in PWL for the hotplate test presents some unique challenges. Although the hotplate is a well-established and validated pain assay (599), variability in baseline data makes it difficult to interpret changes over time between groups when the baseline PWL is significantly increased in one or more groups of mice.

Like many of the pain-related behaviour tests used in mice, the hotplate involves exposure to two stressors, physical confinement or restraint and a noxious stimulus (heat). In the case of the hotplate, the relatively wider and open-ended holding space (see Chapter 2, figure 2.3b) may provide a greater stimulus for the flight response in some mice. Therefore, it is likely that in some mice the primary stimulus leading to a behavioural response is exposure to a noxious temperature, while in other mice the behaviour they display is not a pain response or an indication of thermal hyperalgesia, but rather a stress driven escape response. This could account for the variability in baseline response latency that is reported (599) and that was observed in this

experiment. This is despite the use of two combined endpoints to define PWL (hind paw lick and jump), which were selected because they have been shown to increase both specificity and sensitivity (600) when investigating non-analgesic drug effects.

The variability in response latency also occurs following the administration of analgesics. When large numbers of mice were tested to determine baseline PWL and the effects of variable doses of morphine, there was great repeatability within cohorts but significant repeatable disagreement between cohorts (535). It is still unclear whether this simply represents individual variability or whether it is due to unknown environmental factors that only affected a given cohort at a particular test period.

It has been suggested that matching subjects into groups based on baseline (pre-treatment) PWL would remove the confounding effect of individual differences in sensitivity within different cohorts and allow data to be examined for any interactions between individual differences and treatments effects (517).

The reason this strategy was not adopted is because of the evidence that exists for the effects of habituation leading to behavioural tolerance and a reduction in both baseline response latency and response to some analgesic agents. A progressive decrease in response time and disappearance of licking behaviour has been demonstrated with repeated testing (601) and prior exposure of mice to an unheated hotplate chamber significantly decreased response latency to a 55 degree hotplate. Therefore, behavioural tolerance cannot be ruled out as the cause of the decrease in PWL observed in treatment and sham groups at the early time points. However, it was unavoidable to test individual mice repeatedly over a two-week period in order to investigate early changes in PWL following induction of arthritis.

5.4.6 Summary

Pain assessment in patients with knee OA involves numerous tests that measure many parameters including range of motion, weight bearing, gait analysis and mechanical pain thresholds, as well as self-report questionnaires such as the MPQ and the WOMAC (268). Using multiple tests allows more complete characterisation of OA pain. It also helps to clearly define the pain experience unique to an individual patient and facilitates tracking of its progression and evaluation of its management.

While the use of self-report questionnaires is not an option in preclinical animal studies, the use of multiple pain assessment tools gives greater clarity to the type of pain that develops in any particular animal model (pain phenotype) and provides greater ability to test and quantify the efficacy of novel therapeutics.

In this chapter I have reported on the use of a range of pain-related behaviour tests to characterise pain in the DMM and AIA model and described how the pain changes over time with disease progression. Each model demonstrates a unique pain phenotype despite both models displaying very similar OA-like knee joint pathology at week 16 (refer to chapter 4). Table 5.8 summarises the pain phenotype for each animal model at different phases of OA joint disease (early acute inflammatory, acute OA, chronic OA).

Table 5.8. Summary of pain phenotype for AIA and DMM at different phases of OA
Phases of OA joint disease are based on histopathology changes (early acute, acute OA, chronic OA) and phentotype is defined based on different pain related behaviours (allodynia, mechanical hyperalgesia, thermal hyperalgesia, hind limb weight distribution and stride length). Plus symbol (+) = pain-related behaviour demonstrated; minus symbol (-) = pain-related behaviour not demonstrated.

OA Disease Phase	Pain-related behaviour	Test	AIA	DMM
Early acute (0-2 weeks)	Tactile allodynia	V□□□□□□□	□□	+
	Thermal hyperalgesia	Hotplate	-	-
	Mechanical hyperalgesia	PAM	++	+
	Hind limb weight distribution	Forceplate	++	+
	Gait changes	Reduced stride length	+	-
Acute OA (4-8 weeks)	Tactile allodynia	V□□□□□□□	+	+
	Thermal hyperalgesia	Hotplate	-	+
	Mechanical hyperalgesia	PAM	+	+
	Hind limb weight distribution	Forceplate	+	-
	Gait changes	Reduced stride length	-	+
Chronic OA (12-16 weeks)	Tactile allodynia	V□□□□□□□	+	+
	Thermal hyperalgesia	Hotplate	+	+
	Mechanical hyperalgesia	PAM	-	++
	Hind limb weight distribution	Forceplate	-	+
	Gait changes	Reduced stride length	+	+

The failure to demonstrate any correlation between the different pain related behaviours in this study highlights the importance of not relying on one single pain assay when evaluating the efficacy of therapeutics that are targeting the symptoms of OA (pain and mobility) in pre clinical models.

The pain experienced by patients with OA has been well characterised. Peripheral mechanisms such as inflammation play an important role in its development. But, human OA pain is also driven in part by complex mechanisms that don't directly correlate with joint pathology. These mechanisms lead to sensory nervous system modulation and subsequent development of central sensitisation (230). This explains why the degree of pain does not always correlate with the degree of joint pathology or inflammation and why patients with knee OA display mechanical hyperalgesia and tactile allodynia (284). It explains why OA patients experience movement-evoked pain and pain at rest. It also explains why patients with low pain thresholds and evidence of hyperalgesia may continue to experience pain following knee joint arthroplasty (602).

Evaluation of the effect of both time and treatment on different pain related behaviour further demonstrates the complex nature of OA pain. When time was corrected for, weight bearing on the affected limb significantly decreased in AIA mice relative to both saline injected and DMM mice, indicating that regardless of the stage of disease HL weight bearing changes are determined by what mechanisms trigger OA to develop in the first place. In contrast, no treatment effect was demonstrated for the development of mechanical or thermal hyperalgesia when corrected for time, indicating that the observed changes are more likely associated with the stage of disease development rather than the disease etiology or animal model used to induce OA. Interestingly, the opposing treatment effect observed with stride length (FSLL)

between DMM and AIA indicates the changes in stride are model specific because any change in gait reflects the combined effect of joint pathology on biomechanics, proprioception and pain.

The findings in this chapter demonstrate that the DMM and AIA models lead to a complex pain state that is in part driven by central sensitisation and that has many of the hallmarks of what many human OA patients experience. What isn't clear is which specific joint pathology processes trigger and maintain any given pain behaviour? The absence of any associations between the different pain behaviours indicates that the mechanisms may be different for different types of pain and at different stages of the disease. For example, tactile allodynia appears to persist long after the initiating trigger has resolved. This may be because other pathological processes take over as the drivers of the pain in the later stages of OA disease, or as with other neuropathic pain states, the allodynia is maintained by activity independent (late phase) sensory signal plasticity that is sustained beyond the initiating signal.

This reinforces the need to investigate the underlying changes to sensory innervation that accompany the different pain-related behaviours. The relationship between tissue specific joint pathology and pain, and how it changes over time can then be characterised and a better understanding of OA pain mechanisms arrived at. In the following chapter the changes in gene expression of key inflammatory mediators and neuropeptides in the dorsal root ganglia that innervate the knee joint are investigated.

CHAPTER 6: Gene expression profile of inflammatory mediators and neurotransmitters in the DRG following destabilization of the medial meniscus (DMM) and antigen-induced arthritis (AIA) in mice

6.1 Introduction and aims

In the previous chapter, activity-based and evoked pain-response behaviours were measured to characterise and compare the pain that develops with knee joint arthritis induced by DMM and AIA. Model specific temporal patterns of change in pain response were identified, establishing that both the DMM and AIA models lead to a complex pain state that is partly driven by central sensitisation and that demonstrates many of the characteristics of the pain experienced by human OA patients. These findings highlight the need to investigate the changes in sensory neurons that accompany the different pain behaviours observed in each model in order to better understand differences in pain phenotype between the two models.

In this chapter, gene expression of key inflammatory mediators and neuropeptides in the peripheral sensory neurons that innervate the knee joint were measured following induction of arthritis using DMM and AIA. In addition, gene expression of the major aggrecanases (ADAMTS-4 and ADAMTS-5) involved in articular cartilage degradation was also measured in an attempt to identify any biomolecular links between joint pathology and the mechanisms that drive OA pain. This enabled further characterisation of the pain phenotype in the two models through evaluation of the changes in sensory neurons that may be contributing to the observed pain-related behaviours reported in the previous chapter.

Studies have mapped the cell bodies of afferent neurons that innervate the knee joint in mice to the lumbar DRG (L1 – L5) (226). Retrograde tracing and immunohistochemistry methods have been used to characterise the number, distribution and neuropeptide content of neurons residing in the DRG that innervate the knee joint, with the majority (approximately 90%) residing in L3 and L4 (169). The knee joint sensory afferents make up a small proportion of the total cell population in these DRG (<1 in 15) (603) and only a subset of these are the small myelinated (Aδ fibre) and unmyelinated (C fibre) nociceptors. The remainder comprises large, low threshold mechanoreceptors (169). This has implications for the ability to identify small changes in gene expression in this subset of nociceptor neurons using the method described in this thesis where the entire DRG is processed for RNA extraction and PCR. To avoid further dilution of any change in expression in the nociceptor neurons that specifically innervate the knee joint, only L3 and L4 DRG were processed.

The proteins and neuropeptides that drive and modulate pain signaling in the OA joint have been investigated in a number of pre-clinical animal models (485, 604-607). These studies add to the huge body of knowledge that already exists about pain mechanisms and the role of neuronal plasticity in chronic pain states (230, 432, 596, 608-611). It is well established that inflammatory neuropeptides such as Substance P and CGRP, and numerous inflammatory cytokines, including IL-1β, are involved in the development of chronic pain and sensitisation (89, 469, 612). In addition, nociceptor ion channels such as members of the transient receptor potential family of channels, TRPV1, TRPV2, TRPV4 and TRPA1, are no longer viewed simply as sensory transducers that translate physical stimuli into electrical signals. Their role in the inflammatory and neuropathic mechanisms that contribute to the development of

chronic pain and sensitisation has been established through numerous investigations using preclinical pain models (613). The endogenous opioid and cannabinoid systems are also primary drivers of the inhibitory mechanisms that contribute to modulation of pain signaling (265, 312).

In short, a number of local inflammatory and neurogenic mechanisms have been identified as potentially contributing to OA pain and could therefore lead to the development of suitable therapeutic targets for treating OA specific pain (reviewed in (271, 287)). However, the significance of these channels, neuropeptides and pro-inflammatory cytokines in the establishment of specific sub-types of OA pain and their activity at different stages of disease development is still unclear. This is largely because previous investigations have not taken the approach that pain may be different for different sub types (phenotypes) of OA and at different stages of the disease. In fact, very few studies have investigated pain mechanisms in different animal models in parallel, to differentiate mechanisms that are model (phenotype) specific, and those that reflect more generic mechanisms associated with the development of chronic pain. The failure to translate the current understanding of acute and chronic pain mechanisms highlights the need for a more targeted approach to OA pain (363).

This means that the development and testing of future OA pain therapeutics should target specific OA phenotypes (391). For example, it has been postulated that a more targeted approach that focuses on local (joint specific) and peripheral (DRG) mediators of OA pain is more likely to lead to the development of effective therapeutics that are void of unwanted systemic side effects (307). In line with this new way of thinking, peripheral pain mechanisms were investigated simultaneously in two animal models over a defined time period that corresponded to joint disease

progression (Chapter 4) and model specific pain-related behaviour (Chapter 5). The lumbar DRG were targeted as the site of investigation because it is where the cell bodies of the sensory neurons that innervate the knee joint reside and therefore arguably where OA pain starts. Chronic pain and the development of central sensitisation involve changes in cell signaling, membrane excitability and gene transcription in neurons at the level of the DRG and the spinal cord, as well as supporting cells (astrocytes), immune cells (microglia)(614) and peripheral monocytes that migrate into the DRG and spinal cord (reviewed in (255, 615-618)). As a first step in unraveling these complexities for OA pain, investigation of gene expression alterations in the DRG following induction of arthritis have been undertaken.

The aims of chapter 6 are:

1. To characterise and compare temporal changes in gene expression in the lumbar (L3 and L4) DRG following development of knee joint arthritis induced by DMM and AIA.
2. To identify any associations between the expression of different genes in the DRG and compare these in the two arthritis models.
3. To investigate differences in protein expression in the lumbar (L3-L4) DRG following development of knee joint arthritis induced by DMM and AIA, using immunohistochemistry techniques.

6.2 Methods, statistical analysis and data presentation

Details of the methods used to induce the two models of arthritis, DMM and AIA, are described in chapter 2, section 2.1. The methods used for harvesting DRG and real time Reverse Transcription-Polymerase Chain Reaction (RT-PCR) are described in chapter 2, section 2.4. The methods used for immunohistochemistry are described in chapter 2, section 2.5.

Comparison of gene expression between treatment groups was analysed using the nonparametric ranked Kruskal-Wallis analysis for multiple groups and, where there was significance, post hoc analysis using the Mann Whitney U-test (for unpaired data) was performed for between group comparisons. Within treatment group comparisons between right and left DRG gene expression were conducted using the Wilcoxon signed-rank test (StataSE software, Stata corporation, TX, USA). Analysis focussed on gene expression in the right DRG because both arthritis models induced a mono-articular arthritis with joint pathology in the right knee joint. However, changes in both ipsilateral and contralateral DRG have been reported in animal models of single joint arthritis (375). So for completeness changes in the right and left DRG were compared and the R/L DRG ratio was also compared between treatment groups.

The gene expression results are presented as the mean fold change relative to the respective sham or saline control group and graphed as log of the means with error bars depicting the standard error of each data set (Figures 6.1a-i and 6.2a-i). Bars above 1 represent a relative increase in gene expression and bars below 1 represent a relative decrease.

Due to the current gaps that exist in our understanding of the mechanisms that drive OA pain, the experiments reported in this chapter were designed to be hypothesis generating, with a suite of genes tested. Although, the genes investigated in this

chapter have been implicated in a number of pain states, including arthritis, their pattern of expression in the peripheral nervous system at different stages of OA disease development using different animal models, has not previously been investigated. For this reason, when testing the significance of between and within treatment group changes in gene expression, the alpha value was set at 0.05 and the Benjamini-Hochberg correction was not applied to the *P* values to correct for repeated measures.

Linear regression on log transformed gene expression data was used to determine whether gene expression changed over time regardless of treatment; and when correcting for time, whether there was a difference between arthritis models.

Associations between the different genes within each model (when corrected for time) were also determined by generating Pearson partial correlation coefficients, using Kendall's tau-b (565). This nonparametric process uses pairwise ranked data values between the two variables under study (ordinal scores) and thus does not require data to be normally distributed or the relationship between the variables to be linear. The Benjamini-Hochberg correction was applied to the P values of the associations for each gene pair, resulting in $P < 0.040$ being considered significant when the alpha value was set at 0.05.

CNR1 was excluded from both linear regression and partial correlation analysis because of the reduced data set available for this gene, with only 1 time point in the AIA and saline groups and only 3 time points in the DMM and sham groups.

In the results, 'significance' refers to statistical significance, with *P* values included in the relevant tables.

Protein expression, based on immunohistochemical staining, in each of the treatment groups and at different time points were not measured quantitatively due to the small

sample size (n=2) and the challenges of maintaining the same quality of tissue integrity across all DRG samples and consistent staining patterns between tissue samples that had been stored for different periods of time. Representative images of DRG sections depicting protein expression trends based on immunohistochemical staining are presented in figures 6.4a – 6.4h.

6.3 Results

6.3.1 DRG gene expression (real time RT-PCR)

When comparing gene expression in the R versus L DRG (within animal comparison) for each treatment group at different time points (Table 6.1), there was no significant difference in the saline or sham groups at any measured time point. The genes that showed a significant difference in expression between the R and L DRG of AIA or DMM mice, are displayed in Figure 6.1(a – g). In AIA, differences in gene expression between the R and L DRG occurred at day 3 (R DRG decreased IL-1β); week 1 (R DRG increased TRPV2); week 2 (R DRG decreased ATF3, and ADAMTS-5); week 4 (R DRG decreased CGRP, Oprm1, and ADAMTS-4); week 8 (R DRG decreased CGRP, and TRPA1); and week 12 (R DRG decreased TRPV1). In DMM differences in gene expression between R and L DRG occurred at week 1 (R DRG decreased IL-1β), week 4 (R DRG increased TRPA1, CNR1); week 8 (R DRG decreased TRPV1), week 12 (R DRG decreased CGRP, TRPA1, TRPV1); and week 16 (R DRG increased CGRP, TRPA1, TRPV1, TRPV2).

In AIA there were more differences in gene expression between R and L DRG at the early stages of disease progression (up to week 4). In DMM the reverse trend was observed, with more differences in gene expression profile between R and L DRG at the chronic stages of disease (weeks12-16).

Table 6.1. Gene expression of the right vs. left L3/L4 DRG

Time	Treatment	Gene	P-value
Day 3			
	Saline	n.c.	-
	AIA	**IL-1b**	**0.046**
	Sham	n.c.	
	DMM	n.c.	
Week 1			
	Saline	n.c.	
	AIA	**TRPV2**	**0.046**
	Sham	n.c.	
	DMM	**IL-1b**	**0.028**
Week 2			
	Saline	n.c.	
	AIA	**ATF3**	**0.028**
		ADAMTS-5	**0.028**
	Sham	n.c.	
	DMM	n.c.	
Week 4			
	Saline	n.c.	
	AIA	**CGRP**	**0.043**
		Oprm1	**0.043**
		ADAMTS-4	**0.042**
	Sham	n.c.	
	DMM	**TRPA1**	**0.045**
		CNR1	**0.043**
Week 8			
	Saline	n.c.	
	AIA	**CGRP**	**0.028**
		TRPA1	**0.046**
	Sham	n.c.	
	DMM	**TRPV1**	**0.043**
Week 12			
	Saline	n.c.	
	AIA	**TRPV1**	**0.028**
	Sham	n.c.	
	DMM	**CGRP**	**0.003**
		TRPA1	**0.026**
		TRPV1	**0.013**
Week 16			
	Saline	n.c.	
	AIA	n.c.	
	Sham	n.c.	
	DMM	**CGRP**	**0.003**
		TRPA1	**0.026**
		TRPV1	**0.013**
		TRPV2	**0.043**

DRG gene expression in DMM and AIA mice at day 3, week 1, 2, 4, 8, 12 and 16 post arthritis induction. No significant differences (n.c.) observed in saline and sham mice. Only genes that demonstrated a significant difference ($P<0.05$) are listed.

Figure 6.1a-g. Gene expression for R vs. L L3/L4 DRG

Presented as the mean fold change relative to the respective sham or saline control group and graphed as log of the means with error bars depicting the standard error of each data set. Bars above 1 represent a relative increase in gene expression and bars below 1 represent a relative decrease. Significance for R vs. L within treatment comparisons = $P<0.05$ (§); and $P<0.01$ (§§).

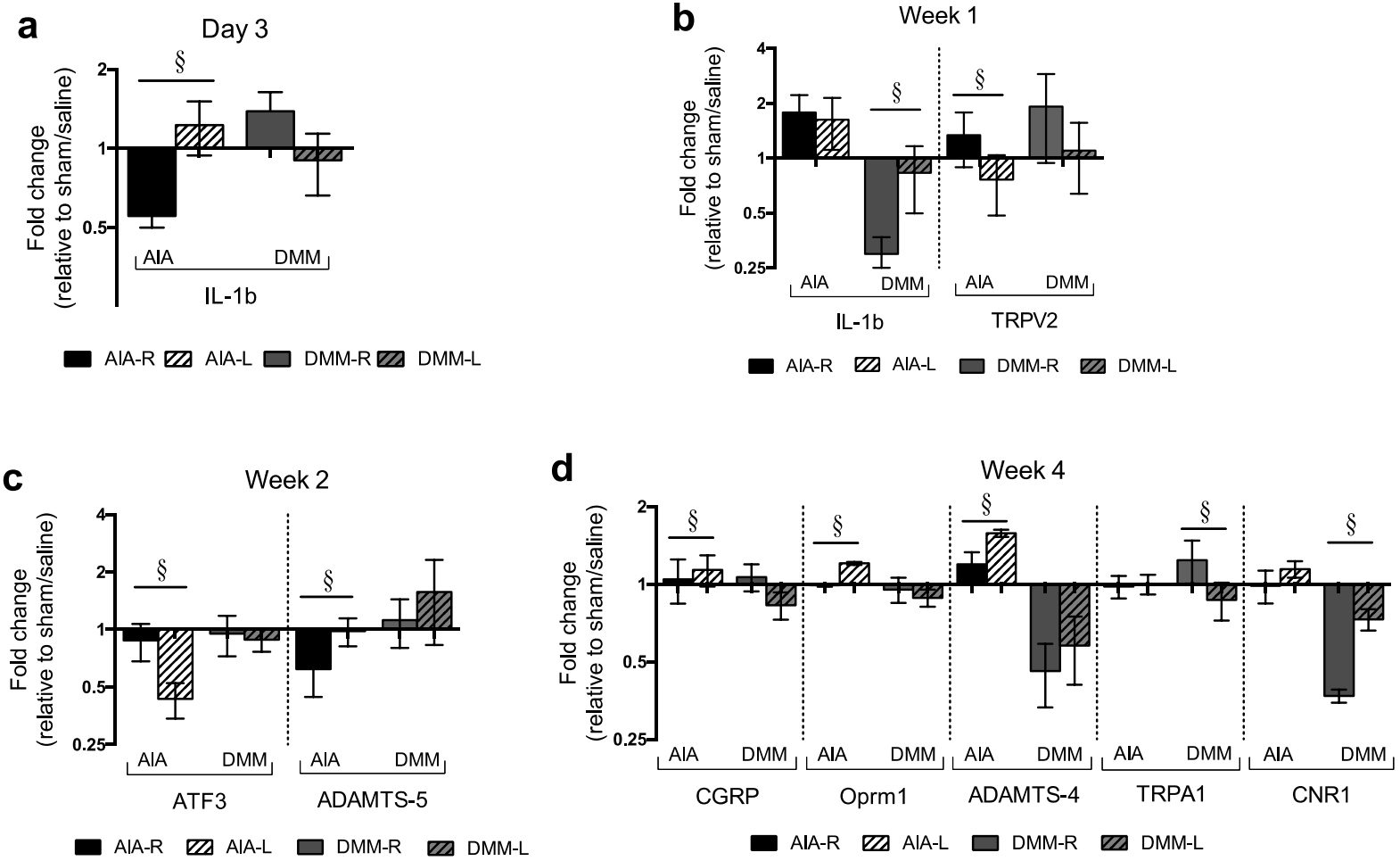

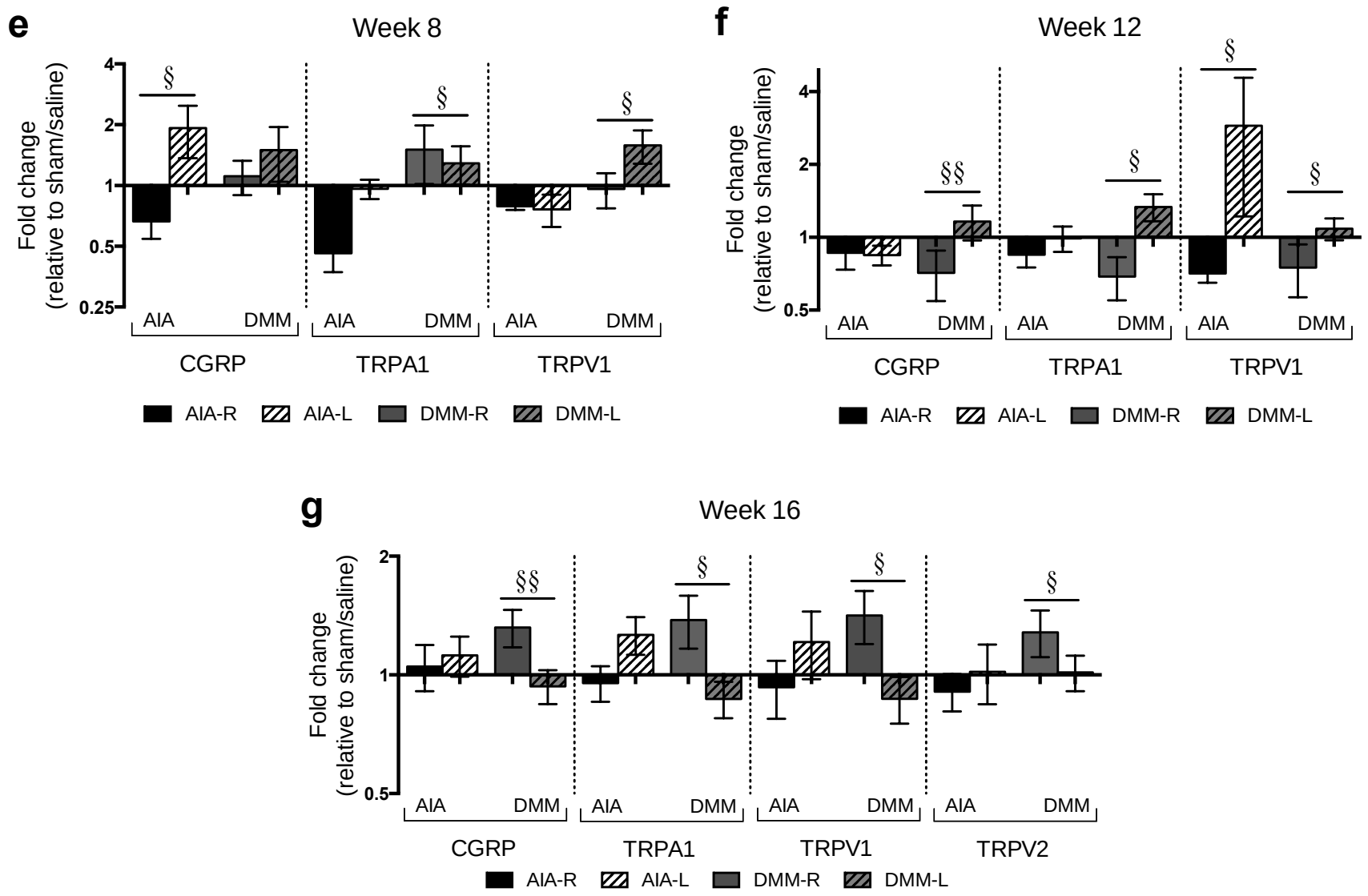
e
Week 8
Fold change
(relative to sham/saline)
4
2
1
0.5
0.25
§
§
§
AIA
DMM
AIA
DMM
AIA
DMM
CGRP
TRPA1
TRPV1
AIA-R
AIA-L
DMM-R
DMM-L
f
Week 12
Fold change
(relative to sham/saline)
4
2
1
0.5
§§
§
§
§
AIA
DMM
AIA
DMM
AIA
DMM
CGRP
TRPA1
TRPV1
AIA-R
AIA-L
DMM-R
DMM-L
g
Week 16
Fold change
(relative to sham/saline)
2
1
0.5
§§
§
§
§
AIA
DMM
AIA
DMM
AIA
DMM
AIA
DMM
CGRP
TRPA1
TRPV1
TRPV2
AIA-R
AIA-L
DMM-R
DMM-L

To investigate these observations further, gene expression in the ipsilateral R DRG was compared in each model against the relevant sham or saline group, as well as between the two models (Table 6.2 and Figures 6.2a – 6.2l). Differences in R DRG gene expression between AIA and saline mice were only observed at week 8: at this time point, both ATF3 (P=0.004) and TRPA1 (P=0.004) expression was decreased in AIA compared to saline. Differences in R DRG gene expression between DMM and sham mice were observed much earlier where at day 3 TRPA1 expression was increased in DMM compared to sham (P = 0.020). Differences between the two models (DMM vs. AIA) occurred at day 3 (IL-1β, ADAMTS-5); week 1 (IL-1β); week 4 (ATF3, CNR1, ADAMTS-4); and week 8 (ATF3, CGRP, TRPA1). Interestingly, when differences between the two models were observed, changes in gene expression were generally in the opposite direction with one model having increased expression and the other model having decreased expression. For example: ADAMTS-5 at day 3 (Figure 6.2l); IL-1β at week 1 (Figure 6.2c); ATF3 at week 4 (Figure 6.2a); and TRPA1 at week 8 (Figure 6.2f).

Table 6.2. Gene expression of the right L3/L4 DRG

Treatment comparison	Time	Gene	P-value
DMM vs Sham	Day 3	TRPA1	0.020
AIA vs Saline	Week 8	ATF3	0.004
		TRPA1	0.004
DMM vs AIA	Day 3	IL1b	0.016
		ADTS5	0.005
	Week 1	IL1b	0.006
	Week 4	ATF3	0.007
		CBR1	0.004
		ADTS4	0.004
	Week 8	ATF3	0.006
		CGRP	0.029
		TRPA1	0.006

DMM vs, sham; AIA vs. Saline; and DMM vs. AIA mice at day 3, week 1, 2, 4, 8, 12 and 16 post arthritis induction. Only genes that demonstrated a significant difference ($P<0.05$) are listed.

Figure 6.2a-l. Gene expression for R L3/L4 DRG

Presented as the mean fold change relative to the respective sham or saline control group and graphed as log of the means with error bars depicting the standard error of each data set. Bars above 1 represent a relative increase in gene expression and bars below 1 represent a relative decrease. Significance for treatment vs. Sham/Saline = $P<0.05$ (*); and $P<0.01$ (**). Significance for AIA vs. DMM = $P<0.05$ (#); and $P<0.01$ (##).

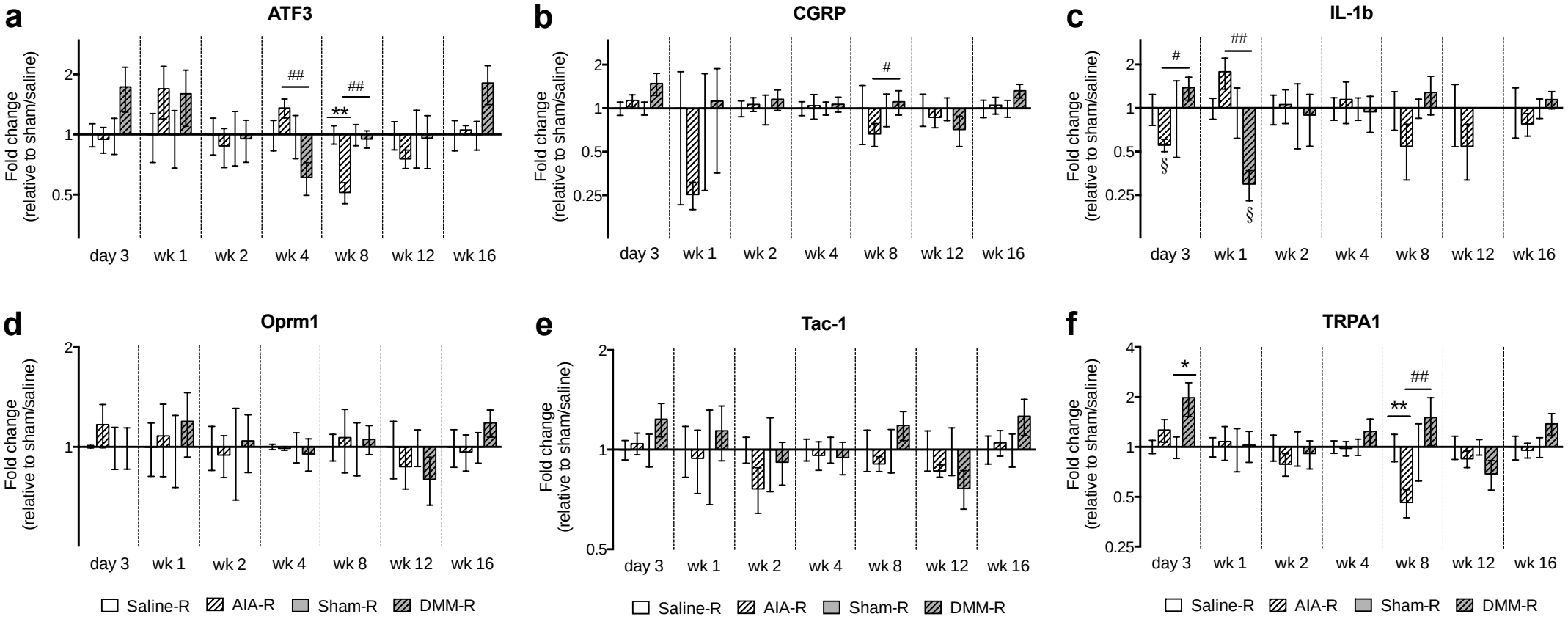

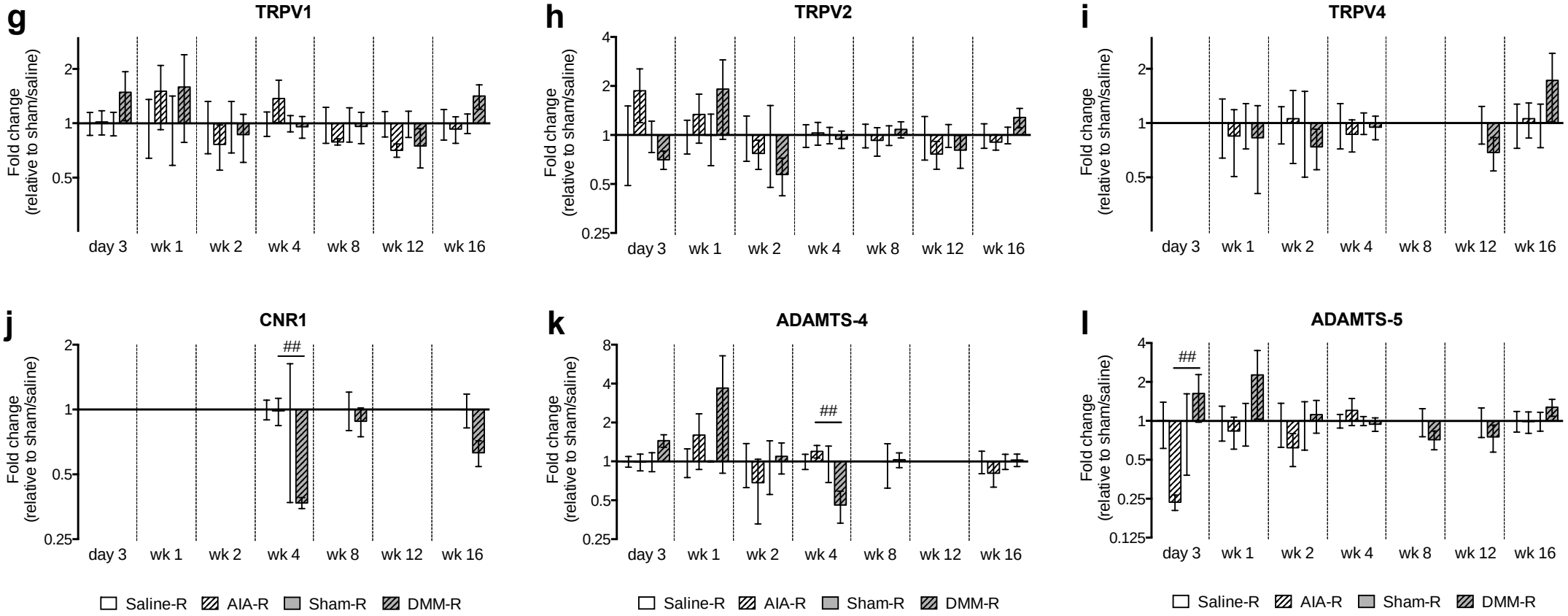
g
TRPV1
h
TRPV2
i
TRPV4
j
CNR1
k
ADAMTS-4
l
ADAMTS-5
Fold change (relative to sham/saline)
day 3
wk 1
wk 2
wk 4
wk 8
wk 12
wk 16
##
Saline-R
AIA-R
Sham-R
DMM-R

To account for any masking of change in ipsilateral R DRG gene expression resulting from changes in the contralateral L DRG, differences in the right to left (R/L) DRG gene expression ratio between treatment groups was also analysed (Table 6.3 and Figures 6.3a-6.3l). The R/L DRG gene expression ratio was different between DMM and sham mice at week 8, week 12 and week 16 but not at the early time points. CGRP, Tac-1, Oprm1, TRPA1 and TRPV1 all displayed significant changes at one or more time point in DMM. In marked contrast, there was no difference in R/L gene expression ratio between AIA and Saline at any of the measured time points. There were differences between DMM and AIA at all measured time points in one or more of the genes tested. Most of the differences between DMM and AIA occurred at week 4, with differences observed in 8 of the 12 genes tested (CGRP, Oprm1, TRPA1, TRPV2, TRPV4, CNR1, ADAMTS-4, ADAMTS-5). The direction of change differed for each gene indicating both up regulation and down regulation at different time points for different treatments.

Table 6.3. Right to left DRG (L3 and L4) gene expression ratio

Treatment comparison	Time	Gene	P-value
DMM vs Sham	Week 8	TRPV1*	0.050
	Week 12	CGRP*	0.006
		SP*	0.045
		MOR*	0.029
		TRPA1*	0.018
	Week 16	CGRP	0.017
		TRPV1	0.015
AIA vs Saline	n.d.	n.d.	n.d.
DMM vs AIA	Day 3	IL1b	0.025
		TRPV2**	0.015
	Week 2	ATF3**	0.037
	Week 4	CGRP	0.002
		MOR	0.006
		TRPA1	0.004
		TRPV2	0.015
		TRPV4	0.004
		CBR1	0.009
		ADTS4	0.014
		ADTS5	0.002
	Week 8	TRPV1**	0.006
	Week 12	SP**	0.037
		TRPA1**	0.010
	Week 16	CGRP	0.035
		TRPV1	0.016

DMM vs, sham; AIA vs. Saline; and DMM vs. AIA mice at day 3, week 1, 2, 4, 8, 12 and 16 post arthritis induction. Only genes that demonstrated a significant difference (P<0.05) are listed. n.d. = no difference; * = DMM < Sham; ** = DMM < AIA

Figure 6.3a-l. Right to left gene expression ratio for L3/L4 DRG

Presented as the mean fold change relative to the respective sham or saline control group and graphed as log of the means with error bars depicting the standard error of each data set. Bars above 1 represent a relative increase in gene expression ration and bars below 1 represent a relative decrease. Significance for treatment vs. Sham/Saline = $P<0.05$ (*); and $P<0.01$ (**). Significance for AIA vs. DMM = $P<0.05$ (#); and $P<0.01$ (##).

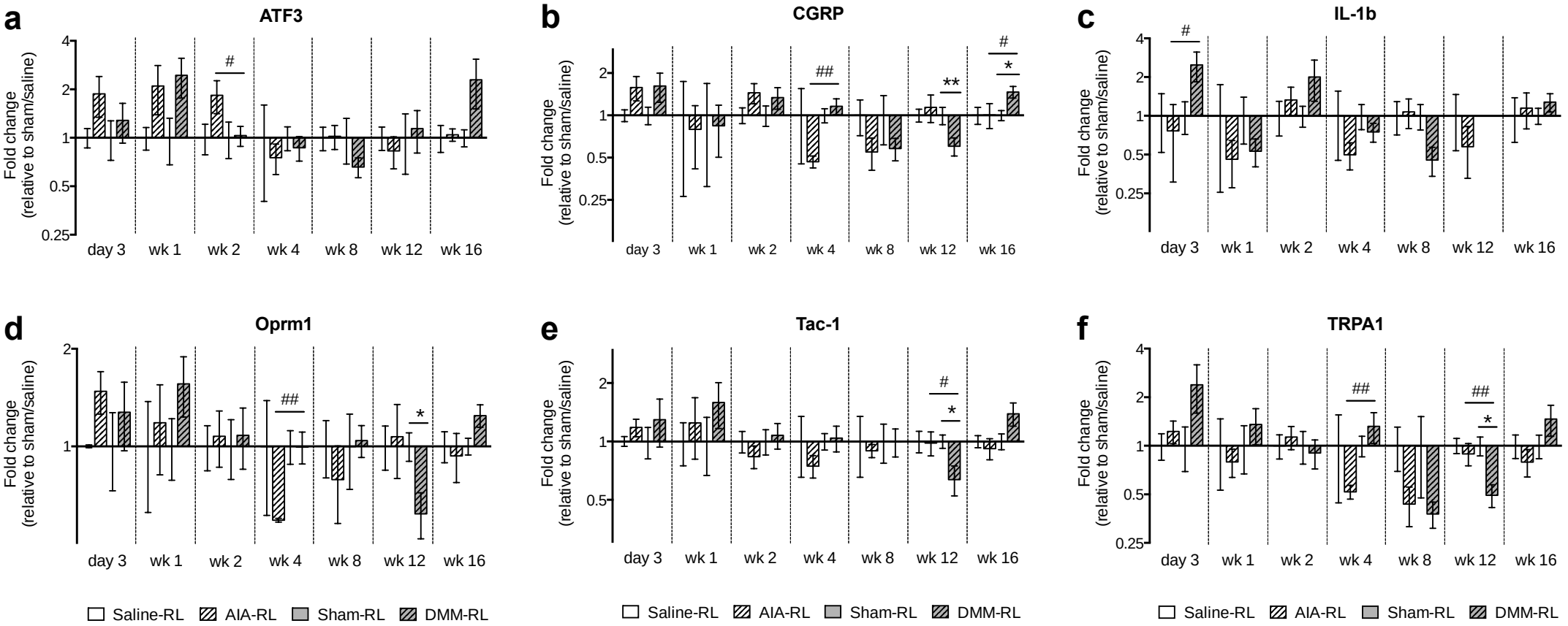

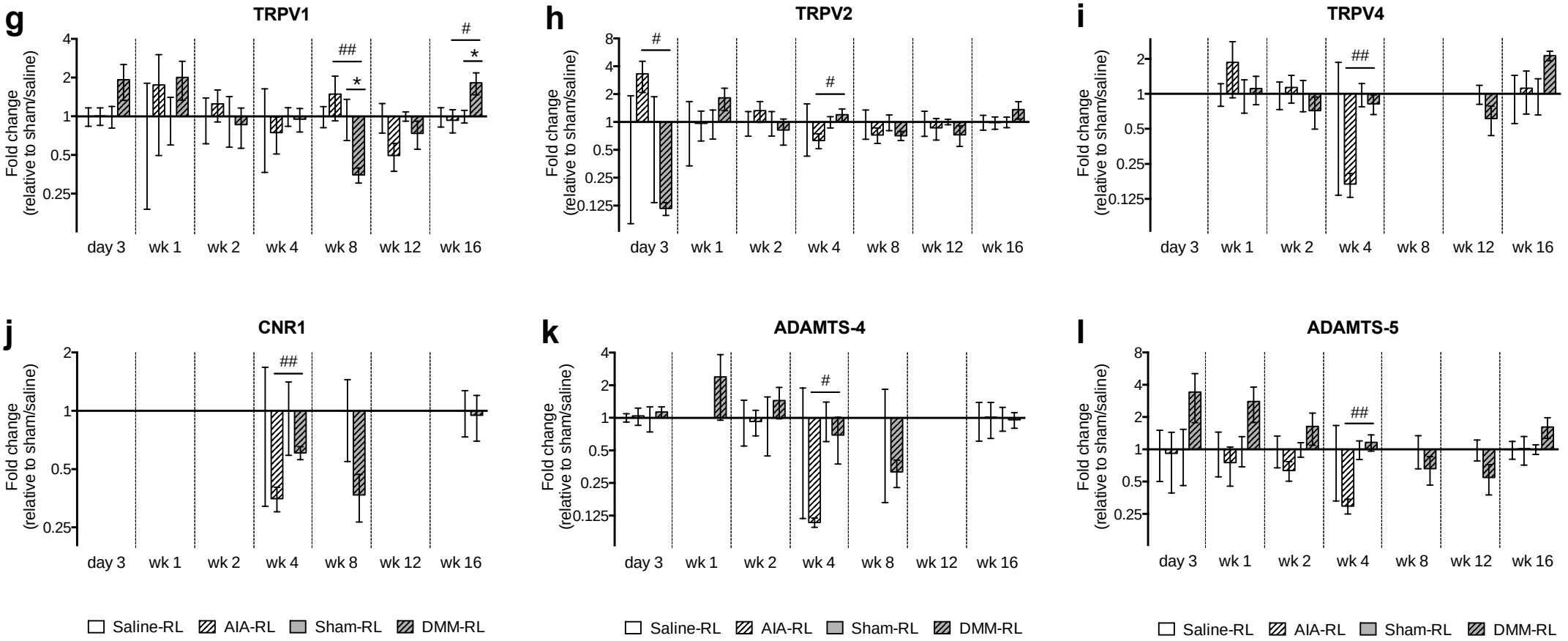
g
TRPV1
h
TRPV2
i
TRPV4
j
CNR1
k
ADAMTS-4
l
ADAMTS-5
Fold change (relative to sham/saline)
day 3
wk 1
wk 2
wk 4
wk 8
wk 12
wk 16
Saline-RL
AIA-RL
Sham-RL
DMM-RL

Table 6.4 summarises the changes in gene expression profile in each model and the differences between the two models at key time points of disease progression. The different phases of OA disease were defined by the histopathology in Chapter 4. The acute inflammatory phase combines day 3, week 1 and week 2 where there is: maximal synovitis; AC proteoglycan loss but mild structural damage; early largely cartilaginous osteophyte development; and SCB remodelling but limited sclerosis. The early-progressive OA phase incorporates week 4 and 8 data and reflects the stage in disease development when: inflammation is decreasing; articular cartilage structural damage and SCB sclerosis is worsening; and osteophytes are approaching maximal size and ossifying. The late OA phase includes week 12 and16 when all the hallmarks of chronic established OA are present and stable at maximal levels in both models, with AC structural damage/erosion, subchondral bone sclerosis and mature boney osteophytes. The genes that displayed differences in R vs L DRG, in the R DRG of arthritic vs sham/saline, or in DMM vs AIA comparisons, at one or more of the time-points included in these different disease phases, have been included in Table 6.4 and the following discussion.

The acute inflammatory phase of disease was characterised by increased ATF3, increased TRPV2 and decreased ADAMTS-5 expression in AIA; increased TRPA1 expression in DMM; and decreased IL-1β in both models (although earlier in AIA). During this acute phase, gene expression for IL-1β (AIA decreased and DMM increased at day 3, AIA increased and DMM decreased at week 1) and ADAMTS-5 (AIA decreased and DMM increased at day 3) was significantly different between the two models.

The early-progressive OA phase of disease was characterised by decreased ATF3, CGRP, TRPA1, Oprm1 and ADAMTS-4 expression in AIA; and increased TRPA1,

decreased TRPV1 and decreased CNR1 expression in DMM. During this phase of OA gene expression for ATF3 (increased AIA and decreased DMM at week 4, decreased AIA and DMM at week 8); CGRP (decrease AIA and increase DMM at week 8); TRPA1 (decrease AIA and increase DMM at week 8); CNR1 (decrease DMM at week 4); and ADAMTS-4 (increase AIA and decrease DMM at week 4) was significantly different between the two models.

The late OA disease phase was characterised by decreased TRPV1 expression in AIA; decreased Tac-1 and Oprm1 expression in DMM; increased TRPV1, TRPV2 and TRPV4 expression in DMM; and interestingly, initial decrease (week 12) and then increase (week 16) CGRP and TRPA1 expression in DMM. During this late phase there were no significant differences in R DRG expression between the two models.

Table 6.4. A summary of changes in gene expression profile in the ipsilateral L3/L4 DRG of DMM and AIA mice.

OA Disease Phase	Gene	DMM[1]	AIA[2]	DMM vs AIA[3]
Acute	ATF3	-	↑	-
	IL-1β	↓	↓	↑↓
	TRPA1	↑	-	-
	TRPV2	-	↑	-
	ADAMTS-5	-	↓	↑
Early OA	ATF3	-	↓	↓↑
	CGRP	-	↓	↑
	TRPA1	↑	↓	↑
	TRPV1	↓	-	-
	Oprm1	-	↓	-
	CNR1	↓	-	↓
	ADAMTS-4	-	↓	↓
Late OA	CGRP	↓↑	-	↑
	Tac-1	↓	-	↓
	TRPA1	↓↑	-	↓↑
	TRPV1	↑	↓	↑
	TRPV2	↑	-	-
	TRPV4	↑	-	-
	Oprm1	↓	-	-

The genes that displayed significant differences in R vs. L DRG or in the R DRG and R/L DRG ratio of arthritis vs. sham/saline and DMM vs. AIA at one or more of the time-points included in the different disease phases (acute inflammatory, early progressive OA, late chronic OA) are presented.

[1.] R DRG and R/L ratio gene expression change compared to sham. [2.] R DRG and R/L ratio gene expression change compared to saline. [3.] R DRG gene expression change DMM compared to AIA (arrow indicates direction of change for DMM relative to AIA). Arrows indicate increase (↑) and decrease (↓)

6.3.2 Time and treatment effect on DRG gene expression (real time RT-PCR)

Linear regression analysis was used to investigate the pattern of change over time for each gene outcome variable (R DRG expression), and within the two arthritis models (Table 6.5). This provides a more robust characterization of the gene expression profile of the different models, by taking time into account and allowing all data to be included in the analyses rather than at individual time points.

When corrected for treatment group (sham, saline, DMM, AIA) only CGRP expression increased significantly with time. None of the genes evaluated displayed a significant decrease in expression with time. When time was corrected for, a significant treatment effect was observed for two genes: both TRPA1 and ADAMTS-5 were increased in DMM relative to AIA. There were no treatment effects for any other genes.

Table 6.5. Time and treatment effect on DRG gene expression

Gene	Time[1]	Time (P)	Treatment[2]		Cf tx[3]	Tx(P)
CGRP	Increased	**0.049**	Sham	–	Saline	0.92
(n=187)			AIA	–	Saline	0.74
			DMM	–	Sham	0.26
			AIA	–	DMM	0.13
IL-1b	–	0.41	Sham	–	Saline	0.95
(n=173)			AIA	–	Saline	0.78
			DMM	–	Sham	0.59
			AIA	–	DMM	0.75
Tac-1	–	0.34	Sham	–	Saline	0.55
(n=184)			AIA	–	Saline	0.32
			DMM	–	Sham	0.52
			AIA	–	DMM	0.29
ATF3	–	0.66	Sham	–	Saline	0.38
(n=187)			AIA	–	Saline	0.83
			DMM	–	Sham	0.28
			AIA	–	DMM	0.70
Oprm1	–	0.99	Sham	–	Saline	0.61
(n=187)			AIA	–	Saline	0.93
			DMM	–	Sham	0.50
			AIA	–	DMM	0.83
TRPA1	–	0.49	Sham	–	Saline	0.43
(n=187)			AIA	–	Saline	0.17
			DMM	–	Sham	0.13
			AIA	**–**	**DMM**	**0.036**
TRPV1	–	0.30	Sham	–	Saline	0.79
(n=187)			AIA	–	Saline	0.94
			DMM	–	Sham	0.57
			AIA	–	DMM	0.75
TRPV2	–	0.17	Sham	–	Saline	0.75
(n=180)			AIA	–	Saline	0.68
			DMM	–	Sham	0.99
			AIA	–	DMM	0.90
TRPV4	–	0.22	Sham	–	Saline	0.96
(n=91)			AIA	–	Saline	0.73
			DMM	–	Sham	0.45
			AIA	–	DMM	0.71
ADAMTS-4	–	0.92	Sham	–	Saline	0.50
(n=135)			AIA	–	Saline	0.70
			DMM	–	Sham	0.96
			AIA	–	DMM	0.76
ADAMTS-5	–	0.12	Sham	–	Saline	0.94
(n=162)			AIA	–	Saline	0.17
			DMM	–	Sham	0.37
			AIA	**–**	**DMM**	**0.028**

Linear regression on log transformed gene expression data of the right L3/L4 DRG in AIA and DMM was used to determine whether gene expression changed over time (1), and when corrected for time whether there was a difference between treatment (2) and comparator treatments (3).

6.3.3 Correlation between different genes in AIA and DMM when corrected for time

Understanding the associations in gene expression in the lumbar DRG provides important information about the mechanisms that may be driving the pain phenotype of the different OA animal models. The existence of any associations was investigated by calculating partial correlation coefficients for the different genes (right DRG gene expression) in the different treatments (AIA, Saline, DMM, Sham) when corrected for time (Table 6.6).

When time was corrected for there were significant associations between all 11 genes in the two control groups (Saline and Sham), with the exception of IL-1β and TRPV4 (no association in sham or saline mice); IL-1β and ADAMTS-4 (no association in sham or saline mice); and TRPV4 and ADAMTS-4 (no association in sham mice). In both AIA and DMM mice the majority of these associations between the 11 genes that were investigated persisted, confirming the interdependence of the neuropeptides, nociceptor channels, inflammatory mediators and other protein receptors involved in pain modulation. These associations reflect the normal network of sensory input regulation at the level of the DRG that are maintained in disease. However, of particular interest were the associations between gene expression that were lost in the two arthritis models, as these indicate disease-specific dysregulation that may be suggesting different pain regulatory pathways in the two arthritis models. Three particular genes showed loss of normal expression association in the two arthritis models; CGRP, IL-1β and ADAMTS-4. In the case of CGRP there were 7 associations lost in AIA (ATF3, IL-1β, Oprm1, TRPV2, TRPV4, ADAMTS-4, ADAMTS-5) but only 2 in DMM (TRPV2, ADAMTS-4). There were 5 associations lost for IL-1β in both AIA (CGRP, Oprm1, TRPV1, TRPV2, ADAMTS-4) and DMM

(ATF3, Oprm1, Tac-1, TRPV2, ADAMTS-5), with only 2 of these (Oprm1, TRPV2) being common to both models. ADAMTS-4 showed the greatest loss of co-expression with other DRG genes, with 6 associations lost in AIA (CGRP, ATF3, IL-1β, Oprm1, TRPV4, ADAMTS-5) and 8 in DMM (CGRP, Oprm1, Tac-1, TRPA1, TRPV1, TRPV2, TRPV4, ADAMTS-5), 4 of these (CGRP, Oprm1, TRPV4, ADAMTS-5) being common to both models.

Table 6.6. Gene expression correlations

Gene comparison	Treatment	r (tau)	*P*
CGRP VS ATF3	**Saline**	**0.374**	**0.003**
	Sham	**0.495**	**<0.001**
	AIA	0.154	0.22
	DMM	**0.320**	**<0.001**
CGRP VS IL-1B	**Saline**	**0.286**	**0.003**
	Sham	**0.322**	**0.001**
	AIA	0.003	0.99
	DMM	**0.379**	**<0.001**
CGRP VS Oprm1	**Saline**	**0.309**	**0.013**
	Sham	**0.442**	**<0.001**
	AIA	0.139	0.29
	DMM	**0.437**	**<0.001**
CGRP VS Tac-1	**Saline**	**0.407**	**<0.001**
	Sham	**0.526**	**<0.001**
	AIA	**0.257**	**0.041**
	DMM	**0.410**	**<0.001**
CGRP VS TRPA1	**Saline**	**0.312**	**0.001**
	Sham	**0.510**	**<0.001**
	AIA	**0.372**	**0.001**
	DMM	**0.483**	**<0.001**
CGRP VS TRPV1	**Saline**	**0.527**	**<0.001**
	Sham	**0.466**	**<0.001**
	AIA	**0.333**	**0.006**
	DMM	**0.480**	**<0.001**
CGRP VS TRPV2	**Saline**	**0.303**	**0.003**
	Sham	**0.468**	**<0.001**
	AIA	0.155	0.22
	DMM	0.227	0.058
CGRP VS TRPV4	**Saline**	**0.323**	**0.005**
	Sham	**0.322**	**0.003**
	AIA	0.287	0.066
	DMM	**0.265**	**0.036**

CGRP VS ADAMTS-4	**Saline**	**0.456**	**<0.001**
	Sham	**0.374**	**<0.001**
	AIA	0.168	0.29
	DMM	0.204	0.11
CGRP VS ADAMTS-5	**Saline**	**0.309**	**0.015**
	Sham	**0.385**	**<0.001**
	AIA	0.031	0.85
	DMM	**0.298**	**0.008**
ATF3 VS IL-1B	**Saline**	**0.299**	**0.001**
	Sham	**0.417**	**<0.001**
	AIA	**0.359**	**0.001**
	DMM	0.111	0.27
ATF3 VS Oprm1	**Saline**	**0.286**	**0.023**
	Sham	**0.506**	**<0.001**
	AIA	**0.295**	**0.026**
	DMM	**0.471**	**<0.001**
ATF3 VS Tac-1	**Saline**	**0.399**	**<0.001**
	Sham	**0.567**	**<0.001**
	AIA	**0.275**	**0.021**
	DMM	**0.407**	**<0.001**
ATF3 VS TRPA1	**Saline**	**0.236**	**0.040**
	Sham	**0.460**	**<0.001**
	AIA	**0.448**	**<0.001**
	DMM	**0.426**	**<0.001**
ATF3 VS TRPV1	**Saline**	**0.414**	**<0.001**
	Sham	**0.493**	**<0.001**
	AIA	**0.347**	**0.004**
	DMM	**0.404**	**<0.001**
ATF3 VS TRPV2	**Saline**	**0.372**	**0.001**
	Sham	**0.536**	**<0.001**
	AIA	**0.331**	**0.009**
	DMM	**0.301**	**0.003**
ATF3 VS TRPV4	**Saline**	**0.449**	**<0.001**
	Sham	**0.315**	**0.004**
	AIA	**0.394**	**0.023**
	DMM	0.241	0.051
ATF3 VS ADAMTS-4	**Saline**	**0.406**	**0.002**
	Sham	**0.375**	**0.001**
	AIA	0.256	0.095
	DMM	**0.406**	**<0.001**
ATF3 VS ADAMTS-5	**Saline**	**0.401**	**0.001**
	Sham	**0.249**	**<0.001**
	AIA	**0.490**	**<0.001**
	DMM	**0.332**	**0.001**
IL-1B VS Oprm1	**Saline**	**0.295**	**0.009**
	Sham	**0.290**	**0.002**
	AIA	0.167	0.19
	DMM	0.115	0.30
IL-1B VS Tac-1	**Saline**	**0.357**	**0.001**
	Sham	**0.376**	**<0.001**
	AIA	**0.239**	**0.035**
	DMM	0.178	0.067
IL-1B VS TRPA1	**Saline**	**0.391**	**<0.001**
	Sham	**0.378**	**<0.001**

	AIA	**0.276**	**0.016**
	DMM	**0.286**	**0.007**
IL-1B VS TRPV1	**Saline**	**0.216**	**0.056**
	Sham	**0.293**	**0.002**
	AIA	0.147	0.23
	DMM	**0.259**	**0.021**
IL-1B VS TRPV2	**Saline**	**0.321**	**0.002**
	Sham	**0.328**	**0.002**
	AIA	0.055	0.65
	DMM	0.037	0.74
IL-1B VS TRPV4	Saline	0.202	0.076
	Sham	0.196	0.14
	AIA	**0.420**	**0.002**
	DMM	0.170	0.21
IL-1B VS ADAMTS-4	Saline	0.237	0.14
	Sham	0.109	0.32
	AIA	0.087	0.63
	DMM	**0.208**	**0.042**
IL-1B VS ADAMTS-5	**Saline**	**0.373**	**0.001**
	Sham	**0.214**	**0.040**
	AIA	**0.458**	**<0.001**
	DMM	0.108	0.32
Oprm1 VS Tac-1	**Saline**	**0.456**	**<0.001**
	Sham	**0.522**	**<0.001**
	AIA	**0.402**	**<0.001**
	DMM	**0.588**	**<0.001**
Oprm1 VS TRPA1	**Saline**	**0.444**	**<0.001**
	Sham	**0.542**	**<0.001**
	AIA	**0.411**	**<0.001**
	DMM	**0.595**	**<0.001**
Oprm1 VS TRPV1	**Saline**	**0.404**	**<0.001**
	Sham	**0.601**	**<0.001**
	AIA	**0.351**	**0.002**
	DMM	**0.569**	**<0.001**
Oprm1 VS TRPV2	**Saline**	**0.505**	**<0.001**
	Sham	**0.634**	**<0.001**
	AIA	**0.419**	**<0.001**
	DMM	**0.443**	**<0.001**
Oprm1 VS TRPV4	**Saline**	**0.399**	**0.002**
	Sham	**0.482**	**<0.001**
	AIA	**0.502**	**<0.001**
	DMM	**0.512**	**<0.001**
Oprm1 VS ADAMTS-4	**Saline**	**0.366**	**0.014**
	Sham	**0.382**	**<0.001**
	AIA	0.164	0.37
	DMM	0.238	0.064
Oprm1 VS ADAMTS-5	**Saline**	**0.483**	**<0.001**
	Sham	**0.481**	**<0.001**
	AIA	**0.415**	**<0.001**
	DMM	**0.500**	**<0.001**
Tac-1 VS TRPA1	**Saline**	**0.443**	**<0.001**
	Sham	**0.641**	**<0.001**
	AIA	**0.513**	**<0.001**
	DMM	**0.578**	**<0.001**

Tac-1 VS TRPV1	**Saline**	**0.366**	**0.001**
	Sham	**0.662**	**<0.001**
	AIA	**0.490**	**<0.001**
	DMM	**0.582**	**<0.001**
Tac-1 VS TRPV2	**Saline**	**0.499**	**<0.001**
	Sham	**0.641**	**<0.001**
	AIA	**0.426**	**<0.001**
	DMM	**0.533**	**<0.001**
Tac-1 VS TRPV4	**Saline**	**0.494**	**<0.001**
	Sham	**0.342**	**0.003**
	AIA	**0.490**	**<0.001**
	DMM	**0.470**	**<0.001**
Tac-1 VS ADAMTS-4	**Saline**	**0.480**	**<0.001**
	Sham	**0.450**	**<0.001**
	AIA	**0.323**	**0.037**
	DMM	0.222	0.089
Tac-1 VS ADAMTS-5	**Saline**	**0.321**	**0.031**
	Sham	**0.385**	**<0.001**
	AIA	**0.367**	**<0.001**
	DMM	**0.371**	**<0.001**
TRPA1 VS TRPV1	**Saline**	**0.368**	**<0.001**
	Sham	**0.548**	**<0.001**
	AIA	**0.484**	**<0.001**
	DMM	**0.592**	**<0.001**
TRPA1 VS TRPV2	**Saline**	**0.517**	**<0.001**
	Sham	**0.529**	**<0.001**
	AIA	**0.410**	**<0.001**
	DMM	**0.496**	**<0.001**
TRPA1 VS TRPV4	**Saline**	**0.433**	**0.001**
	Sham	**0.336**	**0.011**
	AIA	**0.597**	**<0.001**
	DMM	**0.455**	**<0.001**
TRPA1 VS ADAMTS-4	**Saline**	**0.490**	**0.001**
	Sham	**0.333**	**0.002**
	AIA	**0.397**	**0.002**
	DMM	0.176	0.17
TRPA1 VS ADAMTS-5	**Saline**	**0.587**	**<0.001**
	Sham	**0.357**	**<0.001**
	AIA	**0.460**	**<0.001**
	DMM	**0.464**	**<0.001**
TRPV1 VS TRPV2	**Saline**	**0.421**	**<0.001**
	Sham	**0.587**	**<0.001**
	AIA	**0.534**	**<0.001**
	DMM	**0.515**	**<0.001**
TRPV1 VS TRPV4	**Saline**	**0.526**	**<0.001**
	Sham	**0.498**	**<0.001**
	AIA	**0.563**	**<0.001**
	DMM	**0.441**	**<0.001**
TRPV1 VS ADAMTS-4	**Saline**	**0.624**	**<0.001**
	Sham	**0.375**	**<0.001**
	AIA	**0.474**	**<0.001**
	DMM	0.159	0.23
TRPV1 VS ADAMTS-5	**Saline**	**0.471**	**<0.001**
	Sham	**0.447**	**<0.001**

	AIA	**0.443**	**<0.001**
	DMM	**0.431**	**<0.001**
TRPV2 VS TRPV4	**Saline**	**0.598**	**<0.001**
	Sham	**0.603**	**<0.001**
	AIA	**0.528**	**<0.001**
	DMM	**0.409**	**0.001**
TRPV2 VS ADAMTS-4	**Saline**	**0.496**	**<0.001**
	Sham	**0.327**	**0.001**
	AIA	**0.380**	**0.003**
	DMM	-0.003	0.98
TRPV2 VS ADAMTS-5	**Saline**	**0.781**	**<0.001**
	Sham	**0.586**	**<0.001**
	AIA	**0.383**	**0.005**
	DMM	**0.254**	**0.028**
TRPV4 VS ADAMTS-4	**Saline**	**0.470**	**<0.001**
	Sham	0.229	0.18
	AIA	0.215	0.21
	DMM	0.139	0.43
TRPV4 VS ADAMTS-5	**Saline**	**0.593**	**<0.001**
	Sham	**0.438**	**<0.001**
	AIA	**0.493**	**<0.001**
	DMM	**0.479**	**<0.001**
ADAMTS-4 VS ADAMTS-5	**Saline**	**0.403**	**0.002**
	Sham	**0.294**	**0.005**
	AIA	0.216	0.15
	DMM	0.171	0.17

Gene expression Pearson partial correlations on right L3/L4 DRG in AIA and DMM when corrected for time, within treatment. Note: After Benjamini-Hochberg correction, 5% confidence level is $P < 0.040$

6.3.4 DRG protein expression (immunohistochemistry)

Based on the key changes in gene expression and the associations that were identified in the two animal models and at different stages of disease progression (Table 6.4 and Table 6.6), antibodies against ATF3, IL-1β, CGRP, Oprm1, TRPA1, TRPV1, TRPV2, TRPV4, ADAMTS-4 and ADAMTS-5 were used to examine the production of these proteins in the lumbar DRG. Despite using antibodies that had previously been published by other investigators and trying several modifications to the protocol (including heat and enzyme extraction methods and protein blocking techniques), optimisation of staining above the background levels that were observed in negative control stained sections could only be achieved for CGRP and Oprm1. Therefore only these two proteins could be investigated. Figures 6.4a to 6.4h are representative images of the differences in staining intensity and proportion of cells staining positive, that were observed in the two models and at the different time points.

Figure 6.4a-d. CGRP immunoreactivity (IR)

IR (NovaRED staining neurons marked with black arrow) in the right L4 DRG in DMM, Sham, AIA, and Saline-injected mice at week 1 (a), week 4 (b), week 8 (c), and week 16 (d) post arthritis induction. X10 magnification. Inserts represent right L4 DRG negative reagent control (i) and right L4 DRG negative control from naïve mouse (ii).

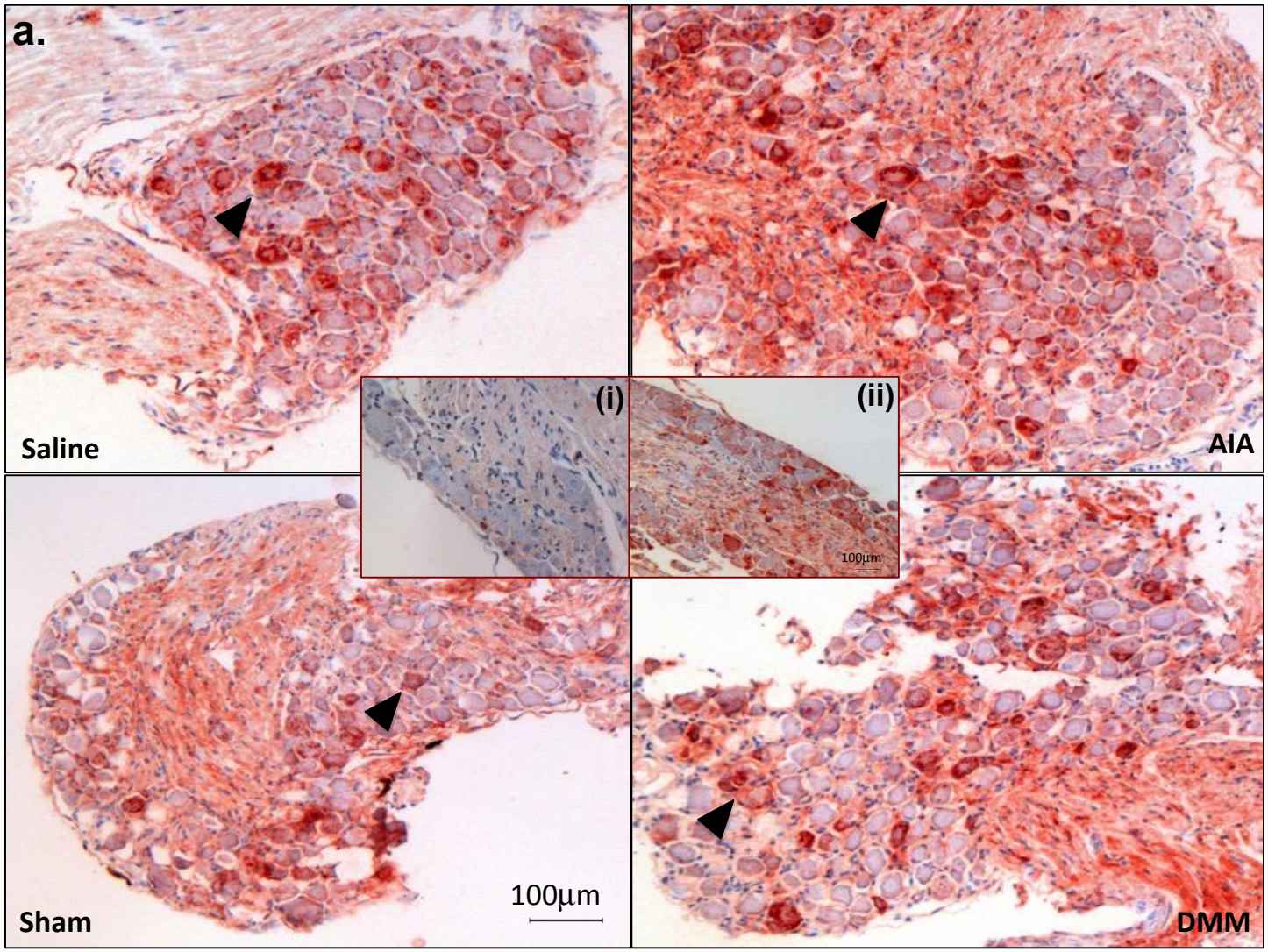

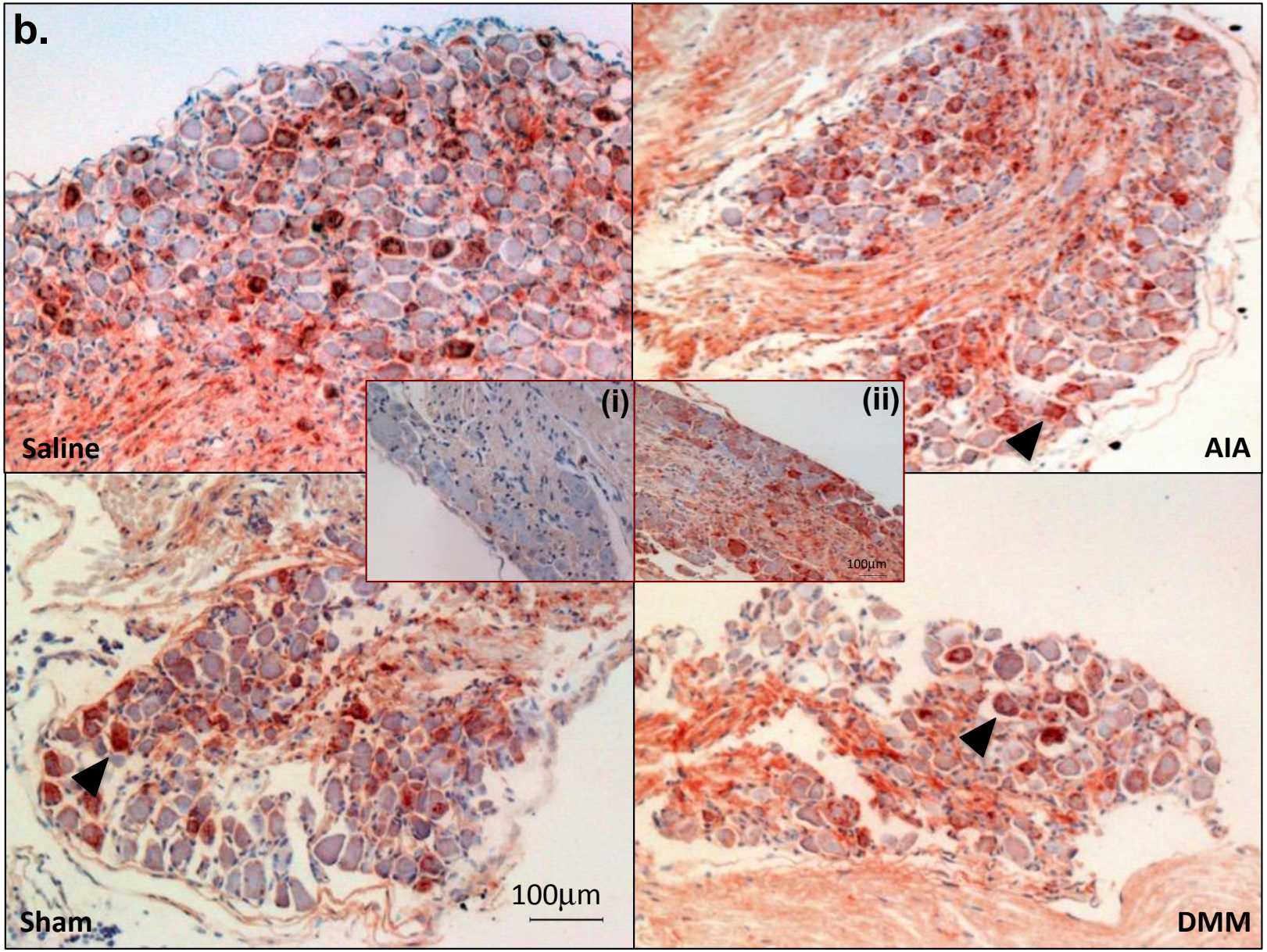
b.
Saline
(i)
(ii)
AIA
100µm
Sham
100µm
DMM

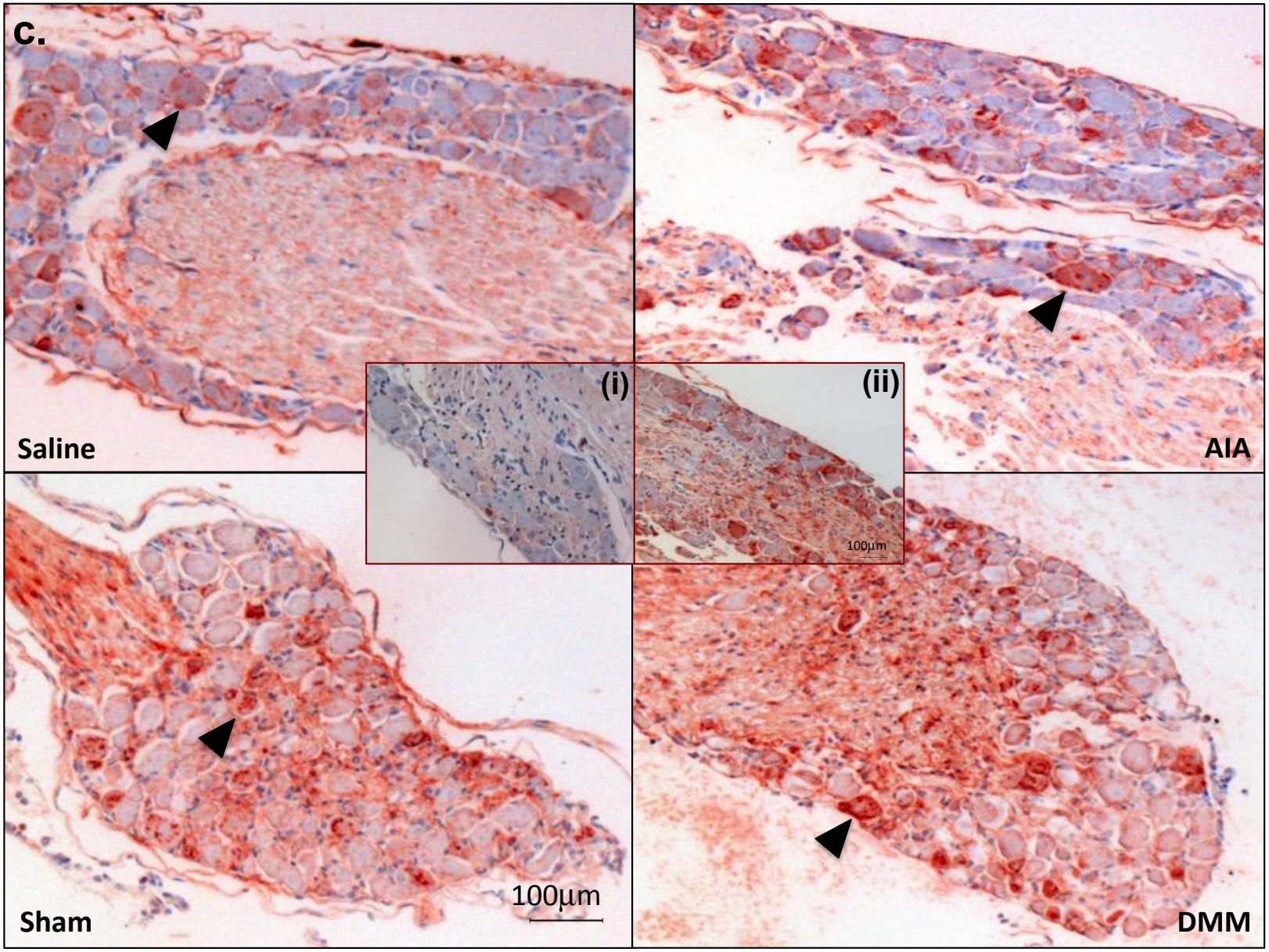
C.
Saline
(i)
(ii)
AIA
100µm
Sham
100µm
DMM

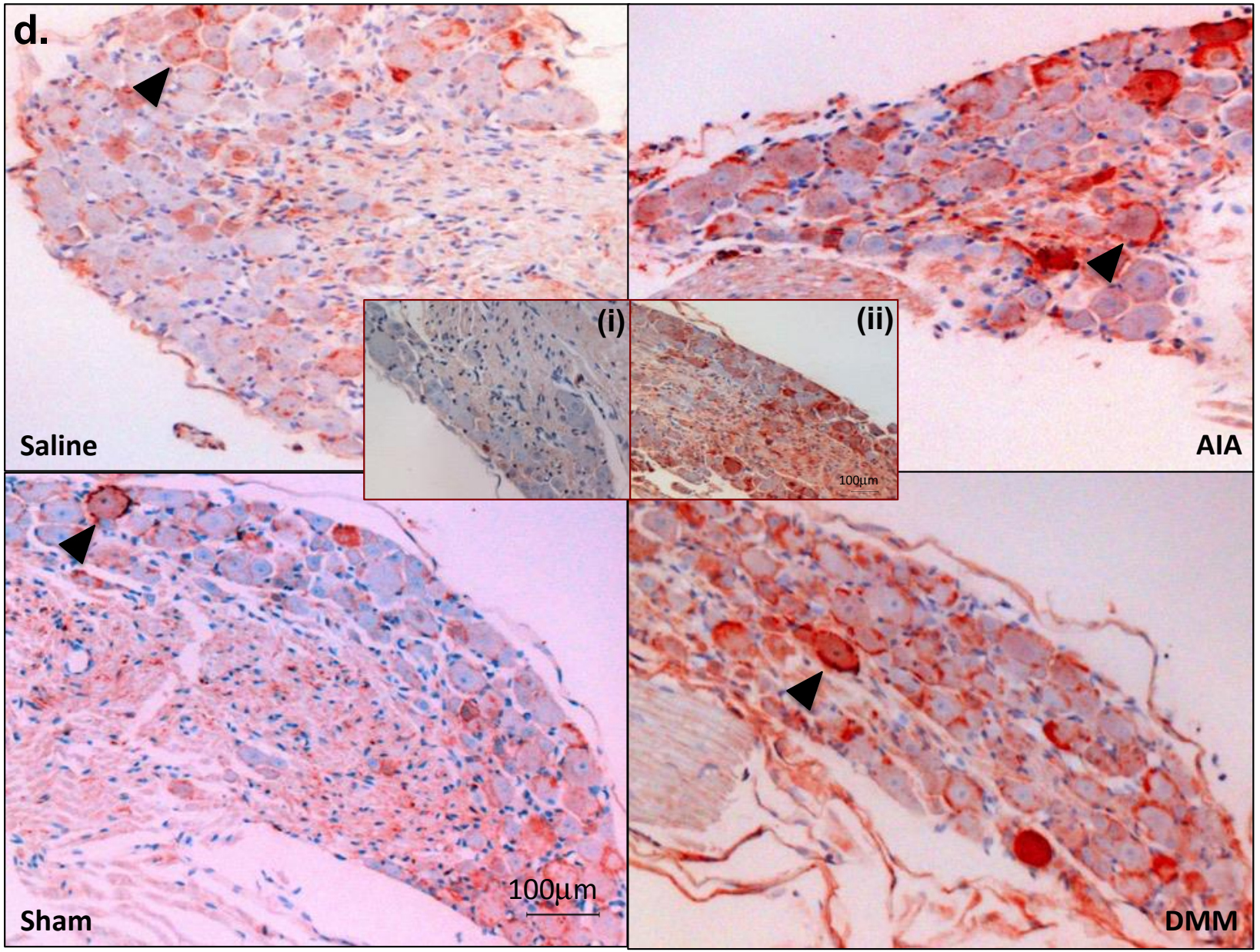
d.
Saline
(i)
(ii)
100µm
AIA
Sham
100µm
DMM

CGRP immunoreactivity (IR) was detected in the right L3 and L4 DRG in all treatment groups at weeks 1, 4, 8 and 16, and was above the levels observed in naïve mice. At week 1, there was a greater level of CGRP-IR in saline, AIA and DMM mice compared to sham. This was reflected in the number of positive staining cells and the staining intensity. In contrast, the increase in CGRP gene expression at day 3 in AIA and DMM was not significant and there were no significant changes in CGRP gene expression observed in the acute inflammatory phase of disease (up to week 2). At week 4, there was greater CGRP-IR in saline and AIA compared to sham and DMM mice (number of positive staining cells and staining intensity). Interestingly, there was greater CGRP-IR in saline mice compared to AIA. This again did not reflect gene expression at this time point. At week 8, expression in all 4 groups was reduced compared to week 1 and 4, but still greater than naïve mice. CGRP-IR was greater in DMM than both sham and AIA based on number of positive staining cells and staining intensity. This difference in IR matched the gene expression changes at this time point where CGRP expression was up regulated compared to AIA (Figure 6.2b). At week 16 CGRP-IR in saline and sham had decreased further to levels similar to naïve mice. CGRP-IR in DMM was similar to week 8 and in AIA it increased to levels similar to DMM.

Figure 6.4e-h. Opmr1 immunoreactivity (IR)

IR (NovaRED staining neurons marked with black arrow) in the right L4 DRG in DMM, Sham, AIA, and Saline-injected mice at week 1 (e), week 4 (f), week 8 (g), and week 16 (h) post arthritis induction. Inserts represent right L4 DRG negative reagent control (i) and right L4 DRG negative control from naïve mouse (ii).

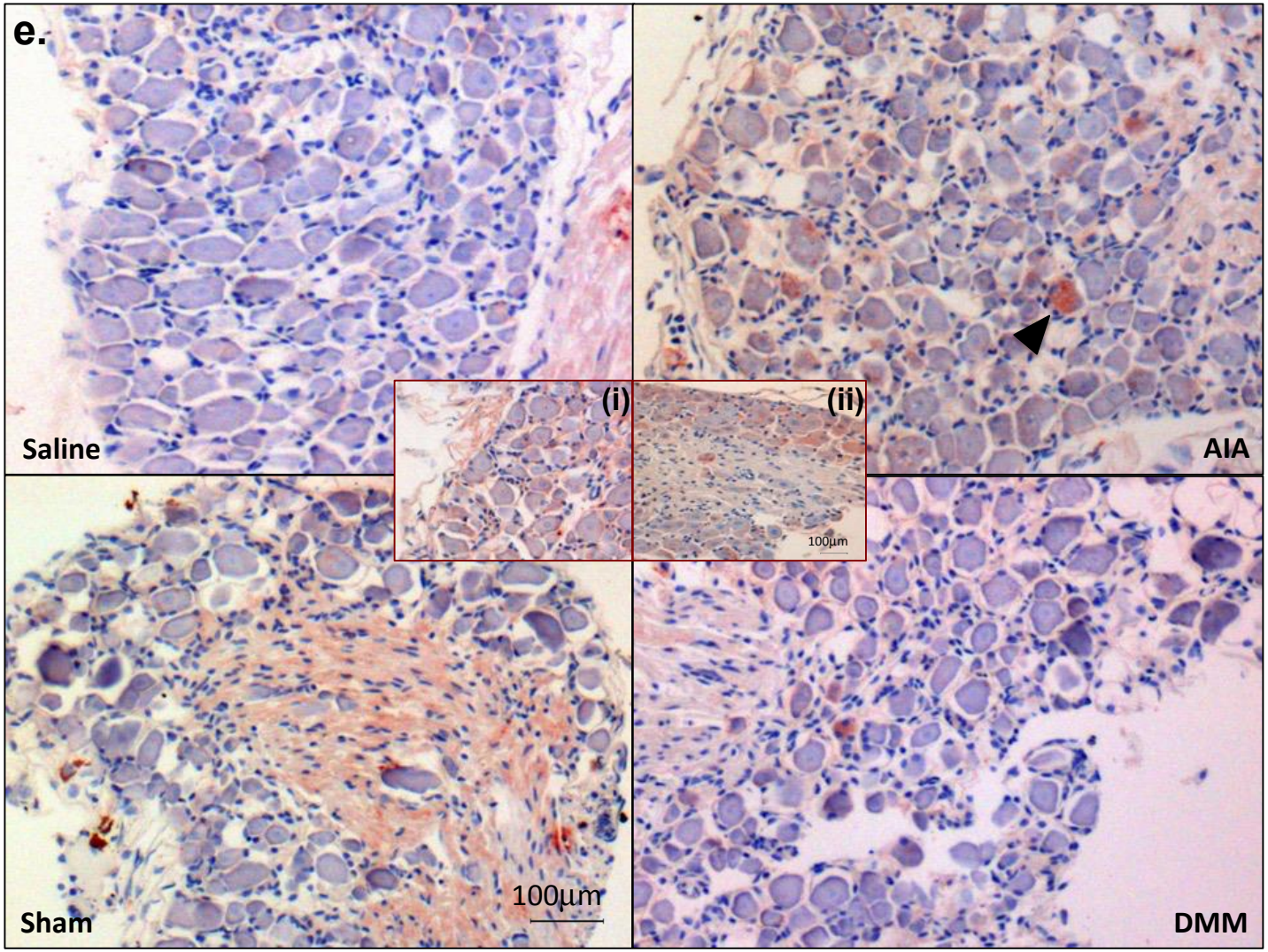

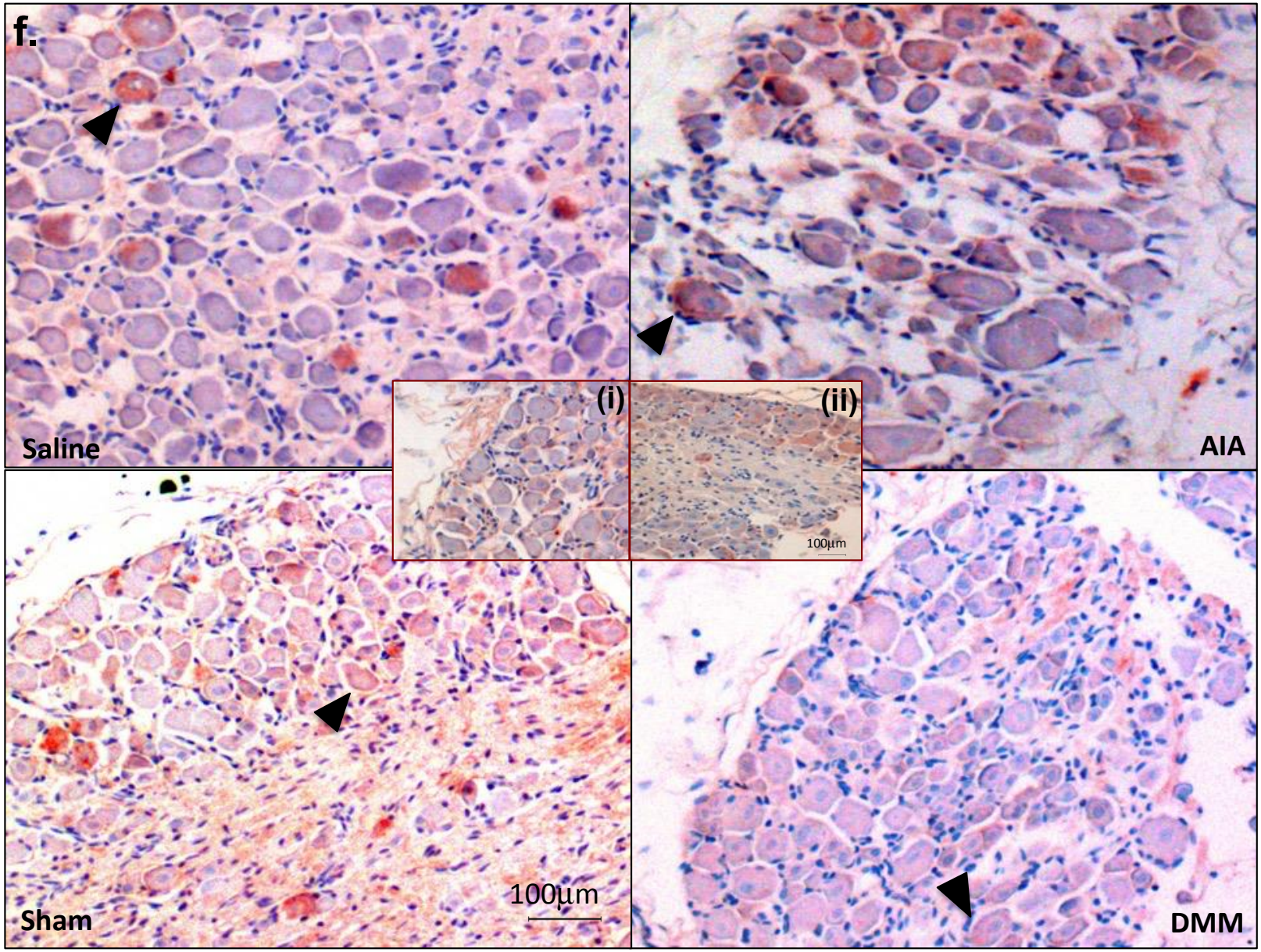
f.
Saline
(i)
(ii)
AIA
100µm
Sham
100µm
DMM

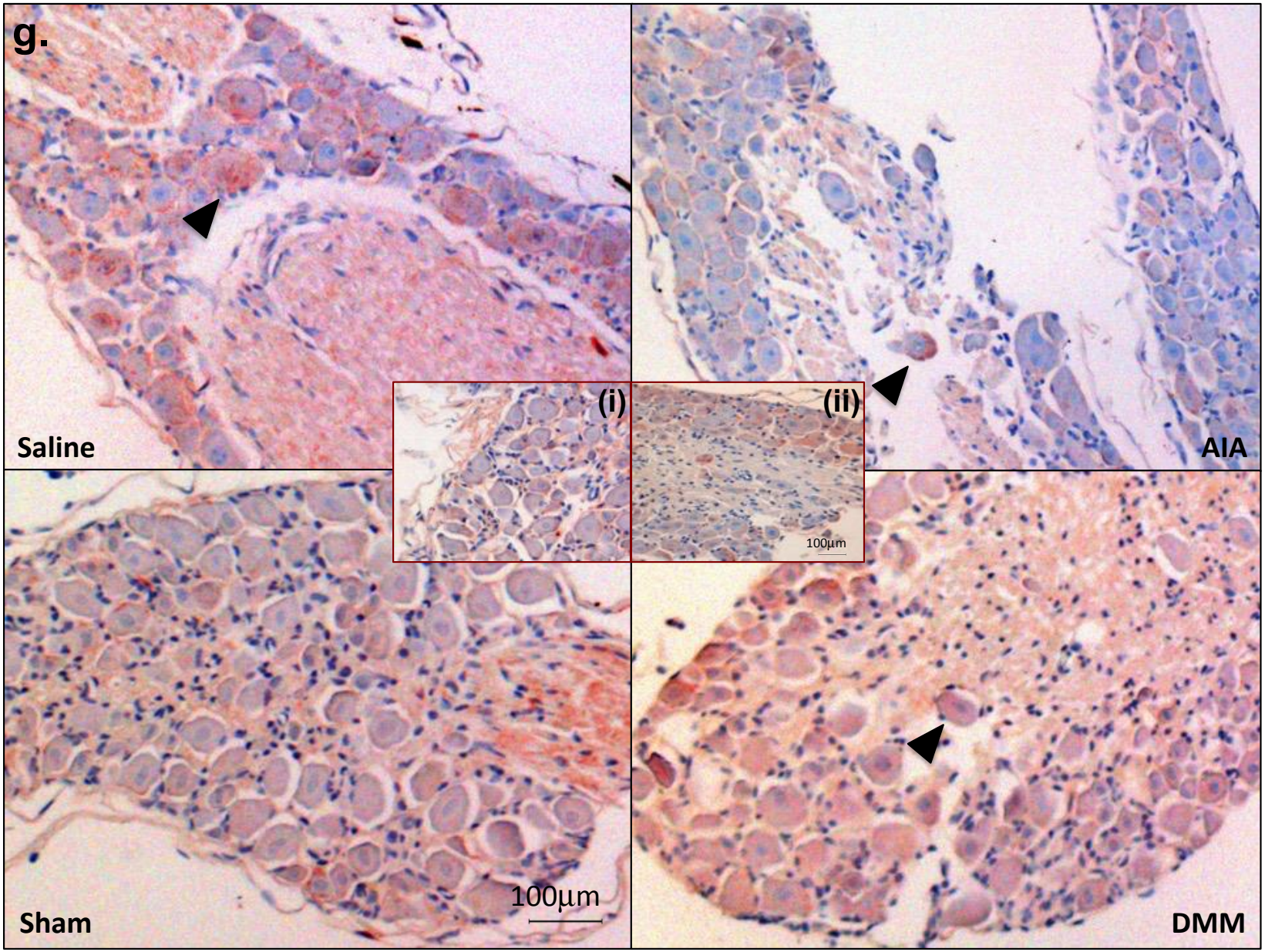
g.
Saline
(i)
(ii)
AIA
100µm
Sham
100µm
DMM

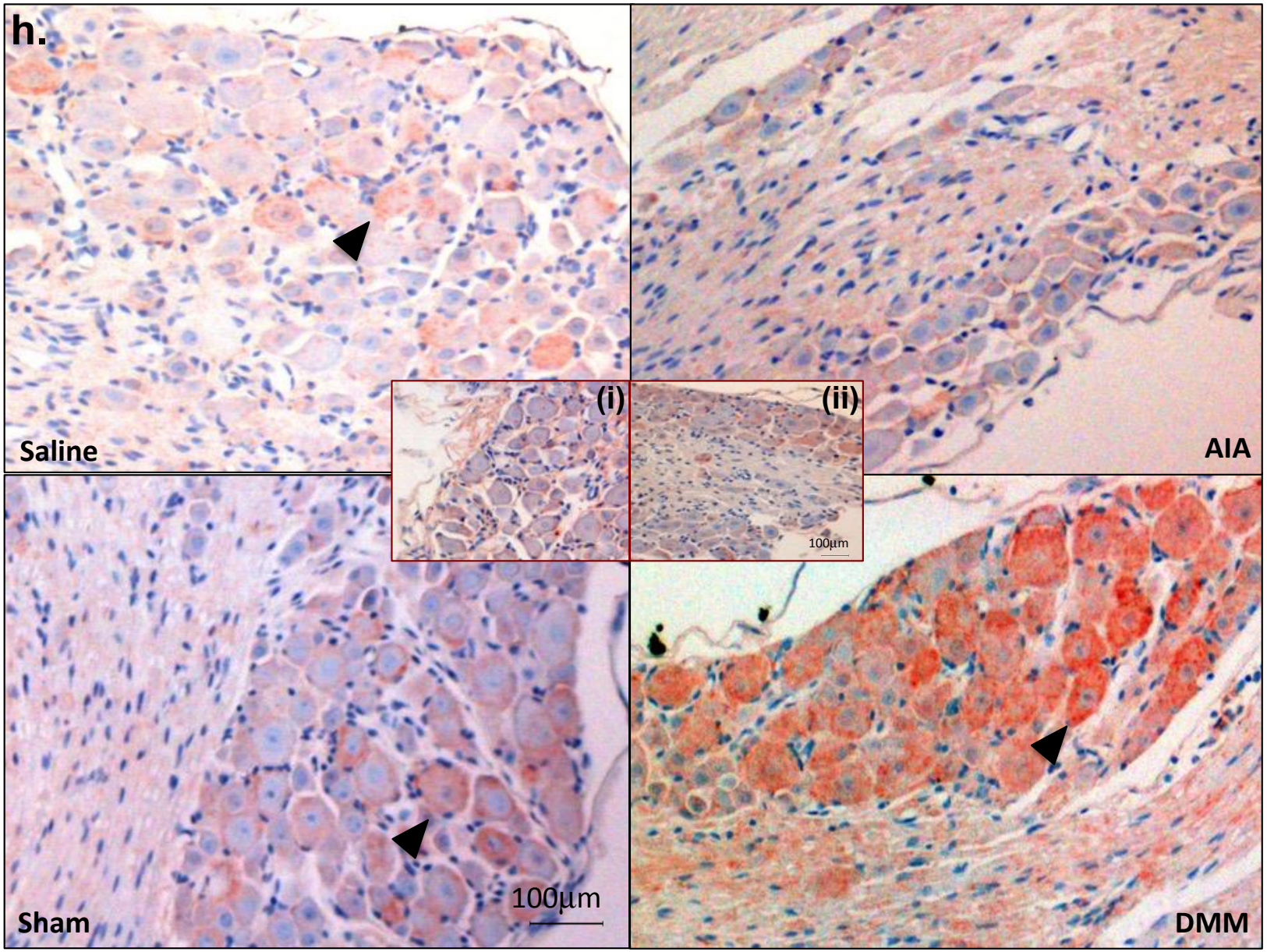
h.
Saline
(i)
(ii)
AIA
100µm
Sham
100µm
DMM

Oprm1-IR above that observed in naïve mice was not detected at all time points and treatment groups. At week 1, Oprm1-IR was detected in a few cells per HPF in all treatment groups and this was comparable to expression in naïve mice. This aligned with the gene expression data where there was no significant change in both model during the acute inflammatory phase (up to week 2). At week 4, Oprm1-IR in saline, AIA and sham mice increased based on number of positive staining cells. Oprm1-IR in DMM was unchanged. At week 8, Oprm1-IR in all treatment groups was similar to age matched naïve mice. At week 16, Oprm1-IR in saline, AIA and sham mice remained similar to age matched naïve. However, in DMM it increased both with respect to number of positive staining cells and staining intensity. This was in contrast to the down regulation in gene expression observed in DMM at week 12.

6.4 Discussion

In summary, this study demonstrated multiple changes in DRG gene expression between arthritic and control (sham/saline) groups as well as between the two arthritis models at each stage of OA disease development (Table 6.4). Differences in expression of IL-1β, ATF3, TRPA1, TRPV2 and ADAMTS-5 were observed in the acute inflammatory stage of disease. Down regulation of IL-1β was the only significant gene expression change observed in both models at this stage. In the early-progressive stage of OA the AIA model was characterised generally by a down regulation in gene expression (ATF3, CGRP, TRPA1, Oprm1 and ADAMTS-4) with fewer changes occurring in DMM. In the late chronic stage of OA the DMM model was generally characterised by an up regulation in gene expression (CGRP, TRPA1, TRPV1, TRPV2, TRPV4) with only one change evident in AIA (TRPV1).

Interestingly, the greatest differences in gene expression profile between the two animal models occurred in the late chronic phase when histological characteristics of OA were well established in both models with no significant differences between the histology observed in AIA and DMM knee joints (Chapter 4). With respect to pain-related behaviour, both models demonstrated ipsilateral tactile allodynia, thermal hyperalgesia and reduced stride length at this late phase of OA disease, with mechanical hyperalgesia and reduced ipsilateral hind limb weight bearing, unique to DMM (Chapter 5). Despite the histological and behavioural similarities between the two models, the DRG gene expression data suggests there are significant differences between the two models when it comes to the mechanisms driving pain at this late phase of OA disease. By week 16 we observed that CGRP, TRPA1, TRPV1, TRPV2 and TRPV4 were all up regulated in DMM; Tac-1 and Oprm1 were down regulated in DMM; and TRPV2 was down regulated in AIA. When corrected for time, the dysregulated DRG gene-expression associations for CGRP, IL-1β and ADAMTS-4, suggest model specific differential effects in the expression profile of these three genes.

This study was not able to clearly demonstrate how the observed changes in gene expression related to gene translation and therefore, changes in protein expression in the DRG. This was in part due to the difficulties encountered in tissue processing and the inability to achieve consistency in antibody immunoreactivity that was above background in 8 of the 10 antibodies tested. For Oprm1 and CGRP where this was achieved, there was no consistent association between gene and protein expression at the different time points. These observed temporal differences may be due to the transient nature of gene transcription and the complex mechanisms that regulate

translation (619). They may also indicate post-transcriptional control of protein levels mediated via proteolysis or other cellular mechanisms.

Taken together, the data presented in this chapter implicates dysregulation of multiple genes including CGRP, IL-1β, ADAMTS-4, ADAMTS-5, ATF3 TRPA1, TRPV1, TRPV2, TRPV4, Tac-1 and Oprm1 in arthritis pain. However, what specific role these changes in the DRG that innervate the knee joint play in the pain phenotype observed in each animal model is still not clear.

A primary role for the sensory neurons of the DRG is to detect noxious mechanical and thermal stimuli in order to protect the body from harm (620). Nociceptive pain detection is clearly an adaptive process that is designed for protection and preservation. However, persistent and exaggerated pain is maladaptive and is driven in part by the plasticity of sensory nociceptor neurons. Modulation following injury or exposure to inflammation starts at the nociceptor and ends with alterations in central nervous system processing. The result is an exaggerated pain state refered to as "sensitisation" that is characterised by hyperalgesia and allodynia. In the case of OA pain, a number of mechanisms have been investigated in an attempt to better understand how chronic pain in this disease develops and identify potential therapeutic targets (432, 604, 605, 608, 621, 622). The genes identified in this study as displaying model-specific alterations in expression have all been shown to play a role in sensitisation and the development of chronic pain (163, 310). The data reported in this chapter sheds further light on the likely significance of their contribution to the development of chronic pain that is specific to different types of OA.

Sensitisation manifests as allodynia, and mechanical and thermal hyperalgesia (230), and is a key component of the OA pain phenotype in humans (284, 596, 623). It contributes to many of the clinical symptoms that patients report such as movement-evoked pain as well as specific tests of hypersensitivity such as mechanical temporal summation (TS) and reduced pressure pain thresholds (PPT) (278, 624, 625). Both TRPV1 and TRPA1 are involved in mediating mechanosensation and thermosensation. Despite TRPA1 being highly co-expressed with TRPV1 at the level of the DRG (626), the two TRP channels play distinct roles in mediating OA pain especially inflammation driven pain (627). Through the use of a TRPA1 specific inhibitor, the role of TRPA1 in development of mechanical hyperalgesia secondary to inflammation has been established (628). More recently, a role for TRPA1 in the development of inflammation driven knee OA sensitisation was demonstrated in TRPA1 KO mice using the MIA model (485). The role of TRPA1 in development of chronic pain in a post-traumatic OA model has not previously been investigated. The findings in this chapter demonstrate an up regulation of TRPA1 in DMM mice during both the acute inflammatory and chronic phase of OA disease, suggesting that in a post-injury OA phenotype, TRPA1 may play an important role in development of sensitisation in the early inflammatory phase of OA disease and the development of mechanical hyperalgesia in the late chronic phase of OA disease that, based on joint histopathology, is likely not driven by inflammation. These findings were not observed in the AIA model despite the similarities in joint pathology at this time.

The TRPV2 channel is activated by temperatures greater than 52 degrees and is reported to also play a role in inflammation-induced hyperalgesia that is distinct from TRPV1 activity, and manifests as development of thermal hyperlagesia secondary to high temperature stimuli (211). The study in this chapter identified that TRPV2 was

only up regulated in the AIA model during the acute inflammatory phase prior to the development of OA specific joint pathology. In the DMM model, TRPV2 was up regulated during the early phase of OA disease when AC damage was developing, osteophytes were well established and moderate joint inflammation was still present (Chapter 4). Interestingly, at this time point thermal hyperalgesia was present in DMM but not in AIA mice (Chapter 5). This suggests the role of TRPV2 in development of thermal hyperalgesia is model and time specific. DRG culture studies, using a cannabinoid TRPV2 specific agonist, cannabidiol, have also demonstrated that TRPV2 mediates CGRP release (629). The findings in this chapter also demonstrated that CGRP was up regulated along side TRPV2 during the early phase of OA disease.

TRPV4 is a polymodal receptor that is activated by many different stimuli including shear stress, hypotonicity and heat (> 27 degrees); and is expressed by low and high threshold neurons in the DRG (221). The observed increase in mechanical nociceptive threshold following disruption of TRPV4 in 129/Sv mice (221) and establishment of TRPV4 as a high threshold mechanoreceptor (219), suggests a role for TRPV4 in mediating mechanical hyperalgesia. This has been demonstrated with inflammatory mediator driven sensitisation (630) and neuropathic pain (631). Investigators have also demonstrated that up regulation of TRPV4 drives mechanical hyperalgesia induced by DRG exposed to the pro-inflammatory cytokine, IL-17 (632). In addition, TRPV4 plays an important role in temperomandibular joint inflammatory pain via the trigeminal ganglion (633).

TRPV4's important role in maintaining joint homeostasis is evident by the numerous inherited skeletal dysplasias and arthropathies seen in humans with TRPV4 mutations (634-636). TRPV4 is found in bone (osteoblasts and osteoclasts) where it plays a role

in bone remodelling activity, and articular chondrocytes where it mediates cellular responses to hyposmotic stress (637). More recently, it has been demonstrated that TRPV4 KO mice are more susceptible to obesity-induced OA when fed a high fat diet (638). All of this makes TRPV4 an attractive therapeutic target for OA as both a DMOAD (639) and for treating OA pain. Yet little is known about the role that TRPV4 plays in mediating chronic OA pain that is not driven primarily by inflammation. There are currently no studies that have reported on the role of TRPV4 in the development of chronic pain that is induced using a joint instability model such as DMM to identify if it plays a role in the chronic pain of a post-injury OA phenotype. In this study, both the upregulation of TRPV4 and the development of mechanical hyperalgesia occurred in the chronic stage of OA disease and were only observed in the DMM model.

CGRP is co-expressed with TRPV1 in a subset of small sized sensory neurons in the DRG and its receptors are located in both the dorsal horn of the spinal cord and in several regions of the brain. CGRP increases synaptic transmission and neuronal responsiveness to noxious stimuli at the level of the spinal cord (dorsal horn neurons), and therefore contributes to the development of central sensitisation. Specific to arthritis pain, it has been demonstrated in the MIA model using retrograde tracing techniques, that there is greater expression of both CGRP and TRPV1 in sensory afferents that innervate the knee joint compared to the general DRG sensory neuron population (192). With the recent development of small molecule CGRP receptor antagonists and antibodies to treat migraine headache, and evidence of their potential for treating inflammation driven pain (640) as well as arthritis pain (641), a better understanding of the role CGRP plays in development of chronic OA pain is needed

in order to take advantage of these emerging novel therapeutics that may prove to be effective at treating some types of chronic OA pain.

Interestingly, the study reported in this chapter identified that in the early phase of OA CGRP gene expression was down regulated in AIA mice, while in the late phase of OA CGRP gene expression was up regulated in DMM mice. Previous knee OA animal model studies have demonstrated an increase in CGRP gene expression in the sensory neurons innervating the knee joint (192, 642). Both these studies used the MIA model of arthritis, which results in severe joint inflammation and chondrocyte death. Changes in CGRP gene expression following surgically induced OA have been reported in one study that compared MIA induced arthritis with two post-injury OA models, DMM and Anterior cruciate ligament transection (ACLT) (426). In all three models the sensory neuronal response to the induced knee joint pathology was a down regulation of both CGRP and Tac-1 gene expression at the level of the lumbar DRG. For MIA lumbar DRG gene expression was measured 5 weeks after intra articular injection of 2mg MIA. PG loss was the only histological joint pathology change that was measured. For DMM and ACLT DRG gene expression at a single time point was measured, but investigators did not report what this time point was or what joint pathology was observed at this time point. Therefore it is difficult to compare it with the findings reported in this chapter, where at week 16 (late phase OA) CGRP was up regulated and Substance P was down regulated in the DMM model. The effects of CGRP receptor blockade have also been investigated in a surgically induced OA model (medial meniscal transection). In this study, blockade of the CGRP receptor resulted in reversal of OA induced pain as measured by changes in hind limb weight distribution (469).

ATF3 regulates transcription by binding to DNA sites as a homodimer to inhibit transcription (643), or heterodimer to activate transcription (644). ATF3 is induced by different stress signals from a range of tissues including the liver, heart and kidneys (645). ATF3 is induced following transection of sensory and motor neurons (362) and is considered a marker of peripheral neuronal injury. ATF3 expression in the DRG has also been reported in inflammatory pain models following injection of CFA (646). In contrast to previous studies that reported no expression of ATF3 in naïve adult rodents (362, 647), the study reported in this chapter demonstrates ATF3 gene expression in both naïve and sham/saline mice (Appendix D). In peripheral neuronal tissue (DRG) ATF3 promotes nerve regeneration in injured neurons (648).

ATF3 expression in animal models of arthritis has been investigated in an effort to identify common nociceptive pathways between OA pain and neuropathic pain following nerve injury. In a study using the rat AIA model investigators were unable to demonstrate any ATF3-positive neurons in the lumbar DRG using IHC techniques at day 1,3 and 21 following induction of arthritis (452). Similarly, in a study using the DMM model investigators reported no ATF3-positive neurons in the L4/L5 lumbar DRG at any time point (316). However, a study using a collagen-induced arthritis model did report ATF3 expression following induction of arthritis (649).

This chapter reports on gene expression in the innervating DRG of DMM and AIA induced arthritis at key stages of disease progression. Up regulation of ATF3 occurred in AIA mice early following knee joint injection (week 2) and during the early OA phase of disease (week 8). In DMM mice there was no significant change in ATF3 expression detected early but ATF3 was increased in late-stage disease. It is difficult to compare these findings with previous studies because gene expression does not always translate to protein expression, and up regulation of gene expression can be

transient, only occurring at specific time points. Therefore, comparisons between studies can only be made if the time points investigated are equivalent with respect to stage of disease. Nevertheless, the current findings suggest that model specific acute inflammation (AIA) and chronic post-traumatic OA knee joint pathology (DMM) either cause peripheral neuronal injury or mimic the biomolecular alterations that signal the need for neuronal transcription regulation, whether it be inhibition or activation.

The peripheral effects of opioids have previously been investigated in an attempt to identify a safer alternative to the systemic use of opioids, such as morphine, to treat severe pain (307). Freund's complete adjuvant induced inflammation results in up regulation of Oprm1 and an increase in Oprm1 G-protein coupling in the DRG but not the spinal cord or hypothalamus suggesting a local adaptive change in the mu receptor in response to acute inflammation rather than a response to systemically released mediators (317). Local injection of MOR agonists in rat models of inflammatory and neuropathic pain result in a reduced pain response and the resolution of allodynia (314). The role of MOR in regulating pain in animal models of OA has also been investigated (316). In this study up regulation of the MOR occurred at week 8 post surgery when affected mice displayed no pain (as measured by forceplate) until treated with a peripherally active MOR antagonist (naloxone methiodide). No change in MOR expression was detected early at 4 weeks or late at 16 weeks after surgery. This differs to the findings in the current study where in the chronic phase of OA a down regulation in Oprm1 gene expression was detected at week 12 and an increase in Oprm1-IR was observed in the L3/L4 DRG at week 16.

ADAMTS-5 is expressed in chondrocytes and fibroblasts, and is the principle aggrecanase in mouse cartilage and plays a key role in cartilage degradation and the

development of OA joint pathology (26, 27). A wider physiological role for ADAMTS-5 has been suggested with the establishment of its constitutive expression in a number of adult tissues including DRG (34). ADAMTS-5 KO mice are protected from development of OA joint pathology (articular cartilage damage, SCB sclerosis and osteophyte formation)(26). Interestingly, ADAMTS-5 KO mice have also been shown to not develop mechanical allodynia when subjected to DMM surgery (441). The investigators did not look at what changes in sensory innervation might be driving this protection from sensitisation. So it remains unclear whether the different pain phenotype observed in the ADAMTS-5 KO is primarily due to the protection from joint pathology or whether ADAMTS-5 plays a direct role in sensory modulation at the level of the DRG. Expression of ADAMTS-5 and other MMP's in the DRG following induction of arthritis has not previously been reported. In the present study, up regulation of ADAMTS-5 expression in the DRG occurred early (week 2) following DMM surgery but was not present at week 4 or beyond, once OA specific joint pathology and mechanical allodynia were well established.

ADAMTS-4 is the other principle aggrecanase expressed in human and mouse cartilage, however its role in development of OA joint pathology is less clear. Unlike ADAMTS-5, ADAMTS-4 is inducible by pro-inflammatory cytokines (650) and although ADAMTS-4 is expressed in many tissues, its role in these tissues is still under investigation. Characterisation of the ADAMTS-4 KO mouse identified no gross or histological abnormalities in any tissues and no difference in susceptibility to the development or severity of OA between KO and wild type mice at 4 and 8 weeks after DMM surgery (25). ADAMTS-4 is the most expressed ADAMTS in the central nervous system (CNS) (ventral horn and cortex) and is thought to play a role in controlling synaptic plasticity during CNS development (478). Whilst it is associated

with neuronal repair after spinal cord injury, investigators have also demonstrated a neurodegenerative effect on motor neurons in a model of neurodegenerative disease (651). Despite its important role in the CNS, there are no previous reports of its expression in the DRG or the role it may play in the peripheral sensory nervous system and the development of OA pain. In this study, down regulation of ADAMTS-4 expression in the DRG was observed during the early progressive OA phase in both models (AIA > DMM). Importantly, in the DMM model ADAMTS-4 showed the greatest loss of association with DRG genes involved in pain signalling (CGRP, Tac-1, Oprm1, TRPV1, TRPV2, TRPV4, TRPA1). This loss of co-regulation of ADAMTS-4 gene expression may implicate this aggrecanase in having an important role in OA pain modulation, in particular in a post-injury OA phenotype.

6.4.1 Summary

In this chapter, the pain phenotype of the two arthritis models under investigation was further characterised by measuring gene expression in the DRG that innervate the knee joint. Some of the key protein and neuropeptide candidates that are associated with both inflammatory and chronic pain states were measured, and the alterations in expression at different phases of arthritis disease that were identified, indicate which of these may play a role in pain signal modulation in each model.

Together, the findings in this chapter demonstrate two distinct peripheral sensory neuronal responses to OA joint pathology that change over time and are animal model specific. The different DRG gene expression profiles that were observed confirm that despite the similarities in histopathology and pain related behaviour that develops in both AIA and DMM in the chronic phase of OA disease, the molecular mechanisms that initiate and sustain the pain state are different.

This confirms that pain is different for different sub types (phenotypes) of OA and at different stages of the disease. By investigating an important aspect of sensory modulation in two models, it has allowed the differentiation of mechanisms that are model specific and therefore relevant for certain sub-types of OA. By focussing the investigation at the level of the DRG, peripheral mediators that may be a suitable therapeutic target for OA pain have been identified to allow for a more targeted approach to developing treatments that are devoid of systemic side effects.

In the next chapter the relationships between the changes in sensory neurons, as measured by gene expression, the observed pain-related behaviour and the joint histopathology that develops over time, are investigated. Combining the findings on OA pain and OA joint pathology will provide a better understanding of what initiates and drives chronic OA pain, and may reveal associations between the two processes that will guide selection of therapeutic targets that modify joint disease and treat pain.

CHAPTER 7: Associations between knee joint histopathology, pain behavior and peripheral sensory innervation following destabilization of the medial meniscus (DMM) and antigen-induced arthritis (AIA) in mice

7.1 Introduction and aims

The previous chapters of this thesis reported individually on the joint histopathology, pain-related behaviour outcomes and gene expression profiles of the innervating DRG in two animal models commonly used to study OA joint pathology (DMM) and arthritis pain (AIA) mechanisms. The two models under investigation both result in a consistent and reproducible chronic joint disease phenotype and ultimately lead to OA-like joint pathology. However, they differ in a number of ways. The DMM model induces altered joint biomechanics that leads to joint instability and greater loading strain on the medial femoro-tibial cartilage and underlying subchondral bone (SCB) (437). This model mimics a post-traumatic OA phenotype but has broader clinical relevance since meniscal tear and degeneration is also associated with non-traumatic age associated OA in patients (298). The AIA model on the other hand relies on an exogenously triggered joint immune response that leads to severe joint inflammation and other joint tissue pathologies. Although less directly-clinically relevant than DMM, this model has been used extensively to investigate the role of inflammation in the development of joint pain, and enabled investigators to begin to unravel the molecular mechanisms that drive arthritis pain (reviewed in (449, 612).

Histological investigation (Chapter 4) revealed that by 16 weeks both DMM and AIA mice display the hallmark histopathological features of human OA (AC erosion, SCB sclerosis, marginal osteophytes, mild synovitis), and by definition both DMM and AIA mice had therefore developed "knee joint OA". However, significant temporal differences in joint tissue pathology progression, model specific pathology associations between the major tissue structures in the joint (AC, SCB and synovium), and different significant risk factors for development/progression of OA (as defined by AC damage), indicate that at the latest time points each model represents a different OA phenotype; "post-traumatic OA" (Pt-OA) for DMM vs. "post-inflammatory OA" (Pi-OA) for AIA.

When tested for pain (Chapter 5), the DMM and AIA models demonstrated distinct temporal patterns of pain-related behaviours, reflecting the development of a complex pain state that is partly driven by central sensitisation and that displays many of the hallmarks of human OA pain. In contrast to the joint pathology outcomes, there was an absence of any association between the different pain behaviours that were measured in either model. This highlighted the importance of using multiple pain assays to more accurately define the pain phenotype in a particular animal model, and by extrapolation, evaluate the response to any given therapy in a model. The absence of any associations between the different pain behaviours likely indicates differences in the underlying mechanisms that drive pain at different stages of joint disease development, and reflects the complex nature of the relationship between tissue specific joint pathology and OA pain.

Following from this, an investigation into the gene expression changes in the DRG (Chapter 6) identified multiple alterations in gene expression that were again model-

specific. The gene expression profiles were also different at each phase of disease development (acute inflammatory, early progressive OA, late chronic OA), with the greatest differences paradoxically observed in the late chronic phase when histologically both models displayed most similarity with all the features of OA joint pathology. The genes investigated were highly associated in both control groups (sham and saline injected mice), reflecting the normal co-ordinated network of sensory input regulation in the DRG. For three of the genes (CGRP, IL-1β and ADAMTS-4), this association was lost in one or both models with different cohorts of other genes, and the disease-specific dysregulation suggests there are different pain regulatory pathways in the two arthritis phenotypes.

Overall, these findings support the theory that OA pain, and at least the peripheral mechanisms that drive it, are unique for each sub-type of OA. This puts into question the current practice of extrapolating findings from pre-clinical investigations to human OA pain, without first considering which human OA phenotype the animal model represents, and in the case of the most commonly used model for pain research, MIA, perhaps any human OA phenotype at all (399). The experimental data generated in this thesis have demonstrated in separate analyses that joint tissue pathology, pain-behaviour, and peripheral sensory modulation are each animal model specific. However, if the associations between these three disease components are the same in different models then, which model is selected to investigate what initiates and drives OA pain may ultimately not be critical to the predictive validity for human translation. To determine if the animal model does matter, any significant associations between OA disease (joint tissue histopathology), OA symptoms (pain behaviour) and sensory innervation (DRG gene expression) need to be characterised in different animal models.

In this chapter the relationships between joint pathology, pain behaviour and peripheral sensory modulation are investigated using statistical modelling to confirm whether the mechanisms that drive OA pain are specific to the pathophysiology of the disease and therefore, unique to each OA phenotype.

The aims of chapter 7 are:

1. To identify any associations between knee joint tissue pathology and gene expression in the innervating DRG of mice with knee joint arthritis induced by DMM and AIA.

2. To identify any associations between pain-related behaviour and gene expression in the innervating DRG of mice with knee joint arthritis induced by DMM and AIA.

3. To identify any associations between knee joint tissue pathology and pain-related behaviour in mice with knee joint arthritis induced by DMM and AIA.

7.2 Methods, statistical analysis and data presentation

Details of the methods used to induce the two models of arthritis, DMM and AIA, are described in chapter 2, section 2.1. The methods used for histological processing, sectioning and staining are described in chapter 2, section 2.2. The scoring system used is outlined in Appendix C. Development and validation of this scoring system is described in chapter 3, section 3.2. The pain assays used in this chapter have previously been reported and validated (316, 465, 493, 517, 545), and the exact methods used for carrying out the pain tests were developed by the researcher (chapter 3, section 3.1) and described in chapter 2, section 2.3. The methods used for

harvesting DRG and real time Reverse Transcription-Polymerase Chain Reaction (RT-PCR) are described in chapter 2, section 2.4.

Associations between the different joint tissue pathologies and gene expression in the right L3/L4 DRG; the different pain behaviours and gene expression in the right L3/L4 DRG; and the different joint tissue pathologies and pain behaviours, were determined for each model (when corrected for time) by generating Pearson partial correlation coefficients, using Kendall's tau-b (565). This nonparametric process uses pairwise ranked data values between the two variables under study (ordinal scores) and thus does not require data to be normally distributed or the relationship between the variables to be linear.

The experiments in this thesis investigating pain behavior (Chapter 5) and gene expression (Chapter 6) were designed to be hypothesis generating due to the lack of standardisation of pain behavior tests that currently exists and the fact that so little is known about which genes are key drivers of OA pain specifically. To this end, the results in this chapter are also presented without correcting for repeated measures to ensure identification of all significant associations between joint tissue histopathology, pain behavior and DRG gene expression, that may otherwise be overlooked once correction for repeated measures has been applied, but which may still be worthy of further investigation.

Correlation analysis was conducted for AIA and DMM only, and not for the equivalent sham/saline data. This was done because the aim of this study was to characterise the relationship between joint tissue pathology, pain behavior and DRG gene expression changes in two models of arthritis where significant joint disease develops. The results in chapter 4 confirm that only mild and transient joint pathology

is observed in the sham surgery and saline injected mice and neither group develops knee joint arthritis.

7.3 Results

7.3.1 Correlation between joint tissues histopathology and gene expression in right L3/L4 DRG in DMM and AIA when corrected for time

An interesting pattern of associations emerged from the data (Table 7.1), with more correlation between joint tissue histopathology and DRG gene-expression observed in the DMM model compared to the AIA model (14 vs. 11). In DMM the DRG-expression correlations were primarily with bone pathology changes (SCB sclerosis, SCB vascular invasion, osteophyte size and osteophyte maturity). In AIA in contrast, the correlations were with inflammatory change and osteophyte formation (synovitis, osteophyte size and osteophyte maturity). The majority but not all associations in both models were negative – i.e. as pathology worsened the DRG gene expression decreased. The positive correlations suggestive of a positive association between joint pathology and DRG gene-expression were: IL-1β with synovitis and AC damage in AIA, and CGRP, TRPV1 and CBR1 with SCB sclerosis in DMM.

The genes whose expression was significantly dysregulated in the association analysis in Chapter 6 (CGRP, IL-1β and ADAMTS-4) also displayed unique associations with joint tissue pathology: CGRP & IL-1β as noted above, and ADAMTS-4 which was negatively correlated with osteophyte size and maturity in DMM. There were a number of pathology:DRG-expression correlations that were shared in the two models: TRPA1 and CBR1 negatively with synovitis; and ATF3 and MOR negatively

with osteophyte size. IL-1β was unique in having a significant positive correlation with synovitis in one model (AIA) but negative in the other (DMM). All other pathology:DRG-expression correlations were specific to one or other of the models. The strongest correlations (>0.4) were with CBR1, which was negatively associated with synovitis in both AIA and DMM (r = -0.596 and -0.517, respectively), and with SCB vascular invasion in DMM (r = -0.413).

Table 7.1. Histopathology and gene expression correlations

Comparison		Treatment	r (tau)	*P*
AC damage	IL-1b	AIA (n=35)	0.201	0.044
AC PG loss	ATF3	DMM (n=46)	-0.281	0.008
	TRPA1	AIA (n=36)	-0.265	0.014
Synovitis	Tac-1	AIA (n=36)	-0.365	0.001
	CNR1	AIA (n=6)	-0.596	0.040
	CNR1	DMM (n=11)	-0.517	0.002
	IL-1b	AIA (n=35)	0.208	0.004
	IL-1b	DMM (n=39)	-0.257	0.010
	TRPA1	AIA (n=36)	-0.324	0.003
	TRPA1	DMM (n=46)	-0.175	0.039
SCB invasion	CNR1	DMM (n=11)	-0.413	<0.001
SCB sclerosis	CGRP	DMM (n=46)	0.249	0.019
	TRPV1	DMM (n=46)	0.233	0.037
	CNR1	DMM (n=11)	0.380	0.033
OP size	ATF3	AIA (n=36)	-0.228	0.021
	ATF3	DMM (n=46)	-0.204	0.050
	Oprm1	AIA (n=36)	-0.303	0.008
	Oprm1	DMM (n=46)	-0.213	0.043
	TRPV4	DMM (n=35)	-0.245	0.044
	ADAMTS-4	DMM (n=34)	-0.275	0.006
	ADAMTS-5	AIA (n=30)	-0.165	0.038
OP maturity	Oprm1	AIA (n=36)	-0.292	0.003
	TRPV1	DMM (n=46)	-0.147	0.023
	ADAMTS-4	DMM (n=34)	-0.240	0.041
	ADAMTS-5	AIA (n=30)	-0.157	0.036

Spearman partial correlations on joint tissue histopathology outcomes and gene expression in right L3/L4 DRG (corrected for time) within treatment. Alpha value set at 0.05. Only significant correlations ($P < 0.05$) are listed.

7.3.2 Correlation between pain behaviour and gene expression in right L3/L4 DRG in DMM and AIA when corrected for time

Even more so than with joint histopathology, there were a great number of significant associations between pain behavior and DRG gene expression in the DMM model compared to the AIA model (7 vs. 2; Table 7.2). In contrast with histopathology, for all behavioural outcomes, a negative correlation indicates an association with worsening pain/disability. This is because pain (including sensitisation) was defined as a decrease in the relevant pain behaviour measurement (PWT, PWL, stride length, R/L hind limb weight distribution).

Only one of the significant DRG-expression:pain-behaviour correlations was negative (TRPV1 and PAM in AIA); suggesting that for the remaining genes, an increase in gene expression was associated with decreasing pain and vice versa. In DMM, stride length was positively correlated with 6 genes (CGRP, Tac-1, TRPV1, TRPV2, TRPV4, ADAMTS-5), and hotplate was positively correlated with 1 gene (ADAMTS-4). In AIA, PAM was positively correlated with IL-1β. There were no significant associations between tactile allodynia (Von Frey) or hind-limb weight distribution (forceplate), and expression of any genes in the DRG in either model.

Table 7.2. Pain behavior and gene expression correlations

Comparison		Treatment	r (tau)	*P*
Stride[1]	CGRP	DMM (n=11)	0.406	0.033
	Tac-1	DMM (n=11)	0.451	0.007
	TRPV1	DMM (n=11)	0.406	0.025
	TRPV2	DMM (n=11)	0.445	0.016
	TRPV4	DMM (n=11)	0.570	<0.001
	ADAMTS-5	DMM (n=11)	0.474	0.034
PAM[2]	IL-1β	AIA (n=5)	0.527	0.015
	TRPV1	AIA (n=5)	-0.788	<0.001
Hotplate[3]	ADAMTS-4	DMM (n=18)	0.267	0.035

Spearman partial correlations on pain outcomes and gene expression in right L3/L4 DRG (corrected for time) within treatment. Alpha value set at 0.05. Only significant correlations ($P < 0.05$) are listed. (1) Stride = full stride length (left to left hind limb) measurement; (2) PAM = right hind limb withdrawal threshold (average of medial and lateral knee joint); and (3) Hotplate = hind limb withdrawal latency with plate set at 52 degrees.

7.3.3 Correlation between joint tissue histopathology and pain behaviour in DMM and AIA when corrected for time

Overall, there were fewer associations between joint tissue histopathology and pain behavior in the DMM model (4) than in the AIA model (7). As above, negative correlation with any behavioral outcome indicates a positive association between that pain measure and histopathologic change. Interestingly, the AIA correlations were predominately (5 of the 7) in a negative direction whereas in DMM the associations were all positive, suggesting a lack of association between pain and worse pathology in this model.

In AIA, synovitis was negatively correlated with PAM and stride length; SCB invasion was negatively correlated with forceplate; AC damage and chondrocyte hypertrophy were negatively correlated with PAM; AC damage was positively correlated with hotplate; and OP maturity was positively correlated with forceplate. In DMM, synovitis was positively correlated with forceplate and stride length; SCB invasion was also positively correlated with forceplate; and AC damage was positively correlated with von Frey.

Table 7.3. Histopathology and pain behaviour correlations

Comparison		Treatment	r (tau)	*P*
Synovitis	Forceplate[1]	DMM (n=23)	0.273	<0.001
	PAM[2]	AIA (n=18)	-0.415	0.014
	Stride[3]	AIA (n=12)	-0.464	0.001
	Stride	DMM (n=11)	0.415	0.003
SCB invasion	Forceplate	AIA (n=38)	-0.263	0.002
	Forceplate	DMM (n=23)	0.335	0.024
AC damage	Von Frey[4]	DMM (n=9)	0.549	0.041
	PAM	AIA (n=18)	-0.349	0.001
	Hotplate[5]	AIA (n=38)	0.172	0.054
Chondrocyte hypertrophy/apoptosis	PAM	AIA (n=18)	-0.398	0.006
OP maturity	Forceplate	AIA (n=38)	0.220	0.050

Spearman partial correlations on joint tissue histopathology outcomes and pain outcomes (corrected for time) within treatment. Alpha value set at 0.05. Only significant correlations ($P < 0.05$) are listed. (1) Forceplate = right to left hind limb weight bearing ratio (average over 30 seconds); (2) PAM = right hind limb withdrawal threshold (average of medial and lateral knee joint); (3) Stride = full stride length (left to left hind limb) measurement; (4) Von Frey = right hind limb 50% withdrawal threshold; and (5) Hotplate = hind limb withdrawal latency with plate set at 52 degrees.

7.4 Discussion

The “cause-effect” relevance of the correlations between knee joint histopathology and DRG gene expression is unclear, but along with the joint tissue pathology associations reported in chapter 4 (figure 4.11), they further demonstrate differences between the two models with respect to joint disease pathophysiology and how these relate to pain mechanisms. Acutely, AIA is a model of inflammatory arthritis and since synovitis is a predominant feature of joint inflammation in this model (448), it would be expected to be a key driver of pain. Only 4 of the 11 significant gene associations in AIA were with synovitis *per se*, 5 being with osteophyte formation suggesting that osteophytes may also play an important role in driving pain in this model. Osteophytes in AIA were late to form and mature to bone compared to the DMM model, and occurred after joint inflammation started to decrease, suggesting a need for resolution of specific pro-inflammatory signals in AIA before bone formation can occur as previously reported for DKK-1 in TNF-transgenic mice (578). Early formation of enthesophytes observed in AIA could be driven by the initiation or inhibition of these same pro-inflammatory signals early in the disease. If this is the case, then the DRG gene correlations with osteophyte formation may in fact reflect an indirect mechanism by which inflammation drives pain in this model.

The joint histopathology and DRG gene expression associations observed in AIA were primarily negative indicating a down regulation in expression of the associated genes with increasing joint tissue pathology. This is not surprising given the pattern of DRG gene expression reported in chapter 4 where the changes in gene expression observed in AIA beyond the acute inflammatory phase of disease were down regulations in expression.

The exception to this is IL-1β, which was positively correlated with synovitis and AC damage. The role of pro-inflammatory cytokines such as IL-1β and TNF-α in mediating AC destruction and synovial inflammation, as well as the development of joint pain and sensitisation has been investigated using the AIA model. Use of neutralising antibodies to block IL-1β and TNF-α activity in the joint previously demonstrated their role in the early establishment of destructive joint pathology in AIA (652), and has led to further investigation of their role in pain modulation more specifically. Joint inflammation and associated mechanical hyperalgesia in the first 7 hours following induction of AIA is attenuated in IL-1 receptor type I (IL-1RI) KO mice, and IL-17 induced mechanical hyperalgesia in WT mice is inhibited by pretreatment with an IL-1RI antagonist in the first 3 days following induction of AIA (653). Furthermore, development of mechanical hyperalgesia following induction of AIA occurs in conjunction with increased production of IL-1β and neutrophil infiltration into the joint, and intra-articular administration of an IL-1β antagonist 30 minutes prior to induction of AIA, attenuates both inflammation and pain (654). However, during the later stages of arthritis disease, the role of IL-1β may be different. Investigators have demonstrated that mechanical hyperalgesia persists following the administration of an IL-1RI antagonist from day 0 to day 21 after induction of AIA, while thermal hyperalgesia is attenuated from day 7 (453). This demonstrates IL-1β's role in development of thermal hyperalgesia but puts into question the role of IL-1β in driving mechanosensitivity of joint nociceptors.

The data presented in this thesis supports these previously reported findings on the role of IL-1β in development of joint inflammation (synovitis) and pain, although which type of pain, remains unclear. However, these previous studies only tracked the

acute phase of the disease and did not establish what role IL-1β plays once significant bone and cartilage pathology is established. The positive association between IL-1β and both synovitis and AC damage suggests a significant role for IL-1β in the establishment of joint OA pathology beyond the early acute phase of disease as reported in previous studies. This is further supported by the fact that synovitis was identified as a risk factor for development of AC damage in AIA (Chapter 4).

Unlike AIA, in the DMM model IL-1β was negatively correlated with synovitis. This suggests that in the DMM model synovitis contributes to OA pain via other pro-inflammatory signaling pathways in the DRG. There is little doubt that IL-1β is a key cytokine in OA pathogenesis (reviewed in (88)); acting to block chondrocyte synthesis of extra cellular matrix components, stimulate production of ADAMTS-4 (655), and promoting chondrocyte apoptosis (656). Yet few studies have looked at whether the role of inflammation and the expression of IL-1β and other inflammatory cytokines, changes with disease severity (reviewed in (77)). Evaluation of synovial tissue from OA patients undergoing arthroscopy or arthroplasty identified greater expression of IL-1β and TNF-α in the synovium of the patients with less severe OA disease (657, 658). Here we demonstrate a similar association with respect to expression of IL-1β in the DRG and OA disease severity/progression.

In DMM, there is a co-dependent relationship between articular cartilage and subchondral bone pathology (49, 407, 583), and data from patients would suggest that subchondral bone is a key driver of OA pain (292, 294). The joint histopathology and DRG gene expression associations observed in DMM (10 of the 14 are with SCB and osteophyte formation) supports a similar association in this mouse model. Furthermore the only positive pathology:DRG-gene-expression correlations in DMM

were all with SCB sclerosis suggesting this may be a major driver of pain in this model.

Logistic regression modeling (chapter 4) identified synovitis as an independent risk factor for pathology progression (as defined by progressive AC damage) in AIA but not DMM, while SCB sclerosis as an independent risk factor for OA progression in DMM but not in AIA. The above results confirm these same model-specific tissue pathology associations, but now with potential molecular drivers of pain/sensitisation as well as progression of cartilage erosion. This further differentiates the uniqueness of each OA phenotype, and highlights the need for additional exploration of the mechanisms underlying these associations to understand any causal effects and how specific joint pathologies might drive DRG-expression changes and pain in each model.

In the case of pain behavior and DRG gene expression correlations, the cause-effect relationship would seem clearer, particularly with differentially regulated neuropeptides, nociceptor cation channels and inflammatory cytokines, where changes might directly alter neuronal excitability. The significance of stride length as a marker of the changes that are occurring in the sensory neurons to initiate and drive DMM-induced OA pain, provides evidence that the changes in stride length are not simply due to the biomechanical changes that occur when a joint is surgically destabilized, but rather they are a reflection of a gait adjustment that is driven by pain. In particular, since the genes that were associated with this pain-related behavior include neuropeptides (CGRP and SP), and nociceptor channels implicated in inflammation driven sensitisation (TRPV1 and TRPV2) and the development of mechanical hyperalgesia (TRPV1 and TRPV4). Stride length demonstrated a

treatment effect only in DMM mice, when corrected for time (Chapter 5), again suggesting that stride length is a relevant behavior marker for studying pain mechanisms in the DMM model. Interestingly though, all of the correlations between DRG-gene-expression and stride length were positive, suggesting the decrease in stride length that was observed is paradoxically not associated with an increase in expression of these genes.

However, this does not exclude CGRP, Tac-1or the TRP channels from playing a significant role in the development of chronic OA pain via mechanisms other than an upregulation in gene transcription. For example, the TRPV1 channel is an important mediator of inflammatory pain (182), yet many studies have not been able to demonstrate an increase in DRG TRPV1 mRNA following induction of inflammation (181, 194). However, an increase in the number of DRG neurons expressing TRPV1 immunoreactivity has been demonstrated in numerous models of inflammation and nerve injury pain (184, 194), including the MIA model of OA (192). In vitro culture studies have been able to demonstrate an increase in both expression and signalling of TRPV1 in DRG neurons (340). Synovium from patients with OA also demonstrates increased TRPV1 immunoreactivity (190). Sensitisation of TRPV1 following the release of inflammatory mediators is reported in both inflammatory and nerve injury models (609) and results in increased nociceptor signalling. Combined, these findings highlight the need to investigate multiple mechanisms of enhanced activity when determining the key molecular pathways involved in development of OA pain and sensitisation.

Further investigation to enable accurate assessment of therapeutic interventions using the DMM model is also required into other gait characteristics and methods for measuring them, in order to develop pain assays that are clinically relevant, easier to measure and more sensitive than stride length alone. One alternative has been to view movement provoked pain, which stride length is an indirect measure of, more broadly and look at measures of other spontaneous activities using purpose built automated instrumentation such as the LABORAS (Metris: Laboratory animal behavior observation, registration and analysis system). Activity based monitoring as a measure of both movement provoked pain and spontaneous pain has previously been reported in the DMM model (316, 339, 441). However, automated instruments such as the LABORAS produce numerous movement-based activity and behavior measurements, therefore a more detailed evaluation of the most sensitive of these measures for detecting changes with disease progression and predicting therapeutic efficacy needs to be conducted in the DMM model.

The positive correlation between ADAMTS-5 expression in the DRG and stride length is interesting, given that ADAMTS-5 is the principle aggrecanase in mouse cartilage (26, 27) and ADAMTS-5 KO mice are not only protected from cartilage degradation and associated SCB sclerosis but also development of allodynia in the DMM model (441, 659). Administration of anti-ADAMTS-5 antibodies ameliorates allodynia in established OA induced by DMM in wild type mice, suggesting that analgesic effects may occur through blocking ADAMTS-5 activity in the DRG and reducing macrophage activation and gliosis (660, 661). It is therefore difficult to reconcile how decreased ADAMTS-5 expression (and presumably activity) in the DRG is associated with reduced stride length (increased pain) in DMM in the current study. In contrast to ADAMTS-5, there was a negative correlation (i.e. positive

association) between DRG-expression of ADAMTS-4 and osteophyte formation (table 7.1). Dysregulation of ADAMTS-4 gene expression in the DRG was unique to the DMM model (Chapter 6). While ADAMTS-4 can cleave aggrecan and play a role in cartilage degradation (662) is still has an undefined role in OA development (25), and there has been no study of its substrates or role in the DRG. Together these findings suggest that both ADAMTS-4 and ADAMTS-5 may play significant but different roles in OA pain mechanisms in a post-traumatic OA phenotype, although the mechanisms remain to be established.

The negative correlation between TRPV1 and PAM in AIA is not surprising, as this indicates an association with local mechanical hyperalgesia and TRPV1 is known to play a significant role in the development of inflammation driven mechanical sensitisation (187). More unexpected was the positive correlation between PAM and IL-1β observed in this model, which means that increased DRG expression of IL-1β is associated with a decrease rather than an increase in sensitisation and local hyperalgesia (ie an increase in the paw withdrawal threshold when a mechanical force is applied to the knee joint). Why this association is positive is not clear, given that IL-1β is an important pro-inflammatory cytokine involved in both the pathogenesis of OA (reviewed in (88, 322)) and the development of pain and sensitisation (reviewed in (89, 663). However, this finding is an important reminder that there are still many unknown complexities in the relationship between inflammation, pain and pathology that still require further investigation. This is evident if we look at the role of IL-1β in OA pathogenesis. Here, it has been shown to promote cartilage degradation (328), yet development of OA has been reported to be accelerated in the IL-1β KO mouse (327), and there is now some evidence that IL-1β can paradoxically play a protective role in articular cartilage homeostasis (664).

The associations between pain behaviour and joint tissue histopathology in the current study also demonstrated interesting trends. The correlations observed in the AIA model were primarily negative, while in DMM they were positive. This suggests a greater association between specific joint pathologies and pain in AIA, with measures of increased joint inflammation (synovitis and SCB vascular invasion) associated with more joint mechanical hyperalgesia, reduced stride length and decreased hind limb weight bearing. PAM, stride length and forceplate may therefore be particularly useful markers for monitoring the degree of joint inflammation in this model. It also confirms that reducing joint inflammation may reduce localised knee joint pain that can impact mobility.

There were fewer associations in the DMM model, and in contrast to what might be expected measures of increased joint inflammation (synovitis and SCB vascular invasion) correlated with increased rather than decreased stride length and ipsilateral hind limb weight bearing. A positive correlation with force plate perhaps reflects the low levels of inflammation that persist throughout the time course of this model and the lack of significant change in weight distribution (right to left hind limb ratio) beyond the significant decrease that occurs at day 3 and week 1 (chapter 5). The correlation between von Frey and AC damage was also positive, but more likely reflects the small data set (n=9) that included only 2 time points (week 4 and week 8), rather than any true reflection of the relationship between AC damage and development of allodynia. These incongruent findings in the DMM model highlight the need for further histological evaluation of knee joints from the same mice in which pain behavior measurements have also been collected. Some researchers have reported development of allodynia in the DMM model that demonstrates a similar temporal pattern to the one observed in this thesis (339, 441), however the

relationship between the observed allodynia and the knee joint pathology in any given animal has not previously been investigated to enable comparisons with the findings from this thesis. Interestingly, others investigators have reported a very different temporal pattern of allodynia in the DMM model (604).

7.4.1 Summary

In summary, the correlation analyses reported in this chapter have identified model-specific associations that further define the complex relationship between joint pathology, pain and gene transcriptional changes in the DRG (an important aspect of peripheral sensory modulation). Not only are joint tissue pathology, pain behaviour and peripheral sensory modulation animal model specific; the associations between these three disease components are also unique to the animal model under investigation. This confirms the importance of mapping pre-clinical findings to the human disease phenotype that best fits the animal model. It would appear that the selection of animal model and pain assay investigators use to study OA pain mechanisms and test therapeutic targets, does matter.

CHAPTER 8: Conclusions and future directions

The research in this thesis investigated the mechanisms that drive osteoarthritis (OA) pain, and whether these change over time, and differ between different OA phenotypes. This was done by characterising the changes that occur in OA joint histopathology, OA pain behaviour and dorsal root ganglia (DRG) gene transcription, over the different phases of OA disease development, using two distinct animal models (a post traumatic model of OA and an antigen-induced inflammatory model of arthritis). The relationship between OA joint tissue pathology and OA pain was explored further by determining if any associations existed between the various outcomes that were measured.

8.1 Summary

1. Each model demonstrated a distinct temporal pattern of joint tissue histopathological change, model-specific associations between the three major tissue structures in the joint (articular cartilage, synovium and subchondral bone), and a different set of risk factors for development of OA cartilage degradation.

a) Moderate synovial inflammation peaking at week 2 and low-grade inflammation persisting until week 16, was observed in DMM. Severe synovial inflammation peaking at week 2 and persisting until week 12 before declining to levels comparable to DMM (week 16) was observed in AIA.

b) Osteophyte formation was a feature of both models, however in DMM osteophytes formed early (week 2) and persisted, and in AIA they formed late (week 12).

c) Unique to the AIA model was the formation of enthesophytes. Their site of origin and early development suggest that inflammation is a key factor in driving their formation.

d) In DMM articular cartilage (AC) proteoglycan loss and AC damage appeared early (week 1 and 2) and developed gradually. In AIA AC proteoglycan loss was immediate (day 3) and complete, and AC damage was more delayed in developing (week 8).

e) The transition from subchondral bone (SCB) vascularisation to SCB sclerosis was different in the two models and reflected the differences in joint inflammation severity, with SCB vascularity persisting for longer (week 4) in AIA.

f) Despite these temporal differences, by 16 weeks both models displayed all the hallmark features of human OA; defined radiographically as joint space narrowing and the presence of osteophytes; and observed histologically as AC proteoglycan loss, AC erosion, SCB sclerosis and osteophyte maturity and ossification.

g) Risk factors for OA development/progression (defined as AC damage) in the DMM model are surgery/joint injury, AC PG loss, chondrocyte hypertrophy/cell death, osteophyte size and SCB sclerosis. Risk factors for OA development/progression (defined as AC damage) in the AIA model are time, synovitis, chondrocyte hypertrophy/cell death and osteophyte size.

These risk factors suggest that different tissue-specific mechanisms; largely determined by the initiating cause, drive the joint pathology changes that lead eventually to OA. Therefore, AIA and DMM are both models of OA based on joint pathology but represent different phenotypes of OA based on their pathophysiology.

2. Both AIA and DMM models displayed tactile allodynia, knee joint mechanical hyperalgesia, reduced weight bearing of the ipsilateral hind limb, thermal hyperalgesia and alterations in stride length, during different stages of disease development. However, the severity and temporal pattern in which these pain behaviours occurred were different in each model.

a) Ipsilateral tactile allodynia developed early in all treatment and sham/saline injected groups (by week 2), suggesting that tissue trauma and inflammation (caused by surgery, immunisation and knee joint injection) initiates sensitisation in both models. Persistence of tactile allodynia in DMM mice and resolution in the shams indicates that different mechanisms are involved in the initiation (surgical trauma and inflammation) and maintenance (OA disease pathology) of sensitisation. Persistence of tactile allodynia in all AIA mice (including immunised only) indicates that sensitisation in this model is largely driven by immunisation and highlights the confounding effect immunisation has on the alteration of pain pathways.

b) Pressure pain sensitivity (as measured by PAM) occurred in the early (week 6) and late phase (week 16) of OA in DMM mice, indicating that mechanical hyperalgesia is driven by local joint pathology changes in this model. In contrast, AIA mice displayed greater pressure pain sensitivity in the early phase of disease with a similar pattern of response also observed in immunised-only mice. This suggests that inflammation (both localised and systemic) drives the development of mechanical hyperalgesia in this model, and again highlights the confounding effect of using a model with both systemic and localised effects.

c) Reduced ipsilateral hind limb weight bearing was observed in DMM, sham and AIA mice only, indicating that this is a measure of locally driven pain mechanisms in both models.

d) Gait changes in DMM mice manifested as a decrease in left-to-right stride and full stride length from week 4 that persisted until week 16. AIA and saline injected mice demonstrated the same temporal pattern of change in stride length and this was different to DMM. At week 16 both were decreased compared to baseline. The changes in stride that occurred after week 4 are likely driven by joint tissue pathology that develops earlier in DMM compared to AIA (AC damage, osteophyte formation and SCB sclerosis), rather than by joint inflammation. However, the added effect of immunisation cannot be overlooked given the changes observed in saline mice.

Overall, each model demonstrated a unique temporal pattern of pain behaviour and despite both AIA and DMM displaying the same OA histopathological changes at week 16, the pain behaviour observed at this time point was different in each model. DMM was characterised by tactile allodynia, mechanical and thermal hyperalgesia, reduced weight bearing on the ipsilateral hindlimb and reduced full stride length. AIA was characterised by tactile allodynia, thermal hyperalgesia and increased full stride length. However, since tactile allodynia and reduced stride length were also observed in immunised-only mice, it is difficult to attribute these pain behaviours solely to the development of knee joint OA in the AIA model.

Importantly, there were no associations between any of the pain behaviours in either model. This highlights the complex nature of pain and the importance of not relying

on one single pain assay when evaluating the efficacy of potential therapeutics in pre-clinical studies, no matter which disease model is used.

Also implicit in the pain behaviour findings is the difficulty in interpreting pain outcomes and investigating pain mechanisms using the AIA model. Models that induce a systemic immune or inflammatory response such as AIA may not be suitable for studying pain mechanisms of arthritis phenotypes where initiation of the disease process is locally driven (e.g. post-traumatic OA) rather than systemically driven (e.g. rheumatoid arthritis), due to the confounding effect immunisation can potentially have on all the outcomes.

3. Changes in gene expression in the innervating DRG were observed during each phase of OA disease in both AIA and DMM, with the greatest differences occurring in the late chronic phase of OA. Despite the histological similarities between AIA and DMM during this phase of disease, the gene expression data suggests there are different mechanisms driving OA pain in the two models.

a) In the acute inflammatory phase of disease, DRG gene expression changes in DMM (relative to sham) occurred for IL-1β and ADAMTS-5, and in AIA (relative to saline) changes occurred for ATF3, IL-1β, TRPV2 and ADAMTS-5.

b) In the early progressive phase of OA, DRG gene expression changes in DMM (relative to sham) occurred for TRPA1, TRPV1 and CNR1, and in AIA (relative to saline) for ATF3, CGRP, TRPA1, Oprm1 and ADAMTS-4.

c) In the late chronic phase of OA, DRG gene expression changes in DMM (relative to sham) occurred for CGRP, Tac-1, TRPA1, TRPV1, TRPV2, TRPV4 and Oprm1, but only for TRPV1 in AIA.

d) Consistent gene expression associations were observed in sham and saline mice. Dysregulation of these associations was identified in both AIA and DMM for CGRP, IL-1β and ADAMTS-4, but with loss of association with different subsets of genes in the two models. This suggests model specific differential effects in the expression profile of these three genes and therefore, supports the existence of different pain regulatory pathways in the two models.

e) The observed temporal pattern of gene expression changes in each model could not be related directly to protein expression in the DRG using immunohistochemistry. For the two genes where antibody immunoreactivity above background was achieved there was no consistent association between gene expression and protein expression at different phases of disease.

4. Correlation analysis proved to be a useful tool for understanding the complex relationship between joint pathology, pain and gene transcriptional changes in the DRG, and defining the differences between different animal model phenotypes.

a) Associations between joint histopathology and DRG gene expression suggest that the synovium may be the primary tissue that drives pain in the AIA model and SCB may be the primary tissue that drives pain in the DMM model.

b) Associations between pain behaviour and DRG gene expression suggest that stride length, and perhaps gait characteristics more generally, is a suitable pain behaviour for investigating pain mechanisms in the DMM model.
c) Associations between joint histopathology and pain behaviour suggest that PAM, stride length and forceplate may be useful markers of joint inflammation.

So not only are joint tissue pathology, pain behaviour and peripheral sensory modulation animal model specific, but the associations between these three components of OA disease are also unique to the animal model under investigation. This confirms the importance of mapping pre-clinical findings to the human disease phenotype that best fits the animal model. Yet currently this does not occur for OA pain, where much of what we know is informed by studies conducted in animal models that don't correspond to a human OA phenotype.

The findings reported in this thesis support the hypothesis that the mechanisms that drive osteoarthritis pain are specific to the pathophysiology and stage of the disease, and differ between different OA phenotypes. Which model researchers use to study different aspects of OA pain is important to our overall understanding of its mechanisms and our ability to translate pre-clinical findings to effective therapeutics. The findings also suggest that OA joint disease and OA pain share common pathways and as such, the study of OA pain and pre-clinical investigation of therapeutics should be carried out in animal models that are phenotypically similar to specific human OA conditions of interest.

8.2 Study limitations

This research challenges how we currently use animal models to inform our understanding of OA pain and make decisions about the potential efficacy of novel therapeutic targets. However, there are a number of study limitations that need to be highlighted.

Model specific tissue pathology associations, pathology-pain associations, and pain-DRG gene expression associations were identified. But establishing causal relationships for these associations was beyond the scope of this thesis, and further investigation is required.

Interpretation of any pain behavior test is complicated by the fact that in most instances these tests involve exposure to two stressors, physical confinement or restraint, and a noxious stimulus (e.g. heat, mechanical, tactile, joint loading). Therefore, a behavioural response that is interpreted as pain may in fact be a stress driven escape response. Acclimatisation aims to familiarise mice to a particular restraint mechanism or procedure in order to minimise the stress response, however, it is unlikely to ever be completely eliminated.

A relationship between the observed changes in gene expression and changes in protein expression in the DRG was not demonstrated. An investigation into the numerous post-transcriptional mechanisms that control protein levels was not within the scope of this study, but would provide a clearer understanding of the significance of the unique pattern of gene dysregulation that was observed in the two arthritis models.

Although a number of key protein and neuropeptide candidates that are associated with both inflammatory and chronic pain states were measured, investigation of all genes implicated in pain signal modulation was also not within the scope of this

study. Investigating gene expression in the DRG was a starting point for characterising the sensory modulation that gives rise to sensitisation and the manifestation of chronic OA pain. Further investigation into pain mechanisms at the level of the spinal cord and brain are required in order to gain a more complete understanding of the mechanisms at play, and better inform gene selection for therapeutic targets in the future.

8.3 Questions arising

A number of key questions about the mechanisms of OA pain emerge from the findings of this research.

1. How suitable is the DMM model as a pre-clinical model for investigating pain mechanisms in a human post-traumatic OA phenotype?
2. What other genes play a role in peripheral (DRG) and central (spinal cord) sensory modulation in OA pain?
3. How important are changes in gene transcription relative to other processes that together account for sensory modulation in OA pain?
4. How does inflammation contribute to pain and sensitisation at different stages of OA disease in a post-traumatic OA phenotype?
5. How useful are different measurements of gait and mobility for tracking OA joint disease progression and testing the efficacy of potential therapeutics?
6. What is the relationship between tactile allodynia (as measured by von frey) and joint tissue pathology at different phases of OA disease?

8.4 Future directions

The broad investigations into pain-related behaviours and changes in DRG gene transcription conducted in this thesis were designed to be hypothesis generating to pave a path for future studies that can build on the findings from this thesis.

The studies reported demonstrate that the DMM model is suitable for investigating both the histopathology and pain behaviour of a post-traumatic OA phenotype. Additional experiments, utilising gene array analysis, are required to fully characterise the DRG gene expression profile at different stages of OA in this model. This will then enable the selection of target genes for investigation in KO mice studies to characterise the role of specific genes in the initiation and progression of OA pain, by utilising the suite of pain assays and the histological scoring method reported in this thesis. The suitability of a particular gene as a future therapeutic target can then be evaluated. Based on the findings reported in this thesis TRPA1, TRPV1, TRPV4 and ADAMTS-4 KO mice are suitable candidates for further investigation, however there are likely to be others.

In addition to characterising gene transcription profiles for each phase of OA, the role of gene translation (protein expression) also requires further investigation. This was commenced in this thesis but due to technical problems with optimising antibodies, the scope of the experiment was very limited. Further work is required to investigate protein expression of the other target genes identified, using a combination of IHC and tissue culture methods to determine the triggers that promote or inhibit protein expression. An investigation into sensory neuron protein expression using DRG tissue culture methods was commenced and preliminary data is presented in Appendix E.

However, because of the time required optimising the protocols and methods for this technique the investigation was not completed as part of the scope of this thesis.

The DRG were selected as a starting point for characterising the sensory modulation that gives rise to sensitisation and the manifestation of chronic OA pain. However, in addition to identifying target genes at the level of the DRG, investigations into pain mechanisms at the level of the spinal cord (dorsal horn) and brain (e.g. thalamas, prefrontal cortex, somatosensory cortex, amygdala) are also required. There are clear advantages to targeting OA pain at the periphery, but this does not exclude the need to have a full understanding of the mechanisms at play all along the pain pathway to better inform gene selection for therapeutic targets that are likely to be effective when administered into the affected joint.

The significant role that inflammation plays in OA pain was observed in both AIA and DMM, but was clearly different for each model. This was evident from the model-specific independent risk factors for developing OA that emerged from regression modelling and joint tissue associations that emerged from the correlation data. It was also demonstrated in the different gene expression profiles for each model at different phases of OA, and importantly in the model-specific associations between joint tissue histopathology, pain behaviour and DRG gene expression. The role of inflammation in OA pain is currently under investigation by numerous researchers and this needs to continue. In particular, greater clarification of the role of macrophage migration and differentiation of sub sets of macrophages and how each may alter sensory signalling differently at different stages of OA disease is required.

Finally, it will be important to build on the pain behaviour methods that were described and used in this thesis, to further investigate associations between pain

behaviour and joint tissue pathology, especially the relevance of tactile allodynia as a measure of sensitisation, its association with AC damage and SCB sclerosis, and its value as a measure of pain when investigating therapeutic targets. Further examination of gait analysis and spontaneous activity based measures to optimise the measures used to detect changes with disease progression and to test potential therapeutics is also required.

Appendix A: Reagents and Equipment

1. Animal Models

1.1 Complete Freund's adjuvant preparation

Material/Equipment	**Supplier**
Incomplete Freund's Adjuvant	SIGMA (order #F5506)
Mycobacterium tuberculosis (M.tb)	DIFCO (6 x 100mg vials, order #231141)
Mortar and pestle	

1.2 Emulsion preparation

Material/Equipment	**Supplier**
Methylated Bovine Serum Albumin	SIGMA (order #A1009)
1ml glass Tb syringe with leur lock	Becton Dickson (order #512027)
10ml glass syringe with leur lock	Becton Dickson (order #512027)
18 gauge drawing needles	Becton Dickson (order #300204)
30 gauge ½ inch needles	Becton Dickson (order #305106)
Dumont tweezers (#7, curved, superfine)	ProSciTech (T017D)
Flat bottomed 5 ml tube with cap	
Double edged razor blades	
Dissection microscope	
Anaesthetic machine (Isoflurane)	
Gloves and safety goggles	

1.3 DMM Surgery

Material/Equipment	**Supplier**
Westcott spring scissors 11.5 cm long with straight tips	ProSciTech (order #T106)
Dumont tweezers – number 7 (curved with superfine points, dumostar steel)	ProSciTech (order #T017D)
Dumont tweezers – number 5 (straight with superfine points, dumostar steel)	ProSciTech (order #T015D)
Castroveijo Ophthalmic needle holder, curved	ProSciTech (order #TT1A03C);
Scalpel blades (no. 11)	ProSciTech
Scalpel handle (no. 3)	ProSciTech
Suture material (8/0 Vicryl)	Ethicon (order # J548G)
Tissue adhesive (Vetbond)	3M
0.9% NaCl sterile irrigation solution	
Double-edged razor blades	Schick
Tuberculin syringes	BD Medical
Sterile gloves	
Paper drapes and sterile gauze	
Surgical microscope	
Anaesthetic machine (Isoflurane)	

2. Polymerase Chain Reaction Primers

Molecule	Species Accession #	Pos'n	Oligo Bases	Sequence 5' to 3'	T °C	Product (bp)
ADAMTS4	Mus musc NM172845	1549F 1793R	24 24	F – TAA CTT GAA TGG GCA GGG GGG TTC R – AAT GGC TTG AGT CAG GAC CGA AGG	60	245
ADAMTS5	Mus musc NM011782	2058F 2355R	21 24	F – TCT CCA AAG GTT ACG GAT GGG R – TCT TCT TCA GGG CTA AGT AGG CAG	55	298
ATF3	Mus Musc AB291912	269F 379R	23 23	F – AGG ATT TTG CTA ACC TGA CAC CC R – TGT TGA CGG TAA CTG ACT CCA GC	55	111
Calcitonin (CGRP)	Mus musc NM007587	716F 853R	24 22	F – CCA CAG GCT AAA AGA GAA TCA CCC R – CCC AAA CAA CCA ACA CTT CCA G	55	138
Cannabinoid receptor 1 (Cnr1)	Mus musc NM007726.3	987F 1149R	22 23	F – TGG AGA ACC TGC TGG TGC TAT G R – GGA CTA TCT TTG CGG TGG AAC AC	57	163
GAPDH	Mus musc BC083149	880F 1079R	20 20	F – TGC GAC TTC AAC AGC AAC TC R – CCT GCT CAG TGT CCT TGC TG	55	200
IL1B	Mus musc BC011437	127F 243R	24 23	F – ACC TGT TCT TTG AAG TTG ACG GAC R – TCT TGT TGA TGT GCT GCT GTG AG	55	117
Opioid receptor mu (Oprm1)	Mus musc AB441736	701F 822R	23 23	F – TCT GTG TCT TCA TCT TCG CCT TC R – GTT CCT GTC CTT TTC TTT GGA GC	55	122
Tachykinin-1 (Substance P)	Mus musc NM009311	754F 859R	22 22	F – CGC AGT CTC CAA AGA AAG GAC C R – TGA AAG CAG AAC CAG GGG TAG C	57	106
TRPA1	Mus musc BC131963	364F 530R	23 21	F – AAG TTT CTT CTC AGC CAA GGA GC R –ATC AAA GCC GTG TTC CCA TTC	55	167
TRPV1	Mus musc AY445519	105F 283R	20 24	F – AGC CAA GCC CCA CAT CTT TG R – TGA GAC AGG TAG GTC CAT CCA CAG	58	179
TRPV2	Mus musc NM011706	1846F 2014R	24 22	F – TAC CTC CCC CTG TTA GTG TCA TCC R – CAG CAA AGC CGA AAA GGA AGA C	56	169
TRPV4	Mus musc NM022017	1454F 1693R	24 21	F – GAG AGA CAA GTG GCG TAA GTT TGG R – CCA GGG CAT TTC TTC GTG AAC	58	240

3. Immunohistochemistry

3.1 Materials

Materials	**Details**	**Supplier**
Slides	Adhesive Slides	Dako K802021
Cover slips	Menzel-Glaser 22x50mm	Trajan Scientific & Medical CS2250100
Mountant	Euckitt mounting media	Trajan Scientific & Medical EUCKITT
Staining chamber	Sequenza Shandon coverplates	ThermoFisher
Xylene	Xylene AR	POCD (Point of care diagnostics) XYL5
Ethanol 100%	Absolute Ethanol, non denatured	POCD ETHABS5
Ethanol 95%	Dilute 100% stock in milliQ water	
Ethanol 70%	Dilute 100% stock in milliQ water	
Heat retrieval solution	0.01M Citrate buffer, pH 6.0	Dako S1699
Enzymatic retrieval	Proteinase K	Dako S3020
0.3% Hydrogen Peroxide	Diluted 30% stock in milliQ water 1:100	Trajan Scientific & Medical UnivarAjax 260-500ml
TBST wash buffer	0.05M Tris, 0.15M NaCl, 0.05% Tween 20, pH 7.6	Dako K800
Blocking reagent	Serum-free Protein Block	Dako X0909
Antibody diluent	Antibody diluent	Dako S0809
Detection	Envision + Rabbit	Dako K4003
	Envision + Mouse	Dako K4001
Stain	NovaRED™	VectorLabs SK4805
Counterstain	Mayer's Haematoxylin	Refer to appendix B for details on preparation
	Scott's Blue	

3.2 Antibodies

Antibody	**Details**	**Source**
CGRP	Monoclonal Anti-Calcitonin Gene-Related Peptide (CGRP) Clone CD8, in mouse, purified immunoglobulin	Sigma C 9487
F4/80	Monoclonal Anti-F4/80 antibody, in rat, purified immunogobulin	Abcam ab6640
Opmr1	Rabbit polyclonal antibody raised against synthetic peptide of opioid mu receptor, affinity purified	Abnova PAB18103
PGP	Polyclonal anti-PGP9.5 antibody raised against synthetic peptide, in rat, affinity purified	Abcam ab27053

4. DRG Tissue Culture reagents and materials

Reagent	**Supplier**
HBSS buffer solution	Invitrogen 14025-092
Poly-L-Lysine	Sigma p1274-25MG
N2	Invitrogen 17502048
Laminin	Sigma L2020-1MG
Collagenase type 4	Fisher NC9620402
Papain	Fisher NC9212788
F12 media	Invitrogen 11765-054
Fetal bovine serum	Invitrogen
Penicillin/Streptomycin	Sigma P4333-20ML
glass coverslips	Fisher 12-545-102
glass pipettes	Fisher 136786B

Appendix B: Reagent Preparation

1. Antigen Induced Arthritis Model

a. Freund's Complete Adjuvant (2mg/ml)

A mask, safety glasses and gloves are worn during preparation.

Place 1-2ml of Incomplete Freund's adjuvant in a mortar and add 1 vial (100mg) of Mycobacterium turberculosis (M.tb). This avoids aerolisation of the powder during preparation. Pulverize the M.tb powder in the Incomplete Freund's for about 10 minutes, adding a little more Freund's as you go but keeping the volume to a minimum so as to give best pulverization.

Transfer the pulverized M.tb to a glass tube with lid. Add more Freund's Incomplete to the mortar and use to "wash out" more of the M.tb

Repeat several times until all of the M.tb has been transferred to the tube.

Make the final volume of the Freund's Complete adjuvant to 50 ml (5 x 10 ml vials) to achieve a concentration of 2mg/ml

b. Methylated Bovine Serum Albumin (mBSA) (2mg/ml)

Weigh out 20mg mBSA in 10 ml tube. Add 10ml sterile water. DO NOT MIX but place in 37°C water bath over ~1hr to allow to dissolve. Check every 15 min and gently flick.

NB *mBSA is prepared as a large batch (20mg in 10 ml), stored as 1ml aliquots at -20 degrees, then thawed on the day it is needed to make emulsion.*

c. mBSA emulsion (100μl/mouse)

Make up more than the calculated amount to compensate for the losses that occur during preparation. For example, for 10 mice prepare 2ml emulsion, for 20 mice prepare 4ml emulsion, and for 30 mice prepare 5ml emulsion.

Safety glasses and gloves are worn during preparation.

Transfer the required amount of Freund's complete adjuvant (FCA) (2mg/ml), using a 1ml Gilson tip, to a 5ml flat bottom tube. Add an equal volume of dissolved 2mg/ml mBSA using a drop wise technique with continual vortexing of the tube. Once all the mBSA has been added, use an autoclaved 10 ml glass syringe with an 18-gauge drawing needle to create a stable emulsion using the following technique.

- Aspirate some of the mixture into the syringe, invert syringe and pull the plunger back most of the way to "coat" the walls of the syringe and provide a better seal. Then expel this back into the tube.

- Draw up all of the emulsion, invert the syringe and expel the air. Expel the emulsion (with force) back into the tube with the needle above the liquid to avoid any overflow and production of bubbles. Repeat the procedure 2-3 times then put the tube and 10 ml syringe on ice for a few minutes to avoid heating the emulsion.

- Minimise handling of syringe around the barrel to avoid warming it up.

- Repeat the above process 3-5 times until a thick and stable white emulsion is formed.

Test the stability of the emulsion by placing one drop of emulsion onto cold water in a beaker. If the drop stays together and little or no oil disperses onto surface of the water then the emulsion is suitable for use.

NB *Emulsion is made fresh on the day of the immunization and stored on ice until injected.*

d. mBSA (20mg/ml)

Weigh out 20mg mBSA into a 1.5 ml tube. Add 1ml sterile water. DO NOT MIX but place in 37°C water bath over ~1hr to allow to dissolve. Check every 15 min and gently flick.

NB *A larger batch is made up (200mg in 10 ml saline) and frozen at -20 degrees, in ½ and 1 ml aliquots, then thawed on the day it is required.*

When required, thaw and add 50µl of a sterile 3M NaCl solution to the 1ml aliquot and mix immediately. This solution is prepared the morning of injection, as the mBSA precipitates out over time.

2. Real Time-PCR: Reverse transcription (RT) Master mix

Total volume = 1000µl

- 400 µl 10x RT buffer (Qiagen Omniscript kit)
- 200 µl RT dNTP (Qiagen Omniscript kit)
- 200 µl rand om primers (pentadecamers)
- 100 µl RNAse inhibitor (Bioline)
- 50 µl RNAse -free glycerol
- 50 µl RT enzyme (Qiagen Omniscript kit)

3. Immunohistochemistry: Mice perfusion protocol

a. Flush solution - 9g NaCl + 5g Na_2NO_4 in 1L milliQ water

Add 1500 IU/500mL heparin (1500 IU = 300µL)

b. Fixative solution - Phosphate buffered saline (PBS) + 4 % Paraformaldehyde (PFA)

Set pH to 7.4 by adding NaOH or HCl. (Use pH meter)

Prepare no sooner than day before and store at 4°C

4. DRG Culture (All procedures carried out under a laminar flow hood)

a. Preparation of Coverslips

- Place sterilized glass coverslips in tissue culture wells (2 x 6 well plates) and coat with Poly-L-Lysine (PLL) (2ml/well) and leave at 4°C overnight

Note: The coating of these coverslips was done ahead of time and stored at 4°C

- Turn coverslips over. Wash coverslips three times with sterile water. Use 2 ml for each was and suction with a glass pipette. Allow coverslips to dry.
- Before use, coat the PLL-coated coverslips with Laminin (200 µl per coverslip) and incubate for 2 hrs in the incubator at 37°C.
- After incubation, remove excess laminin from each coverslip by suctioning with glass pipette, and allow to air dry.

b. Solutions and Culture Mediums

Poly-L-Lysine (PLL):- Add 250 ml of sterile tissue culture grade water to 25 mg of PLL. Store as 50 ml aliquots (100 µg/ml) at -20°C.

N2:- Thaw 5 mL vial and store as 1 mL aliquots at -20°C

Laminin: - Dilute 50x with sterile water (supplied at 1mg/ml concentration). Store as 50 µl aliquots at -20°C. Thaw at room temperature and make working dilution of 50□l in 2.5ml MB water.

Collagenase type 4: - Dissolve 50 mg of Collagenase 4 into 50 ml of Hank's Balanced Salt solution (HBSS) (1mg/ml). Store as 1 ml aliquots at 4-8°C. Thaw in 37°C water bath before use.

Papain; - Dissolve 1 vial of papain in 5ml of HBSS. Store as 500 µl aliquots at 4-8°C.

F12 DRG medium and 10% FBS: - Add 5 ml of Fetal Bovine Serum (FBS) into 45 ml of F12 media. Make up in small quantities as required (0.5ml in 4.5ml for total of 5ml).

F12 DRG Medium - Make up 100ml at a time in filter top bottles and store @ 4°C for up to 4wks.

- 98 ml F12 media (use fresh bottle of F12 every ~6 weeks)
- 0.5 ml FBS
- 1 ml N2 supplement
- 0.5 ml Penicillin/Streptomycin

Appendix C: Histology Scoring

Scoring system used for histopathological assessment of Toluidine blue stained osteochondral sections of mouse knees following DMM or AIA. Sagittal sections. Only score a single slide for each animal/joint and try to score the same area of the joint in all animals – the slide near the central weight-bearing region of the joint.

Table 1. STRUCTURAL CARTILAGE DAMAGE

Scoring system used for histopathological assessment of Toluidine blue stained osteochondral sections of mouse knees following DMM or AIA, modified from that of Glasson et al (Arthritis Rhem 2004). The tibial plateau and the femoral condyle are scored separately. Only the central weight-bearing region of the joint was evaluated.

0	Normal cartilage
1	Roughened surface AND/OR superficial fibrillation <10% of cartilage depth (any % of joint surface area),
2	Fibrillation extending >10% of cartilage depth but not reaching the calcified cartilage AND/OR loss of surface lamina (any % or joint surface area)
3	Horizontal cracks/separations between calcified and non-calcified cartilage OR clefts down to calcified cartilage BUT no loss of non-calcified cartilage
4	Fibrillation to the calcified layer OR loss of non-calcified cartilage lesion for 1-25% of the joint surface
5	Fibrillation to the calcified layer OR loss of non-calcified cartilage lesion for 25-50% of the joint surface
6	Fibrillation to the calcified layer OR loss of non-calcified cartilage lesion for 50-75% of the joint surface
7	Fibrillation to the calcified layer OR loss of non-calcified cartilage lesion for >75% of the joint surface
8.	Lesion extends through the calcified cartilage (any % joint surface area)

Table 2. PROTEOGLYCAN LOSS

Scoring system used for histopathological assessment of Toluidine blue stained osteochondral sections of mouse knees following DMM or AIA. The tibial plateau and the femoral condyle are scored separately. Serial sections across the width of the medial tibial plateau are stained. Only the central weight-bearing region of the joint is evaluated.

0	Normal cartilage
1	Decreased but not complete loss of toluidine blue staining over any % of surface area
2	Complete loss of toluidine blue staining in the non-calcified cartilage extending to <25% of the articular surface
3	Complete loss of toluidine blue staining in the non-calcified cartilage extending to 25-50% of the articular surface
4	Complete loss of toluidine blue staining in the non-calcified cartilage extending to 50-75% of the articular surface
5	Complete loss of toluidine blue staining in the non-calcified cartilage extending to >75% of the articular surface

Table 3. CHONDROCYTE HYPERTROPHY/APOPTOSIS/CELL DEATH – non-calcified articular cartilage

Scoring system used for histopathological assessment of Toluidine blue stained osteochondral sections of mouse knees following DMM or AIA. POSITIVE SCORE - defined as enlarged chondrocyte/lacunae in non-calcified cartilage – appears as empty space around collapsed chondrocyte typical of cells in calcified zone PLUS the nucleus of the cell is dark stained and pyknotic (shrunken).

NOTE: If the nucleus is missing from the lacunae this is considered apoptotic. If there is empty space around nucleus but it is not collapsed/dark staining this is not considered positive (compare with hypertrophic/apoptotic cells in calcified cartilage as an example). Tibia and femur examined separately as below.

0	No hypertrophy/apoptosis
1	<1/3rd of cells in non-calcified cartilage across the width of the joint are hypertrophic/apoptotic/missing nuclei
2	1/3rd – 2/3rd of cells in non-calcified cartilage across the width of the joint are hypertrophic/apoptotic/missing nuclei
3	>2/3rd of cells in non-calcified cartilage across the width of the joint are hypertrophic/apoptotic/missing nuclei

Table 4. OSTEOPHYTE FORMATION/MATURATION

Scoring system used for histopathological assessment of Toluidine blue stained osteochondral sections of mouse knees following DMM or AIA. Only the major osteophyte that forms on the anterior/medial margin of the tibia is scored. Only a single section is scored for each mouse. The section that is scored is that just at the point when separation of the anterior and posterior meniscal elements becomes apparent. The osteophyte in the DMM model is invariably closer to the medial margin of the joint in sagittal sections and the same site is scored in each mouse.

Osteophyte "maturity"	
0	No Osteophyte
1	Predominantly cartilaginous - little or no active endochondral ossification
2	Mixed cartilage and bone with active endochondral ossification – chondrocyte hypertophy and active vascular invasion and new bone formation
3	Predominantly bone (often with mature trabeculae and marrow space) with little active endochondral ossification.

Osteophyte size	
This is judged by an "internal" standard which is the thickness of the nearby normal full depth articular cartilage (i.e surface to base of calcified cartilage).	
0	No Osteophyte
1	Small = up to 1x (same) thickness of the adjacent normal cartilage
2	Medium = 1-3 x the thickness of the adjacent normal cartilage
3	Large = > 3 x the thickness of the adjacent normal cartilage

Table 5. SUBCHONDRAL BONE

Scoring system used for histopathological assessment of Toluidine blue stained osteochondral sections of mouse knees following DMM or AIA. Only the tibia is scored. NOTE *"solid"* trabeculae bone or cortical-type bone is seen as predominantly (>90%) green stained bone with canaliculi but may contain small marrow spaces and extends from the articular to the growth plate cartilage. For a score of 1-3 the changes must be on 2 or more consecutive sections.

0	Normal trabecular bone with > 50% marrow space
1	2 or more "wide" vertical trabecular struts of bone that extend from the cartilage to the growth plate OR "solid" bone spanning up to 1/3rd of the width of the epiphysis
2	"solid" bone spanning > 1/3rd but < 2/3rd of the width of the epiphysis
3	"solid" bone spanning > 2/3rd of the width of the epiphysis.

Table 6. SUBCHONDRAL BONE Vascular Invasion/erosion

Scoring system used for histopathological assessment of Toluidine blue stained osteochondral sections of mouse knees following DMM. Only the tibia is scored. Score by evaluating the number of points at which the subchondral bone is "breached" such that vessels or marrow WBC touch or invade the calcified cartilage.

0	Normal: intact SC bone layer
1	Mild: 1 or 2 points of vascular invasion to touch but not invade the calcified AC in tibia
2	Moderate: 3 or more points of vascular invasion to touch but not invade the calcified AC in tibia; OR any number of points that invade into the calcified AC but do not reach the non calcified AC
3	Severe: any number of points that invade through the calcified AC and reach/invade the non calcified AC

Synovial Inflammation Scoring

Scoring system used for histopathological assessment of Toluidine blue stained osteochondral sections of mouse knees following DMM or AIA. Sagittal sections. Only score a single slide for each animal/joint and try to score the same area of the joint in all animals – the slide near the central weight-bearing region of the joint. Only the synovium superior (femoral side) to the meniscal remnant is scored. Both anterior and posterior aspects of the joint are scored.

PANUS

Panus, defined as fibrous tissue/synovium/inflammatory cell out growth spreading OVER the bone at the osteochondral junction joint margin and ultimately over the surface of the cartilage at the joint margins. Score the maximum distance over which the panus (see definition above) has spread. Use an "internal standard" to measure the distance which is the full thickness depth of the articular cartilage (non-calcified plus calcified – i.e. tol blue positive tissue) at a point 1/4 of the way across the joint (see figure) from the respective adjacent/affected joint margin.

0 No panus

1 mild: panus (2> cells thickness) is present on the bone at the joint margin but has not has migrated over cartilage surface

2 moderate: panus has migrated over cartilage surface < 1 x cartilage depth

3 severe: panus has migrated over cartilage surface > 1 x cartilage depth

Bone Erosion By Panus Or Inflammatory Cell Inflitrate

As well as migrating over the surface of the cartilage the panus/inflammatory cell infiltrate can erode into the cortical bone at the joint margin. Look at the anterior and posterior margin of the femur between joint capsule attachment and cartilage margin. Bone erosion by pannus/inflammatory cells is considered to be present when there is loss of any depth of the cortical bone from the outside in towards the marrow cavity with hyperplastic synovial cells/inflammatory cells attached to and invading into this area of bone loss. The depth of cortical bone loss can vary from partial thickness, appearing as a rough and/or scalloped bone surface with attached panus through to complete loss of cortical bone with panus extending into the marrow.

BONE EROSION

Score the maximum erosion severity at the joint margin.

0 no cortical bone erosion at any site

1 partial thickness loss of cortical bone only

2 focal complete loss of cortical bone - communication with the marrow cavity one small “vascular” communication site

3 widespread complete loss of cortical bone - communication with the marrow cavity multiple sites or broad area of loss of cortical bone

SYNOVIAL HYPERPLASIA - SEVERITY

Do not score the cells in the area actually attached to the tibia or femur (this is recorded in panus) OR cells on the surface of the meniscus itself or immediately adjacent (synovial plica here often has multiple synovial cell thickness in normal joints). Score the maximum hyperplasia seen anywhere along this area even if only focal.

0 1 cell thick
1 mild = 2-3 cells thick
2 moderate = 4-5 cells thick
3 severe = >5 cells thick

SUB-SYNOVIAL INFLAMMATION / WBC INFILTRATION

The infiltration of inflammatory cells (neutrophils, macrophages and/or lymphocytes) is evaluated.

0 no inflammatory cells
1 occasional scattered inflammatory cells - perivascular
2 FOCAL areas of dense subsynovial wbc infiltrate - but still predominantly normal subsynovial areolar connective tissue present
3 WIDESPREAD dense subsynovial wbc infiltrate – markedly reduced or little/no normal areolar connective tissue evident OR
LYMPHOID FOLLICLE formation – distinct accumulations of mononuclear cells organised into rounded masses reminiscent of lymph nodules

SYNOVIAL EXUDATE

The infiltration of inflammatory cells (neutrophils, macrophages and/or lymphocytes) is evaluated.

0 no inflammatory cells or fibrin in the synovial cavity
1 inflammatory cells and/or fibrin clot restricted in the synovial cavity – may be restricted to recesses

Appendix D: Melt curves for real time RT-PCR

For real time RT-PCR, primer specificity was confirmed for each gene by performing a melt curve analysis and demonstrating a single amplicon of appropriate size. Representative melt curves for the 12 genes investigated in this study are included below. Each graph includes samples for DMM, AIA, sham and saline injected mice.

ADAMTS-4

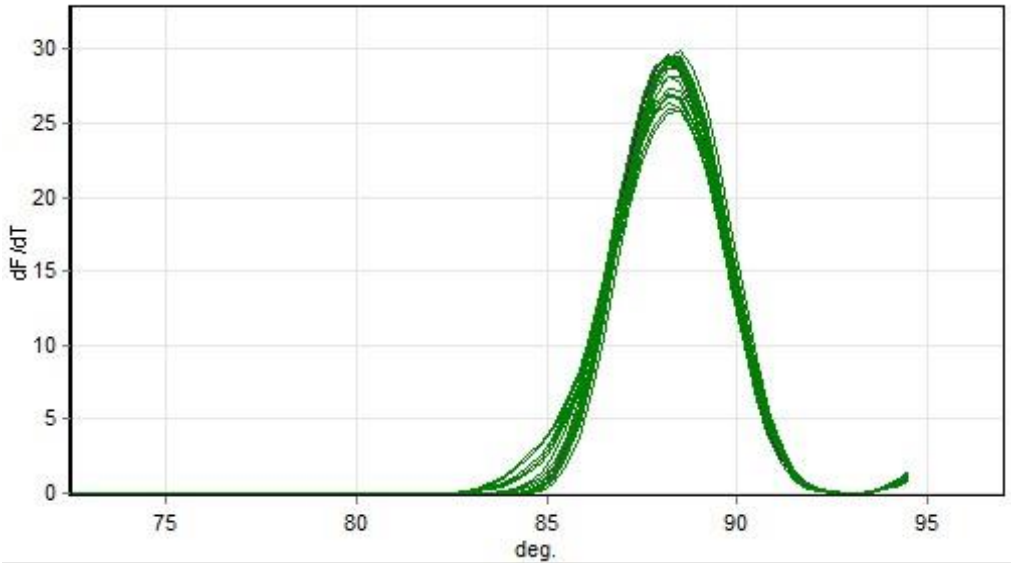

ADAMTS-5

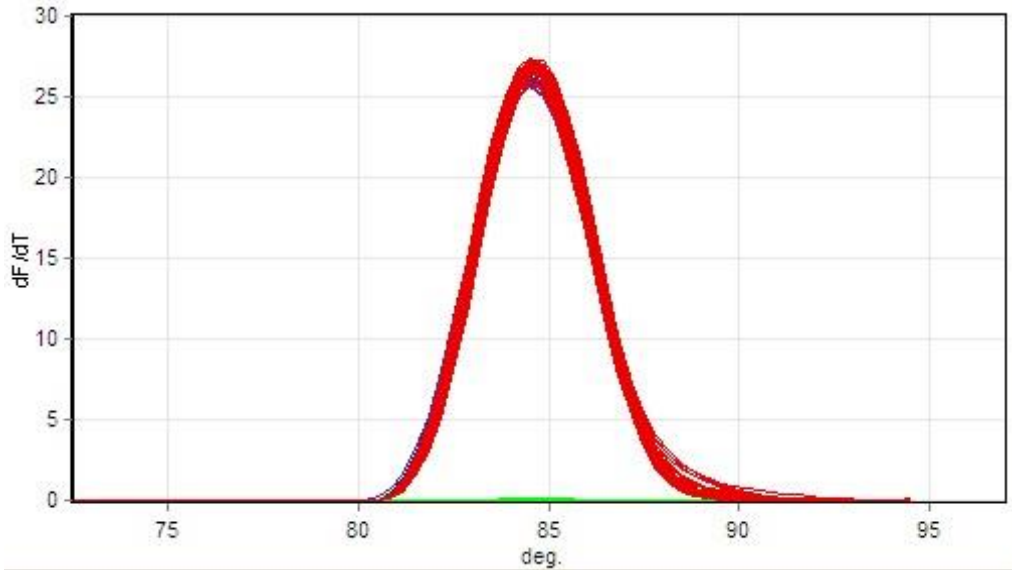

ATF3

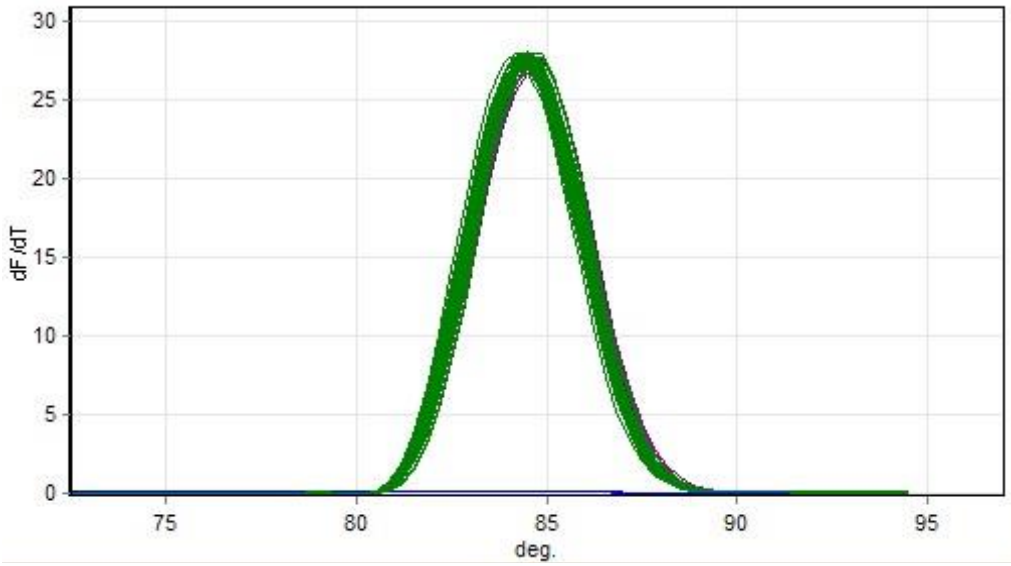
30
25
20
15
10
5
0
dF /dT
75
80
85
90
95
deg.

CGRP

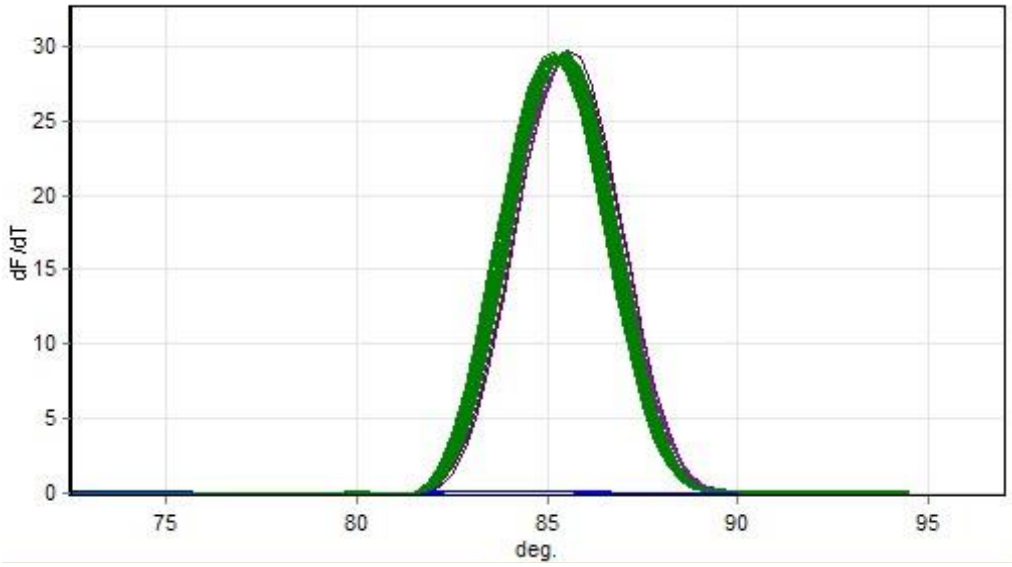
30
25
20
15
10
5
0
dF /dT
75
80
85
90
95
deg.

CNR1

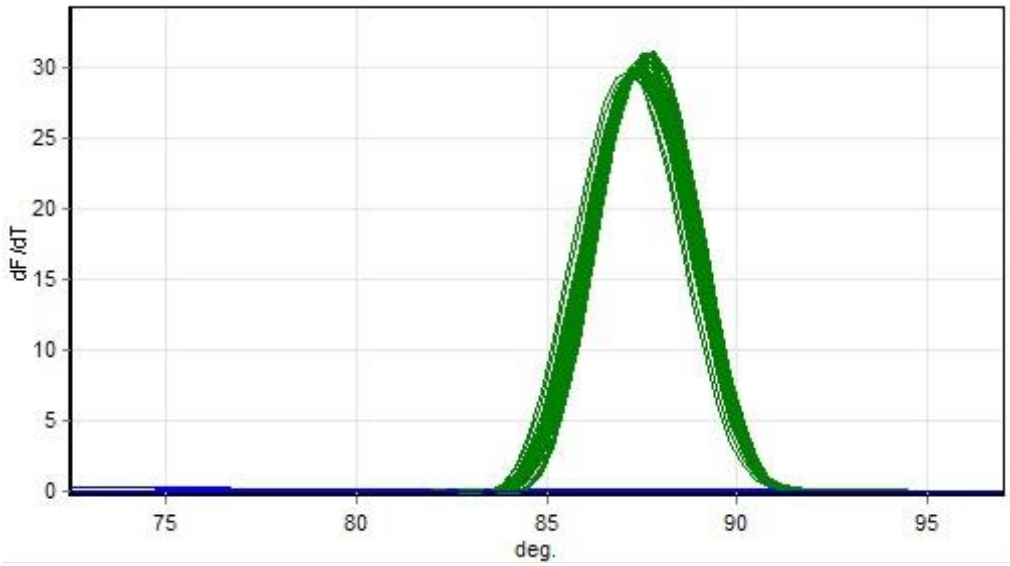
30
25
20
15
10
5
0
dF/dT
75
80
85
90
95
deg.

IL-1β

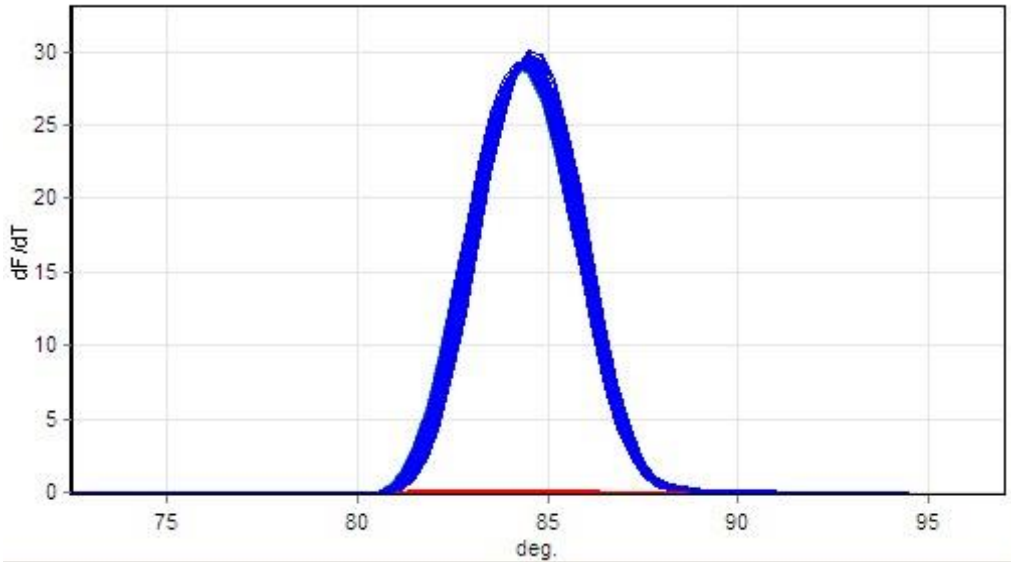
30
25
20
15
10
5
0
dF/dT
75
80
85
90
95
deg.

Oprm1

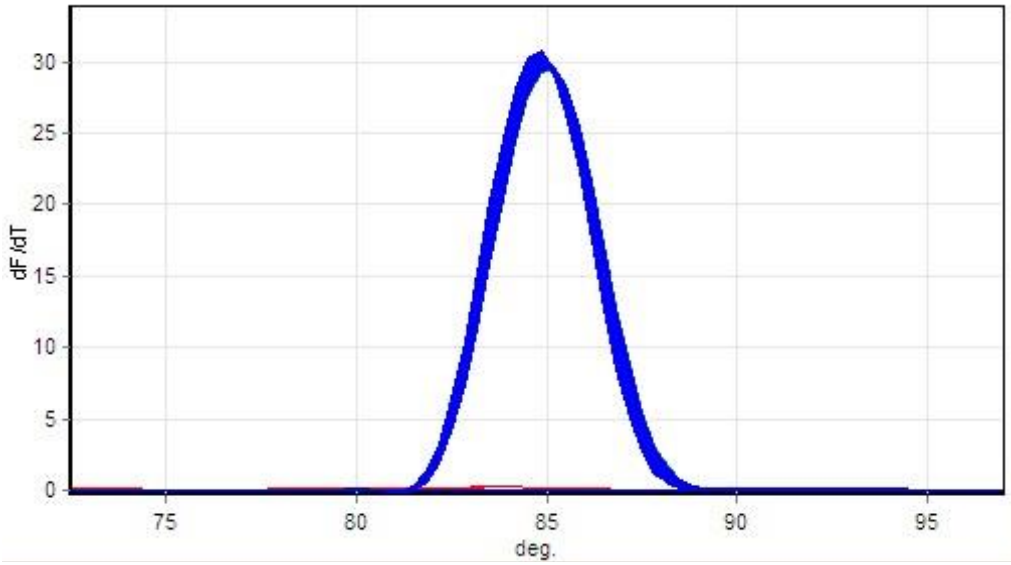
30
25
20
15
10
5
0
dF/dT
75
80
85
90
95
deg.

Tac-1

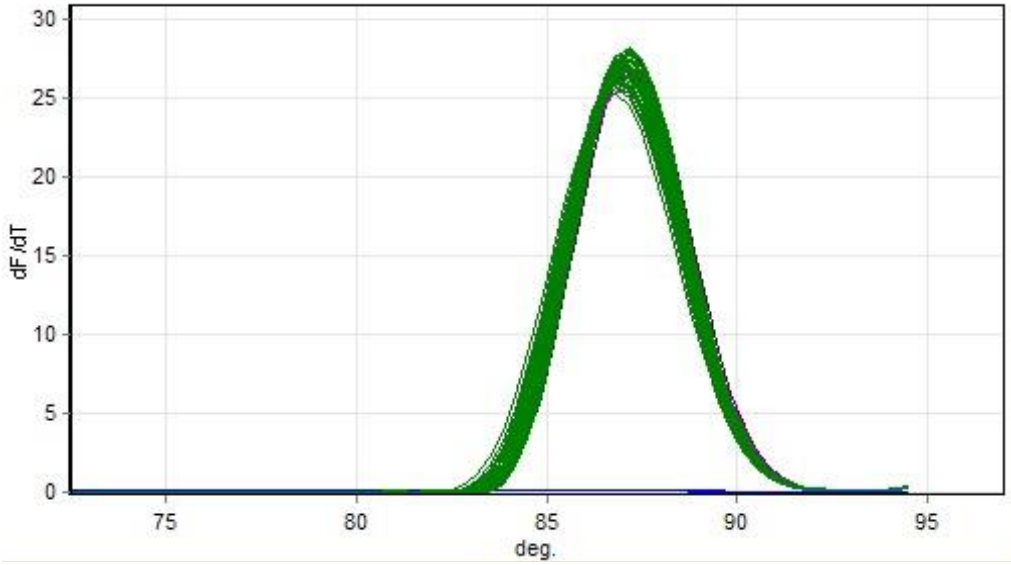
30
25
20
15
10
5
0
dF/dT
75
80
85
90
95
deg.

TRPV1

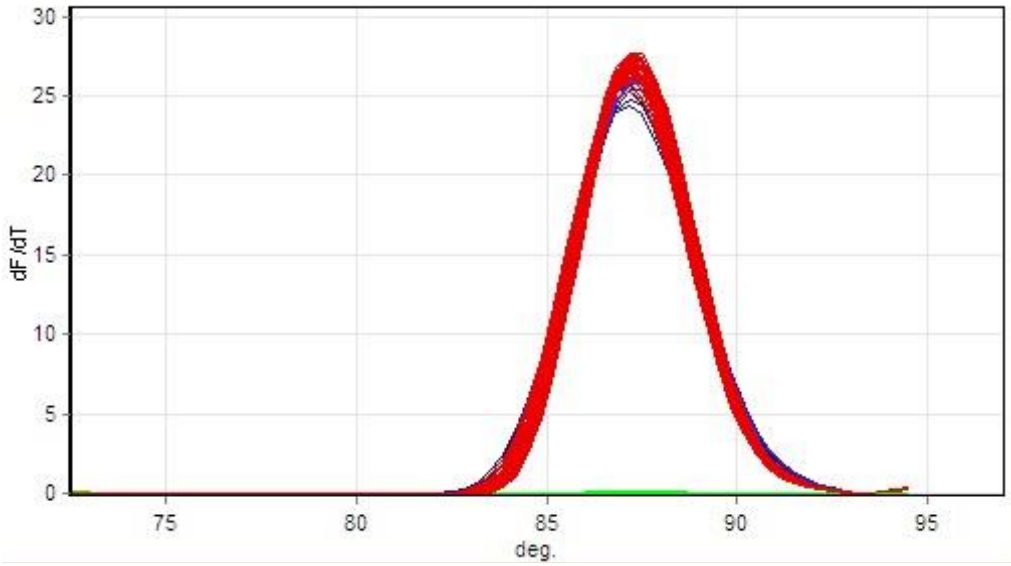
30
25
20
15
10
5
0
dF/dT
75
80
85
90
95
deg.

TRPV2

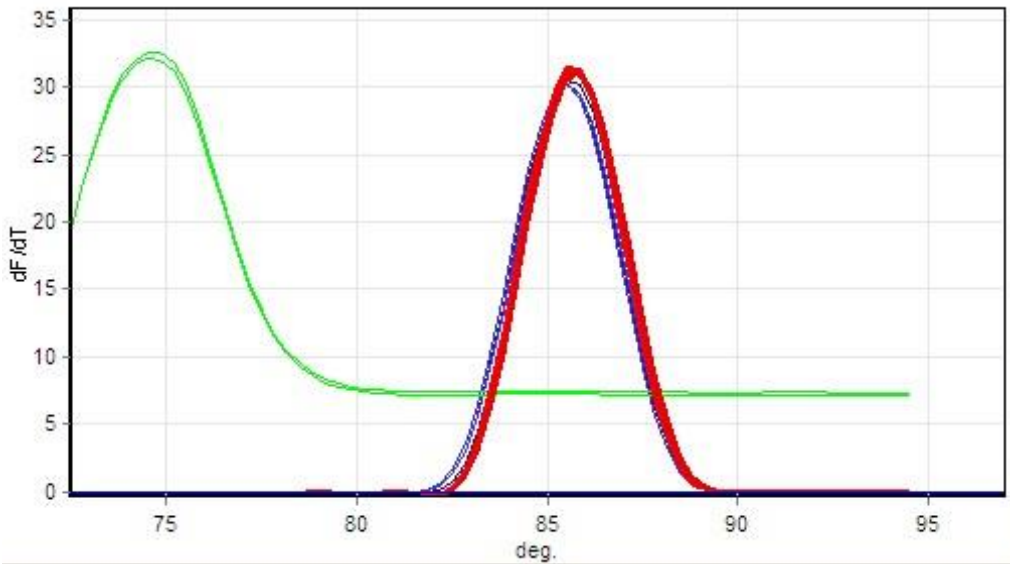
35
30
25
20
15
10
5
0
dF/dT
75
80
85
90
95
deg.

TRPV4

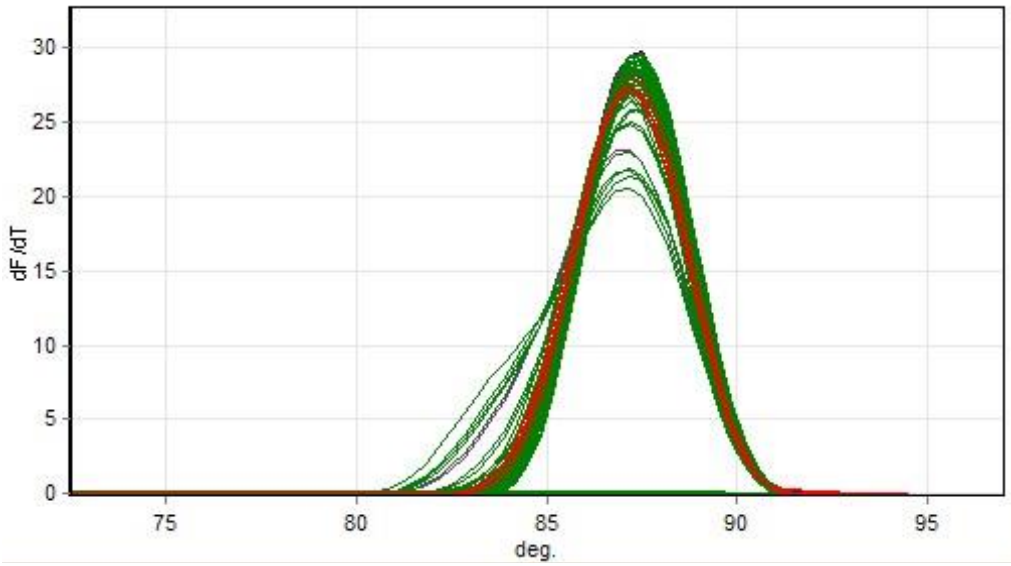
30
25
20
15
10
5
0
dF/dT
75
80
85
90
95
deg.

TRPA1

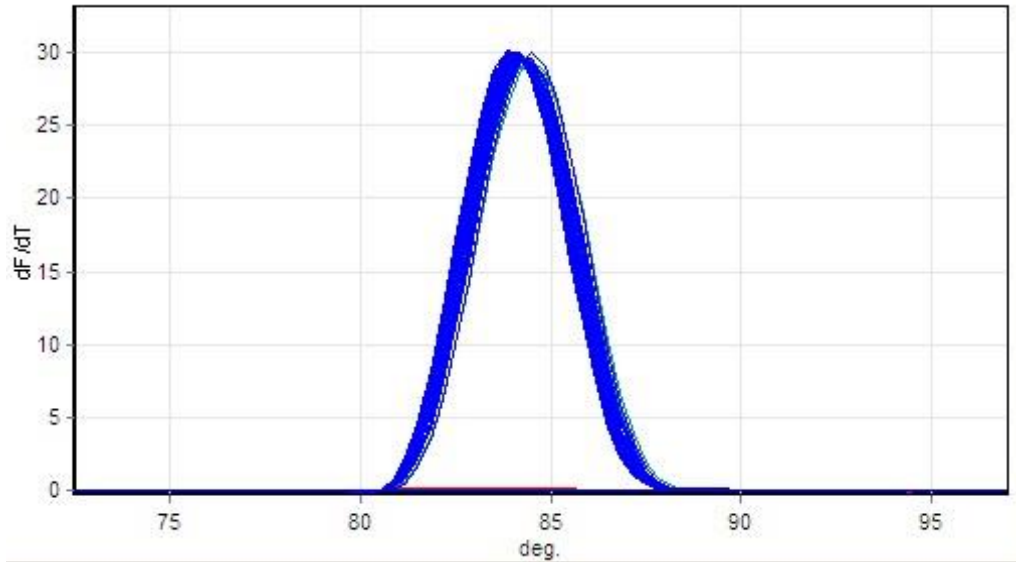
30
25
20
15
10
5
0
dF/dT
75
80
85
90
95
deg.

ATF3 quantitative data graph represents DMM, Sham, AIA and saline injected mice DRG. Expression of ATF3 was demonstrated in both treatment and control groups at all measured time points. The graphs below represent week 4 (a) and week 8 (b) data.

a.

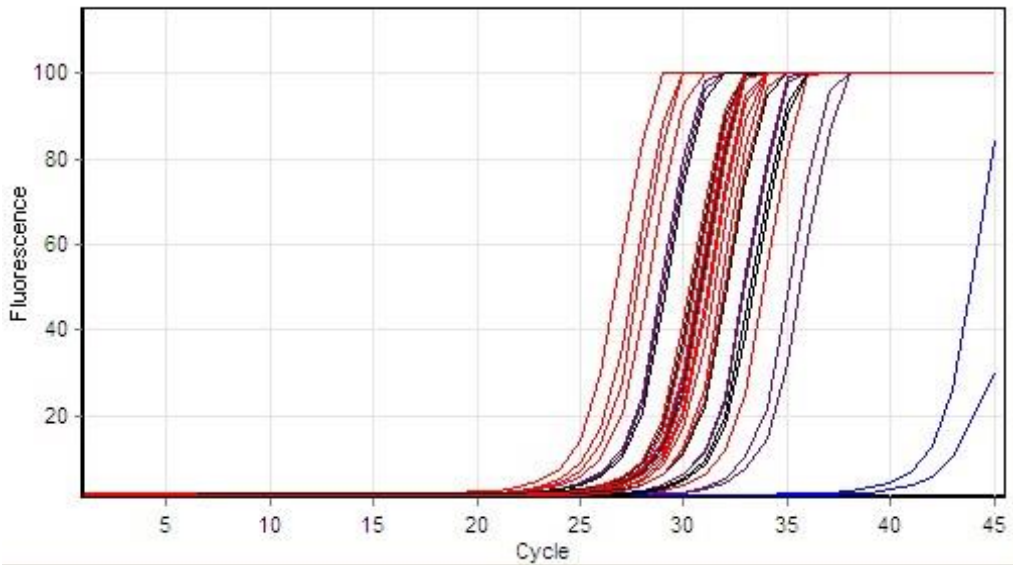

b.

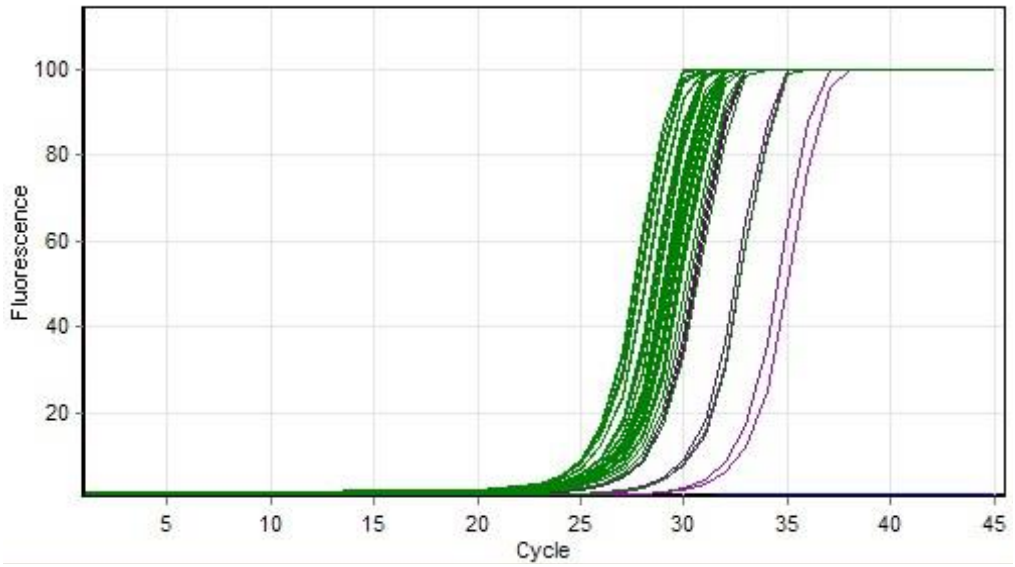

Appendix E: the role of macrophage infiltration and chemokine production by sensory neurones in development of OA pain - preliminary findings using IHC and DRG tissue culture methods.

Introduction and aims

Recently, macrophage infiltration has been implicated in pain and sensitisation in animal models of OA. Researchers have demonstrated that peripheral inflammation alone in the absence of peripheral nerve injury is a trigger for macrophage infiltration into innervating DRG, and that this macrophage infiltration correlates with OA pain related behaviour. MCP-1 (monocyte chemo-attractant protein-1) is a chemotactic cytokine that mediates increased pain signaling by attracting macrophages to the DRG, and has also been shown to directly mediate excitatory effects at the level of the DRG in nerve-injury models of pain. However, the relationship between DRG macrophage infiltration, pain, and progression of joint pathology has not been studied. To further investigate the mechanisms involved in sensitisation at the level of the DRG (both early and late in the development of OA), IHC and DRG tissue culture methods were used. Immunoreactivity for F4-80 (a macrophage marker) and production of MCP-1 by sensory neurons *in vitro*, was measured in the lumbar DRG of AIA and DMM mice (and their respective controls).

Aims:

1. To investigate differences in F4-80 expression in the lumbar (L3-L4) DRG following development of knee joint arthritis induced by DMM and AIA, using immunohistochemistry techniques.
2. To measure and compare the levels of MCP-1 protein produced in culture by lumbar DRG from mice with knee joint arthritis induced by DMM and AIA.

Methods and data presentation

Details of the methods used to induce the two models of arthritis, DMM and AIA, are described in chapter 2, section 2.1. The methods used for immunohistochemistry are described in chapter 2, section 2.5. The methods used for tissue culture are described below. Details of the composition and preparation of all solutions and culture mediums used in DRG culture are found in Appendix B.

a. DRG harvesting

At week 1, 4, 8 and 16, post arthritis induction, cells were harvested and isolated from the innervating DRG of the knee joint (L3-L5). Due to the limited cell yield from each individual DRG, left and right DRG were combined, and DRG 4 mice from each treatment group (DMM, sham, AIA, saline, immunised-control, control) were pooled for each 12-plate culture.

Mice were euthanised using CO_2 inhalation. The coat was sprayed liberally with 70% ethanol to minimise contamination. Using a dissection microscope, the skin covering the dorsum was dissected away to expose the underlying muscle layers and allow visualisation of the vertebral column and ribs. Using iris scissors an incision was made through the interveterbral disc space at the level of the thoracolumbar region. The dorsal vertebral column was then trimmed away to expose the spinal cord. The

spinal cord was gently lifted starting at the thoracolumbar junction and working towards the sacral region, to enable visualisation of the DRG. Left and right DRG (L3 to L5) were lifted with forceps and dissected out by cutting the attaching nerve roots. The DRG were placed in a collection dish containing cold Hank's Balanced Salt Solution (HBSS). They sat on ice for approximately one hour, until DRG from all 4 mice (24 DRG in total) had been harvested.

b. DRG digest

All tissue culture procedures were done inside a laminar flow hood. Using a 1ml pipette, the DRGs were transferred to a 15 ml centrifuge tube (falcon tube) and centrifuged at 700 rpm for 5 minutes. The supernatant was removed and 500□l of pre-warmed Collagenase type 4 added to the DRG and incubated for 20-25 minutes at 37^{o}C. A further 500□l of pre-warmed papain was added to the DRG, followed by gently vortexing and incubation for 20-25 minutes at 37^{o}C.

Ham's F12 medium containing 10% Fetal Bovine Serum (FBS) (0.5ml) was then added and the DRG digest titurated with a glass pipette for several minutes to gently break up the tissue. The resultant cell suspension was filtered through a 70□m cell strainer to remove non-dissociated cells and remaining connective tissue. The tube containing the digest was 'washed' by adding 4.5 ml of Ham's F12 medium with 10% FBS, and this also filtered through the cell strainer. The filtered cell digest was centrifuged at 1500 rpm for 10 minutes.

c. DRG culture

The supernatant was removed, leaving only 0.5ml. The DRG cells were re-suspended in 1.2ml of serum free Ham's F12 medium by gentle mixing, and 100µl of cell suspension was plated onto the centre of sterile coverslips (previously coated with Poly-L-Lysine and laminin) that sat in 6 well tissue culture plates. A total of 12 wells

were plated with cells. These were then incubated at 37oC with 5% CO2 for 1.5 hours to allow cells to adhere before an additional 2ml of serum free Ham's F12 medium was added to each cover slip, making sure not to add directly to the cells but rather the side of the well. The plate was gently moved from side to side to ensure the coverslips were fully coated with media before placing them back in the incubator and cultured for two days at 37oC with 5% CO2. After two days in culture, the media was changed and the cells cultured for an additional two days, this media being used for subsequent analysis.

d. Conditioned media harvest

Before harvesting, each well was viewed under the microscope and graded 1-3 based on the density and viability of the cell population. Cell culture supernatant from each well was transferred to an assembled 3-kDa molecular weight cut-off Millipore centrifugal filter tube, using a 1ml pipette. The tubes were centrifuged at 5000 rpm (10^{o}C) for 30 minutes. The bottom of the filter tubes were discarded and the tubes inverted, before centrifuging at 1000 rpm for an additional 2 minutes. The concentrated supernatant was then transferred to low binding tubes and stored at -80^{o}C.

e. Protein analysis of conditioned media

Total protein was determined using a BCA assay (Thermo Fisher Scientific). Briefly 25□l of each unknown sample replicate and a series of diluted protein standards was pipetted into microplate wells (Pierce 96-well plate, Thermo Scientific). To each well 200□l of working reagent was added, and the plate mixed thoroughly on a plate shaker for 30 seconds. The plate was then covered and incubated at 37°C for 30 minutes. The plate was then cooled to room temperature before measuring the absorbance at 562nm using a plate reader.

Levels of MCP-1 protein were determined using an ELISA (R&D systems) following the manufacturer's instructions. MCP-1 values were then expressed relative to total protein.

Results

Representative images of F4-80 IR are displayed in Figure I. Levels of MPC-1 in conditioned media are represented in Figure II.

Figure I. F4-80 Immunoreactivity

IR (NovaRED staining) in the right L3/L4 DRG in DMM, Sham, AIA, and Saline-injected mice at week 1 (a), week 4 (b), week 8 (c), and week 16 (d) post arthritis induction. X10 magnification

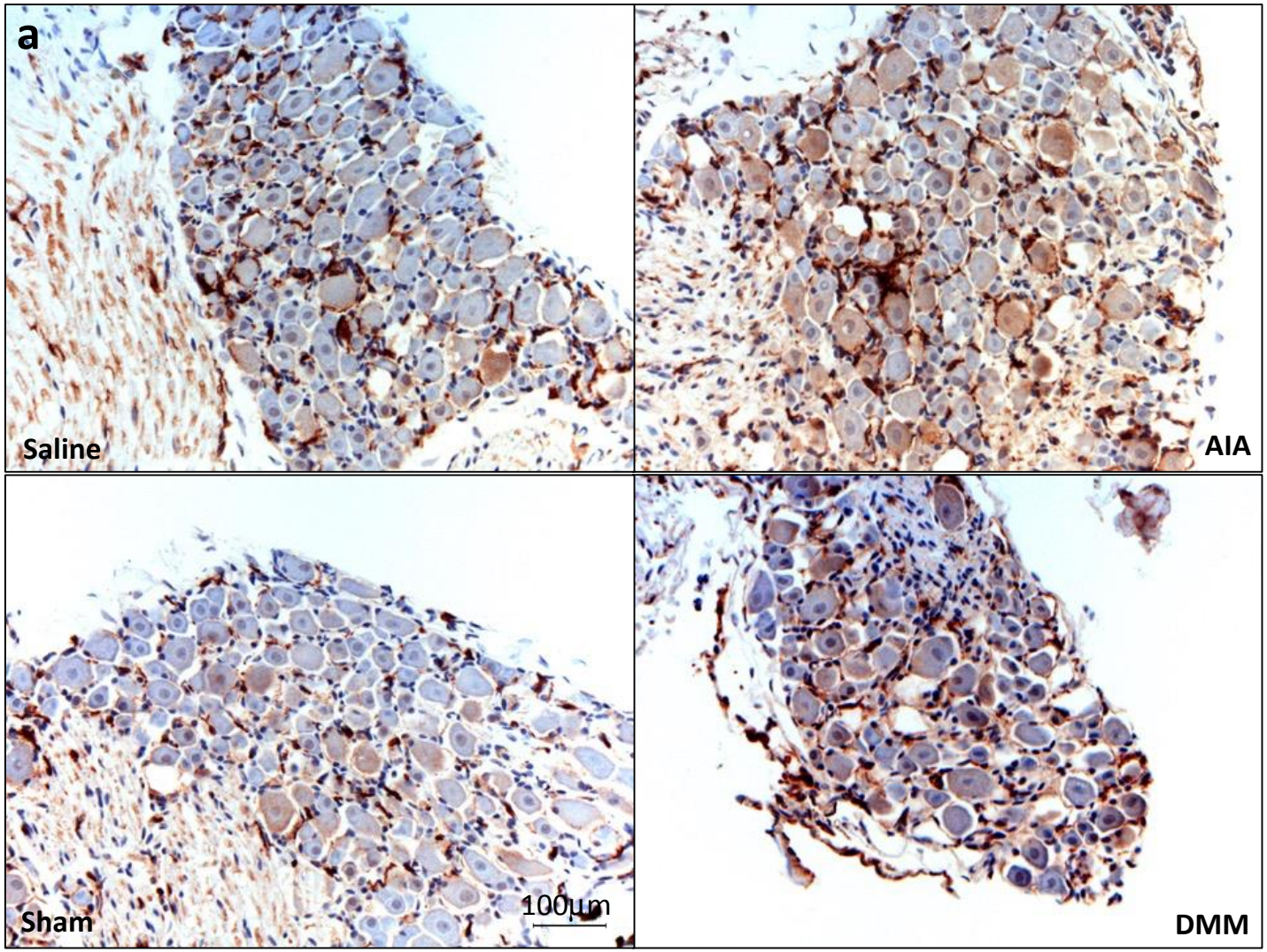

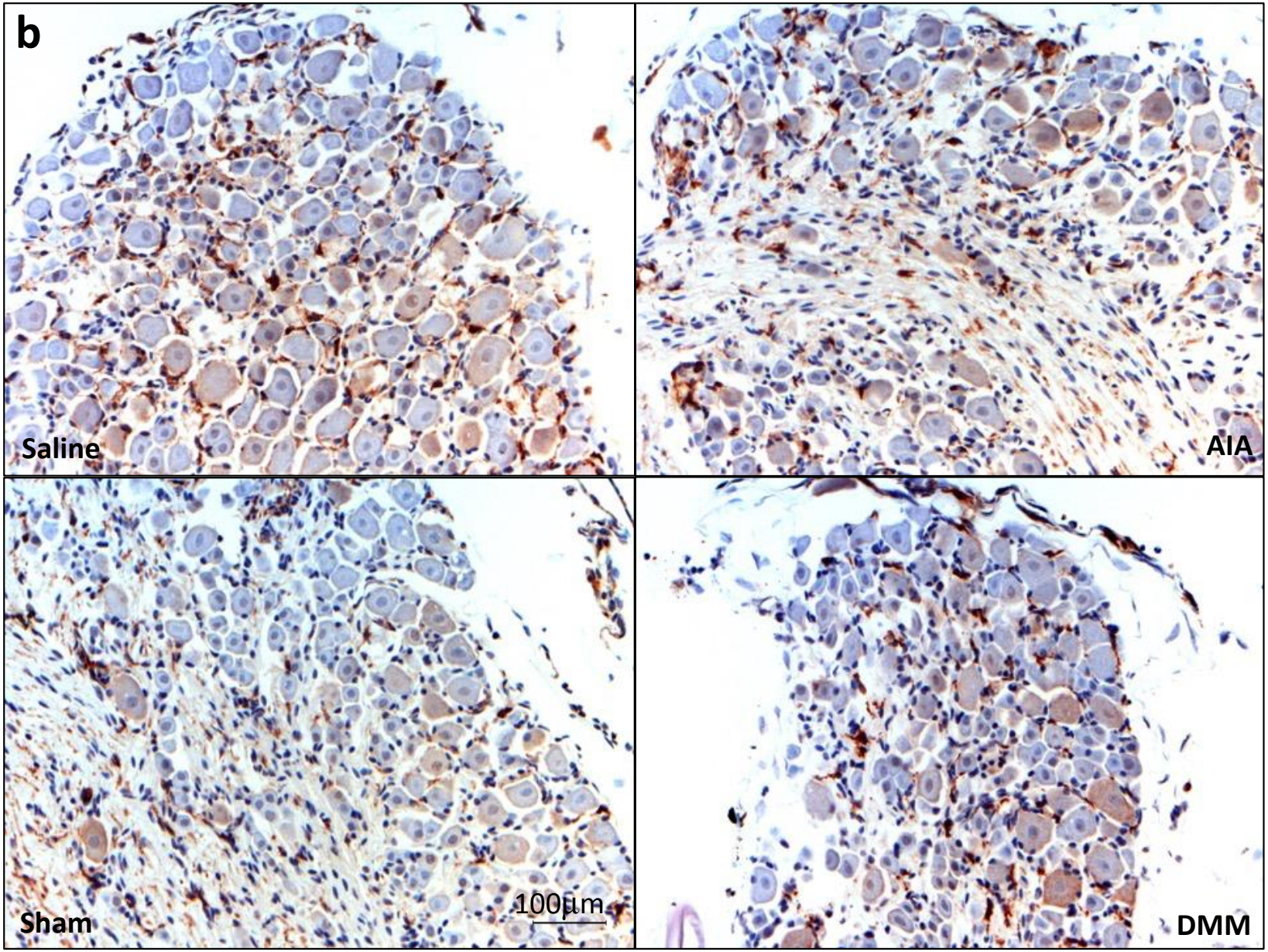
b
Saline
AIA
Sham
100μm
DMM

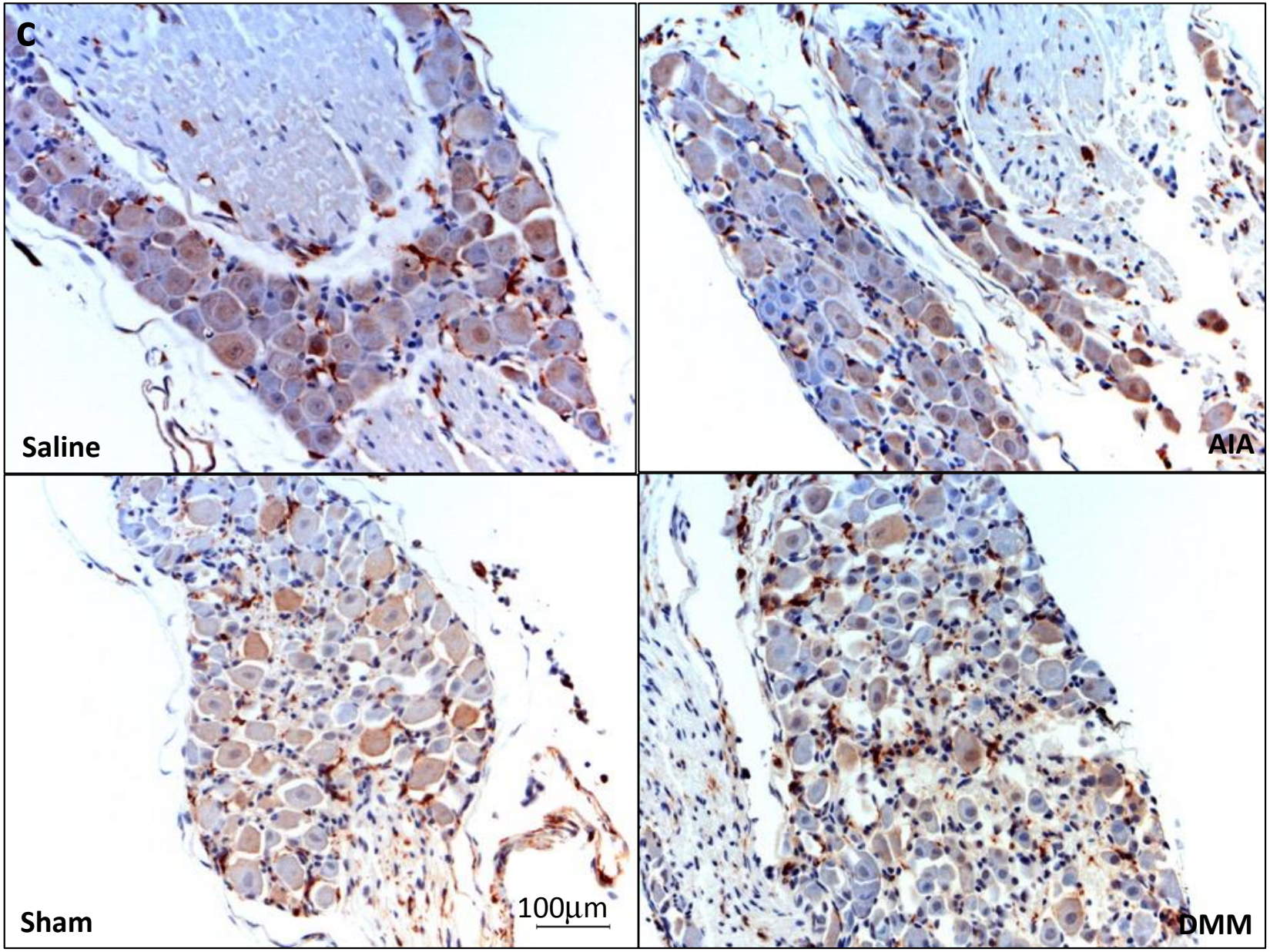
C
Saline
AIA
Sham
100µm
DMM

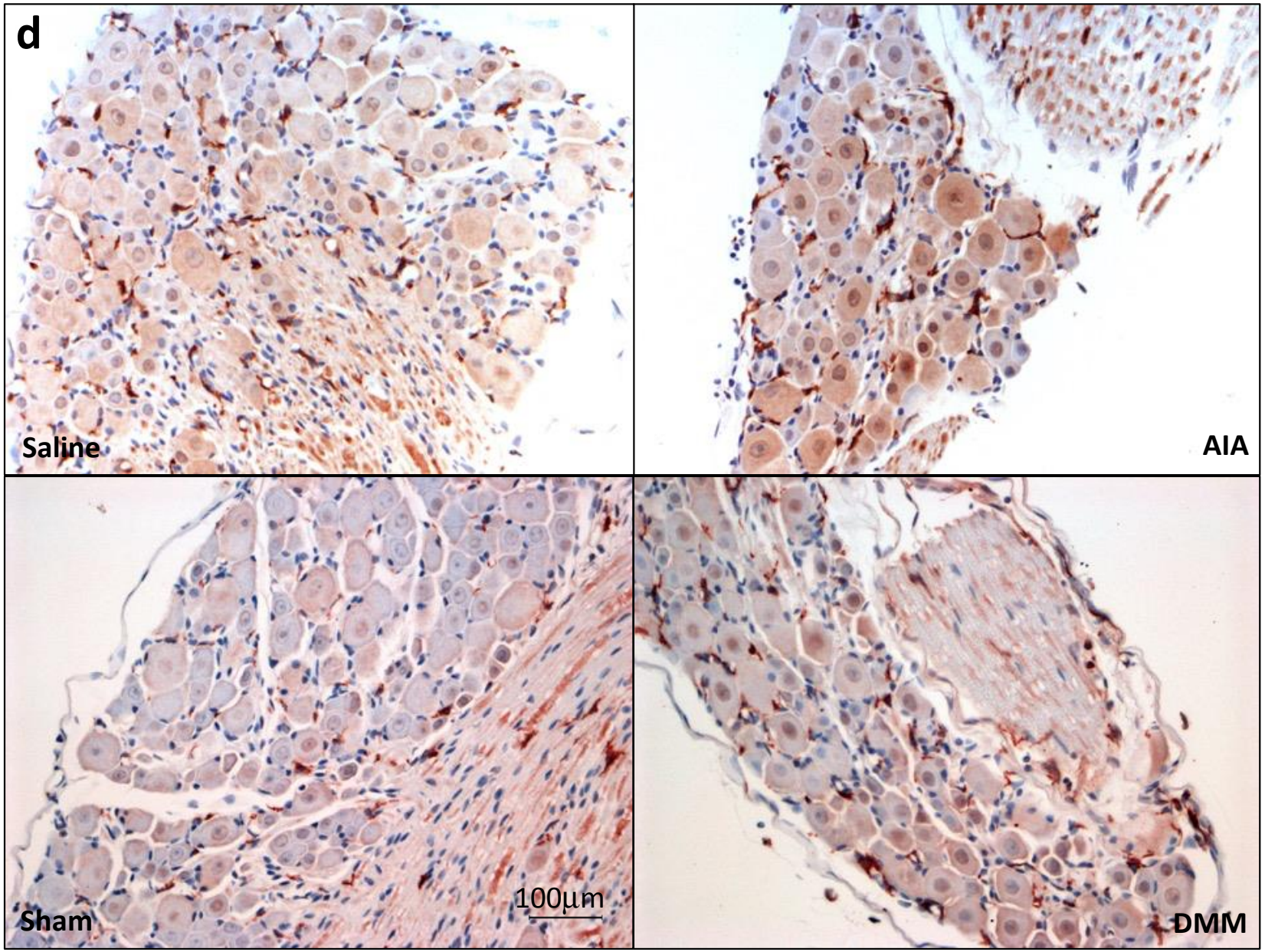
d
Saline
AIA
Sham
100µm
DMM

Figure II. MCP-1 production in conditioned media

Levels of MCP-1, expressed relative to total protein in conditioned media, L3-L45 DRG (pooled from 4 mice) in DMM, Sham, AIA, Saline-injected and control (untreated) mice at week 1, 4, 8 and 16 post arthritis induction. Values are presented graphically as a scatter plot (mean and SEM)

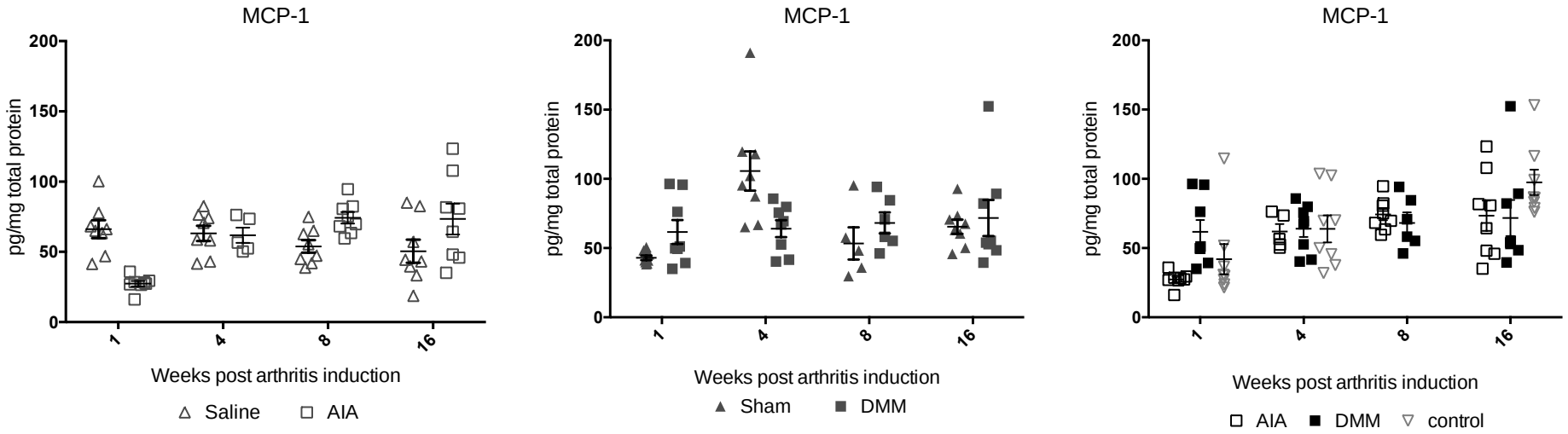

References:

1. Vos T, Flaxman AD, Naghavi M, Lozano R, Michaud C, Ezzati M, et al. Years lived with disability (YLDs) for 1160 sequelae of 289 diseases and injuries 1990-2010: a systematic analysis for the Global Burden of Disease Study 2010. Lancet. 2012;380(9859):2163-96.
2. Cross M, Smith E, Hoy D, Nolte S, Ackerman I, Fransen M, et al. The global burden of hip and knee osteoarthritis: estimates from the Global Burden of Disease 2010 study. Ann Rheum Dis. 2014;73(7):1323-30.
3. Neogi T. The epidemiology and impact of pain in osteoarthritis. Osteoarthritis Cartilage. 2013;21(9):1145-53.
4. NHS. National Health Survey: First Results (2014-15). Australian Bureau of Statistics, Canberra; 2015. Contract No.: 4364.0.55.001.
5. AccessEconomics. Painful Realities: The economic impact of arthritis in Australia. 2007.
6. ArthritisAustralia. The Voice of Arthritis 2011 Survey. 2011.
7. Henderson JV, Harrison CM, Britt HC, Bayram CF, Miller GC. Prevalence, causes, severity, impact, and management of chronic pain in Australian general practice patients. Pain medicine (Malden, Mass). 2013;14(9):1346-61.
8. Hawker GA, Stewart L, French MR, Cibere J, Jordan JM, March L, et al. Understanding the pain experience in hip and knee osteoarthritis--an OARSI/OMERACT initiative. Osteoarthritis Cartilage. 2008;16(4):415-22.
9. Chen A, Gupte C, Akhtar K, Smith P, Cobb J. The Global Economic Cost of Osteoarthritis: How the UK Compares. Arthritis. 2012;2012:698709.
10. Hiligsmann M, Cooper C, Arden N, Boers M, Branco JC, Luisa Brandi M, et al. Health economics in the field of osteoarthritis: an expert's consensus paper from the European Society for Clinical and Economic Aspects of Osteoporosis and Osteoarthritis (ESCEO). Semin Arthritis Rheum. 2013;43(3):303-13.
11. Zhang W, Nuki G, Moskowitz RW, Abramson S, Altman RD, Arden NK, et al. OARSI recommendations for the management of hip and knee osteoarthritis: part III: Changes in evidence following systematic cumulative update of research published through January 2009. Osteoarthritis and cartilage / OARS, Osteoarthritis Research Society. 2010;18(4):476-99.
12. Wylde V, Hewlett S, Learmonth ID, Dieppe P. Persistent pain after joint replacement: prevalence, sensory qualities, and postoperative determinants. Pain. 2011;152(3):566-72.
13. McAlindon TE, Bannuru RR, Sullivan MC, Arden NK, Berenbaum F, Bierma-Zeinstra SM, et al. OARSI guidelines for the non-surgical management of knee osteoarthritis. Osteoarthritis Cartilage. 2014;22(3):363-88.
14. Hardingham TE, Fosang AJ. The structure of aggrecan and its turnover in cartilage. J Rheumatol Suppl. 1995;43:86-90.
15. Cohen NP, Foster RJ, Mow VC. Composition and dynamics of articular cartilage: structure, function, and maintaining healthy state. The Journal of orthopaedic and sports physical therapy. 1998;28(4):203-15.
16. Poole CA. Articular cartilage chondrons: form, function and failure. Journal of anatomy. 1997;191 (Pt 1):1-13.
17. Kempson GE, Freeman MA, Swanson SA. Tensile properties of articular cartilage. Nature. 1968;220(5172):1127-8.

18. Murphy G, Knauper V, Atkinson S, Butler G, English W, Hutton M, et al. Matrix metalloproteinases in arthritic disease. Arthritis Res. 2002;4 Suppl 3:S39-49.
19. Fosang AJ, Last K, Maciewicz RA. Aggrecan is degraded by matrix metalloproteinases in human arthritis. Evidence that matrix metalloproteinase and aggrecanase activities can be independent. J Clin Invest. 1996;98(10):2292-9.
20. Stanton H, Melrose J, Little CB, Fosang AJ. Proteoglycan degradation by the ADAMTS family of proteinases. Biochimica et biophysica acta. 2011;1812(12):1616-29.
21. Tortorella MD, Burn TC, Pratta MA, Abbaszade I, Hollis JM, Liu R, et al. Purification and cloning of aggrecanase-1: a member of the ADAMTS family of proteins. Science (New York, NY). 1999;284(5420):1664-6.
22. Abbaszade I, Liu RQ, Yang F, Rosenfeld SA, Ross OH, Link JR, et al. Cloning and characterization of ADAMTS11, an aggrecanase from the ADAMTS family. J Biol Chem. 1999;274(33):23443-50.
23. Little CB, Hughes CE, Curtis CL, Jones SA, Caterson B, Flannery CR. Cyclosporin A inhibition of aggrecanase-mediated proteoglycan catabolism in articular cartilage. Arthritis Rheum. 2002;46(1):124-9.
24. Bau B, Gebhard PM, Haag J, Knorr T, Bartnik E, Aigner T. Relative messenger RNA expression profiling of collagenases and aggrecanases in human articular chondrocytes in vivo and in vitro. Arthritis Rheum. 2002;46(10):2648-57.
25. Glasson SS, Askew R, Sheppard B, Carito BA, Blanchet T, Ma H-L, et al. Characterization of and osteoarthritis susceptibility in ADAMTS-4-knockout mice. Arthritis Rheum. 2004;50(8):2547-58.
26. Glasson SS, Askew R, Sheppard B, Carito B, Blanchet T, Ma H-L, et al. Deletion of active ADAMTS5 prevents cartilage degradation in a murine model of osteoarthritis. Nature. 2005;434(7033):644-8.
27. Stanton H, Rogerson FM, East CJ, Golub SB, Lawlor KE, Meeker CT, et al. ADAMTS5 is the major aggrecanase in mouse cartilage in vivo and in vitro. Nature. 2005;434(7033):648-52.
28. Majumdar MK, Askew R, Schelling S, Stedman N, Blanchet T, Hopkins B, et al. Double-knockout of ADAMTS-4 and ADAMTS-5 in mice results in physiologically normal animals and prevents the progression of osteoarthritis. Arthritis Rheum. 2007;56(11):3670-4.
29. Zhen EY, Brittain IJ, Laska DA, Mitchell PG, Sumer EU, Karsdal MA, et al. Characterization of metalloprotease cleavage products of human articular cartilage. Arthritis Rheum. 2008;58(8):2420-31.
30. Rogerson FM, Stanton H, East CJ, Golub SB, Tutolo L, Farmer PJ, et al. Evidence of a novel aggrecan-degrading activity in cartilage: Studies of mice deficient in both ADAMTS-4 and ADAMTS-5. Arthritis Rheum. 2008;58(6):1664-73.
31. Fosang AJ, Rogerson FM, East CJ, Stanton H. ADAMTS-5: the story so far. European cells & materials. 2008;15:11-26.
32. Borden P, Heller RA. Transcriptional control of matrix metalloproteinases and the tissue inhibitors of matrix metalloproteinases. Crit Rev Eukaryot Gene Expr. 1997;7(1-2):159-78.
33. Benbow U, Brinckerhoff CE. The AP-1 site and MMP gene regulation: what is all the fuss about? Matrix Biol. 1997;15(8-9):519-26.
34. McCulloch DR, Goff CL, Bhatt S, Dixon LJ, Sandy JD, Apte SS. Adamts5, the gene encoding a proteoglycan-degrading metalloprotease, is expressed by specific

cell lineages during mouse embryonic development and in adult tissues. Gene Expr Patterns. 2009;9(5):314-23.
35. Helminen HJ, Kiraly K, Pelttari A, Tammi MI, Vandenberg P, Pereira R, et al. An inbred line of transgenic mice expressing an internally deleted gene for type II procollagen (COL2A1). Young mice have a variable phenotype of a chondrodysplasia and older mice have osteoarthritic changes in joints. J Clin Invest. 1993;92(2):582-95.
36. Stoop R, van der Kraan PM, Buma P, Hollander AP, Poole AR, van den Berg WB. Denaturation of type II collagen in articular cartilage in experimental murine arthritis. Evidence for collagen degradation in both reversible and irreversible cartilage damage. J Pathol. 1999;188(3):329-37.
37. Maroudas AI. Balance between swelling pressure and collagen tension in normal and degenerate cartilage. Nature. 1976;260(5554):808-9.
38. Sah RL, Yang AS, Chen AC, Hant JJ, Halili RB, Yoshioka M, et al. Physical properties of rabbit articular cartilage after transection of the anterior cruciate ligament. J Orthop Res. 1997;15(2):197-203.
39. Chayen J, Bitensky L, Chambers MG. Modulation of murine osteoarthritis. Cell biochemistry and function. 1996;14(1):57-61.
40. Stoop R, van der Kraan PM, Buma P, Hollander AP, Billinghurst RC, Poole AR, et al. Type II collagen degradation in spontaneous osteoarthritis in C57Bl/6 and BALB/c mice. Arthritis Rheum. 1999;42(11):2381-9.
41. Caterson B, Flannery CR, Hughes CE, Little CB. Mechanisms involved in cartilage proteoglycan catabolism. Matrix Biol. 2000;19(4):333-44.
42. Mitchell PG, Magna HA, Reeves LM, Lopresti-Morrow LL, Yocum SA, Rosner PJ, et al. Cloning, expression, and type II collagenolytic activity of matrix metalloproteinase-13 from human osteoarthritic cartilage. J Clin Invest. 1996;97(3):761-8.
43. Billinghurst RC, Dahlberg L, Ionescu M, Reiner A, Bourne R, Rorabeck C, et al. Enhanced cleavage of type II collagen by collagenases in osteoarthritic articular cartilage. J Clin Invest. 1997;99(7):1534-45.
44. Neuhold LA, Killar L, Zhao W, Sung ML, Warner L, Kulik J, et al. Postnatal expression in hyaline cartilage of constitutively active human collagenase-3 (MMP-13) induces osteoarthritis in mice. J Clin Invest. 2001;107(1):35-44.
45. Takaishi H, Kimura T, Dalal S, Okada Y, D'Armiento J. Joint diseases and matrix metalloproteinases: a role for MMP-13. Current pharmaceutical biotechnology. 2008;9(1):47-54.
46. Kosaki N, Takaishi H, Kamekura S, Kimura T, Okada Y, Minqi L, et al. Impaired bone fracture healing in matrix metalloproteinase-13 deficient mice. Biochemical and biophysical research communications. 2007;354(4):846-51.
47. Little CB, Barai A, Burkhardt D, Smith SM, Fosang AJ, Werb Z, et al. Matrix metalloproteinase 13-deficient mice are resistant to osteoarthritic cartilage erosion but not chondrocyte hypertrophy or osteophyte development. Arthritis and rheumatism. 2009;60(12):3723-33.
48. Miller RE, Lu Y, Tortorella MD, Malfait AM. Genetically Engineered Mouse Models Reveal the Importance of Proteases as Osteoarthritis Drug Targets. Current rheumatology reports. 2013;15(8):350.
49. Hayami T, Zhuo Y, Wesolowski GA, Pickarski M, Duong LT. Inhibition of cathepsin K reduces cartilage degeneration in the anterior cruciate ligament transection rabbit and murine models of osteoarthritis. Bone. 2012;50(6):1250-9.

50. Vinardell T, Dejica V, Poole AR, Mort JS, Richard H, Laverty S. Evidence to suggest that cathepsin K degrades articular cartilage in naturally occurring equine osteoarthritis. Osteoarthritis Cartilage. 2009;17(3):375-83.
51. Kozawa E, Nishida Y, Cheng XW, Urakawa H, Arai E, Futamura N, et al. Osteoarthritic change is delayed in a Ctsk-knockout mouse model of osteoarthritis. Arthritis Rheum. 2012;64(2):454-64.
52. Kozawa E, Cheng XW, Urakawa H, Arai E, Yamada Y, Kitamura S, et al. Increased expression and activation of cathepsin K in human osteoarthritic cartilage and synovial tissues. J Orthop Res. 2015.
53. Baker AH, Edwards DR, Murphy G. Metalloproteinase inhibitors: biological actions and therapeutic opportunities. Journal of cell science. 2002;115(Pt 19):3719-27.
54. Kashiwagi M, Tortorella M, Nagase H, Brew K. TIMP-3 is a potent inhibitor of aggrecanase 1 (ADAM-TS4) and aggrecanase 2 (ADAM-TS5). J Biol Chem. 2001;276(16):12501-4.
55. Sahebjam S, Khokha R, Mort JS. Increased collagen and aggrecan degradation with age in the joints of Timp3(-/-) mice. Arthritis Rheum. 2007;56(3):905-9.
56. Yu D, Liu F, Liu M, Zhao X, Wang X, Li Y, et al. The inhibition of subchondral bone lesions significantly reversed the weight-bearing deficit and the overexpression of CGRP in DRG neurons, GFAP and Iba-1 in the spinal dorsal horn in the monosodium iodoacetate induced model of osteoarthritis pain. PloS one. 2013;8(10):e77824.
57. Felson DT, Chaisson CE, Hill CL, Totterman SM, Gale ME, Skinner KM, et al. The association of bone marrow lesions with pain in knee osteoarthritis. Annals of internal medicine. 2001;134(7):541-9.
58. Hunter DJ, Conaghan PG. Imaging outcomes and their role in determining outcomes in osteoarthritis and rheumatoid arthritis. Current opinion in rheumatology. 2006;18(2):157-62.
59. Buckland-Wright C. Subchondral bone changes in hand and knee osteoarthritis detected by radiography. Osteoarthritis Cartilage. 2004;12 Suppl A:S10-9.
60. Goldring SR. Role of bone in osteoarthritis pathogenesis. Med Clin North Am. 2009;93(1):25-35, xv.
61. Karsdal MA, Bay-Jensen AC, Lories RJ, Abramson S, Spector T, Pastoureau P, et al. The coupling of bone and cartilage turnover in osteoarthritis: opportunities for bone antiresorptives and anabolics as potential treatments? Ann Rheum Dis. 2014;73(2):336-48.
62. Conaghan PG, Felson D, Gold G, Lohmander S, Totterman S, Altman R. MRI and non-cartilaginous structures in knee osteoarthritis. Osteoarthritis Cartilage. 2006;14 Suppl A:A87-94.
63. Roemer FW, Neogi T, Nevitt MC, Felson DT, Zhu Y, Zhang Y, et al. Subchondral bone marrow lesions are highly associated with, and predict subchondral bone attrition longitudinally: the MOST study. Osteoarthritis and cartilage / OARS, Osteoarthritis Research Society. 2010;18(1):47-53.
64. Neogi T, Felson D, Niu J, Lynch J, Nevitt M, Guermazi A, et al. Cartilage loss occurs in the same subregions as subchondral bone attrition: a within-knee subregion-matched approach from the Multicenter Osteoarthritis Study. Arthritis Rheum. 2009;61(11):1539-44.
65. Intema F, Thomas TP, Anderson DD, Elkins JM, Brown TD, Amendola A, et al. Subchondral bone remodeling is related to clinical improvement after joint

distraction in the treatment of ankle osteoarthritis. Osteoarthritis Cartilage. 2011;19(6):668-75.
66. Roemer FW, Guermazi A, Javaid MK, Lynch JA, Niu J, Zhang Y, et al. Change in MRI-detected subchondral bone marrow lesions is associated with cartilage loss: the MOST Study. A longitudinal multicentre study of knee osteoarthritis. Annals of the rheumatic diseases. 2009;68(9):1461-5.
67. Strassle BW, Mark L, Leventhal L, Piesla MJ, Jian Li X, Kennedy JD, et al. Inhibition of osteoclasts prevents cartilage loss and pain in a rat model of degenerative joint disease. Osteoarthritis Cartilage. 2010;18(10):1319-28.
68. Nettelbladt E, Sundblad L. Protein patterns in synovial fluid and serum in rheumatoid arthritis and osteoarthritis. Arthritis Rheum. 1959;2(2):144-51.
69. Soren A, Klein W, Huth F. Microscopic comparison of the synovial changes in posttraumatic synovitis and osteoarthritis. Clin Orthop Relat Res. 1976(121):191-5.
70. Scanzello CR, Goldring SR. The role of synovitis in osteoarthritis pathogenesis. Bone. 2012;51(2):249-57.
71. Roemer FW, Guermazi A, Felson DT, Niu J, Nevitt MC, Crema MD, et al. Presence of MRI-detected joint effusion and synovitis increases the risk of cartilage loss in knees without osteoarthritis at 30-month follow-up: the MOST study. Ann Rheum Dis. 2011;70(10):1804-9.
72. Ayral X, Pickering EH, Woodworth TG, Mackillop N, Dougados M. Synovitis: a potential predictive factor of structural progression of medial tibiofemoral knee osteoarthritis -- results of a 1 year longitudinal arthroscopic study in 422 patients. Osteoarthritis Cartilage. 2005;13(5):361-7.
73. Torres L, Dunlop DD, Peterfy C, Guermazi A, Prasad P, Hayes KW, et al. The relationship between specific tissue lesions and pain severity in persons with knee osteoarthritis. Osteoarthritis Cartilage. 2006;14(10):1033-40.
74. Baker K, Grainger A, Niu J, Clancy M, Guermazi A, Crema M, et al. Relation of synovitis to knee pain using contrast-enhanced MRIs. Annals of the rheumatic diseases. 2010;69(10):1779-83.
75. Sowers M, Karvonen-Gutierrez CA, Jacobson JA, Jiang Y, Yosef M. Associations of anatomical measures from MRI with radiographically defined knee osteoarthritis score, pain, and physical functioning. J Bone Joint Surg Am. 2011;93(3):241-51.
76. Sokolove J, Lepus CM. Role of inflammation in the pathogenesis of osteoarthritis: latest findings and interpretations. Therapeutic advances in musculoskeletal disease. 2013;5(2):77-94.
77. de Lange-Brokaar BJ, Ioan-Facsinay A, van Osch GJ, Zuurmond AM, Schoones J, Toes RE, et al. Synovial inflammation, immune cells and their cytokines in osteoarthritis: a review. Osteoarthritis Cartilage. 2012;20(12):1484-99.
78. Kawai T, Akira S. The role of pattern-recognition receptors in innate immunity: update on Toll-like receptors. Nature immunology. 2010;11(5):373-84.
79. Termeer C, Benedix F, Sleeman J, Fieber C, Voith U, Ahrens T, et al. Oligosaccharides of Hyaluronan activate dendritic cells via toll-like receptor 4. J Exp Med. 2002;195(1):99-111.
80. Su SL, Tsai CD, Lee CH, Salter DM, Lee HS. Expression and regulation of Toll-like receptor 2 by IL-1beta and fibronectin fragments in human articular chondrocytes. Osteoarthritis Cartilage. 2005;13(10):879-86.
81. Sohn DH, Sokolove J, Sharpe O, Erhart JC, Chandra PE, Lahey LJ, et al. Plasma proteins present in osteoarthritic synovial fluid can stimulate cytokine production via Toll-like receptor 4. Arthritis Res Ther. 2012;14(1):R7.

82. Wang Q, Rozelle AL, Lepus CM, Scanzello CR, Song JJ, Larsen DM, et al. Identification of a central role for complement in osteoarthritis. Nat Med. 2011;17(12):1674-9.
83. Bondeson J, Wainwright SD, Lauder S, Amos N, Hughes CE. The role of synovial macrophages and macrophage-produced cytokines in driving aggrecanases, matrix metalloproteinases, and other destructive and inflammatory responses in osteoarthritis. Arthritis Res Ther. 2006;8(6):R187.
84. Zhao XY, Yang ZB, Zhang ZJ, Zhang ZQ, Kang Y, Huang GX, et al. CCL3 serves as a potential plasma biomarker in knee degeneration (osteoarthritis). Osteoarthritis Cartilage. 2015;23(8):1405-11.
85. Zhou Y, Chen J, Yang G. Serum and synovial fluid levels of CCL18 are correlated with radiographic grading of knee osteoarthritis. Medical science monitor : international medical journal of experimental and clinical research. 2015;21:840-4.
86. Nair A, Gan J, Bush-Joseph C, Verma N, Tetreault MW, Saha K, et al. Synovial chemokine expression and relationship with knee symptoms in patients with meniscal tears. Osteoarthritis Cartilage. 2015;23(7):1158-64.
87. Alaaeddine N, Antoniou J, Moussa M, Hilal G, Kreichaty G, Ghanem I, et al. The chemokine CCL20 induces proinflammatory and matrix degradative responses in cartilage. Inflamm Res. 2015;64(9):721-31.
88. Wojdasiewicz P, Poniatowski LA, Szukiewicz D. The role of inflammatory and anti-inflammatory cytokines in the pathogenesis of osteoarthritis. Mediators of inflammation. 2014;2014:561459.
89. Miller RE, Miller RJ, Malfait AM. Osteoarthritis joint pain: The cytokine connection. Cytokine. 2014.
90. Lane NE, Brandt K, Hawker G, Peeva E, Schreyer E, Tsuji W, et al. OARSI-FDA initiative: defining the disease state of osteoarthritis. Osteoarthritis and cartilage / OARS, Osteoarthritis Research Society. 2011;19(5):478-82.
91. Sandell LJ. Etiology of osteoarthritis: genetics and synovial joint development. Nat Rev Rheumatol. 2012;8(2):77-89.
92. Valdes AM, Spector TD. The clinical relevance of genetic susceptibility to osteoarthritis. Best practice & research Clinical rheumatology. 2010;24(1):3-14.
93. Block JA, Shakoor N. The biomechanics of osteoarthritis: implications for therapy. Current rheumatology reports. 2009;11(1):15-22.
94. Shin D. Association between metabolic syndrome, radiographic knee osteoarthritis, and intensity of knee pain: results of a national survey. The Journal of clinical endocrinology and metabolism. 2014:jc20141043.
95. Visser AW, de Mutsert R, Loef M, le Cessie S, den Heijer M, Bloem JL, et al. The role of fat mass and skeletal muscle mass in knee osteoarthritis is different for men and women: the NEO study. Osteoarthritis Cartilage. 2014;22(2):197-202.
96. Sacitharan PK, Snelling SJ, Edwards JR. Aging mechanisms in arthritic disease. Discovery medicine. 2012;14(78):345-52.
97. Lee R, Kean WF. Obesity and knee osteoarthritis. Inflammopharmacology. 2012;20(2):53-8.
98. Visser AW, de Mutsert R, le Cessie S, den Heijer M, Rosendaal FR, Kloppenburg M. The relative contribution of mechanical stress and systemic processes in different types of osteoarthritis: the NEO study. Ann Rheum Dis. 2014.
99. Herrero-Beaumont G, Roman-Blas JA, Castaneda S, Jimenez SA. Primary osteoarthritis no longer primary: three subsets with distinct etiological, clinical, and therapeutic characteristics. Semin Arthritis Rheum. 2009;39(2):71-80.

100. Felson DT. Identifying different osteoarthritis phenotypes through epidemiology. Osteoarthritis and cartilage / OARS, Osteoarthritis Research Society. 2010;18(5):601-4.
101. Kinds MB, Marijnissen AC, Viergever MA, Emans PJ, Lafeber FP, Welsing PM. Identifying phenotypes of knee osteoarthritis by separate quantitative radiographic features may improve patient selection for more targeted treatment. J Rheumatol. 2013;40(6):891-902.
102. Nelson AE, Golightly YM, Renner JB, Schwartz TA, Kraus VB, Helmick CG, et al. Brief report: differences in multijoint symptomatic osteoarthritis phenotypes by race and sex: the Johnston County Osteoarthritis Project. Arthritis Rheum. 2013;65(2):373-7.
103. Cruz-Almeida Y, Sibille KT, Goodin BR, Ruiter M, Bartley EJ, Riley JL, et al. Racial and ethnic differences in older adults with knee osteoarthritis. Arthritis rheumatol. 2014.
104. Parmelee PA, Harralson TL, McPherron JA, DeCoster J, Schumacher HR. Pain, disability, and depression in osteoarthritis: effects of race and sex. Journal of aging and health. 2012;24(1):168-87.
105. Castaneda S, Roman-Blas JA, Largo R, Herrero-Beaumont G. Osteoarthritis: a progressive disease with changing phenotypes. Rheumatology (Oxford). 2014;53(1):1-3.
106. Conaghan PG. Osteoarthritis in 2012: Parallel evolution of OA phenotypes and therapies. Nat Rev Rheumatol. 2013;9(2):68-70.
107. Little CB, Ghosh P. Variation in proteoglycan metabolism by articular chondrocytes in different joint regions is determined by post-natal mechanical loading. Osteoarthritis Cartilage. 1997;5(1):49-62.
108. Flannery CR, Little CB, Hughes CE, Caterson B. Expression of ADAMTS homologues in articular cartilage. Biochemical and biophysical research communications. 1999;260(2):318-22.
109. Flannery CR, Little CB, Caterson B, Hughes CE. Effects of culture conditions and exposure to catabolic stimulators (IL-1 and retinoic acid) on the expression of matrix metalloproteinases (MMPs) and disintegrin metalloproteinases (ADAMs) by articular cartilage chondrocytes. Matrix Biol. 1999;18(3):225-37.
110. Flannery CR, Little CB, Hughes CE, Caterson B. Expression and activity of articular cartilage hyaluronidases. Biochemical and biophysical research communications. 1998;251(3):824-9.
111. Fosang AJ, Stanton H, Little CB, Atley LM. Neoepitopes as biomarkers of cartilage catabolism. Inflamm Res. 2003;52(7):277-82.
112. Caterson B, Flannery CR, Hughes CE, Little CB. Mechanisms of proteoglycan metabolism that lead to cartilage destruction in the pathogenesis of arthritis. Drugs Today (Barc). 1999;35(4-5):397-402.
113. Little CB, Flannery CR, Hughes CE, Goodship A, Caterson B. Cytokine induced metalloproteinase expression and activity does not correlate with focal susceptibility of articular cartilage to degeneration. Osteoarthritis Cartilage. 2005;13(2):162-70.
114. Goldring MB, Goldring SR. Osteoarthritis. Journal of cellular physiology. 2007;213(3):626-34.
115. Hardingham T. Extracellular matrix and pathogenic mechanisms in osteoarthritis. Current rheumatology reports. 2008;10(1):30-6.
116. Lee P, Rooney PJ, Sturrock RD, Kennedy AC, Dick WC. The etiology and pathogenesis of osteoarthrosis: a review. Semin Arthritis Rheum. 1974;3(3):189-218.

117. Stephens RW, Ghosh P, Taylor TK. The pathogenesis of osteoarthrosis. Medical hypotheses. 1979;5(7):809-16.
118. Howell DS, Sapolsky AI, Pita JC, Woessner JF. The pathogenesis of osteoarthritis. Semin Arthritis Rheum. 1976;4(4):365-83.
119. Hunziker EB. Articular cartilage repair: basic science and clinical progress. A review of the current status and prospects. Osteoarthritis Cartilage. 2002;10(6):432-63.
120. Pitsillides AA, Beier F. Cartilage biology in osteoarthritis--lessons from developmental biology. Nat Rev Rheumatol. 2011;7(11):654-63.
121. van den Berg WB. Osteoarthritis year 2010 in review: pathomechanisms. Osteoarthritis Cartilage. 2011;19(4):338-41.
122. Little CB, Fosang AJ. Is cartilage matrix breakdown an appropriate therapeutic target in osteoarthritis--insights from studies of aggrecan and collagen proteolysis? Current drug targets. 2010;11(5):561-75.
123. Schmitz N, Kraus VB, Aigner T. Targets to tackle--the pathophysiology of the disease. Current drug targets. 2010;11(5):521-7.
124. Tortorella MD, Malfait AM. Will the real aggrecanase(s) step up: evaluating the criteria that define aggrecanase activity in osteoarthritis. Current pharmaceutical biotechnology. 2008;9(1):16-23.
125. Tortorella MD, Malfait F, Barve RA, Shieh H-S, Malfait A-M. A review of the ADAMTS family, pharmaceutical targets of the future. Curr Pharm Des. 2009;15(20):2359-74.
126. Fosang AJ, Little CB. Drug insight: aggrecanases as therapeutic targets for osteoarthritis. Nature clinical practice Rheumatology. 2008;4(8):420-7.
127. Miller RE, Lu Y, Tortorella MD, Malfait A-M. Genetically Engineered Mouse Models Reveal the Importance of Proteases as Osteoarthritis Drug Targets. Current rheumatology reports. 2013;15(8):350.
128. Malfait AM, Little CB. On the predictive utility of animal models of osteoarthritis. Arthritis Res Ther. 2015;17:225.
129. Karsdal MA, Byrjalsen I, Alexandersen P, Bihlet A, Andersen JR, Riis BJ, et al. Treatment of Symptomatic Knee Osteoarthritis with Oral Salmon Calcitonin: Results from two Phase 3 Trials. Osteoarthritis Cartilage. 2015.
130. Nielsen RH, Bay-Jensen AC, Byrjalsen I, Karsdal MA. Oral salmon calcitonin reduces cartilage and bone pathology in an osteoarthritis rat model with increased subchondral bone turnover. Osteoarthritis Cartilage. 2011;19(4):466-73.
131. El Hajjaji H, Williams JM, Devogelaer JP, Lenz ME, Thonar EJ, Manicourt DH. Treatment with calcitonin prevents the net loss of collagen, hyaluronan and proteoglycan aggregates from cartilage in the early stages of canine experimental osteoarthritis. Osteoarthritis Cartilage. 2004;12(11):904-11.
132. Sondergaard BC, Catala-Lehnen P, Huebner AK, Bay-Jensen AC, Schinke T, Henriksen K, et al. Mice over-expressing salmon calcitonin have strongly attenuated osteoarthritic histopathological changes after destabilization of the medial meniscus. Osteoarthritis Cartilage. 2012;20(2):136-43.
133. Lohmander LS, Hellot S, Dreher D, Krantz EF, Kruger DS, Guermazi A, et al. Intraarticular sprifermin (recombinant human fibroblast growth factor 18) in knee osteoarthritis: a randomized, double-blind, placebo-controlled trial. Arthritis Rheumatol. 2014;66(7):1820-31.
134. Moore EE, Bendele AM, Thompson DL, Littau A, Waggie KS, Reardon B, et al. Fibroblast growth factor-18 stimulates chondrogenesis and cartilage repair in a rat model of injury-induced osteoarthritis. Osteoarthritis Cartilage. 2005;13(7):623-31.

135. Reginster JY, Badurski J, Bellamy N, Bensen W, Chapurlat R, Chevalier X, et al. Efficacy and safety of strontium ranelate in the treatment of knee osteoarthritis: results of a double-blind, randomised placebo-controlled trial. Ann Rheum Dis. 2013;72(2):179-86.
136. Pelletier JP, Kapoor M, Fahmi H, Lajeunesse D, Blesius A, Maillet J, et al. Strontium ranelate reduces the progression of experimental dog osteoarthritis by inhibiting the expression of key proteases in cartilage and of IL-1beta in the synovium. Ann Rheum Dis. 2013;72(2):250-7.
137. Yu DG, Ding HF, Mao YQ, Liu M, Yu B, Zhao X, et al. Strontium ranelate reduces cartilage degeneration and subchondral bone remodeling in rat osteoarthritis model. Acta Pharmacol Sin. 2013;34(3):393-402.
138. Hellio le Graverand MP, Clemmer RS, Redifer P, Brunell RM, Hayes CW, Brandt KD, et al. A 2-year randomised, double-blind, placebo-controlled, multicentre study of oral selective iNOS inhibitor, cindunistat (SD-6010), in patients with symptomatic osteoarthritis of the knee. Ann Rheum Dis. 2013;72(2):187-95.
139. Pelletier JP, Jovanovic D, Fernandes JC, Manning P, Connor JR, Currie MG, et al. Reduced progression of experimental osteoarthritis in vivo by selective inhibition of inducible nitric oxide synthase. Arthritis Rheum. 1998;41(7):1275-86.
140. Pelletier J, Jovanovic D, Fernandes JC, Manning P, Connor JR, Currie MG, et al. Reduction in the structural changes of experimental osteoarthritis by a nitric oxide inhibitor. Osteoarthritis Cartilage. 1999;7(4):416-8.
141. van den Berg WB, van de Loo F, Joosten LA, Arntz OJ. Animal models of arthritis in NOS2-deficient mice. Osteoarthritis Cartilage. 1999;7(4):413-5.
142. Connor J, Rogers K, Sunyer T, Hellio le Graverand MP, Manning P, . Efficacy of the selective inducible nitric oxide synthase inhibitor sd-6010 in nonclinical inflammatory, neuropathic, and osteoarthritis pain. Osteoarthritis Cartilage. 2012;20(Suupl 1):S64-S5.
143. Laslett LL, Dore DA, Quinn SJ, Boon P, Ryan E, Winzenberg TM, et al. Zoledronic acid reduces knee pain and bone marrow lesions over 1 year: a randomised controlled trial. Ann Rheum Dis. 2012;71(8):1322-8.
144. Strassle BW, Mark L, Leventhal L, Piesla MJ, Jian Li X, Kennedy JD, et al. Inhibition of osteoclasts prevents cartilage loss and pain in a rat model of degenerative joint disease. Osteoarthritis Cartilage. 2010;18(10):1319-28.
145. Yu DG, Yu B, Mao YQ, Zhao X, Wang XQ, Ding HF, et al. Efficacy of zoledronic acid in treatment of teoarthritis is dependent on the disease progression stage in rat medial meniscal tear model. Acta Pharmacol Sin. 2012;33(7):924-34.
146. McAlindon T, LaValley M, Schneider E, Nuite M, Lee JY, Price LL, et al. Effect of vitamin D supplementation on progression of knee pain and cartilage volume loss in patients with symptomatic osteoarthritis: a randomized controlled trial. Jama. 2013;309(2):155-62.
147. Castillo EC, Hernandez-Cueto MA, Vega-Lopez MA, Lavalle C, Kouri JB, Ortiz-Navarrete V. Effects of Vitamin D Supplementation during the Induction and Progression of Osteoarthritis in a Rat Model. Evid Based Complement Alternat Med. 2012;2012:156563.
148. Jefferies D, Farquharson C, Thomson J, Smith W, Seawright E, McCormack H, et al. Differences in metabolic parameters and gene expression related to osteochondrosis/osteoarthrosis in pigs fed 25-hydroxyvitamin D3. Vet Res. 2002;33(4):383-96.
149. Raynauld JP, Martel-Pelletier J, Bias P, Laufer S, Haraoui B, Choquette D, et al. Protective effects of licofelone, a 5-lipoxygenase and cyclo-oxygenase inhibitor,

versus naproxen on cartilage loss in knee osteoarthritis: a first multicentre clinical trial using quantitative MRI. Ann Rheum Dis. 2009;68(6):938-47.
150. Moreau M, Boileau C, Martel-Pelletier J, Brunet J, Laufer S, Pelletier JP. Licofelone reduces progression of structural changes in a canine model of osteoarthritis under curative conditions: effect on protease expression and activity. J Rheumatol. 2006;33(6):1176-83.
151. Spector TD, Conaghan PG, Buckland-Wright JC, Garnero P, Cline GA, Beary JF, et al. Effect of risedronate on joint structure and symptoms of knee osteoarthritis: results of the BRISK randomized, controlled trial [ISRCTN01928173]. Arthritis Res Ther. 2005;7(3):R625-33.
152. Bingham CO, 3rd, Buckland-Wright JC, Garnero P, Cohen SB, Dougados M, Adami S, et al. Risedronate decreases biochemical markers of cartilage degradation but does not decrease symptoms or slow radiographic progression in patients with medial compartment osteoarthritis of the knee: results of the two-year multinational knee osteoarthritis structural arthritis study. Arthritis Rheum. 2006;54(11):3494-507.
153. Buckland-Wright JC, Messent EA, Bingham CO, 3rd, Ward RJ, Tonkin C. A 2 yr longitudinal radiographic study examining the effect of a bisphosphonate (risedronate) upon subchondral bone loss in osteoarthritic knee patients. Rheumatology (Oxford). 2007;46(2):257-64.
154. Thomsen JS, Straarup TS, Danielsen CC, Oxlund H, Bruel A. No effect of risedronate on articular cartilage damage in the Dunkin Hartley guinea pig model of osteoarthritis. Scand J Rheumatol. 2013;42(5):408-16.
155. Permuy M, Guede D, Lopez-Pena M, Munoz F, Gonzalez-Cantalapiedra A, Caeiro JR. Effects of glucosamine and risedronate alone or in combination in an experimental rabbit model of osteoarthritis. BMC Vet Res. 2014;10:97.
156. Krzeski P, Buckland-Wright C, Balint G, Cline GA, Stoner K, Lyon R, et al. Development of musculoskeletal toxicity without clear benefit after administration of PG-116800, a matrix metalloproteinase inhibitor, to patients with knee osteoarthritis: a randomized, 12-month, double-blind, placebo-controlled study. Arthritis Res Ther. 2007;9(5):R109.
157. Janusz MJ, Hookfin EB, Heitmeyer SA, Woessner JF, Freemont AJ, Hoyland JA, et al. Moderation of iodoacetate-induced experimental osteoarthritis in rats by matrix metalloproteinase inhibitors. Osteoarthritis Cartilage. 2001;9(8):751-60.
158. Brewster M, Lewis EJ, Wilson KL, Greenham AK, Bottomley KM. Ro 32-3555, an orally active collagenase selective inhibitor, prevents structural damage in the STR/ORT mouse model of osteoarthritis. Arthritis Rheum. 1998;41(9):1639-44.
159. Brandt KD, Mazzuca SA, Katz BP, Lane KA, Buckwalter KA, Yocum DE, et al. Effects of doxycycline on progression of osteoarthritis: results of a randomized, placebo-controlled, double-blind trial. Arthritis Rheum. 2005;52(7):2015-25.
160. Yu LP, Jr., Smith GN, Jr., Brandt KD, Myers SL, O'Connor BL, Brandt DA. Reduction of the severity of canine osteoarthritis by prophylactic treatment with oral doxycycline. Arthritis Rheum. 1992;35(10):1150-9.
161. Bowyer J, Heapy CG, Flannelly JK, Waterton JC, Maciewicz RA. Evaluation of a magnetic resonance biomarker of osteoarthritis disease progression: doxycycline slows tibial cartilage loss in the Dunkin Hartley guinea pig. Int J Exp Pathol. 2009;90(2):174-81.
162. Silva J, Fanning P, O'Connell S, Mason-Savas A, Walcott M, Hays P, et al. Effects of Disease-modifying Osteoarthritis Drugs in an in-vivo Animal Model. J Orthopedic Research Society. 2009;abstract.

163. von Hehn CA, Baron R, Woolf CJ. Deconstructing the neuropathic pain phenotype to reveal neural mechanisms. Neuron. 2012;73(4):638-52.
164. Mogil JS, Ritchie J, Sotocinal SG, Smith SB, Croteau S, Levitin DJ, et al. Screening for pain phenotypes: analysis of three congenic mouse strains on a battery of nine nociceptive assays. Pain. 2006;126(1-3):24-34.
165. Pouli N, Das Nair R, Lincoln NB, Walsh D. The experience of living with knee osteoarthritis: exploring illness and treatment beliefs through thematic analysis. Disability and rehabilitation. 2014;36(7):600-7.
166. Englund M. The role of biomechanics in the initiation and progression of OA of the knee. Best practice & research Clinical rheumatology. 2010;24(1):39-46.
167. Ray L, Lipton RB, Zimmerman ME, Katz MJ, Derby CA. Mechanisms of association between obesity and chronic pain in the elderly. Pain. 2011;152(1):53-9.
168. Hildebrand C, Oqvist G, Brax L, Tuisku F. Anatomy of the rat knee joint and fibre composition of a major articular nerve. Anat Rec. 1991;229(4):545-55.
169. Salo PT, Theriault E. Number, distribution and neuropeptide content of rat knee joint afferents. Journal of anatomy. 1997;190 (Pt 4):515-22.
170. Ebinger M, Schmidt RF, Heppelmann B. Composition of the medial and posterior articular nerves of the mouse knee joint. Somatosensory & motor research. 2001;18(1):62-5.
171. Schaible HG, Schmidt RF, Willis WD. Responses of spinal cord neurones to stimulation of articular afferent fibres in the cat. The Journal of physiology. 1986;372:575-93.
172. Weihe E, Nohr D, Millan MJ, Stein C, Muller S, Gramsch C, et al. Peptide neuroanatomy of adjuvant-induced arthritic inflammation in rat. Agents Actions. 1988;25(3-4):255-9.
173. Konttinen YT, Gronblad M, Hukkanen M, Kinnunen E, Santavirta S, Polak JM, et al. Pain fibers in osteoarthritis: a review. Semin Arthritis Rheum. 1989;18(4 Suppl 2):35-40.
174. Kuraishi Y, Nanayama T, Ohno H, Fujii N, Otaka A, Yajima H, et al. Calcitonin gene-related peptide increases in the dorsal root ganglia of adjuvant arthritic rat. Peptides. 1989;10(2):447-52.
175. Widenfalk B, Wiberg M. Origin of sympathetic and sensory innervation of the knee joint. A retrograde axonal tracing study in the rat. Anat Embryol (Berl). 1989;180(4):317-23.
176. Kar S, Gibson SJ, Rees RG, Jura WG, Brewerton DA, Polak JM. Increased calcitonin gene-related peptide (CGRP), substance P, and enkephalin immunoreactivities in dorsal spinal cord and loss of CGRP-immunoreactive motoneurons in arthritic rats depend on intact peripheral nerve supply. J Mol Neurosci. 1991;3(1):7-18.
177. Marlier L, Poulat P, Rajaofetra N, Privat A. Modifications of serotonin-, substance P- and calcitonin gene-related peptide-like immunoreactivities in the dorsal horn of the spinal cord of arthritic rats: a quantitative immunocytochemical study. Exp Brain Res. 1991;85(3):482-90.
178. Buma P, Verschuren C, Versleyen D, Van der Kraan P, Oestreicher AB. Calcitonin gene-related peptide, substance P and GAP-43/B-50 immunoreactivity in the normal and arthrotic knee joint of the mouse. Histochemistry. 1992;98(5):327-39.
179. Barker RA, Barasi S, Neal MJ, editors. Neuroscience at a Glance. 2nd ed. Oxford OX4 2DQ, UK: Blackwell Publishing Ltd; 2003.
180. Levine JD, Alessandri-Haber N. TRP channels: targets for the relief of pain. Biochim Biophys Acta. 2007;1772(8):989-1003.

181. Sanchez JF, Krause JE, Cortright DN. The distribution and regulation of vanilloid receptor VR1 and VR1 5' splice variant RNA expression in rat. Neuroscience. 2001;107(3):373-81.
182. Davis JB, Gray J, Gunthorpe MJ, Hatcher JP, Davey PT, Overend P, et al. Vanilloid receptor-1 is essential for inflammatory thermal hyperalgesia. Nature. 2000;405(6783):183-7.
183. Bolcskei K, Helyes Z, Szabo A, Sandor K, Elekes K, Nemeth J, et al. Investigation of the role of TRPV1 receptors in acute and chronic nociceptive processes using gene-deficient mice. Pain. 2005;117(3):368-76.
184. Hudson LJ, Bevan S, Wotherspoon G, Gentry C, Fox A, Winter J. VR1 protein expression increases in undamaged DRG neurons after partial nerve injury. Eur J Neurosci. 2001;13(11):2105-14.
185. Fukuoka T, Tokunaga A, Tachibana T, Dai Y, Yamanaka H, Noguchi K. VR1, but not P2X(3), increases in the spared L4 DRG in rats with L5 spinal nerve ligation. Pain. 2002;99(1-2):111-20.
186. Keeble JE, Brain SD. Capsaicin-induced vasoconstriction in the mouse knee joint: a study using TRPV1 knockout mice. Neurosci Lett. 2006;401(1-2):55-8.
187. Szabo A, Helyes Z, Sandor K, Bite A, Pinter E, Nemeth J, et al. Role of transient receptor potential vanilloid 1 receptors in adjuvant-induced chronic arthritis: in vivo study using gene-deficient mice. J Pharmacol Exp Ther. 2005;314(1):111-9.
188. Barton NJ, McQueen DS, Thomson D, Gauldie SD, Wilson AW, Salter DM, et al. Attenuation of experimental arthritis in TRPV1R knockout mice. Exp Mol Pathol. 2006;81(2):166-70.
189. Kalff KM, El Mouedden M, van Egmond J, Veening J, Joosten L, Scheffer GJ, et al. Pre-treatment with capsaicin in a rat osteoarthritis model reduces the symptoms of pain and bone damage induced by monosodium iodoacetate. Eur J Pharmacol. 2010;641(2-3):108-13.
190. Kelly S, Chapman RJ, Woodhams S, Sagar DR, Turner J, Burston JJ, et al. Increased function of pronociceptive TRPV1 at the level of the joint in a rat model of osteoarthritis pain. Ann Rheum Dis. 2013.
191. Cho WG, Valtschanoff JG. Vanilloid receptor TRPV1-positive sensory afferents in the mouse ankle and knee joints. Brain Res. 2008;1219:59-65.
192. Fernihough J, Gentry C, Bevan S, Winter J. Regulation of calcitonin gene-related peptide and TRPV1 in a rat model of osteoarthritis. Neuroscience letters. 2005;388(2):75-80.
193. Bar K-J, Schaible H-G, Brauer R, Halbhuber K-J, von Banchet GS. The proportion of TRPV1 protein-positive lumbar DRG neurones does not increase in the course of acute and chronic antigen-induced arthritis in the knee joint of the rat. Neuroscience letters. 2004;361(1-3):172-5.
194. Ji R-R, Samad TA, Jin S-X, Schmoll R, Woolf CJ. p38 MAPK activation by NGF in primary sensory neurons after inflammation increases TRPV1 levels and maintains heat hyperalgesia. Neuron. 2002;36(1):57-68.
195. Carlton SM, Coggeshall RE. Peripheral capsaicin receptors increase in the inflamed rat hindpaw: a possible mechanism for peripheral sensitization. Neurosci Lett. 2001;310(1):53-6.
196. Amaya F, Oh-hashi K, Naruse Y, Iijima N, Ueda M, Shimosato G, et al. Local inflammation increases vanilloid receptor 1 expression within distinct subgroups of DRG neurons. Brain Res. 2003;963(1-2):190-6.

197. Chen Y, Willcockson HH, Valtschanoff JG. Vanilloid receptor TRPV1-mediated phosphorylation of ERK in murine adjuvant arthritis. Osteoarthritis Cartilage. 2009;17(2):244-51.
198. von Banchet GS, Richter J, Huckel M, Rose C, Brauer R, Schaible H-G. Fibroblast-like synovial cells from normal and inflamed knee joints differently affect the expression of pain-related receptors in sensory neurones: a co-culture study. Arthritis Res Ther. 2007;9(1):R6.
199. Bautista DM, Movahed P, Hinman A, Axelsson HE, Sterner O, Hogestatt ED, et al. Pungent products from garlic activate the sensory ion channel TRPA1. Proc Natl Acad Sci U S A. 2005;102(34):12248-52.
200. Bautista DM, Jordt SE, Nikai T, Tsuruda PR, Read AJ, Poblete J, et al. TRPA1 mediates the inflammatory actions of environmental irritants and proalgesic agents. Cell. 2006;124(6):1269-82.
201. Story GM, Peier AM, Reeve AJ, Eid SR, Mosbacher J, Hricik TR, et al. ANKTM1, a TRP-like channel expressed in nociceptive neurons, is activated by cold temperatures. Cell. 2003;112(6):819-29.
202. Kwan KY, Allchorne AJ, Vollrath MA, Christensen AP, Zhang DS, Woolf CJ, et al. TRPA1 contributes to cold, mechanical, and chemical nociception but is not essential for hair-cell transduction. Neuron. 2006;50(2):277-89.
203. Corey DP, Garcia-Anoveros J, Holt JR, Kwan KY, Lin SY, Vollrath MA, et al. TRPA1 is a candidate for the mechanosensitive transduction channel of vertebrate hair cells. Nature. 2004;432(7018):723-30.
204. Petrus M, Peier AM, Bandell M, Hwang SW, Huynh T, Olney N, et al. A role of TRPA1 in mechanical hyperalgesia is revealed by pharmacological inhibition. Mol Pain. 2007;3:40.
205. Bandell M, Story GM, Hwang SW, Viswanath V, Eid SR, Petrus MJ, et al. Noxious cold ion channel TRPA1 is activated by pungent compounds and bradykinin. Neuron. 2004;41(6):849-57.
206. Caterina MJ, Rosen TA, Tominaga M, Brake AJ, Julius D. A capsaicin-receptor homologue with a high threshold for noxious heat. Nature. 1999;398(6726):436-41.
207. Woodbury CJ, Zwick M, Wang S, Lawson JJ, Caterina MJ, Koltzenburg M, et al. Nociceptors lacking TRPV1 and TRPV2 have normal heat responses. The Journal of neuroscience : the official journal of the Society for Neuroscience. 2004;24(28):6410-5.
208. Lewinter RD, Skinner K, Julius D, Basbaum AI. Immunoreactive TRPV-2 (VRL-1), a capsaicin receptor homolog, in the spinal cord of the rat. The Journal of comparative neurology. 2004;470(4):400-8.
209. Kojima I, Nagasawa M. TRPV2. Handb Exp Pharmacol. 2014;222:247-72.
210. Park U, Vastani N, Guan Y, Raja SN, Koltzenburg M, Caterina MJ. TRP vanilloid 2 knock-out mice are susceptible to perinatal lethality but display normal thermal and mechanical nociception. The Journal of neuroscience : the official journal of the Society for Neuroscience. 2011;31(32):11425-36.
211. Shimosato G, Amaya F, Ueda M, Tanaka Y, Decosterd I, Tanaka M. Peripheral inflammation induces up-regulation of TRPV2 expression in rat DRG. Pain. 2005;119(1-3):225-32.
212. Petitjean H, Hugel S, Barthas F, Bohren Y, Barrot M, Yalcin I, et al. Activation of transient receptor potential vanilloid 2-expressing primary afferents stimulates synaptic transmission in the deep dorsal horn of the rat spinal cord and elicits mechanical hyperalgesia. Eur J Neurosci. 2014.

213. Katanosaka Y, Iwasaki K, Ujihara Y, Takatsu S, Nishitsuji K, Kanagawa M, et al. TRPV2 is critical for the maintenance of cardiac structure and function in mice. Nature communications. 2014;5:3932.
214. Rubinstein J, Lasko VM, Koch SE, Singh VP, Carreira V, Robbins N, et al. Novel role of transient receptor potential vanilloid 2 in the regulation of cardiac performance. American journal of physiology Heart and circulatory physiology. 2014;306(4):H574-84.
215. Liberati S, Morelli MB, Amantini C, Farfariello V, Santoni M, Conti A, et al. Loss of TRPV2 Homeostatic Control of Cell Proliferation Drives Tumor Progression. Cells. 2014;3(1):112-28.
216. Guler AD, Lee H, Iida T, Shimizu I, Tominaga M, Caterina M. Heat-evoked activation of the ion channel, TRPV4. The Journal of neuroscience : the official journal of the Society for Neuroscience. 2002;22(15):6408-14.
217. Alessandri-Haber N, Yeh JJ, Boyd AE, Parada CA, Chen X, Reichling DB, et al. Hypotonicity induces TRPV4-mediated nociception in rat. Neuron. 2003;39(3):497-511.
218. Vriens J, Watanabe H, Janssens A, Droogmans G, Voets T, Nilius B. Cell swelling, heat, and chemical agonists use distinct pathways for the activation of the cation channel TRPV4. Proc Natl Acad Sci U S A. 2004;101(1):396-401.
219. Suzuki M, Watanabe Y, Oyama Y, Mizuno A, Kusano E, Hirao A, et al. Localization of mechanosensitive channel TRPV4 in mouse skin. Neurosci Lett. 2003;353(3):189-92.
220. Mizuno A, Matsumoto N, Imai M, Suzuki M. Impaired osmotic sensation in mice lacking TRPV4. American journal of physiology Cell physiology. 2003;285(1):C96-101.
221. Suzuki M, Mizuno A, Kodaira K, Imai M. Impaired pressure sensation in mice lacking TRPV4. J Biol Chem. 2003;278(25):22664-8.
222. Grant AD, Cottrell GS, Amadesi S, Trevisani M, Nicoletti P, Materazzi S, et al. Protease-activated receptor 2 sensitizes the transient receptor potential vanilloid 4 ion channel to cause mechanical hyperalgesia in mice. The Journal of physiology. 2007;578(Pt 3):715-33.
223. Alessandri-Haber N, Joseph E, Dina OA, Liedtke W, Levine JD. TRPV4 mediates pain-related behavior induced by mild hypertonic stimuli in the presence of inflammatory mediator. Pain. 2005;118(1-2):70-9.
224. Alessandri-Haber N, Dina OA, Joseph EK, Reichling D, Levine JD. A transient receptor potential vanilloid 4-dependent mechanism of hyperalgesia is engaged by concerted action of inflammatory mediators. The Journal of neuroscience : the official journal of the Society for Neuroscience. 2006;26(14):3864-74.
225. Alessandri-Haber N, Dina OA, Yeh JJ, Parada CA, Reichling DB, Levine JD. Transient receptor potential vanilloid 4 is essential in chemotherapy-induced neuropathic pain in the rat. The Journal of neuroscience : the official journal of the Society for Neuroscience. 2004;24(18):4444-52.
226. Salo PT, Tatton WG. Age-related loss of knee joint afferents in mice. J Neurosci Res. 1993;35(6):664-77.
227. Salo PT, Seeratten RA, Erwin WM, Bray RC. Evidence for a neuropathic contribution to the development of spontaneous knee osteoarthrosis in a mouse model. Acta orthopaedica Scandinavica. 2002;73(1):77-84.
228. Hunter DJ, McDougall JJ, Keefe FJ. The symptoms of osteoarthritis and the genesis of pain. Rheum Dis Clin North Am. 2008;34(3):623-43.

229. Dieppe PA, Lohmander LS. Pathogenesis and management of pain in osteoarthritis. Lancet. 2005;365(9463):965-73.
230. Woolf CJ. Central sensitization: implications for the diagnosis and treatment of pain. Pain. 2011;152(3 Suppl):S2-15.
231. Melzack R, Wall PD. Pain mechanisms: a new theory. Science (New York, NY). 1965;150(3699):971-9.
232. Cesselin F, Montastruc JL, Gros C, Bourgoin S, Hamon M. Met-enkephalin levels and opiate receptors in the spinal cord of chronic suffering rats. Brain research. 1980;191(1):289-93.
233. Calvino B, Le Bars D. The response to viscero-peritoneal nociceptive stimuli is reduced in experimental arthritic rats. Brain research. 1986;370(1):191-5.
234. Cesselin F. [Endomorphins and nociception]. Rev Neurol (Paris). 1986;142(8-9):649-70.
235. Kudo T, Wei EQ, Inoki R, Terasawa M, Nakao T. Influence of Y-20003, an analgesic agent, on the endogenous opioid peptide system in rats. NIDA Res Monogr. 1986;75:236-9.
236. Millan MJ, Millan MH, Czlonkowski A, Hollt V, Pilcher CW, Herz A, et al. A model of chronic pain in the rat: response of multiple opioid systems to adjuvant-induced arthritis. Journal of Neuroscience. 1986;6(4):899-906.
237. Neil A, Kayser V, Gacel G, Besson JM, Guilbaud G. Opioid receptor types and antinociceptive activity in chronic inflammation: both kappa- and mu-opiate agonistic effects are enhanced in arthritic rats. European journal of pharmacology. 1986;130(3):203-8.
238. Przewlocki R, Lason W, Silberring J, Herz A, Przewlocka B. Release of opioid peptides from the spinal cord of rats subjected to chronic pain. NIDA Res Monogr. 1986;75:422-5.
239. Millan MJ, Czlonkowski A, Pilcher CW, Almeida OF, Millan MH, Colpaert FC, et al. A model of chronic pain in the rat: functional correlates of alterations in the activity of opioid systems. Journal of Neuroscience. 1987;7(1):77-87.
240. Panerai AE, Sacerdote P, Bianchi M, Brini A, Mantegazza P. Brain and spinal cord neuropeptides in adjuvant induced arthritis in rats. Life sciences. 1987;41(10):1297-303.
241. Herz A, Millan MJ, Stein C. Arthritic inflammation in rats as a model of chronic pain: role of opioid systems. NIDA Res Monogr. 1989;95:110-5.
242. Lombard MC, Besson JM. Electrophysiological evidence for a tonic activity of the spinal cord intrinsic opioid systems in a chronic pain model. Brain research. 1989;477(1-2):48-56.
243. Perl ER, Kumazawa T, Lynn B, Kenins P. Sensitization of high threshold receptors with unmyelinated (C) afferent fibers. Progress in brain research. 1976;43:263-77.
244. Kocher L, Anton F, Reeh PW, Handwerker HO. The effect of carrageenan-induced inflammation on the sensitivity of unmyelinated skin nociceptors in the rat. Pain. 1987;29(3):363-73.
245. Reeh PW, Bayer J, Kocher L, Handwerker HO. Sensitization of nociceptive cutaneous nerve fibers from the rat's tail by noxious mechanical stimulation. Exp Brain Res. 1987;65(3):505-12.
246. Campbell JN, Khan AA, Meyer RA, Raja SN. Responses to heat of C-fiber nociceptors in monkey are altered by injury in the receptive field but not by adjacent injury. Pain. 1988;32(3):327-32.

247. Binshtok AM, Wang H, Zimmermann K, Amaya F, Vardeh D, Shi L, et al. Nociceptors are interleukin-1beta sensors. The Journal of neuroscience : the official journal of the Society for Neuroscience. 2008;28(52):14062-73.
248. Mendell LM, Wall PD. Responses of single dorsal cord cells to peripheral cutaneous unmyelinated fibres. Nature. 1965;206:97-9.
249. Torebjork HE, Lundberg LE, LaMotte RH. Central changes in processing of mechanoreceptive input in capsaicin-induced secondary hyperalgesia in humans. The Journal of physiology. 1992;448:765-80.
250. Woolf CJ. Windup and central sensitization are not equivalent. Pain. 1996;66(2-3):105-8.
251. Woolf CJ, Shortland P, Sivilotti LG. Sensitization of high mechanothreshold superficial dorsal horn and flexor motor neurones following chemosensitive primary afferent activation. Pain. 1994;58(2):141-55.
252. Neumann S, Doubell TP, Leslie T, Woolf CJ. Inflammatory pain hypersensitivity mediated by phenotypic switch in myelinated primary sensory neurons. Nature. 1996;384(6607):360-4.
253. Woolf CJ. Phenotypic modification of primary sensory neurons: the role of nerve growth factor in the production of persistent pain. Philos Trans R Soc Lond B Biol Sci. 1996;351(1338):441-8.
254. Weihe E, Nohr D, Muller S, Buchler M, Friess H, Zentel HJ. The tachykinin neuroimmune connection in inflammatory pain. Annals of the New York Academy of Sciences. 1991;632:283-95.
255. Woolf CJ, Costigan M. Transcriptional and posttranslational plasticity and the generation of inflammatory pain. Proc Natl Acad Sci U S A. 1999;96(14):7723-30.
256. Woolf CJ, Salter MW. Neuronal plasticity: increasing the gain in pain. Science (New York, NY). 2000;288(5472):1765-9.
257. Ikeda H, Heinke B, Ruscheweyh R, Sandkuhler J. Synaptic plasticity in spinal lamina I projection neurons that mediate hyperalgesia. Science (New York, NY). 2003;299(5610):1237-40.
258. Chiang CY, Li Z, Dostrovsky JO, Sessle BJ. Central sensitization in medullary dorsal horn involves gap junctions and hemichannels. Neuroreport. 2010;21(3):233-7.
259. Woolf CJ, Safieh-Garabedian B, Ma QP, Crilly P, Winter J. Nerve growth factor contributes to the generation of inflammatory sensory hypersensitivity. Neuroscience. 1994;62(2):327-31.
260. Woolf CJ, Allchorne A, Safieh-Garabedian B, Poole S. Cytokines, nerve growth factor and inflammatory hyperalgesia: the contribution of tumour necrosis factor alpha. Br J Pharmacol. 1997;121(3):417-24.
261. von Banchet GS, Petrow PK, Brauer R, Schaible HG. Monoarticular antigen-induced arthritis leads to pronounced bilateral upregulation of the expression of neurokinin 1 and bradykinin 2 receptors in dorsal root ganglion neurons of rats. Arthritis research. 2000;2(5):424-7.
262. Vikman KS, Duggan AW, Siddall PJ. Increased ability to induce long-term potentiation of spinal dorsal horn neurones in monoarthritic rats. Brain research. 2003;990(1-2):51-7.
263. McDougall JJ, Watkins L, Li Z. Vasoactive intestinal peptide (VIP) is a modulator of joint pain in a rat model of osteoarthritis. Pain. 2006;123(1-2):98-105.
264. McNamee KE, Burleigh A, Gompels LL, Feldmann M, Allen SJ, Williams RO, et al. Treatment of murine osteoarthritis with TrkAd5 reveals a pivotal role for nerve growth factor in non-inflammatory joint pain. Pain. 2010;149(2):386-92.

265. Przewlocki R, Przewlocka B. Opioids in chronic pain. European journal of pharmacology. 2001;429(1-3):79-91.
266. Straub RH, Wolff C, Fassold A, Hofbauer R, Chover-Gonzalez A, Richards LJ, et al. Antiinflammatory role of endomorphins in osteoarthritis, rheumatoid arthritis, and adjuvant-induced polyarthritis. Arthritis & Rheumatism. 2008;58(2):456-66.
267. Burston JJ, Woodhams SG. Endocannabinoid system and pain: an introduction. The Proceedings of the Nutrition Society. 2014;73(1):106-17.
268. Neugebauer V, Han JS, Adwanikar H, Fu Y, Ji G. Techniques for assessing knee joint pain in arthritis. Molecular pain. 2007;3:8.
269. Henriksen M, Graven-Nielsen T, Aaboe J, Andriacchi TP, Bliddal H. Gait changes in patients with knee osteoarthritis are replicated by experimental knee pain. Arthritis care & research. 2010;62(4):501-9.
270. Pincus T, Sokka T. Quantitative measures and indices to assess rheumatoid arthritis in clinical trials and clinical care. Rheum Dis Clin North Am. 2004;30(4):725-51, vi.
271. Schaible HG. Mechanisms of Chronic Pain in Osteoarthritis. Current rheumatology reports. 2012.
272. Salaffi F, Ciapetti A, Carotti M. The sources of pain in osteoarthritis: a pathophysiological review. Reumatismo. 2014;66(1):57-71.
273. Dimitroulas T, Duarte RV, Behura A, Kitas GD, Raphael JH. Neuropathic pain in osteoarthritis: A review of pathophysiological mechanisms and implications for treatment. Semin Arthritis Rheum. 2014.
274. Hassan H, Walsh DA. Central pain processing in osteoarthritis: implications for treatment. Pain management. 2014;4(1):45-56.
275. Lluch E, Torres R, Nijs J, Van Oosterwijck J. Evidence for central sensitization in patients with osteoarthritis pain: A systematic literature review. Eur J Pain. 2014.
276. Neogi T, Frey-Law L, Scholz J, Niu J, Arendt-Nielsen L, Woolf C, et al. Sensitivity and sensitisation in relation to pain severity in knee osteoarthritis: trait or state? Ann Rheum Dis. 2013.
277. King CD, Sibille KT, Goodin BR, Cruz-Almeida Y, Glover TL, Bartley E, et al. Experimental pain sensitivity differs as a function of clinical pain severity in symptomatic knee osteoarthritis. Osteoarthritis Cartilage. 2013;21(9):1243-52.
278. Wylde V, Palmer S, Learmonth ID, Dieppe P. Somatosensory abnormalities in knee OA. Rheumatology (Oxford). 2012;51(3):535-43.
279. Kavchak AJ, Fernandez-de-Las-Penas C, Rubin LH, Arendt-Nielsen L, Chmell SJ, Durr RK, et al. Association between altered somatosensation, pain, and knee stability in patients with severe knee osteoarthrosis. The Clinical journal of pain. 2012;28(7):589-94.
280. Hendiani JA, Westlund KN, Lawand N, Goel N, Lisse J, McNearney T. Mechanical sensation and pain thresholds in patients with chronic arthropathies. The journal of pain : official journal of the American Pain Society. 2003;4(4):203-11.
281. Graven-Nielsen T, Wodehouse T, Langford RM, Arendt-Nielsen L, Kidd BL. Normalization of widespread hyperesthesia and facilitated spatial summation of deep-tissue pain in knee osteoarthritis patients after knee replacement. Arthritis Rheum. 2012;64(9):2907-16.
282. Staud R. Evidence for shared pain mechanisms in osteoarthritis, low back pain, and fibromyalgia. Current rheumatology reports. 2011;13(6):513-20.

283. Sofat N, Ejindu V, Kiely P. What makes osteoarthritis painful? The evidence for local and central pain processing. Rheumatology (Oxford). 2011;50(12):2157-65.
284. Arendt-Nielsen L, Nie H, Laursen MB, Laursen BS, Madeleine P, Simonsen OH, et al. Sensitization in patients with painful knee osteoarthritis. Pain. 2010;149(3):573-81.
285. Hochman JR, Davis AM, Elkayam J, Gagliese L, Hawker GA. Neuropathic pain symptoms on the modified painDETECT correlate with signs of central sensitization in knee osteoarthritis. Osteoarthritis Cartilage. 2013;21(9):1236-42.
286. Murphy SL, Phillips K, Williams DA, Clauw DJ. The role of the central nervous system in osteoarthritis pain and implications for rehabilitation. Current rheumatology reports. 2012;14(6):576-82.
287. Mease PJ, Hanna S, Frakes EP, Altman RD. Pain mechanisms in osteoarthritis: understanding the role of central pain and current approaches to its treatment. J Rheumatol. 2011;38(8):1546-51.
288. Lee YC, Nassikas NJ, Clauw DJ. The role of the central nervous system in the generation and maintenance of chronic pain in rheumatoid arthritis, osteoarthritis and fibromyalgia. Arthritis Res Ther. 2011;13(2):211.
289. Kobayashi K, Imaizumi R, Sumichika H, Tanaka H, Goda M, Fukunari A, et al. Sodium iodoacetate-induced experimental osteoarthritis and associated pain model in rats. The Journal of veterinary medical science / the Japanese Society of Veterinary Science. 2003;65(11):1195-9.
290. Chandran P, Pai M, Blomme EA, Hsieh GC, Decker MW, Honore P. Pharmacological modulation of movement-evoked pain in a rat model of osteoarthritis. European journal of pharmacology. 2009;613(1-3):39-45.
291. Zhang RX, Ren K, Dubner R. Osteoarthritis pain mechanisms: basic studies in animal models. Osteoarthritis Cartilage. 2013;21(9):1308-15.
292. Felson DT, Niu J, Guermazi A, Roemer F, Aliabadi P, Clancy M, et al. Correlation of the development of knee pain with enlarging bone marrow lesions on magnetic resonance imaging. Arthritis and rheumatism. 2007;56(9):2986-92.
293. Javaid MK, Lynch JA, Tolstykh I, Guermazi A, Roemer F, Aliabadi P, et al. Pre-radiographic MRI findings are associated with onset of knee symptoms: the most study. Osteoarthritis and cartilage / OARS, Osteoarthritis Research Society. 2010;18(3):323-8.
294. Felson DT. Imaging abnormalities that correlate with joint pain. British journal of sports medicine. 2011;45(4):289-91.
295. Hunter DJ, Guermazi A, Roemer F, Zhang Y, Neogi T. Structural correlates of pain in joints with osteoarthritis. Osteoarthritis Cartilage. 2013;21(9):1170-8.
296. McDougall JJ, Andruski B, Schuelert N, Hallgrimsson B, Matyas JR. Unravelling the relationship between age, nociception and joint destruction in naturally occurring osteoarthritis of Dunkin Hartley guinea pigs. Pain. 2009;141(3):222-32.
297. Hunter DJ, Lo GH, Gale D, Grainger AJ, Guermazi A, Conaghan PG. The reliability of a new scoring system for knee osteoarthritis MRI and the validity of bone marrow lesion assessment: BLOKS (Boston Leeds Osteoarthritis Knee Score). Ann Rheum Dis. 2008;67(2):206-11.
298. Lo GH, Hunter DJ, Nevitt M, Lynch J, McAlindon TE. Strong association of MRI meniscal derangement and bone marrow lesions in knee osteoarthritis: data from the osteoarthritis initiative. Osteoarthritis Cartilage. 2009;17(6):743-7.
299. Pelletier JP, Raynauld JP, Abram F, Haraoui B, Choquette D, Martel-Pelletier J. A new non-invasive method to assess synovitis severity in relation to symptoms and

cartilage volume loss in knee osteoarthritis patients using MRI. Osteoarthritis Cartilage. 2008;16 Suppl 3:S8-13.
300. Hill CL, Gale DG, Chaisson CE, Skinner K, Kazis L, Gale ME, et al. Knee effusions, popliteal cysts, and synovial thickening: association with knee pain in osteoarthritis. J Rheumatol. 2001;28(6):1330-7.
301. Kornaat PR, Bloem JL, Ceulemans RY, Riyazi N, Rosendaal FR, Nelissen RG, et al. Osteoarthritis of the knee: association between clinical features and MR imaging findings. Radiology. 2006;239(3):811-7.
302. Sowers MF, Hayes C, Jamadar D, Capul D, Lachance L, Jannausch M, et al. Magnetic resonance-detected subchondral bone marrow and cartilage defect characteristics associated with pain and X-ray-defined knee osteoarthritis. Osteoarthritis Cartilage. 2003;11(6):387-93.
303. Wluka AE, Wolfe R, Stuckey S, Cicuttini FM. How does tibial cartilage volume relate to symptoms in subjects with knee osteoarthritis? Ann Rheum Dis. 2004;63(3):264-8.
304. Appleton CT, Pitelka V, Henry J, Beier F. Global analyses of gene expression in early experimental osteoarthritis. Arthritis Rheum. 2007;56(6):1854-68.
305. Hunter DJ, McDougall JJ, Keefe FJ. The symptoms of osteoarthritis and the genesis of pain. Med Clin North Am. 2009;93(1):83-100, xi.
306. Wade JB, Riddle DL, Price DD, Dumenci L. Role of pain catastrophizing during pain processing in a cohort of patients with chronic and severe arthritic knee pain. Pain. 2011;152(2):314-9.
307. McDougall JJ. Peripheral analgesia: Hitting pain where it hurts. Biochim Biophys Acta. 2011;1812(4):459-67.
308. Franchi S, Moretti S, Castelli M, Lattuada D, Scavullo C, Panerai AE, et al. Mu opioid receptor activation modulates Toll like receptor 4 in murine macrophages. Brain, behavior, and immunity. 2012;26(3):480-8.
309. Kraus J. Expression and functions of mu-opioid receptors and cannabinoid receptors type 1 in T lymphocytes. Annals of the New York Academy of Sciences. 2012;1261:1-6.
310. McDougall JJ, Linton P. Neurophysiology of arthritis pain. Current pain and headache reports. 2012;16(6):485-91.
311. La Porta C, Bura SA, Negrete R, Maldonado R. Involvement of the endocannabinoid system in osteoarthritis pain. Eur J Neurosci. 2014;39(3):485-500.
312. La Porta C, Bura SA, Aracil-Fernandez A, Manzanares J, Maldonado R. Role of CB1 and CB2 cannabinoid receptors in the development of joint pain induced by monosodium iodoacetate. Pain. 2013;154(1):160-74.
313. Schuelert N, Johnson MP, Oskins JL, Jassal K, Chambers MG, McDougall JJ. Local application of the endocannabinoid hydrolysis inhibitor URB597 reduces nociception in spontaneous and chemically induced models of osteoarthritis. Pain. 2011;152(5):975-81.
314. Obara I, Parkitna JR, Korostynski M, Makuch W, Kaminska D, Przewlocka B, et al. Local peripheral opioid effects and expression of opioid genes in the spinal cord and dorsal root ganglia in neuropathic and inflammatory pain. Pain. 2009;141(3):283-91.
315. Mousa SA, Straub RH, Schafer M, Stein C. Beta-endorphin, Met-enkephalin and corresponding opioid receptors within synovium of patients with joint trauma, osteoarthritis and rheumatoid arthritis. Ann Rheum Dis. 2007;66(7):871-9.

316. Inglis JJ, McNamee KE, Chia S-L, Essex D, Feldmann M, Williams RO, et al. Regulation of pain sensitivity in experimental osteoarthritis by the endogenous peripheral opioid system. Arthritis Rheum. 2008;58(10):3110-9.
317. Shaqura MA, Zollner C, Mousa SA, Stein C, Schafer M. Characterization of mu opioid receptor binding and G protein coupling in rat hypothalamus, spinal cord, and primary afferent neurons during inflammatory pain. The Journal of pharmacology and experimental therapeutics. 2004;308(2):712-8.
318. Stein C, Kuchler S. Non-analgesic effects of opioids: peripheral opioid effects on inflammation and wound healing. Current pharmaceutical design. 2012;18(37):6053-69.
319. Bodnar RJ. Endogenous opiates and behavior: 2012. Peptides. 2013;50:55-95.
320. Sellam J, Berenbaum F. The role of synovitis in pathophysiology and clinical symptoms of osteoarthritis. Nat Rev Rheumatol. 2010;6(11):625-35.
321. Coggeshall RE, Hong KA, Langford LA, Schaible HG, Schmidt RF. Discharge characteristics of fine medial articular afferents at rest and during passive movements of inflamed knee joints. Brain Res. 1983;272(1):185-8.
322. Kapoor M, Martel-Pelletier J, Lajeunesse D, Pelletier JP, Fahmi H. Role of proinflammatory cytokines in the pathophysiology of osteoarthritis. Nat Rev Rheumatol. 2011;7(1):33-42.
323. Hensellek S, Brell P, Schaible H-G, Brauer R, Segond von Banchet G. The cytokine TNFalpha increases the proportion of DRG neurones expressing the TRPV1 receptor via the TNFR1 receptor and ERK activation. Mol Cell Neurosci. 2007;36(3):381-91.
324. White FA, Sun J, Waters SM, Ma C, Ren D, Ripsch M, et al. Excitatory monocyte chemoattractant protein-1 signaling is up-regulated in sensory neurons after chronic compression of the dorsal root ganglion. Proc Natl Acad Sci U S A. 2005;102(39):14092-7.
325. Lai Y-C, Shaftel SS, Miller J-nH, Tallents RH, Chang Y, Pinkert CA, et al. Intraarticular induction of interleukin-1beta expression in the adult mouse, with resultant temporomandibular joint pathologic changes, dysfunction, and pain. Arthritis and rheumatism. 2006;54(4):1184-97.
326. van de Loo AA, Arntz OJ, Otterness IG, van den Berg WB. Proteoglycan loss and subsequent replenishment in articular cartilage after a mild arthritic insult by IL-1 in mice: impaired proteoglycan turnover in the recovery phase. Agents Actions. 1994;41(3-4):200-8.
327. Clements KM, Price JS, Chambers MG, Visco DM, Poole AR, Mason RM. Gene deletion of either interleukin-1beta, interleukin-1beta-converting enzyme, inducible nitric oxide synthase, or stromelysin 1 accelerates the development of knee osteoarthritis in mice after surgical transection of the medial collateral ligament and partial medial meniscectomy. Arthritis Rheum. 2003;48(12):3452-63.
328. Daheshia M, Yao JQ. The interleukin 1beta pathway in the pathogenesis of osteoarthritis. J Rheumatol. 2008;35(12):2306-12.
329. Richter F, Natura G, Ebbinghaus M, von Banchet GS, Hensellek S, Konig C, et al. Interleukin-17 sensitizes joint nociceptors to mechanical stimuli and contributes to arthritic pain through neuronal interleukin-17 receptors in rodents. Arthritis & Rheumatism. 2012;64(12):4125-34.
330. Willemen HLDM, Eijkelkamp N, Garza Carbajal A, Wang H, Mack M, Zijlstra J, et al. Monocytes/Macrophages Control Resolution of Transient Inflammatory Pain. The Journal of Pain. 2014;15(5):496-506.

331. Oh SB, Tran PB, Gillard SE, Hurley RW, Hammond DL, Miller RJ. Chemokines and glycoprotein120 produce pain hypersensitivity by directly exciting primary nociceptive neurons. The Journal of neuroscience : the official journal of the Society for Neuroscience. 2001;21(14):5027-35.
332. Zhu X, Cao S, Zhu M-D, Liu J-Q, Chen J-J, Gao Y-J. Contribution of Chemokine CCL2/CCR2 Signaling in the Dorsal Root Ganglion and Spinal Cord to the Maintenance of Neuropathic Pain in a Rat Model of Lumbar Disc Herniation. The Journal of Pain. 2014;15(5):516-26.
333. Kim D, You B, Lim H, Lee SJ. Toll-like receptor 2 contributes to chemokine gene expression and macrophage infiltration in the dorsal root ganglia after peripheral nerve injury. Mol Pain. 2011;7:74.
334. Jeon SM, Sung JK, Cho HJ. Expression of monocyte chemoattractant protein-1 and its induction by tumor necrosis factor receptor 1 in sensory neurons in the ventral rhizotomy model of neuropathic pain. Neuroscience. 2011;190:354-66.
335. Jeon SM, Lee KM, Park ES, Jeon YH, Cho HJ. Monocyte chemoattractant protein-1 immunoreactivity in sensory ganglia and hindpaw after adjuvant injection. Neuroreport. 2008;19(2):183-6.
336. Jung H, Toth PT, White FA, Miller RJ. Monocyte chemoattractant protein-1 functions as a neuromodulator in dorsal root ganglia neurons. J Neurochem. 2008;104(1):254-63.
337. Jeon SM, Lee KM, Cho HJ. Expression of monocyte chemoattractant protein-1 in rat dorsal root ganglia and spinal cord in experimental models of neuropathic pain. Brain Res. 2009;1251:103-11.
338. Wang CH, Zou LJ, Zhang YL, Jiao YF, Sun JH. The excitatory effects of the chemokine CCL2 on DRG somata are greater after an injury of the ganglion than after an injury of the spinal or peripheral nerve. Neurosci Lett. 2010;475(1):48-52.
339. Miller RE, Tran PB, Das R, Ghoreishi-Haack N, Ren D, Miller RJ, et al. CCR2 chemokine receptor signaling mediates pain in experimental osteoarthritis. Proc Natl Acad Sci U S A. 2012;109(50):20602-7.
340. Kao DJ, Li AH, Chen JC, Luo RS, Chen YL, Lu JC, et al. CC chemokine ligand 2 upregulates the current density and expression of TRPV1 channels and Nav1.8 sodium channels in dorsal root ganglion neurons. Journal of neuroinflammation. 2012;9:189.
341. Dib-Hajj SD, Binshtok AM, Cummins TR, Jarvis MF, Samad T, Zimmermann K. Voltage-gated sodium channels in pain states: role in pathophysiology and targets for treatment. Brain Res Rev. 2009;60(1):65-83.
342. Rahman W, Dickenson AH. Osteoarthritis-dependent changes in antinociceptive action of Nav1.7 and Nav1.8 sodium channel blockers: An in vivo electrophysiological study in the rat. Neuroscience. 2015;295:103-16.
343. Mapp PI, Walsh DA. Mechanisms and targets of angiogenesis and nerve growth in osteoarthritis. Nat Rev Rheumatol. 2012;8(7):390-8.
344. Haywood L, McWilliams DF, Pearson CI, Gill SE, Ganesan A, Wilson D, et al. Inflammation and angiogenesis in osteoarthritis. Arthritis Rheum. 2003;48(8):2173-7.
345. Walsh DA, McWilliams DF, Turley MJ, Dixon MR, Franses RE, Mapp PI, et al. Angiogenesis and nerve growth factor at the osteochondral junction in rheumatoid arthritis and osteoarthritis. Rheumatology (Oxford). 2010;49(10):1852-61.
346. McDougall JJ. Arthritis and pain. Neurogenic origin of joint pain. Arthritis Res Ther. 2006;8(6):220.

347. Schaible HG, Schmidt RF. Effects of an experimental arthritis on the sensory properties of fine articular afferent units. J Neurophysiol. 1985;54(5):1109-22.
348. Neugebauer V, Rumenapp P, Schaible HG. Calcitonin gene-related peptide is involved in the spinal processing of mechanosensory input from the rat's knee joint and in the generation and maintenance of hyperexcitability of dorsal horn-neurons during development of acute inflammation. Neuroscience. 1996;71(4):1095-109.
349. McDougall JJ, Zhang C, Cellars L, Joubert E, Dixon CM, Vergnolle N. Triggering of proteinase-activated receptor 4 leads to joint pain and inflammation in mice. Arthritis Rheum. 2009;60(3):728-37.
350. Russell FA, McDougall JJ. Proteinase activated receptor (PAR) involvement in mediating arthritis pain and inflammation. Inflamm Res. 2009;58(3):119-26.
351. Martin L, Auge C, Boue J, Buresi MC, Chapman K, Asfaha S, et al. Thrombin receptor: An endogenous inhibitor of inflammatory pain, activating opioid pathways. Pain. 2009;146(1-2):121-9.
352. Helyes Z, Sandor K, Borbely E, Tekus V, Pinter E, Elekes K, et al. Involvement of transient receptor potential vanilloid 1 receptors in protease-activated receptor-2-induced joint inflammation and nociception. Eur J Pain. 2010;14(4):351-8.
353. Russell FA, Schuelert N, Veldhoen VE, Hollenberg MD, McDougall JJ. Activation of PAR(2) receptors sensitizes primary afferents and causes leukocyte rolling and adherence in the rat knee joint. Br J Pharmacol. 2012;167(8):1665-78.
354. Russell FA, Veldhoen VE, Tchitchkan D, McDougall JJ. Proteinase-activated receptor-4 (PAR4) activation leads to sensitization of rat joint primary afferents via a bradykinin B2 receptor-dependent mechanism. Journal of Neurophysiology. 2010;103(1):155-63.
355. Russell FA, Veldhoen VE, Tchitchkan D, McDougall JJ. Proteinase-activated receptor-4 (PAR4) activation leads to sensitization of rat joint primary afferents via a bradykinin B2 receptor-dependent mechanism. J Neurophysiol. 2009;103(1):155-63.
356. Russell FA, Zhan S, Dumas A, Lagarde S, Pouliot M, McDougall JJ. The pronociceptive effect of proteinase-activated receptor-4 stimulation in rat knee joints is dependent on mast cell activation. Pain. 2011;152(2):354-60.
357. Asfaha S, Cenac N, Houle S, Altier C, Papez MD, Nguyen C, et al. Protease-activated receptor-4: a novel mechanism of inflammatory pain modulation. Br J Pharmacol. 2007;150(2):176-85.
358. McDougall JJ, Barin AK. The role of joint nerves and mast cells in the alteration of vasoactive intestinal peptide (VIP) sensitivity during inflammation progression in rats. Br J Pharmacol. 2005;145(1):104-13.
359. Schuelert N, McDougall JJ. Electrophysiological evidence that the vasoactive intestinal peptide receptor antagonist VIP6-28 reduces nociception in an animal model of osteoarthritis. Osteoarthritis and cartilage / OARS, Osteoarthritis Research Society. 2006;14(11):1155-62.
360. Kawasaki Y, Xu Z-Z, Wang X, Park JY, Zhuang Z-Y, Tan P-H, et al. Distinct roles of matrix metalloproteases in the early- and late-phase development of neuropathic pain. Nat Med. 2008;14(3):331-6.
361. Ivanavicius SP, Ball AD, Heapy CG, Westwood FR, Murray F, Read SJ. Structural pathology in a rodent model of osteoarthritis is associated with neuropathic pain: increased expression of ATF-3 and pharmacological characterisation. Pain. 2007;128(3):272-82.
362. Tsujino H, Kondo E, Fukuoka T, Dai Y, Tokunaga A, Miki K, et al. Activating transcription factor 3 (ATF3) induction by axotomy in sensory and

motoneurons: A novel neuronal marker of nerve injury. Mol Cell Neurosci. 2000;15(2):170-82.
363. Malfait AM, Little CB, McDougall JJ. A commentary on modelling osteoarthritis pain in small animals. Osteoarthritis Cartilage. 2013;21(9):1316-26.
364. Fernihough J, Gentry C, Malcangio M, Fox A, Rediske J, Pellas T, et al. Pain related behaviour in two models of osteoarthritis in the rat knee. Pain. 2004;112(1-2):83-93.
365. Trevisani M, Siemens J, Materazzi S, Bautista DM, Nassini R, Campi B, et al. 4-Hydroxynonenal, an endogenous aldehyde, causes pain and neurogenic inflammation through activation of the irritant receptor TRPA1. Proc Natl Acad Sci U S A. 2007;104(33):13519-24.
366. Shi Q, Vaillancourt F, Cote V, Fahmi H, Lavigne P, Afif H, et al. Alterations of metabolic activity in human osteoarthritic osteoblasts by lipid peroxidation end product 4-hydroxynonenal. Arthritis Res Ther. 2006;8(6):R159.
367. Morquette B, Shi Q, Lavigne P, Ranger P, Fernandes JC, Benderdour M. Production of lipid peroxidation products in osteoarthritic tissues: new evidence linking 4-hydroxynonenal to cartilage degradation. Arthritis Rheum. 2006;54(1):271-81.
368. Shah R, Raska K, Jr., Tiku ML. The presence of molecular markers of in vivo lipid peroxidation in osteoarthritic cartilage: a pathogenic role in osteoarthritis. Arthritis Rheum. 2005;52(9):2799-807.
369. Tiku ML, Shah R, Allison GT. Evidence linking chondrocyte lipid peroxidation to cartilage matrix protein degradation. Possible role in cartilage aging and the pathogenesis of osteoarthritis. J Biol Chem. 2000;275(26):20069-76.
370. Wolfe MM, Lichtenstein DR, Singh G. Gastrointestinal toxicity of nonsteroidal antiinflammatory drugs. N Engl J Med. 1999;340(24):1888-99.
371. Akhtar N, Haqqi TM. Current nutraceuticals in the management of osteoarthritis: a review. Therapeutic advances in musculoskeletal disease. 2012;4(3):181-207.
372. Ragle RL, Sawitzke AD. Nutraceuticals in the management of osteoarthritis : a critical review. Drugs Aging. 2012;29(9):717-31.
373. Levi-Montalcini R, Cohen S. IN VITRO AND IN VIVO EFFECTS OF A NERVE GROWTH-STIMULATING AGENT ISOLATED FROM SNAKE VENOM. Proc Natl Acad Sci U S A. 1956;42(9):695-9.
374. Lewin GR, Lechner SG, Smith ES. Nerve growth factor and nociception: from experimental embryology to new analgesic therapy. Handb Exp Pharmacol. 2014;220:251-82.
375. Ashraf S, Mapp PI, Burston J, Bennett AJ, Chapman V, Walsh DA. Augmented pain behavioural responses to intra-articular injection of nerve growth factor in two animal models of osteoarthritis. Ann Rheum Dis. 2013.
376. Lewin GR, Rueff A, Mendell LM. Peripheral and central mechanisms of NGF-induced hyperalgesia. Eur J Neurosci. 1994;6(12):1903-12.
377. Driscoll C, Chanalaris A, Knights C, Ismail H, Sacitharan PK, Gentry C, et al. Nociceptive sensitizers are regulated in damaged joint tissues, including the articular cartilage, when osteoarthritic mice display pain behaviour. Arthritis rheumatol. 2015.
378. Seidel MF, Herguijuela M, Forkert R, Otten U. Nerve growth factor in rheumatic diseases. Seminars in Arthritis & Rheumatism. 2010;40(2):109-26.
379. Stoppiello LA, Mapp PI, Wilson D, Hill R, Scammell BE, Walsh DA. Structural Associations of Symptomatic Knee Osteoarthritis. Arthritis rheumatol. 2014;66(11):3018-27.

380. Aso K, Ikeuchi M, Izumi M, Sugimura N, Kato T, Ushida T, et al. Nociceptive phenotype of dorsal root ganglia neurons innervating the subchondral bone in rat knee joints. Eur J Pain. 2014;18(2):174-81.
381. Sagar DR, Nwosu L, Walsh DA, Chapman V. Dissecting the contribution of knee joint NGF to spinal nociceptive sensitization in a model of OA pain in the rat. Osteoarthritis Cartilage. 2015.
382. Watson JJ, Allen SJ, Dawbarn D. Targeting nerve growth factor in pain: what is the therapeutic potential? BioDrugs. 2008;22(6):349-59.
383. Lane NE, Schnitzer TJ, Birbara CA, Mokhtarani M, Shelton DL, Smith MD, et al. Tanezumab for the treatment of pain from osteoarthritis of the knee. The New England journal of medicine. 2010;363(16):1521-31.
384. Nagashima H, Suzuki M, Araki S, Yamabe T, Muto C. Preliminary assessment of the safety and efficacy of tanezumab in Japanese patients with moderate to severe osteoarthritis of the knee: a randomized, double-blind, dose-escalation, placebo-controlled study. Osteoarthritis Cartilage. 2011;19(12):1405-12.
385. Seidel MF, Wise BL, Lane NE. Nerve growth factor: an update on the science and therapy. Osteoarthritis Cartilage. 2013;21(9):1223-8.
386. Schnitzer TJ, Lane NE, Birbara C, Smith MD, Simpson SL, Brown MT. Long-term open-label study of tanezumab for moderate to severe osteoarthritic knee pain. Osteoarthritis and cartilage / OARS, Osteoarthritis Research Society. 2011;19(6):639-46.
387. Brown MT, Murphy FT, Radin DM, Davignon I, Smith MD, West CR. Tanezumab reduces osteoarthritic knee pain: results of a randomized, double-blind, placebo-controlled phase III trial. The journal of pain : official journal of the American Pain Society. 2012;13(8):790-8.
388. Brown MT, Murphy FT, Radin DM, Davignon I, Smith MD, West CR. Tanezumab reduces osteoarthritic hip pain: results of a randomized, double-blind, placebo-controlled phase III trial. Arthritis Rheum. 2013;65(7):1795-803.
389. Hoffman EM, Zhang Z, Anderson MB, Schechter R, Miller KE. Potential mechanisms for hypoalgesia induced by anti-nerve growth factor immunoglobulin are identified using autoimmune nerve growth factor deprivation. Neuroscience. 2011;193:452-65.
390. Brown MT, Herrmann DN, Goldstein M, Burr AM, Smith MD, West CR, et al. Nerve safety of tanezumab, a nerve growth factor inhibitor for pain treatment. Journal of the neurological sciences. 2014.
391. Malfait A-M, Schnitzer TJ. Towards a mechanism-based approach to pain management in osteoarthritis. Nature Reviews Rheumatology. 2013;9(11):654-64.
392. Smith MM, Little CB, Rodgers K, Ghosh P. Animal models used for the evaluation of anti-osteoarthritis drugs. Pathologie-biologie. 1997;45(4):313-20.
393. Lotsch J, Oertel BG, Ultsch A. Human models of pain for the prediction of clinical analgesia. Pain. 2014.
394. Rice AS, Cimino-Brown D, Eisenach JC, Kontinen VK, Lacroix-Fralish ML, Machin I, et al. Animal models and the prediction of efficacy in clinical trials of analgesic drugs: a critical appraisal and call for uniform reporting standards. Pain. 2008;139(2):243-7.
395. Kilkenny C, Browne WJ, Cuthill IC, Emerson M, Altman DG. Improving bioscience research reporting: the ARRIVE guidelines for reporting animal research. PLoS biology. 2010;8(6):e1000412.

396. van der Worp HB, Howells DW, Sena ES, Porritt MJ, Rewell S, O'Collins V, et al. Can animal models of disease reliably inform human studies? PLoS medicine. 2010;7(3):e1000245.
397. Teeple E, Jay GD, Elsaid KA, Fleming BC. Animal models of osteoarthritis: challenges of model selection and analysis. The AAPS journal. 2013;15(2):438-46.
398. Gregory MH, Capito N, Kuroki K, Stoker AM, Cook JL, Sherman SL. A review of translational animal models for knee osteoarthritis. Arthritis. 2012;2012:764621.
399. Little CB, Zaki S. What constitutes an "animal model of osteoarthritis"--the need for consensus? Osteoarthritis and cartilage / OARS, Osteoarthritis Research Society. 2012;20(4):261-7.
400. Little C, Smith M. Animal Models of Osteoarthritis. Current Rheumatology Reviews. 2008;4:175-82.
401. Lorenz J, Grassel S. Experimental osteoarthritis models in mice. Methods Mol Biol. 2014;1194:401-19.
402. Fang H, Beier F. Mouse models of osteoarthritis: modelling risk factors and assessing outcomes. Nat Rev Rheumatol. 2014.
403. Griffin TM, Fermor B, Huebner JL, Kraus VB, Rodriguiz RM, Wetsel WC, et al. Diet-induced obesity differentially regulates behavioral, biomechanical, and molecular risk factors for osteoarthritis in mice. Arthritis research & therapy. 2010;12(4):R130.
404. Bluteau G, Conrozier T, Mathieu P, Vignon E, Herbage D, Mallein-Gerin F. Matrix metalloproteinase-1, -3, -13 and aggrecanase-1 and -2 are differentially expressed in experimental osteoarthritis. Biochim Biophys Acta. 2001;1526(2):147-58.
405. Le Graverand M-PH, Eggerer J, Vignon E, Otterness IG, Barclay L, Hart DA. Assessment of specific mRNA levels in cartilage regions in a lapine model of osteoarthritis. J Orthop Res. 2002;20(3):535-44.
406. Knights CB, Gentry C, Bevan S. Partial medial meniscectomy produces osteoarthritis pain-related behaviour in female C57BL/6 mice. Pain. 2012;153(2):281-92.
407. Little CB, Hunter DJ. Post-traumatic osteoarthritis: from mouse models to clinical trials. Nat Rev Rheumatol. 2013;9(8):485-97.
408. van der Kraan PM, Vitters EL, van Beuningen HM, van de Putte LB, van den Berg WB. Degenerative knee joint lesions in mice after a single intra-articular collagenase injection. A new model of osteoarthritis. J Exp Pathol (Oxford). 1990;71(1):19-31.
409. Botter SM, van Osch GJVM, Waarsing JH, Day JS, Verhaar JAN, Pols HAP, et al. Quantification of subchondral bone changes in a murine osteoarthritis model using micro-CT. Biorheology. 2006;43(3-4):379-88.
410. Blaker CL, Clarke EC, Little CB. Using mouse models to investigate the pathophysiology, treatment, and prevention of post-traumatic osteoarthritis. J Orthop Res. 2016.
411. Allen KD, Adams SB, Jr., Mata BA, Shamji MF, Gouze E, Jing L, et al. Gait and behavior in an IL1beta-mediated model of rat knee arthritis and effects of an IL1 antagonist. J Orthop Res. 2011;29(5):694-703.
412. Allen KD, Griffin TM, Rodriguiz RM, Wetsel WC, Kraus VB, Huebner JL, et al. Decreased physical function and increased pain sensitivity in mice deficient for type IX collagen. Arthritis Rheum. 2009;60(9):2684-93.

413. Vincent TL, Williams RO, Maciewicz R, Silman A, Garside P. Mapping pathogenesis of arthritis through small animal models. Rheumatology (Oxford). 2012;51(11):1931-41.
414. Suokas AK, Sagar DR, Mapp PI, Chapman V, Walsh DA. Design, study quality and evidence of analgesic efficacy in studies of drugs in models of OA pain: a systematic review and a meta-analysis. Osteoarthritis Cartilage. 2014.
415. Neogi T, Guermazi A, Roemer F, Nevitt M, Scholz J, Arendt-Nielsen L, et al. Joint inflammation is associated with pain sensitization in knee osteoarthritis: The Multicenter Osteoarthritis Study. Arthritis rheumatol. 2015.
416. Boettger MK, Leuchtweis J, Kummel D, Gajda M, Brauer R, Schaible HG. Differential effects of locally and systemically administered soluble glycoprotein 130 on pain and inflammation in experimental arthritis. Arthritis Res Ther. 2010;12(4):R140.
417. Guingamp C, Gegout-Pottie P, Philippe L, Terlain B, Netter P, Gillet P. Mono-iodoacetate-induced experimental osteoarthritis: a dose-response study of loss of mobility, morphology, and biochemistry. Arthritis Rheum. 1997;40(9):1670-9.
418. Guzman RE, Evans MG, Bove S, Morenko B, Kilgore K. Mono-iodoacetate-induced histologic changes in subchondral bone and articular cartilage of rat femorotibial joints: an animal model of osteoarthritis. Toxicol Pathol. 2003;31(6):619-24.
419. Janusz MJ, Hookfin EB, Heitmeyer SA, Woessner JF, Freemont AJ, Hoyland JA, et al. Moderation of iodoacetate-induced experimental osteoarthritis in rats by matrix metalloproteinase inhibitors. Osteoarthritis Cartilage. 2001;9(8):751-60.
420. Combe R, Bramwell S, Field MJ. The monosodium iodoacetate model of osteoarthritis: a model of chronic nociceptive pain in rats? Neuroscience letters. 2004;370(2-3):236-40.
421. Bove SE, Calcaterra SL, Brooker RM, Huber CM, Guzman RE, Juneau PL, et al. Weight bearing as a measure of disease progression and efficacy of anti-inflammatory compounds in a model of monosodium iodoacetate-induced osteoarthritis. Osteoarthritis Cartilage. 2003;11(11):821-30.
422. Ferreira-Gomes J, Adaes S, Castro-Lopes JM. Assessment of movement-evoked pain in osteoarthritis by the knee-bend and CatWalk tests: a clinically relevant study. The journal of pain : official journal of the American Pain Society. 2008;9(10):945-54.
423. Vonsy JL, Ghandehari J, Dickenson AH. Differential analgesic effects of morphine and gabapentin on behavioural measures of pain and disability in a model of osteoarthritis pain in rats. European journal of pain (London, England). 2009;13(8):786-93.
424. Okun A, Liu P, Davis P, Ren J, Remeniuk B, Brion T, et al. Afferent drive elicits ongoing pain in a model of advanced osteoarthritis. Pain. 2012;153(4):924-33.
425. Dumond H, Presle N, Pottie P, Pacquelet S, Terlain B, Netter P, et al. Site specific changes in gene expression and cartilage metabolism during early experimental osteoarthritis. Osteoarthritis Cartilage. 2004;12(4):284-95.
426. Im H-J, Kim J-S, Li X, Kotwal N, Sumner DR, van Wijnen AJ, et al. Alteration of sensory neurons and spinal response to an experimental osteoarthritis pain model. Arthritis and rheumatism. 2010;62(10):2995-3005.
427. Gerwin N, Bendele AM, Glasson S, Carlson CS. The OARSI histopathology initiative - recommendations for histological assessments of osteoarthritis in the rat. Osteoarthritis and cartilage / OARS, Osteoarthritis Research Society. 2010;18 Suppl 3:S24-34.

428. Janusz MJ, Little CB, King LE, Hookfin EB, Brown KK, Heitmeyer SA, et al. Detection of aggrecanase- and MMP-generated catabolic neoepitopes in the rat iodoacetate model of cartilage degeneration. Osteoarthritis Cartilage. 2004;12(9):720-8.
429. Barve RA, Minnerly JC, Weiss DJ, Meyer DM, Aguiar DJ, Sullivan PM, et al. Transcriptional profiling and pathway analysis of monosodium iodoacetate-induced experimental osteoarthritis in rats: relevance to human disease. Osteoarthritis and Cartilage. 2007;15(10):1190-8.
430. Moreton BJ, Tew V, das Nair R, Wheeler M, Walsh DA, Lincoln NB. Pain phenotype in patients with knee osteoarthritis: classification and measurement properties of painDETECT and self-report Leeds assessment of neuropathic symptoms and signs scale in a cross-sectional study. Arthritis care & research. 2015;67(4):519-28.
431. Dimitroulas T, Duarte RV, Behura A, Kitas GD, Raphael JH. Neuropathic pain in osteoarthritis: a review of pathophysiological mechanisms and implications for treatment. Semin Arthritis Rheum. 2014;44(2):145-54.
432. Thakur M, Dickenson AH, Baron R. Osteoarthritis pain: nociceptive or neuropathic? Nat Rev Rheumatol. 2014;10(6):374-80.
433. Lampropoulou-Adamidou K, Lelovas P, Karadimas EV, Liakou C, Triantafillopoulos IK, Dontas I, et al. Useful animal models for the research of osteoarthritis. European journal of orthopaedic surgery & traumatology : orthopedie traumatologie. 2013.
434. Muthuri SG, McWilliams DF, Doherty M, Zhang W. History of knee injuries and knee osteoarthritis: a meta-analysis of observational studies. Osteoarthritis Cartilage. 2011;19(11):1286-93.
435. Englund M, Guermazi A, Lohmander LS. The meniscus in knee osteoarthritis. Rheum Dis Clin North Am. 2009;35(3):579-90.
436. Englund M, Roemer FW, Hayashi D, Crema MD, Guermazi A. Meniscus pathology, osteoarthritis and the treatment controversy. Nat Rev Rheumatol. 2012;8(7):412-9.
437. Glasson SS, Blanchet TJ, Morris EA. The surgical destabilization of the medial meniscus (DMM) model of osteoarthritis in the 129/SvEv mouse. Osteoarthritis and cartilage / OARS, Osteoarthritis Research Society. 2007;15(9):1061-9.
438. Kamekura S, Hoshi K, Shimoaka T, Chung U, Chikuda H, Yamada T, et al. Osteoarthritis development in novel experimental mouse models induced by knee joint instability. Osteoarthritis Cartilage. 2005;13(7):632-41.
439. Little CB, Meeker CT, Golub SB, Lawlor KE, Farmer PJ, Smith SM, et al. Blocking aggrecanase cleavage in the aggrecan interglobular domain abrogates cartilage erosion and promotes cartilage repair. The Journal of clinical investigation. 2007;117(6):1627-36.
440. Ma HL, Blanchet TJ, Peluso D, Hopkins B, Morris EA, Glasson SS. Osteoarthritis severity is sex dependent in a surgical mouse model. Osteoarthritis and cartilage / OARS, Osteoarthritis Research Society. 2007;15(6):695-700.
441. Malfait AM, Ritchie J, Gil AS, Austin JS, Hartke J, Qin W, et al. ADAMTS-5 deficient mice do not develop mechanical allodynia associated with osteoarthritis following medial meniscal destabilization. Osteoarthritis and cartilage / OARS, Osteoarthritis Research Society. 2010;18(4):572-80.
442. Wehling M. Assessing the translatability of drug projects: what needs to be scored to predict success? Nature reviews Drug discovery. 2009;8(7):541-6.

443. Wendler A, Wehling M. The translatability of animal models for clinical development: biomarkers and disease models. Current opinion in pharmacology. 2010;10(5):601-6.
444. Christiansen BA, Guilak F, Lockwood KA, Olson SA, Pitsillides AA, Sandell LJ, et al. Non-invasive mouse models of post-traumatic osteoarthritis. Osteoarthritis Cartilage. 2015;23(10):1627-38.
445. Kim HA, Kim I, Song YW, Kim DH, Niu J, Guermazi A, et al. The association between meniscal and cruciate ligament damage and knee pain in community residents. Osteoarthritis Cartilage. 2011;19(12):1422-8.
446. Hunter DJ. Imaging insights on the epidemiology and pathophysiology of osteoarthritis. Rheum Dis Clin North Am. 2009;35(3):447-63.
447. Dumonde DC, Glynn LE. The production of arthritis in rabbits by an immunological reaction to fibrin. British journal of experimental pathology. 1962;43:373-83.
448. Brackertz D, Mitchell GF, Mackay IR. Antigen-induced arthritis in mice. I. Induction of arthritis in various strains of mice. Arthritis Rheum. 1977;20(3):841-50.
449. van den Berg WB. Lessons from animal models of arthritis over the past decade. Arthritis Res Ther. 2009;11(5):250.
450. Little CB, Mittaz L, Belluoccio D, Rogerson FM, Campbell IK, Meeker CT, et al. ADAMTS-1-knockout mice do not exhibit abnormalities in aggrecan turnover in vitro or in vivo. Arthritis and rheumatism. 2005;52(5):1461-72.
451. Yang YH, Hall P, Little CB, Fosang AJ, Milenkovski G, Santos L, et al. Reduction of arthritis severity in protease-activated receptor-deficient mice. Arthritis and rheumatism. 2005;52(4):1325-32.
452. Segond von Banchet G, Boettger MK, Fischer N, Gajda M, Brauer R, Schaible HG. Experimental arthritis causes tumor necrosis factor-alpha-dependent infiltration of macrophages into rat dorsal root ganglia which correlates with pain-related behavior. Pain. 2009;145(1-2):151-9.
453. Ebbinghaus M, Uhlig B, Richter F, von Banchet GS, Gajda M, Brauer R, et al. The role of interleukin-1beta in arthritic pain: main involvement in thermal, but not mechanical, hyperalgesia in rat antigen-induced arthritis. Arthritis & Rheumatism. 2012;64(12):3897-907.
454. Somerville JM, Aspden RM, Armour KE, Armour KJ, Reid DM. Growth of C57BL/6 mice and the material and mechanical properties of cortical bone from the tibia. Calcified tissue international. 2004;74(5):469-75.
455. Langford DJ, Tuttle AH, Brown K, Deschenes S, Fischer DB, Mutso A, et al. Social approach to pain in laboratory mice. Social neuroscience. 2010;5(2):163-70.
456. Langford DJ, Crager SE, Shehzad Z, Smith SB, Sotocinal SG, Levenstadt JS, et al. Social modulation of pain as evidence for empathy in mice. Science (New York, NY). 2006;312(5782):1967-70.
457. Gioiosa L, Chiarotti F, Alleva E, Laviola G. A trouble shared is a trouble halved: social context and status affect pain in mouse dyads. PloS one. 2009;4(1):e4143.
458. Langford DJ, Tuttle AH, Briscoe C, Harvey-Lewis C, Baran I, Gleeson P, et al. Varying perceived social threat modulates pain behavior in male mice. The journal of pain : official journal of the American Pain Society. 2011;12(1):125-32.
459. Englund M, Guermazi A, Roemer FW, Aliabadi P, Yang M, Lewis CE, et al. Meniscal tear in knees without surgery and the development of radiographic osteoarthritis among middle-aged and elderly persons: The Multicenter Osteoarthritis Study. Arthritis Rheum. 2009;60(3):831-9.

460. Lohmander LS, Englund PM, Dahl LL, Roos EM. The long-term consequence of anterior cruciate ligament and meniscus injuries: osteoarthritis. Am J Sports Med. 2007;35(10):1756-69.
461. Jackson MT, Moradi B, Zaki S, Smith MM, McCracken S, Smith SM, et al. Depletion of protease-activated receptor 2 but not protease-activated receptor 1 may confer protection against osteoarthritis in mice through extracartilaginous mechanisms. Arthritis rheumatol. 2014;66(12):3337-48.
462. Glasson SS, Chambers MG, Van Den Berg WB, Little CB. The OARSI histopathology initiative - recommendations for histological assessments of osteoarthritis in the mouse. Osteoarthritis and cartilage / OARS, Osteoarthritis Research Society. 2010;18 Suppl 3:S17-23.
463. Bytyqi D, Shabani B, Lustig S, Cheze L, Karahoda Gjurgjeala N, Neyret P. Gait knee kinematic alterations in medial osteoarthritis: three dimensional assessment. International orthopaedics. 2014;38(6):1191-8.
464. Imamura M, Imamura ST, Kaziyama HH, Targino RA, Hsing WT, de Souza LP, et al. Impact of nervous system hyperalgesia on pain, disability, and quality of life in patients with knee osteoarthritis: a controlled analysis. Arthritis Rheum. 2008;59(10):1424-31.
465. Chaplan SR, Bach FW, Pogrel JW, Chung JM, Yaksh TL. Quantitative assessment of tactile allodynia in the rat paw. Journal of neuroscience methods. 1994;53(1):55-63.
466. Dixon WJ. Efficient analysis of experimental observations. Annual review of pharmacology and toxicology. 1980;20:441-62.
467. Schaible HG, von Banchet GS, Boettger MK, Brauer R, Gajda M, Richter F, et al. The role of proinflammatory cytokines in the generation and maintenance of joint pain. Annals of the New York Academy of Sciences. 2010;1193:60-9.
468. Zhang L, Hoff AO, Wimalawansa SJ, Cote GJ, Gagel RF, Westlund KN. Arthritic calcitonin/alpha calcitonin gene-related peptide knockout mice have reduced nociceptive hypersensitivity. Pain. 2001;89(2-3):265-73.
469. Bullock CM, Wookey P, Bennett A, Mobasheri A, Dickerson I, Kelly S. Increased peripheral calcitonin gene-related peptide receptor signalling drives mechanical sensitization of the joint in rat models of osteoarthritis pain. Arthritis rheumatol. 2014.
470. McDougall JJ, Karimian SM, Ferrell WR. Alteration of substance P-mediated vasodilatation and sympathetic vasoconstriction in the rat knee joint by adjuvant-induced inflammation. Neurosci Lett. 1994;174(2):127-9.
471. Westlund KN, Kochukov MY, Lu Y, McNearney TA. Impact of central and peripheral TRPV1 and ROS levels on proinflammatory mediators and nociceptive behavior. Molecular pain. 2010;6:46.
472. Zhang Y, Wang Y-H, Ge H-Y, Arendt-Nielsen L, Wang R, Yue S-W. A transient receptor potential vanilloid 4 contributes to mechanical allodynia following chronic compression of dorsal root ganglion in rats. Neurosci Lett. 2008;432(3):222-7.
473. Premkumar LS, Abooj M. TRP channels and analgesia. Life sciences. 2012.
474. McGaraughty S, Chu KL, Perner RJ, Didomenico S, Kort ME, Kym PR. TRPA1 modulation of spontaneous and mechanically evoked firing of spinal neurons in uninjured, osteoarthritic, and inflamed rats. Molecular pain. 2010;6:14.
475. Schuelert N, McDougall JJ. Cannabinoid-mediated antinociception is enhanced in rat osteoarthritic knees. Arthritis Rheum. 2008;58(1):145-53.

476. Nascimento D, Pozza DH, Castro-Lopes JM, Neto FL. Neuronal injury marker ATF-3 is induced in primary afferent neurons of monoarthritic rats. Neurosignals. 2011;19(4):210-21.
477. Thakur M, Rahman W, Hobbs C, Dickenson AH, Bennett DLH. Characterisation of a peripheral neuropathic component of the rat monoiodoacetate model of osteoarthritis. PLoS ONE [Electronic Resource]. 2012;7(3):e33730.
478. Lemarchant S, Pruvost M, Montaner J, Emery E, Vivien D, Kanninen K, et al. ADAMTS proteoglycanases in the physiological and pathological central nervous system. Journal of neuroinflammation. 2013;10:133.
479. Borbely E, Hajna Z, Sandor K, Kereskai L, Toth I, Pinter E, et al. Role of tachykinin 1 and 4 gene-derived neuropeptides and the neurokinin 1 receptor in adjuvant-induced chronic arthritis of the mouse. PLoS ONE [Electronic Resource]. 2013;8(4):e61684.
480. Makino A, Sakai A, Ito H, Suzuki H. Involvement of tachykinins and NK1 receptor in the joint inflammation with collagen type II-specific monoclonal antibody-induced arthritis in mice. J Nippon Med Sch. 2012;79(2):129-38.
481. Saxler G, Loer F, Skumavc M, Pfortner J, Hanesch U. Localization of SP- and CGRP-immunopositive nerve fibers in the hip joint of patients with painful osteoarthritis and of patients with painless failed total hip arthroplasties. Eur J Pain. 2007;11(1):67-74.
482. Wang ZY, McDowell T, Wang P, Alvarez R, Gomez T, Bjorling DE. Activation of CB1 inhibits NGF-induced sensitization of TRPV1 in adult mouse afferent neurons. Neuroscience. 2014;277:679-89.
483. Zhang Y, Wang YH, Ge HY, Arendt-Nielsen L, Wang R, Yue SW. A transient receptor potential vanilloid 4 contributes to mechanical allodynia following chronic compression of dorsal root ganglion in rats. Neurosci Lett. 2008;432(3):222-7.
484. Fernandes ES, Russell FA, Spina D, McDougall JJ, Graepel R, Gentry C, et al. A distinct role for transient receptor potential ankyrin 1, in addition to transient receptor potential vanilloid 1, in tumor necrosis factor alpha-induced inflammatory hyperalgesia and Freund's complete adjuvant-induced monarthritis. Arthritis & Rheumatism. 2011;63(3):819-29.
485. Horvath A, Tekus V, Boros M, Pozsgai G, Botz B, Borbely E, et al. Transient receptor potential ankyrin 1 (TRPA1) receptor is involved in chronic arthritis: in vivo study using TRPA1-deficient mice. Arthritis Res Ther. 2016;18(1):6.
486. Thakur M, Rahman W, Hobbs C, Dickenson AH, Bennett DL. Characterisation of a peripheral neuropathic component of the rat monoiodoacetate model of osteoarthritis. PloS one. 2012;7(3):e33730.
487. Rosenzweig DH, Quinn TM, Haglund L. Low-frequency high-magnitude mechanical strain of articular chondrocytes activates p38 MAPK and induces phenotypic changes associated with osteoarthritis and pain. Int J Mol Sci. 2014;15(8):14427-41.
488. Piller N, Decosterd I, Suter MR. Reverse transcription quantitative real-time polymerase chain reaction reference genes in the spared nerve injury model of neuropathic pain: validation and literature search. BMC research notes. 2013;6:266.
489. Tsantoulas C, Zhu L, Yip P, Grist J, Michael GJ, McMahon SB. Kv2 dysfunction after peripheral axotomy enhances sensory neuron responsiveness to sustained input. Exp Neurol. 2014;251:115-26.
490. Huggett J, Dheda K, Bustin S, Zumla A. Real-time RT-PCR normalisation; strategies and considerations. Genes and immunity. 2005;6(4):279-84.

491. Fundel K, Haag J, Gebhard PM, Zimmer R, Aigner T. Normalization strategies for mRNA expression data in cartilage research. Osteoarthritis Cartilage. 2008;16(8):947-55.
492. Kozera B, Rapacz M. Reference genes in real-time PCR. Journal of applied genetics. 2013;54(4):391-406.
493. Boettger MK, Weber K, Schmidt M, Gajda M, Brauer R, Schaible HG. Gait abnormalities differentially indicate pain or structural joint damage in monoarticular antigen-induced arthritis. Pain. 2009;145(1-2):142-50.
494. Loeser JD, Treede RD. The Kyoto protocol of IASP Basic Pain Terminology. Pain. 2008;137(3):473-7.
495. Gaskill BN, Karas AZ, Garner JP, Pritchett-Corning KR. Nest building as an indicator of health and welfare in laboratory mice. Journal of visualized experiments : JoVE. 2013(82):51012.
496. Jirkof P. Burrowing and nest building behavior as indicators of well-being in mice. J Neurosci Methods. 2014.
497. Jirkof P, Cesarovic N, Rettich A, Nicholls F, Seifert B, Arras M. Burrowing behavior as an indicator of post-laparotomy pain in mice. Frontiers in behavioral neuroscience. 2010;4:165.
498. Jirkof P, Fleischmann T, Cesarovic N, Rettich A, Vogel J, Arras M. Assessment of postsurgical distress and pain in laboratory mice by nest complexity scoring. Lab Anim. 2013;47(3):153-61.
499. Matsumiya LC, Sorge RE, Sotocinal SG, Tabaka JM, Wieskopf JS, Zaloum A, et al. Using the Mouse Grimace Scale to reevaluate the efficacy of postoperative analgesics in laboratory mice. Journal of the American Association for Laboratory Animal Science : JAALAS. 2012;51(1):42-9.
500. Langford DJ, Bailey AL, Chanda ML, Clarke SE, Drummond TE, Echols S, et al. Coding of facial expressions of pain in the laboratory mouse. Nature methods. 2010;7(6):447-9.
501. Keating SC, Thomas AA, Flecknell PA, Leach MC. Evaluation of EMLA cream for preventing pain during tattooing of rabbits: changes in physiological, behavioural and facial expression responses. PloS one. 2012;7(9):e44437.
502. Leach MC, Klaus K, Miller AL, Scotto di Perrotolo M, Sotocinal SG, Flecknell PA. The assessment of post-vasectomy pain in mice using behaviour and the Mouse Grimace Scale. PloS one. 2012;7(4):e35656.
503. Sotocinal SG, Sorge RE, Zaloum A, Tuttle AH, Martin LJ, Wieskopf JS, et al. The Rat Grimace Scale: a partially automated method for quantifying pain in the laboratory rat via facial expressions. Mol Pain. 2011;7:55.
504. Bellamy N, Buchanan WW, Goldsmith CH, Campbell J, Stitt LW. Validation study of WOMAC: a health status instrument for measuring clinically important patient relevant outcomes to antirheumatic drug therapy in patients with osteoarthritis of the hip or knee. J Rheumatol. 1988;15(12):1833-40.
505. Burckhardt CS. The use of the McGill Pain Questionnaire in assessing arthritis pain. Pain. 1984;19(3):305-14.
506. Hawker GA, Mian S, Kendzerska T, French M. Measures of adult pain: Visual Analog Scale for Pain (VAS Pain), Numeric Rating Scale for Pain (NRS Pain), McGill Pain Questionnaire (MPQ), Short-Form McGill Pain Questionnaire (SF-MPQ), Chronic Pain Grade Scale (CPGS), Short Form-36 Bodily Pain Scale (SF-36 BPS), and Measure of Intermittent and Constant Osteoarthritis Pain (ICOAP). Arthritis care & research. 2011;63 Suppl 11:S240-52.

507. Cedraschi C, Delezay S, Marty M, Berenbaum F, Bouhassira D, Henrotin Y, et al. "Let's talk about OA pain": a qualitative analysis of the perceptions of people suffering from OA. Towards the development of a specific pain OA-Related questionnaire, the Osteoarthritis Symptom Inventory Scale (OASIS). PloS one. 2013;8(11):e79988.
508. Osgood E, Trudeau JJ, Eaton TA, Jensen MP, Gammaitoni A, Simon LS, et al. Development of a bedside pain assessment kit for the classification of patients with osteoarthritis. Rheumatology international. 2015;35(6):1005-13.
509. Abhishek A, Doherty M. Diagnosis and clinical presentation of osteoarthritis. Rheum Dis Clin North Am. 2013;39(1):45-66.
510. Sutton BC, Opp MR. Musculoskeletal sensitization and sleep: chronic muscle pain fragments sleep of mice without altering its duration. Sleep. 2014;37(3):505-13.
511. Finan PH, Buenaver LF, Bounds SC, Hussain S, Park RJ, Haque UJ, et al. Discordance between pain and radiographic severity in knee osteoarthritis: Findings from quantitative sensory testing of central sensitization. Arthritis Rheum. 2013;65(2):363-72.
512. Rakel B, Vance C, Zimmerman MB, Petsas-Blodgett N, Amendola A, Sluka KA. Mechanical Hyperalgesia and Reduced Quality of Life Occur in People with Mild Knee Osteoarthritis Pain. The Clinical journal of pain. 2014.
513. Arendt-Nielsen L, Egsgaard LL, Petersen KK, Eskehave TN, Graven-Nielsen T, Hoeck HC, et al. A mechanism-based pain sensitivity index to characterize knee osteoarthritis patients with different disease stages and pain levels. Eur J Pain. 2014.
514. Levinger P, Menz HB, Morrow AD, Feller JA, Bartlett JR, Bergman NR. Foot kinematics in people with medial compartment knee osteoarthritis. Rheumatology (Oxford). 2012;51(12):2191-8.
515. Vincelette J, Xu Y, Zhang LN, Schaefer CJ, Vergona R, Sullivan ME, et al. Gait analysis in a murine model of collagen-induced arthritis. Arthritis Res Ther. 2007;9(6):R123.
516. Poulet B, de Souza R, Knights CB, Gentry C, Wilson AM, Bevan S, et al. Modifications of gait as predictors of natural osteoarthritis progression in STR/Ort mice. Arthritis rheumatol. 2014;66(7):1832-42.
517. Plone MA, Emerich DF, Lindner MD. Individual differences in the hotplate test and effects of habituation on sensitivity to morphine. Pain. 1996;66(2–3):265-70.
518. Barton NJ, Strickland IT, Bond SM, Brash HM, Bate ST, Wilson AW, et al. Pressure application measurement (PAM): a novel behavioural technique for measuring hypersensitivity in a rat model of joint pain. J Neurosci Methods. 2007;163(1):67-75.
519. Boettger MK, Hensellek S, Richter F, Gajda M, Stockigt R, von Banchet GS, et al. Antinociceptive effects of tumor necrosis factor alpha neutralization in a rat model of antigen-induced arthritis: evidence of a neuronal target. Arthritis and rheumatism. 2008;58(8):2368-78.
520. Harvey VL, Dickenson AH. Behavioural and electrophysiological characterisation of experimentally induced osteoarthritis and neuropathy in C57Bl/6 mice. Mol Pain. 2009;5:18.
521. Griffiths RJ. Characterisation and pharmacological sensitivity of antigen arthritis induced by methylated bovine serum albumin in the rat. Agents Actions. 1992;35(1-2):88-95.
522. Schulz KF, Chalmers I, Hayes RJ, Altman DG. Empirical evidence of bias. Dimensions of methodological quality associated with estimates of treatment effects

in controlled trials. JAMA : the journal of the American Medical Association. 1995;273(5):408-12.
523. Kjaergard LL, Villumsen J, Gluud C. Reported methodologic quality and discrepancies between large and small randomized trials in meta-analyses. Annals of internal medicine. 2001;135(11):982-9.
524. Festing MF. Design and statistical methods in studies using animal models of development. Ilar j. 2006;47(1):5-14.
525. Bello S, Krogsboll LT, Gruber J, Zhao ZJ, Fischer D, Hrobjartsson A. Lack of blinding of outcome assessors in animal model experiments implies risk of observer bias. Journal of clinical epidemiology. 2014;67(9):973-83.
526. Von Frey M. Zur physiologie der juckempfindung. Arch Neerland Physiol. 1922;7:142-5.
527. Semmes J, Weinstein S, Ghent L, Teuber HL. Somatosensory changes after penetrating brain wounds in man. Oxford, England: Harvard University Press; 1960. 91 p.
528. Bove G. Mechanical sensory threshold testing using nylon monofilaments: the pain field's "tin standard". Pain. 2006;124(1-2):13-7.
529. Pitcher GM, Ritchie J, Henry JL. Paw withdrawal threshold in the von Frey hair test is influenced by the surface on which the rat stands. J Neurosci Methods. 1999;87(2):185-93.
530. File SE. The interplay of learning and anxiety in the elevated plus-maze. Behavioural brain research. 1993;58(1-2):199-202.
531. Bushnell MC, Duncan GH, Dubner R, Jones RL, Maixner W. Attentional influences on noxious and innocuous cutaneous heat detection in humans and monkeys. The Journal of neuroscience : the official journal of the Society for Neuroscience. 1985;5(5):1103-10.
532. Villemure C, Bushnell MC. Mood influences supraspinal pain processing separately from attention. The Journal of neuroscience : the official journal of the Society for Neuroscience. 2009;29(3):705-15.
533. Callahan BL, Gil ASC, Levesque A, Mogil JS. Modulation of mechanical and thermal nociceptive sensitivity in the laboratory mouse by behavioral state. The journal of pain : official journal of the American Pain Society. 2008;9(2):174-84.
534. Woolfe G, MacDonald AD. The evaluation of analgesic action of pethidine hydrochloride (Demerol). J Pharmacol Exp Ther. 1944;80:300-7.
535. Eddy NB, Leimbach D. Synthetic analgesics. II. Dithienylbutenyl- and dithienylbutylamines. J Pharmacol Exp Ther. 1953;107(3):385-93.
536. O'Callaghan JP, Holtzman SG. Quantification of the analgesic activity of narcotic antagonists by a modified hot-plate procedure. J Pharmacol Exp Ther. 1975;192(3):497-505.
537. Crockett RS, Bornschein RL, Smith RP. Diurnal variation in response to thermal stimulation: mouse-hotplate test. Physiology & behavior. 1977;18(2):193-6.
538. Lotsch J, Tegeder I, Angst MS, Geisslinger G. Antinociceptive effects of morphine-6-glucuronide in homozygous MDR1a P-glycoprotein knockout and in wildtype mice in the hotplate test. Life sciences. 2000;66(24):2393-403.
539. Kiyatkin EA. Nociceptive sensitivity/behavioral reactivity regulation in rats during aversive states of different nature: its mediation by opioid peptides. Int J Neurosci. 1989;44(1-2):91-110.
540. Porro CA, Carli G. Immobilization and restraint effects on pain reactions in animals. Pain. 1988;32(3):289-307.

541. Patapoutian A, Peier AM, Story GM, Viswanath V. ThermoTRP channels and beyond: mechanisms of temperature sensation. Nat Rev Neurosci. 2003;4(7):529-39.
542. Langley GB, Fowles M, Sheppeard H, Wigley RD. A simple pressure dolorimeter for the quantification of joint tenderness in inflammatory arthritis. Rheumatology international. 1983;3(3):109-12.
543. Atkins CJ, Zielinski A, Klinkhoff AV, Chalmers A, Wade J, Williams D, et al. An electronic method for measuring joint tenderness in rheumatoid arthritis. Arthritis Rheum. 1992;35(4):407-10.
544. Wessel J. The reliability and validity of pain threshold measurements in osteoarthritis of the knee. Scandinavian journal of rheumatology. 1995;24(4):238-42.
545. Leuchtweis J, Imhof AK, Montechiaro F, Schaible HG, Boettger MK. Validation of the digital pressure application measurement (PAM) device for detection of primary mechanical hyperalgesia in rat and mouse antigen-induced knee joint arthritis. Methods and findings in experimental and clinical pharmacology. 2010;32(8):575-83.
546. Di Cesare Mannelli L, Micheli L, Zanardelli M, Ghelardini C. Low dose native type II collagen prevents pain in a rat osteoarthritis model. BMC musculoskeletal disorders. 2013;14:228.
547. Amorim D, David-Pereira A, Pertovaara A, Almeida A, Pinto-Ribeiro F. Amitriptyline reverses hyperalgesia and improves associated mood-like disorders in a model of experimental monoarthritis. Behavioural brain research. 2014;265:12-21.
548. Yarnitsky D, Ochoa JL. Studies of heat pain sensation in man: perception thresholds, rate of stimulus rise and reaction time. Pain. 1990;40(1):85-91.
549. Klemm WR. Behavioral arrest: in search of the neural control system. Progress in neurobiology. 2001;65(5):453-71.
550. Amir S, Brown ZW, Amit Z, Ornstein K. Body pinch induces long lasting cataleptic like immobility in mice: behavioral characterization and the effect of naloxone. Life sciences. 1981;28(10):1189-94.
551. Kul-Panza E, Berker N. Pedobarographic findings in patients with knee osteoarthritis. American journal of physical medicine & rehabilitation / Association of Academic Physiatrists. 2006;85(3):228-33.
552. Maly MR, Costigan PA, Olney SJ. Role of knee kinematics and kinetics on performance and disability in people with medial compartment knee osteoarthritis. Clinical biomechanics (Bristol, Avon). 2006;21(10):1051-9.
553. Gok H, Ergin S, Yavuzer G. Kinetic and kinematic characteristics of gait in patients with medial knee arthrosis. Acta orthopaedica Scandinavica. 2002;73(6):647-52.
554. Simjee SU, Pleuvry BJ, Coulthard P. Modulation of the gait deficit in arthritic rats by infusions of muscimol and bicuculline. Pain. 2004;109(3):453-60.
555. Parvathy SS, Masocha W. Gait analysis of C57BL/6 mice with complete Freund's adjuvant-induced arthritis using the CatWalk system. BMC musculoskeletal disorders. 2013;14:14.
556. Plaas A, Li J, Riesco J, Das R, Sandy JD, Harrison A. Intraarticular injection of hyaluronan prevents cartilage erosion, periarticular fibrosis and mechanical allodynia and normalizes stance time in murine knee osteoarthritis. Arthritis Res Ther. 2011;13(2):R46.
557. Hruska RE, Kennedy S, Silbergeld EK. Quantitative aspects of normal locomotion in rats. Life sciences. 1979;25(2):171-9.

558. Coulthard P, Pleuvry BJ, Brewster M, Wilson KL, Macfarlane TV. Gait analysis as an objective measure in a chronic pain model. J Neurosci Methods. 2002;116(2):197-213.
559. Orito K, Kurozumi S, Ishii I, Tanaka A, Sawada J, Matsuda H. A sensitive gait parameter for quantification of arthritis in rats. J Pharmacol Sci. 2007;103(1):113-6.
560. Ruan MZC, Patel RM, Dawson BC, Jiang MM, Lee BHL. Pain, motor and gait assessment of murine osteoarthritis in a cruciate ligament transection model. Osteoarthritis & Cartilage. 2013;21(9):1355-64.
561. Piel MJ, Kroin JS, van Wijnen AJ, Kc R, Im H-J. Pain assessment in animal models of osteoarthritis. Gene. 2014;537(2):184-8.
562. Duncan RC, Hay EM, Saklatvala J, Croft PR. Prevalence of radiographic osteoarthritis--it all depends on your point of view. Rheumatology (Oxford). 2006;45(6):757-60.
563. Ledingham J, Regan M, Jones A, Doherty M. Radiographic patterns and associations of osteoarthritis of the knee in patients referred to hospital. Ann Rheum Dis. 1993;52(7):520-6.
564. Reiner A, Yekutieli D, Benjamini Y. Identifying differentially expressed genes using false discovery rate controlling procedures. Bioinformatics (Oxford, England). 2003;19(3):368-75.
565. Jacobsen E, Dart AJ, Mondori T, Horadogoda N, Jeffcott LB, Little CB, et al. Focal experimental injury leads to widespread gene expression and histologic changes in equine flexor tendons. PloS one. 2015;10(4):e0122220.
566. Emrani PS, Katz JN, Kessler CL, Reichmann WM, Wright EA, McAlindon TE, et al. Joint space narrowing and Kellgren-Lawrence progression in knee osteoarthritis: an analytic literature synthesis. Osteoarthritis Cartilage. 2008;16(8):873-82.
567. Kellgren JH, Lawrence JS. Radiological assessment of osteo-arthrosis. Ann Rheum Dis. 1957;16(4):494-502.
568. Felson DT, Gale DR, Elon Gale M, Niu J, Hunter DJ, Goggins J, et al. Osteophytes and progression of knee osteoarthritis. Rheumatology (Oxford). 2005;44(1):100-4.
569. van der Kraan PM, van den Berg WB. Osteophytes: relevance and biology. Osteoarthritis Cartilage. 2007;15(3):237-44.
570. Schelbergen RF, de Munter W, van den Bosch MH, Lafeber FP, Sloetjes A, Vogl T, et al. Alarmins S100A8/S100A9 aggravate osteophyte formation in experimental osteoarthritis and predict osteophyte progression in early human symptomatic osteoarthritis. Ann Rheum Dis. 2016;75(1):218-25.
571. Schelbergen RF, Geven EJ, van den Bosch MH, Eriksson H, Leanderson T, Vogl T, et al. Prophylactic treatment with S100A9 inhibitor paquinimod reduces pathology in experimental collagenase-induced osteoarthritis. Ann Rheum Dis. 2015;74(12):2254-8.
572. Blaney Davidson EN, Vitters EL, Bennink MB, van Lent PL, van Caam AP, Blom AB, et al. Inducible chondrocyte-specific overexpression of BMP2 in young mice results in severe aggravation of osteophyte formation in experimental OA without altering cartilage damage. Ann Rheum Dis. 2015;74(6):1257-64.
573. Blaney Davidson EN, Vitters EL, van Beuningen HM, van de Loo FA, van den Berg WB, van der Kraan PM. Resemblance of osteophytes in experimental osteoarthritis to transforming growth factor beta-induced osteophytes: limited role of bone morphogenetic protein in early osteoarthritic osteophyte formation. Arthritis Rheum. 2007;56(12):4065-73.

574. Blaney Davidson EN, Vitters EL, van der Kraan PM, van den Berg WB. Expression of transforming growth factor-beta (TGFbeta) and the TGFbeta signalling molecule SMAD-2P in spontaneous and instability-induced osteoarthritis: role in cartilage degradation, chondrogenesis and osteophyte formation. Ann Rheum Dis. 2006;65(11):1414-21.
575. Scharstuhl A, Vitters EL, van der Kraan PM, van den Berg WB. Reduction of osteophyte formation and synovial thickening by adenoviral overexpression of transforming growth factor beta/bone morphogenetic protein inhibitors during experimental osteoarthritis. Arthritis Rheum. 2003;48(12):3442-51.
576. Scharstuhl A, Glansbeek HL, van Beuningen HM, Vitters EL, van der Kraan PM, van den Berg WB. Inhibition of endogenous TGF-beta during experimental osteoarthritis prevents osteophyte formation and impairs cartilage repair. J Immunol. 2002;169(1):507-14.
577. Hsia AW, Anderson MJ, Heffner MA, Lagmay EP, Zavodovskaya R, Christiansen BA. Osteophyte formation after ACL rupture in mice is associated with joint restabilization and loss of range of motion. J Orthop Res. 2016.
578. Diarra D, Stolina M, Polzer K, Zwerina J, Ominsky MS, Dwyer D, et al. Dickkopf-1 is a master regulator of joint remodeling. Nat Med. 2007;13(2):156-63.
579. Resnick D, Niwayama G. Entheses and enthesopathy. Anatomical, pathological, and radiological correlation. Radiology. 1983;146(1):1-9.
580. Rogers J, Shepstone L, Dieppe P. Bone formers: osteophyte and enthesophyte formation are positively associated. Ann Rheum Dis. 1997;56(2):85-90.
581. Hardcastle SA, Dieppe P, Gregson CL, Arden NK, Spector TD, Hart DJ, et al. Osteophytes, enthesophytes, and high bone mass: a bone-forming triad with potential relevance in osteoarthritis. Arthritis rheumatol. 2014;66(9):2429-39.
582. Burr DB. The importance of subchondral bone in osteoarthrosis. Current opinion in rheumatology. 1998;10(3):256-62.
583. Sanchez C, Deberg MA, Piccardi N, Msika P, Reginster JY, Henrotin YE. Subchondral bone osteoblasts induce phenotypic changes in human osteoarthritic chondrocytes. Osteoarthritis Cartilage. 2005;13(11):988-97.
584. Loeser RF. Aging and osteoarthritis. Current opinion in rheumatology. 2011;23(5):492-6.
585. Hwang HS, Kim HA. Chondrocyte Apoptosis in the Pathogenesis of Osteoarthritis. Int J Mol Sci. 2015;16(11):26035-54.
586. Portal-Nunez S, Esbrit P, Alcaraz MJ, Largo R. Oxidative stress, autophagy, epigenetic changes and regulation by miRNAs as potential therapeutic targets in osteoarthritis. Biochem Pharmacol. 2016;108:1-10.
587. Funck-Brentano T, Cohen-Solal M. Subchondral bone and osteoarthritis. Current opinion in rheumatology. 2015;27(4):420-6.
588. Hunter DJ, Gerstenfeld L, Bishop G, Davis AD, Mason ZD, Einhorn TA, et al. Bone marrow lesions from osteoarthritis knees are characterized by sclerotic bone that is less well mineralized. Arthritis Res Ther. 2009;11(1):R11.
589. Kadri A, Funck-Brentano T, Lin H, Ea HK, Hannouche D, Marty C, et al. Inhibition of bone resorption blunts osteoarthritis in mice with high bone remodelling. Ann Rheum Dis. 2010;69(8):1533-8.
590. Funck-Brentano T, Lin H, Hay E, Ah Kioon MD, Schiltz C, Hannouche D, et al. Targeting bone alleviates osteoarthritis in osteopenic mice and modulates cartilage catabolism. PloS one. 2012;7(3):e33543.
591. Glasson SS. In vivo osteoarthritis target validation utilizing genetically-modified mice. Current drug targets. 2007;8(2):367-76.

592. Ryu JH, Yang S, Shin Y, Rhee J, Chun CH, Chun JS. Interleukin-6 plays an essential role in hypoxia-inducible factor 2alpha-induced experimental osteoarthritic cartilage destruction in mice. Arthritis Rheum. 2011;63(9):2732-43.
593. Nasi S, Ea HK, Chobaz V, van Lent P, Liote F, So A, et al. Dispensable role of myeloid differentiation primary response gene 88 (MyD88) and MyD88-dependent toll-like receptors (TLRs) in a murine model of osteoarthritis. Joint, bone, spine : revue du rhumatisme. 2014;81(4):320-4.
594. Leuchtweis J, Boettger MK, Niv F, Redecker C, Schaible HG. Enhanced neurogenesis in the hippocampal dentate gyrus during antigen-induced arthritis in adult rat--a crucial role of immunization. PloS one. 2014;9(2):e89258.
595. Boettger MK, Weber K, Grossmann D, Gajda M, Bauer R, Bar KJ, et al. Spinal tumor necrosis factor alpha neutralization reduces peripheral inflammation and hyperalgesia and suppresses autonomic responses in experimental arthritis: a role for spinal tumor necrosis factor alpha during induction and maintenance of peripheral inflammation. Arthritis Rheum. 2010;62(5):1308-18.
596. Neogi T, Frey-Law L, Scholz J, Niu J, Arendt-Nielsen L, Woolf C, et al. Sensitivity and sensitisation in relation to pain severity in knee osteoarthritis: trait or state? Ann Rheum Dis. 2015;74(4):682-8.
597. Woolf CJ. Evidence for a central component of post-injury pain hypersensitivity. Nature. 1983;306(5944):686-8.
598. Hamilton CB, Pest MA, Pitelka V, Ratneswaran A, Beier F, Chesworth BM. Weight-bearing asymmetry and vertical activity differences in a rat model of post-traumatic knee osteoarthritis. Osteoarthritis & Cartilage. 2015;23(7):1178-85.
599. Le Bars D, Gozariu M, Cadden SW. Animal models of nociception. Pharmacological reviews. 2001;53(4):597-652.
600. Carter RB. Differentiating analgesic and non-analgesic drug activities on rat hot plate: effect of behavioral endpoint. Pain. 1991;47(2):211-20.
601. Espejo EF, Mir D. Structure of the rat's behaviour in the hot plate test. Behavioural brain research. 1993;56(2):171-6.
602. Lundblad H, Kreicbergs A, Jansson KA. Prediction of persistent pain after total knee replacement for osteoarthritis. J Bone Joint Surg Br. 2008;90(2):166-71.
603. Tandrup T. Unbiased estimates of number and size of rat dorsal root ganglion cells in studies of structure and cell survival. Journal of neurocytology. 2004;33(2):173-92.
604. Driscoll C, Chanalaris A, Knights C, Ismail H, Sacitharan PK, Gentry C, et al. Nociceptive Sensitizers Are Regulated in Damaged Joint Tissues, Including Articular Cartilage, When Osteoarthritic Mice Display Pain Behavior. Arthritis rheumatol. 2016;68(4):857-67.
605. Aso K, Izumi M, Sugimura N, Okanoue Y, Ushida T, Ikeuchi M. Nociceptive phenotype alterations of dorsal root ganglia neurons innervating the subchondral bone in osteoarthritic rat knee joints. Osteoarthritis Cartilage. 2016.
606. Walsh DA, Mapp PI, Kelly S. Calcitonin gene-related peptide in the joint: contributions to pain and inflammation. Br J Clin Pharmacol. 2015;80(5):965-78.
607. Taniguchi A, Ishikawa T, Miyagi M, Kamoda H, Sakuma Y, Oikawa Y, et al. Decreased calcitonin gene-related peptide expression in the dorsal root ganglia of TNF-deficient mice in a monoiodoacetate-induced knee osteoarthritis model. International journal of clinical and experimental pathology. 2015;8(10):12967-71.
608. Miller RE, Tran PB, Obeidat AM, Raghu P, Ishihara S, Miller RJ, et al. The Role of Peripheral Nociceptive Neurons in the Pathophysiology of Osteoarthritis Pain. Current osteoporosis reports. 2015;13(5):318-26.

609. Malek N, Pajak A, Kolosowska N, Kucharczyk M, Starowicz K. The importance of TRPV1-sensitisation factors for the development of neuropathic pain. Mol Cell Neurosci. 2015;65:1-10.
610. Perrot S. Osteoarthritis pain. Best practice & research Clinical rheumatology. 2015;29(1):90-7.
611. Latremoliere A, Woolf CJ. Central sensitization: a generator of pain hypersensitivity by central neural plasticity. The journal of pain : official journal of the American Pain Society. 2009;10(9):895-926.
612. Schaible HG, von Banchet GS, Boettger MK, Brauer R, Gajda M, Richter F, et al. The role of proinflammatory cytokines in the generation and maintenance of joint pain. Annals of the New York Academy of Sciences. 2010;1193:60-9.
613. Premkumar LS, Abooj M. TRP channels and analgesia. Life sciences. 2013;92(8-9):415-24.
614. Peng J, Gu N, Zhou L, U BE, Murugan M, Gan WB, et al. Microglia and monocytes synergistically promote the transition from acute to chronic pain after nerve injury. Nature communications. 2016;7:12029.
615. Sofroniew MV, Vinters HV. Astrocytes: biology and pathology. Acta neuropathologica. 2010;119(1):7-35.
616. Scholz J, Woolf CJ. The neuropathic pain triad: neurons, immune cells and glia. Nature neuroscience. 2007;10(11):1361-8.
617. Abbadie C, Bhangoo S, De Koninck Y, Malcangio M, Melik-Parsadaniantz S, White FA. Chemokines and pain mechanisms. Brain Res Rev. 2009;60(1):125-34.
618. Taves S, Berta T, Chen G, Ji RR. Microglia and spinal cord synaptic plasticity in persistent pain. Neural plasticity. 2013;2013:753656.
619. Chekulaeva M, Landthaler M. Eyes on Translation. Molecular cell. 2016;63(6):918-25.
620. Woolf CJ, Ma Q. Nociceptors--noxious stimulus detectors. Neuron. 2007;55(3):353-64.
621. Miller RE, Belmadani A, Ishihara S, Tran PB, Ren D, Miller RJ, et al. Damage-associated molecular patterns generated in osteoarthritis directly excite murine nociceptive neurons through Toll-like receptor 4. Arthritis rheumatol. 2015;67(11):2933-43.
622. Adaes S, Ferreira-Gomes J, Mendonca M, Almeida L, Castro-Lopes JM, Neto FL. Injury of primary afferent neurons may contribute to osteoarthritis induced pain: an experimental study using the collagenase model in rats. Osteoarthritis & Cartilage. 2015;23(6):914-24.
623. Gwilym SE, Keltner JR, Warnaby CE, Carr AJ, Chizh B, Chessell I, et al. Psychophysical and functional imaging evidence supporting the presence of central sensitization in a cohort of osteoarthritis patients. Arthritis Rheum. 2009;61(9):1226-34.
624. Wylde V, Palmer S, Learmonth ID, Dieppe P. Test-retest reliability of Quantitative Sensory Testing in knee osteoarthritis and healthy participants. Osteoarthritis Cartilage. 2011;19(6):655-8.
625. Kosek E, Ordeberg G. Abnormalities of somatosensory perception in patients with painful osteoarthritis normalize following successful treatment. Eur J Pain. 2000;4(3):229-38.
626. Kobayashi K, Fukuoka T, Obata K, Yamanaka H, Dai Y, Tokunaga A, et al. Distinct expression of TRPM8, TRPA1, and TRPV1 mRNAs in rat primary afferent neurons with adelta/c-fibers and colocalization with trk receptors. The Journal of comparative neurology. 2005;493(4):596-606.

627. Fernandes ES, Russell FA, Spina D, McDougall JJ, Graepel R, Gentry C, et al. A distinct role for transient receptor potential ankyrin 1, in addition to transient receptor potential vanilloid 1, in tumor necrosis factor a-induced inflammatory hyperalgesia and Freund's complete adjuvant-induced monarthritis. Arthritis Rheum. 2011;63(3):819-29.
628. Lennertz RC, Kossyreva EA, Smith AK, Stucky CL. TRPA1 mediates mechanical sensitization in nociceptors during inflammation. PloS one. 2012;7(8):e43597.
629. Qin N, Neeper MP, Liu Y, Hutchinson TL, Lubin ML, Flores CM. TRPV2 is activated by cannabidiol and mediates CGRP release in cultured rat dorsal root ganglion neurons. The Journal of neuroscience : the official journal of the Society for Neuroscience. 2008;28(24):6231-8.
630. Chen X, Alessandri-Haber N, Levine JD. Marked attenuation of inflammatory mediator-induced C-fiber sensitization for mechanical and hypotonic stimuli in TRPV4-/- mice. Mol Pain. 2007;3:31.
631. Alessandri-Haber N, Dina OA, Joseph EK, Reichling DB, Levine JD. Interaction of transient receptor potential vanilloid 4, integrin, and SRC tyrosine kinase in mechanical hyperalgesia. The Journal of neuroscience : the official journal of the Society for Neuroscience. 2008;28(5):1046-57.
632. Segond von Banchet G, Boettger MK, Konig C, Iwakura Y, Brauer R, Schaible HG. Neuronal IL-17 receptor upregulates TRPV4 but not TRPV1 receptors in DRG neurons and mediates mechanical but not thermal hyperalgesia. Mol Cell Neurosci. 2013;52:152-60.
633. Chen Y, Williams SH, McNulty AL, Hong JH, Lee SH, Rothfusz NE, et al. Temporomandibular joint pain: a critical role for Trpv4 in the trigeminal ganglion. Pain. 2013;154(8):1295-304.
634. Lamande SR, Yuan Y, Gresshoff IL, Rowley L, Belluoccio D, Kaluarachchi K, et al. Mutations in TRPV4 cause an inherited arthropathy of hands and feet. Nature genetics. 2011;43(11):1142-6.
635. Nilius B, Voets T. The puzzle of TRPV4 channelopathies. EMBO reports. 2013;14(2):152-63.
636. Andreucci E, Aftimos S, Alcausin M, Haan E, Hunter W, Kannu P, et al. TRPV4 related skeletal dysplasias: a phenotypic spectrum highlighted byclinical, radiographic, and molecular studies in 21 new families. Orphanet journal of rare diseases. 2011;6:37.
637. White JP, Cibelli M, Urban L, Nilius B, McGeown JG, Nagy I. TRPV4: Molecular Conductor of a Diverse Orchestra. Physiological reviews. 2016;96(3):911-73.
638. O'Conor CJ, Griffin TM, Liedtke W, Guilak F. Increased susceptibility of Trpv4-deficient mice to obesity and obesity-induced osteoarthritis with very high-fat diet. Ann Rheum Dis. 2013;72(2):300-4.
639. McNulty AL, Leddy HA, Liedtke W, Guilak F. TRPV4 as a therapeutic target for joint diseases. Naunyn Schmiedebergs Arch Pharmacol. 2014.
640. Hirsch S, Corradini L, Just S, Arndt K, Doods H. The CGRP receptor antagonist BIBN4096BS peripherally alleviates inflammatory pain in rats. Pain. 2013;154(5):700-7.
641. Benschop RJ, Collins EC, Darling RJ, Allan BW, Leung D, Conner EM, et al. Development of a novel antibody to calcitonin gene-related peptide for the treatment of osteoarthritis-related pain. Osteoarthritis Cartilage. 2014;22(4):578-85.

642. Ferreira-Gomes J, Adaes S, Sarkander J, Castro-Lopes JM. Phenotypic alterations of neurons that innervate osteoarthritic joints in rats. Arthritis Rheum. 2010;62(12):3677-85.
643. Chen BP, Liang G, Whelan J, Hai T. ATF3 and ATF3 delta Zip. Transcriptional repression versus activation by alternatively spliced isoforms. J Biol Chem. 1994;269(22):15819-26.
644. Hai T, Curran T. Cross-family dimerization of transcription factors Fos/Jun and ATF/CREB alters DNA binding specificity. Proc Natl Acad Sci U S A. 1991;88(9):3720-4.
645. Chen BP, Wolfgang CD, Hai T. Analysis of ATF3, a transcription factor induced by physiological stresses and modulated by gadd153/Chop10. Mol Cell Biol. 1996;16(3):1157-68.
646. Inglis JJ, Nissim A, Lees DM, Hunt SP, Chernajovsky Y, Kidd BL. The differential contribution of tumour necrosis factor to thermal and mechanical hyperalgesia during chronic inflammation. Arthritis Res Ther. 2005;7(4):R807-16.
647. Matsuura Y, Ohtori S, Iwakura N, Suzuki T, Kuniyoshi K, Takahashi K. Expression of activating transcription factor 3 (ATF3) in uninjured dorsal root ganglion neurons in a lower trunk avulsion pain model in rats. European spine journal : official publication of the European Spine Society, the European Spinal Deformity Society, and the European Section of the Cervical Spine Research Society. 2013;22(8):1794-9.
648. Seijffers R, Mills CD, Woolf CJ. ATF3 increases the intrinsic growth state of DRG neurons to enhance peripheral nerve regeneration. The Journal of neuroscience : the official journal of the Society for Neuroscience. 2007;27(30):7911-20.
649. Inglis JJ, Notley CA, Essex D, Wilson AW, Feldmann M, Anand P, et al. Collagen-induced arthritis as a model of hyperalgesia: functional and cellular analysis of the analgesic actions of tumor necrosis factor blockade. Arthritis Rheum. 2007;56(12):4015-23.
650. Yamanishi Y, Boyle DL, Clark M, Maki RA, Tortorella MD, Arner EC, et al. Expression and regulation of aggrecanase in arthritis: the role of TGF-beta. J Immunol. 2002;168(3):1405-12.
651. Lemarchant S, Pomeshchik Y, Kidin I, Karkkainen V, Valonen P, Lehtonen S, et al. ADAMTS-4 promotes neurodegeneration in a mouse model of amyotrophic lateral sclerosis. Molecular neurodegeneration. 2016;11:10.
652. van de Loo FA, Joosten LA, van Lent PL, Arntz OJ, van den Berg WB. Role of interleukin-1, tumor necrosis factor alpha, and interleukin-6 in cartilage proteoglycan metabolism and destruction. Effect of in situ blocking in murine antigen- and zymosan-induced arthritis. Arthritis Rheum. 1995;38(2):164-72.
653. Pinto LG, Talbot J, Peres RS, Franca RF, Ferreira SH, Ryffel B, et al. Joint production of IL-22 participates in the initial phase of antigen-induced arthritis through IL-1beta production. Arthritis Res Ther. 2015;17:235.
654. Sachs D, Coelho FM, Costa VV, Lopes F, Pinho V, Amaral FA, et al. Cooperative role of tumour necrosis factor-alpha, interleukin-1beta and neutrophils in a novel behavioural model that concomitantly demonstrates articular inflammation and hypernociception in mice. Br J Pharmacol. 2011;162(1):72-83.
655. Koshy PJ, Lundy CJ, Rowan AD, Porter S, Edwards DR, Hogan A, et al. The modulation of matrix metalloproteinase and ADAM gene expression in human chondrocytes by interleukin-1 and oncostatin M: a time-course study using real-time quantitative reverse transcription-polymerase chain reaction. Arthritis Rheum. 2002;46(4):961-7.

656. Lopez-Armada MJ, Carames B, Lires-Dean M, Cillero-Pastor B, Ruiz-Romero C, Galdo F, et al. Cytokines, tumor necrosis factor-alpha and interleukin-1beta, differentially regulate apoptosis in osteoarthritis cultured human chondrocytes. Osteoarthritis Cartilage. 2006;14(7):660-9.
657. Benito MJ, Veale DJ, FitzGerald O, van den Berg WB, Bresnihan B. Synovial tissue inflammation in early and late osteoarthritis. Ann Rheum Dis. 2005;64(9):1263-7.
658. Ning L, Ishijima M, Kaneko H, Kurihara H, Arikawa-Hirasawa E, Kubota M, et al. Correlations between both the expression levels of inflammatory mediators and growth factor in medial perimeniscal synovial tissue and the severity of medial knee osteoarthritis. International orthopaedics. 2011;35(6):831-8.
659. Tran PB, Miller RE, Ishihara S, Miller RJ, Malfait AM. Spinal microglial activation in a murine surgical model of knee osteoarthritis. Osteoarthritis Cartilage. 2016.
660. Larkin J, Lohr TA, Elefante L, Shearin J, Matico R, Su JL, et al. Translational development of an ADAMTS-5 antibody for osteoarthritis disease modification. Osteoarthritis & Cartilage. 2015;23(8):1254-66.
661. Miller RE, Tran PB, Ishihara S, Larkin J, Malfait AM. Therapeutic effects of an anti-ADAMTS-5 antibody on joint damage and mechanical allodynia in a murine model of osteoarthritis. Osteoarthritis Cartilage. 2016;24(2):299-306.
662. Tortorella M, Pratta M, Liu RQ, Abbaszade I, Ross H, Burn T, et al. The thrombospondin motif of aggrecanase-1 (ADAMTS-4) is critical for aggrecan substrate recognition and cleavage. J Biol Chem. 2000;275(33):25791-7.
663. Kawasaki Y, Zhang L, Cheng JK, Ji RR. Cytokine mechanisms of central sensitization: distinct and overlapping role of interleukin-1beta, interleukin-6, and tumor necrosis factor-alpha in regulating synaptic and neuronal activity in the superficial spinal cord. The Journal of neuroscience : the official journal of the Society for Neuroscience. 2008;28(20):5189-94.
664. Choi YS, Park JK, Kang EH, Lee YK, Kim TK, Chung JH, et al. Cytokine signaling-1 suppressor is inducible by IL-1beta and inhibits the catabolic effects of IL-1beta in chondrocytes: its implication in the paradoxical joint-protective role of IL-1beta. Arthritis Res Ther. 2013;15(6):R191.